Investigating the feasibility of using dynamic stiffness beam functions in a hybrid structure-borne noise prediction model

University of Salford MANCHESTER

Daniela Duarte Filipe
School of Computing, Science and Engineering
University of Salford
Supervised by Professor A T Moorhouse

Submitted for the degree of
Master of Science by Research
Acoustics
February 2019

Declaration of authorship

I, Daniela Duarte Filipe, hereby declare that this thesis entitled "*Investigating the feasibility of using dynamic stiffness beam functions in a hybrid structure-borne noise prediction model"* is my own work, along with all that is within it. I confirm that:

- The present work was carried out solely during the candidature for a degree at this university;
- No part of this thesis has been submitted for a degree (or any other qualification) at this or other university;
- Where published work by others has been consulted and / or quoted, this is always clearly attributed and the source is always given. With the exception of such quotations, the thesis is entirely my own work.
- All main sources of help have been acknowledged;
- The main body of this thesis consists of approximately 49,240 words.

Signed: _____

Date: _____

Abstract

Ground-borne vibration and structure-borne noise in buildings associated with nearby railway systems, either above ground or underground, is a common occurrence in densely populated areas. This is especially true where new transportation systems are built in proximity to existing noise and vibration sensitive buildings, and where similar buildings are built close to existing rail systems. With the tendency to build closer to railways both overground and underground, there is a need to better understand how to predict the levels of ground-borne vibration and structure-borne noise in buildings from such systems. A review of the mechanisms through which energy is generated from train sources and propagates into buildings, as well as a review of the existing empirical and theoretical models for the prediction of structure-borne noise in buildings has been undertaken.

A proposal for the simplification of an existing hybrid deterministic – statistical model for the prediction of structure-borne noise in buildings has been put forward and its feasibility investigated. The original model consists of a hybrid finite element – statistical energy analysis tool, where low frequencies are modelled deterministically with finite element, and the higher frequencies are modelled statistically. In the simplified model, the deterministic elements of the system, i.e. beams and columns, are proposed to be modelled using a dynamic stiffness approach.

The analytical mobility functions for free-free beams with six degrees of freedom at each end have been derived from first principles. The results from these were compared against a finite element model for the same beam arrangement. Good agreement was found between the results of the analytical and finite element models. The coupling between beams has been accounted for by using the impedance addition method. Various scenarios were modelled. Good agreement was obtained with a finite element model for the two beams in line scenario. Discrepancies were present for some of the degrees of freedom coupled for the beams in L-junctions scenarios. Further works have been suggested to address these.

A comparison between the various stages of the full and simplified hybrid prediction models has been provided, along with suggestions for the next steps to further develop and assemble the proposed simplified model.

Acknowledgments

First and foremost, I would like to thank Professor Andy Moorhouse for his continued support and supervision, and for understanding the time limitations that come with studying part time while in full-time employment.

I would also like to acknowledge the staff at the School of Computing, Science and Engineering's Postgraduate Support Centre, in combination with Professor Andy Moorhouse, for providing continued support and a helping hand during particularly stressful periods.

Thirdly, I would like to thank Sandy Brown Associates, who sponsored this programme and allowed me the opportunity to expand my knowledge of structure-borne noise and vibration while working with them.

Last, but not least, my family have played a crucial part in my personal and academic life. Without their support, this thesis would not have been possible.

Table of contents

List of figures

List of tables

List of symbols

Acronym	Description
ANC	Association of Noise Consultants (UK)
BEM	Boundary Element Method
CONVURT	CONtrol of Vibration from Underground Rail Traffic
FDM	Finite Difference Method
FDTD	Finite Difference Time Domain
FEM	Finite Element Method
FRA	Federal Railroad Association (US)
FTA	Federal Transit Administration (US)
RIVAS	Railway Induced Vibration Abatement Solutions
rms	Root mean square
SEA	Statistical Energy Analysis
TCRP	Transit Cooperative Research Program

The list of symbols below includes the symbols that are most used in this document. Where the same symbol is used, but the parameter it describes is different, a note has been included in the text.

Symbol	Description
Lower-case Greek letters	
α	Absorption coefficient
ε	Strain
η	Loss factor
ϑ	Damping coefficient
λ	Wavelength (m)
ν	Poisson's ratio
ξ	Displacement (m)
ρ	Density (kg/m^3)
ϱ	Reflection efficiency
σ	Stress (N/m^2)

Symbol	Description
τ	Time constant, transmission efficiency, relaxation time (refer to definition in chapters where this is shown)
ω	Angular frequency (rad/s)

Lower-case English letters

c	Phase velocity (m/s)
f	Frequency (Hz)
k	Wavenumber (rad/m)
m'	Mass per unit length (kg/m)
m''	Mass per unit area (kg/m^2)
t	Time (seconds)
v	Linear velocity (m/s)
w	Angular velocity (rad/s)
x	Location on the beam (m)

Upper-case English letters

B	Beam bending stiffness (Nm^2)
D	Longitudinal stiffness (N/m^2)
E	Young's modulus, also known as modulus of elasticity (N/m^2)
F	Force (N)
G	Shear modulus (N/m^2)
I	Moment of inertia (m^4)
M	Moment (Nm)
R	Transmission loss (dB)
S	Cross-sectional area (m^2)
T	Torsional stiffness (N/m^2)
Y	Mobility (m/Ns)
Z	Impedance (Ns/m)

1 Introduction

1.1 Background

With the continued growth of cities and the consequent lack of space above ground, there is an increasing tendency to build transportation systems underground, especially railways. Whilst they are an effective form of transport and they save valuable space above ground, they can sometimes have severe effects on those nearby. Such effects range from annoyance and sleep disturbance caused to people, to cosmetic and potentially structural damage to buildings. The operation of highly sensitive equipment can also be disrupted by such transportation systems.

Energy from the operation of railway systems, both above and below ground can manifest itself as ground-borne vibration generated by a train event, which propagates through the ground and into a receiver, typically a building. Once at the receiver, ground-borne vibration can be perceived by the building occupants as tactile vibration, i.e. vibration that can be felt, and / or as structure-borne noise which is audible. Structure-borne noise is caused by energy radiating from the surfaces within a room that are excited by ground-borne vibration. Structure-borne noise is also known as ground-borne or re-radiated noise. (BSI, 2005) For the purposes of this document, the terms structure-borne noise and ground-borne noise are interchangeable.

On the effect of ground-borne noise and vibration on people and how it is perceived, the Association of Noise Consultants (2012) state "*the human body is a complex structure and its reaction to vibration is variable and subjective*". Numerous field studies have been undertaken on the impact of railway noise and vibration on people over the years. These include, but are not limited to, the TCRP 2009 study (Zapfe, Saurenman, & Fidell, 2009), where more than 1300 interviews were carried out over the phone in five cities in North America. Noted effects of ground-borne vibration and noise on people include annoyance and discomfort at low level, which can escalate to reduced working efficiency and quality of life.

Ground-borne vibration, and sometimes noise, can also affect the operation of highly sensitive equipment, such as electron microscopes, where high levels of precision are required. Colin Gordon & Associates (Gordon, nd) have undertaken research on acceptable levels of vibration for different types of sensitive equipment. They have set vibration criterion (VC) curves for different uses, which are widely used across the industry, especially in science research facilities.

As previously mentioned, vibration can also have a negative impact on buildings. In extreme cases, it can cause structural damage. BS 7385-1:1990 *Evaluation and measurement for vibration in buildings, Part 1. Guide for measurement of vibrations and evaluation of their effect on buildings* (1990), as its name suggests, provides guidance on how the effect of vibration on buildings can be assessed.

Whilst guidance is available from various sources on how to determine the impact of vibration and structure-borne noise in buildings and their occupants, such task is not an easy one, given the large number of unknowns between a vibration source, such as an underground train, and a receiver. Several techniques are available for the prediction of ground-borne vibration and structure-borne noise in buildings. These range from empirical methods developed in the 1970s and 1980s in America (Kurzweil, 1979; Nelson & Saurenman, 1983; Hanson, Towers, & Meister, 2006), which are still widely used nowadays, to specialist numerical techniques, including finite element modelling (Lurcock & Thompson, 2014) and Rupert Taylor Ltd's FDTD FINDWAVE commercial software package (RPS, 2005), with significant computational costs for detailed models.

Various prediction techniques have also been developed to estimate the propagation of ground-borne vibration in the soil before it enters a building. The Pipe-in-Pipe model, first launched in 1999 with various subsequent updates, is an example of a prediction tool frequently used in the industry to model the interaction between a train, a floating-slab track in an underground tunnel and the surrounding soil. Being a semi-analytical technique means the computation time required is significantly lower than that of numerical techniques, making it an attractive model for use in the early design stages of a project. (Hunt & Hussein, 2007; Kuo, Jones, Hussein, & Hunt, 2013)

As most prediction techniques have their limitations, some authors have taken to developing hybrid calculation models, which combine the best characteristics of two or more calculation techniques and provide more accurate results. An example of these is Shorter & Langley's (2005) Hybrid FE-SEA model, which was developed based on work carried out by Langley & Bremner (1999). This uses a combination of methods for the prediction of structure-borne noise in buildings as its name indicates: finite element analysis to model low frequencies and statistical energy analysis to model high frequencies. However, the division between low and high frequencies is not as such a clear line, but a mid-frequency zone, which does not fall entirely within the domain of finite element or statistical energy analysis. For these frequencies, the model makes use of some of the principles of fuzzy structure theory. Further details on Shorter & Langley's Hybrid FE-SEA model, along with a review of other existing tools for the prediction of structure-borne noise in buildings is provided in this thesis.

1.2 Aim and objectives of the research

The overall aim of this thesis is to propose and investigate the feasibility of a simplified hybrid deterministic – statistical model for the prediction of structure-borne sound in beam-framed buildings, building on the work undertaken by Shorter & Langley (2005) on their Hybrid FE-SEA model. As buildings comprise both deterministic and statistical elements, such as beams and walls, respectively, it is considered appropriate to model energy propagation through such coupled elements using a hybrid approach. The main question is whether dynamic stiffness modelling techniques can be used to model the deterministic elements of a building instead of finite element analysis, thus simplifying Shorter & Langley's model.

With the above in mind, the following are the objectives of the present document:

1. Provide an overview of the mechanisms through which ground-borne vibration and structure-borne noise from trains are generated, how energy propagates through the soil and into a receiving structure, to help understand what parameters affect the propagation of vibration and structure-borne noise between a source and a receiver and how these can be modelled;
2. Focussing on the receiving structure, present a review of empirical and theoretical models currently available for the prediction of structure-borne noise in buildings;
3. Derive the mobilities for each degree of freedom of the deterministic elements of the system using analytical beam functions and compare the obtained results with finite element modelling of the same structures. A comparison between the computation time of the analytical and finite element models is also provided;
4. Demonstrate how structures can be coupled together with beam functions using coupling matrices, compare the obtained results with finite element modelling of the same assemblies and comment on the computation time of each model;
5. Compare the various calculation stages of the proposed simplified hybrid model against the full model it is based on, and identify the main differences relating to each, such as the level of detail required.

1.3 Thesis outline

Chapter 2 of the present document provides an overview of the mechanisms through which ground-borne vibration and structure-borne noise from trains are generated, how energy propagates through the soil and into a receiving structure. The parameters and elements that control the propagation of vibration and structure-borne noise through a building are also set out. This chapter is intended to set the scene on the means through which ground-borne vibration and structure-borne noise is generated by a source and transmitted to a receiver. The subsequent chapters will focus on the receiver only.

Chapter 3 discusses the various types of models that can be used to predict structure-borne noise in buildings and their limitations. A review of the existing empirical and theoretical prediction models is provided in Sections 3.2 and 3.3, based on the information available, with a summary of the findings in Section 3.4. Section 3.5 sets out the initial proposal for a simplified hybrid deterministic – statistical prediction model.

In Chapter 4, analytical beam mobilities for each degree of freedom of a free-free beam are derived from first principles. An overview of the impedance, mobility and dynamic stiffness calculation methods is provided in Section 4.1, with a description of the elements being modelled and their degrees of freedom in Section 4.2. Sections 4.3 and 4.4 present the derivation process for the analytical beam mobilities and the validation of the results against a finite element model, respectively.

Chapter 5 sets out the process used for coupling beams together. The global and local coordinate systems are defined in Section 5.1, and the impedance addition methodology for coupling beams together is described in Section 5.2. Sections 5.3 and 5.4 present the derived coupling matrices and coupled impedance matrices for the beams, and the validation of the results against a finite element model, respectively.

Chapter 6 sets out the proposal for a simplified hybrid deterministic – statistical prediction model. A comparison between Shorter & Langley's (2005) Hybrid FE-SEA model and the proposed simplified model is provided in Section 6.1, with the main steps discussed in Sections 6.2 to 6.5.

A summary of the conclusions obtained from the research and suggestions for further work are provided in Chapter 7.

2 Vibration and structure-borne noise theory

The present chapter introduces the theory necessary to understand and predict vibration and structure-borne noise in buildings. The mechanisms through which vibration propagates from a source to a receiver are described and different vibration sources and their characteristics identified. This chapter is intended as a background literature review to guide the reader through the vibration transmission route from a source to a receiver, as per the first objective of this thesis. The subsequent chapters will focus on vibration transmission through a receiver only.

2.1 Vibration transmission route

Vibration and structure-borne noise in buildings can be caused by a number of sources, namely road traffic, surface and underground rail, machinery and construction works. According to BS ISO 14387-1:2005 (BSI, 2005), railways, either on the surface or underground, are the most commonly occurring and significant source of ground-borne vibration and noise, as a result of the interaction between the steel wheels of the train and the steel rails.

Understanding the mechanism through which vibrational energy propagates away from a source and arrives at a receiver is essential for the determination of vibration and structure-borne noise. Such processes have been the subject of numerous and extensive studies, dating back to the 1960s and 1970s. The guidance provided in some of these studies, such as that by Kurzweil (1979), is still widely used nowadays. Kurzweil's study focuses on the propagation of vibration from underground trains in tunnels through the ground and into a building. It proposes a method for estimating A-weighted sound levels, and noise and vibration spectra due to ground-borne vibration in buildings. (Kurzweil, 1979)

Hung & Yang (2001) state that the transmission of noise and vibration from a source, namely trains in underground tunnels, to a receiver includes four main stages:

- Generation: vibration excitation resulting from the movement of a train on rails with irregular surfaces;
- Transmission: propagation of energy through the tunnel structure and soil;
- Reception: vibrational energy admitted to the nearby buildings;
- Interception: attenuation of vibration through barriers, such as building foundations and vibration isolation measures.

Whilst the above stages focus on noise and vibration associated with trains in underground tunnels, vibration from other sources to a receiver would be subject to a similar process. Melke (1988) groups the above stages into three main categories: source, transmission path and receiver. These are also referred to in BS 14387-1:2005 (BSI, 2005) as emission, transmission and immission. Figure 2. 1 provides a sketch showing the source – transmission path – receiver line.

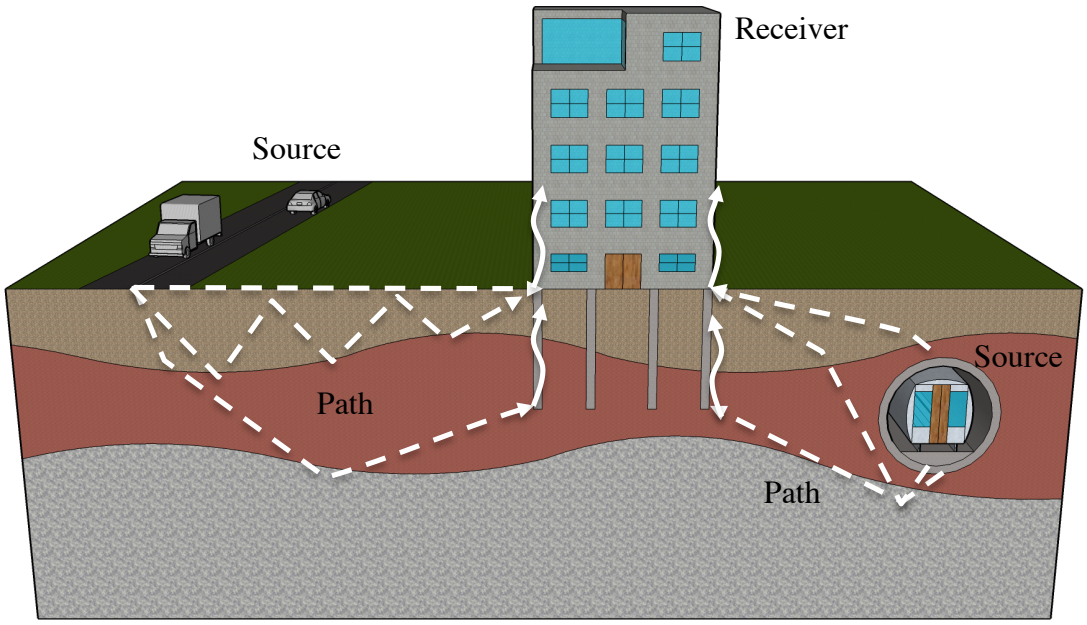

Figure 2. 1 Indicative sketch showing source – transmission path – receiver line

2.2 Source

Road traffic, railways, machinery and construction works are some of the types of sources / activities that generate vibration. In road traffic, vibration is generally caused by heavy goods vehicles (HGVs) passing over imperfections on the road surface, such as potholes, speed humps, changes of road surface, etc. This generates forces, dependent on the suspension system of the vehicle, that propagate along the surface of the ground and the soil underneath to a receiver. (ANC, 2012)

In the case of railways, vibration is generated by the interaction between the steel wheels of the trains and the rails. Heckl et al. (1996) suggest that vibration from trains is most dominant between 40 Hz and 100 Hz, as this is approximately where the resonant frequency of the wheel / track system lies. The following are some of the mechanisms of excitation that govern source vibration in railway systems, as described in BS ISO 14387-1:2005 (BSI, 2005):

1. Moving loads (quasi-static) excitation: the passage of a train on a rail can be regarded as several discrete static forces acting on the rail. However, from the point of view of the rail, these discrete forces are "seen" as a periodic excitation, even though the force applied on it is constant. This effect contributes to the low frequency response of the system between 0 Hz and 20 Hz (Hunt & Hussein, 2007) and it mainly affects the stability of the track in the near field. This quasi-static excitation can be controlled by installing the train bed on stiffer ground and / or foundations.
2. Wheel / rail roughness: irregularities on the rails and wheels occur during the manufacture process and will vary with time and use of the system. Such irregularities cause forced excitations of the vehicle / track and are the main source of vibration in railway systems across a wide range of frequencies. (Hunt & Hussein, 2007)
3. Parametric excitation: in railway tracks supported on periodic structures, such as sleepers on ballast, the wheels of the vehicle will experience different stiffness depending on where they are along the rail. This is influenced by the spacing between the supports and the speed at which the vehicle is travelling. For low speed trains, the excitation frequency would be in the region of 25 Hz, while for high-speed trains it would increase to 150 Hz. (Hunt & Hussein, 2007)

4. Additional wheel / rail defects: irregularities with different wavelengths overlaid periodically along the track are a significant cause of roughness, capable of generating high levels of vibration. Such irregularities are commonly known as corrugation. Wheel flats (from skidding with locked brakes, for example) and other changes in shape of the wheels can also result in corrugation of the wheels.
5. Discontinuities of the track: impact forces are caused by discontinuities of the track, such as joints and switches. An increase in the vibration levels generated will occur where the spacing between bogies of the vehicles is equal to the length of the jointed rails. Hunt & Hussein (2007) state that this mechanism of excitation is becoming less significant with the use of continuously welded tracks.
6. Vehicle suspension: the dynamic excitation forces caused by the vehicle suspension can be reduced through the use of low-stiffness systems. (Hunt & Hussein, 2007)
7. Steel hardness: changes in hardness of the rails, either random or periodic, can generate vibration. Such variations can arise during manufacture, though they occur more frequently during operation.
8. Driving conditions and lateral loads: dynamic forces generated during acceleration or deceleration of the train, and lateral loads resulting from vehicle guidance systems on corners with tight radius, can result in vibration.
9. Environmental conditions: the temperature of the rails and vehicle wheels, along with humidity, can have an impact on the deterioration of the system, affecting the levels of vibration generated.

An additional mechanism of excitation in railway systems, not mentioned in BS ISO 14387-1:2005, occurs when the speed of the train approaches or exceeds the speed of Rayleigh waves in the ground (refer to Section 2.3.1 of the present document), generating high amplitudes of vibration. Such high levels of vibration can also occur when the train speed is equal to or greater than the minimum phase velocity of bending waves in the track. (Hunt & Hussein, 2007)

Industrial machinery, such as generators, compressors, centrifugal fans and pumps, can also generate high levels of vibration. This is caused by the periodic motion of moving parts exciting the system and adjacent structures, especially if the system is unbalanced or not well maintained. Isolation bases are often used to control vibration from impulsive sources. (ANC, 2012)

Construction and demolition works are also major sources of vibration and structure-borne noise. Activities such as driven piling and blasting are some of the most significant sources associated with this type of works. (ANC, 2012) BS 5228-2:2009 (BSI, 2009) provides guidance on the types of vibration generating activities encountered in construction and demolition sites, typical vibration levels generated by each of them, and guidance on how they can be mitigated.

2.2.1 Types of vibration

Vibration is often characterised based on its duration, frequency content, direction and whether it is deterministic or random. (ANC, 2012)

With regard to duration, a vibration signal / event can be continuous or transient. BS 7385-1:1990 (BSI, 1990), now superseded by BS ISO 4866:2010, suggests that whether an event is continuous or transient is related to the time constant of a response. Equation 2. 1 shows the dependency of the time constant on frequency f_r and damping ξ_r.

$$\tau_r = \frac{1}{2\pi\xi_r f_r} \qquad \text{Equation 2. 1}$$

BS 7385-1:1990 considers an event to be continuous if a structure is excited for longer than $5\tau_r$, and transient if the excitation lasts for less than $5\tau_r$. BS 6472-1:2008 (BSI, 2008) goes on to state that impulsive (or transient) vibration consists of a rapid build-up to a peak level followed by a decay. The peak level can be sustained for a certain period, provided it does not exceed $5\tau_r$, while the decay can include several vibration cycles / events.

Vibration which can be perceived in separately identifiable repeated bursts is neither continuous or transient. In such scenarios, like in many real life situations, vibration can also be intermittent. The ANC Guidelines (2012) state that there is no strict approach to describing intermittent vibration based on its frequency of occurrence or on the characteristics of the excitation. Intermittent vibration is random with variable or similar magnitudes and can be defined as a "string of vibration incidents, each of short duration, separated by intervals of much lower vibration levels". Examples of sources of intermittent vibration are HGVs and trains generating ground or airborne vibration.

The duration of a vibration event will affect the dynamic response of a building. For example, dynamic amplification can occur when the duration of an event is sufficiently long with a steady frequency content, and the excitation frequency is similar to the resonant frequency of the structure it is exciting. When assessing building damage, different vibration criteria should therefore be set for continuous and transient vibration. (ANC, 2012)

The spectral content of a vibration event, combined with the natural frequencies of the structure being excited, will influence the frequency content of the event under consideration. The following frequency ranges are often considered when analysing ground-borne vibration and building response (BSI, 1990):

- 1 Hz to 150 Hz when assessing building damage from man-made sources;
- 0.1 Hz to 30 Hz when assessing vibration from natural sources, such as earthquakes;
- 0.1 Hz to 2 Hz when assessing wind excitation.

Another factor that can be used to characterise vibration is its direction. The ANC Guidelines (2012) state that vibration will tend to propagate in all directions away from the source. The direction of the vibration might change when a discontinuity is present in the propagation path. Such discontinuities can alter the direction of propagation, but can also end the propagation in that particular direction.

In addition to the above, whether vibration is deterministic or random can also be used to describe a vibration event. BS 7385-1:1990 (BSI, 1990) states that vibration which can be described by an explicit mathematical function is deterministic. This can be further divided into periodic (sinusoidal or complex) and non-periodic vibration (transient or shock). An example of sinusoidal vibration would be that generated by machinery with rotating parts, such as a centrifugal fan. This type of vibration can be described using the root mean square (rms) or peak-to-peak descriptors. For complex periodic vibration, averaging of energy is required to describe the spectral amplitudes of the vibration accurately. The time history of an event would be required to fully understand non-periodic vibration, such as that caused by the passage of HGVs / trains or blasting. (ANC, 2012)

BS 7385-1:1990 (BSI, 1990) sub-divides random vibration into stationary and non-stationary, depending on whether the statistical properties of the vibration are constant or variable with time. When assessing random vibration, the measurement period should be selected based on the error that can be tolerated in the end analysed result. Random vibration is normally quantified by the power spectral density, i.e. the square of the vibration / acceleration / displacement over frequency. (ANC, 2012)

Time varying and steady state signals are often quantified in terms of their rms value. This is dependent on the averaging time and any time response characteristic associated with this, i.e. whether the measurements were undertaken using a 'slow' or 'fast' time constant. (ANC, 2012)

Additional guidance on the frequency range, and typical displacement, particle velocity and acceleration ranges for different types of vibration sources is provided in Table 1 of BS 7385-1:1990 (BSI, 1990). Part of this table is reproduced in Table 2. 1 below, where the frequency ranges given refer to the response of buildings and of building elements to each type of forcing function shown.

Table 2. 1 Typical range of structural response for various sources (reproduced from BS 7385-1:1990)

Vibration forcing function	Frequency range (Hz)	Amplitude range (μm)	Particle velocity range (mm/s)	Particle acceleration range (mm/s^2)	Time characteristic
Traffic Road, rail, ground-borne	1 – 80	1 – 200	0.2 – 50	0.02 – 1	Continuous / transient
Blasting vibration Ground-borne	1 – 300	100 – 2500	0.2 – 500	0.02 – 50	Transient
Pile driving Ground-borne	1 – 100	10 – 50	0.2 – 50	0.02 – 2	Transient
Machinery outside Ground-borne	1 – 300	10 – 1000	0.2 – 50	0.02 – 1	Continuous / transient
Machinery inside	1 – 1000	1 – 100	0.2 – 30	0.02 – 1	Continuous / transient
Human activities					
a) impact	0.1 – 100	100 – 500	0.2 – 20	0.02 – 5	Transient
b) direct	0.1 – 12	100 – 5000	0.2 – 5	0.02 – 0.2	

2.3 Propagation path

The second stage in Melke's (1988) vibration transmission line is the propagation path. To predict the vibration levels from a source at a given receiver, the propagation path and any effects associated with it need to be considered. For vibration sources located outside buildings, the main propagation path will likely be through the ground. The types of waves propagating away from a vibration source through the ground are described in the following sections.

2.3.1 Types of waves in soil

The ground is often modelled as an elastic half-space, i.e. an elastic solid bound by a single plane. The response of an isotropic elastic half-space to different types of impulsive and harmonic loads was originally studied by Lamb in 1904. His findings still form the basis for understanding wave propagation in an elastic half-space nowadays. (Hunt & Hussein, 2007) Lamb's work (1904) acknowledged that the study would be relevant to understanding earthquakes. However, the vibrational energy from a source such as road / rail traffic would be subject to similar propagation mechanisms in the soil.

The types of waves that can propagate through soil can be divided into two main groups: body waves and surface waves. Body waves propagate spherically away from an excitation point, and can be sub-divided into pressure and shear waves. (Hunt & Hussein, 2007) In a medium without boundaries, i.e. a homogeneous full space, subjected to a vibration source, shear and pressure waves would be the only types of waves that would be generated. However, for a medium with a free surface, such as the ground, pressure and shear waves will interact along the free surface, generating surface waves. Surface waves can also occur along discontinuities in the propagation medium, and include Rayleigh, Love and Stoneley waves. (Eitzenberger, 2008) The characteristics of each wave type are further described in Table 2. 2. Illustrations showing the particle motion in relation of the direction of propagation for each wave type are provided in Figure 2. 2.

Table 2. 2 Types of waves propagating in soil (Hunt & Hussein, 2007 and Eitzenberger, 2008)

Wave types	Sub-division	Particle motion	Characteristics
Body waves	Pressure waves (P-waves)	Parallel to direction of propagation.	P-waves have the highest propagation velocity. This is determined by $c_p = \sqrt{\frac{E(1-\nu)}{\rho(1+\nu)(1-2\nu)}}$ in an unbounded (full) space.
	Shear waves (S-waves)	Perpendicular to direction of propagation.	If the particle motion caused by S-waves is vertical when compared to the direction of propagation, vertical (SV) polarised waves occur. If the particle motion is horizontal, then horizontal (SH) polarised waves occur. S-waves are slower than pressure waves. Their particle velocity is determined by $c_s = \sqrt{\frac{G}{\rho}}$.
Surface waves	Rayleigh waves (R-waves)	Elliptical in a plane perpendicular to the direction of propagation and to the half-space free surface.	R-waves propagate along the surface of the ground. Their propagation velocity is lower than that of body waves. As R-waves occur because of the interaction between body waves, their particle velocity is related to that of S-waves as follows $c_r = \frac{0.862+1.14\nu}{1+\nu} c_s$ (Achenbach, 1973).
	Love waves	Horizontal in a plane parallel to the half-space free surface.	Love waves are the fastest of all surface waves and occur when a layer with different properties is present along the surface of the half-space. They propagate within that layer.
	Stoneley waves	Perpendicular to direction of propagation.	Stoneley waves propagate along the boundary between two half-spaces with different mechanical properties. They occur when the propagation velocity of S-waves in the two half-spaces are similar. Stoneley waves are faster than Rayleigh waves, though slower than S-waves.

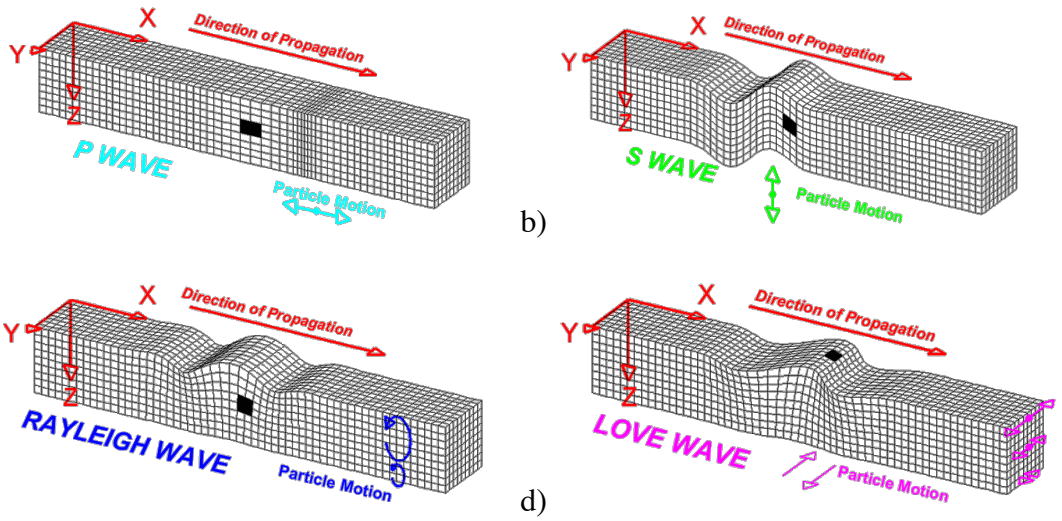

Figure 2. 2 Diagrams showing particle motion of different wave types in the ground (Braile, 2010)

The type of waves arriving at a receiver are dependent on the type and location of the vibration source, and on the monitoring location. BS ISO 14387-1:2005 (BSI, 2005) states that ground-borne vibration from rail systems at grade or on elevated structures is mainly carried by surface waves, while for underground rail systems, pressure and shear waves are the main carrier of vibrational energy. However, at large distances from the source, vibration carried by surface waves may dominate.

Gutowski & Dym (1976) state that for a small rigid disk vibrating on the surface of a half-space, the input energy to the half-space is distributed as follows between each wave type:

- 67% to Rayleigh waves;
- 26% to shear waves;
- 7% to pressure waves.

The above shows that for excitations on the surface of the half-space, such as rail systems at grade, the energy is mostly carried by Rayleigh waves as suggested in BS ISO 14387-1:2005 (BSI, 2005).

Regarding monitoring locations, the response at locations on the surface of the half-space, i.e. at the ground surface, will include both body and surface waves. However, for monitoring locations within the half-space well below the surface, body waves will predominate. (Gutowski & Dym, 1976)

2.3.2 Attenuation through soil

The prediction of vibration through the ground, from sources such as road and rail traffic, is a rather complex process. The somewhat limited knowledge of soil behaviour, combined with difficulties associated with the determination of accurate soil properties and the precision when modelling vibration sources, are some of the problems that affect the degree of accuracy with which vibration propagation through the soil can be predicted.

There are two main mechanisms that affect vibration propagation in an elastic half-space. These are geometric attenuation and material damping. The former consists of the rate of decrease of wave amplitude with distance away from a source. Geometric attenuation is also known as geometric decay, geometric spreading or radiation damping. Material damping is associated with the energy dissipation properties of the elastic half-space. (Gutowski & Dym, 1976)

Geometric attenuation for a given source is dependent on the type of source, propagation distance and on the monitoring location, as mentioned above. The rate at which vibration amplitudes decay with distance away from a given source are set out in Table 2. 3, based on far-field analyses of elastic spaces. (Gutowski & Dym, 1976; Verhas, 1979; Hung & Yang, 2001)

Table 2. 3 Geometrical attenuation for body and surface waves generated by surface sources

Monitoring location	Geometrical attenuation of wave vibration amplitude with distance r from a source in an elastic half-space	
	Body waves	Surface waves
Surface point source (spherical spreading)		
Surface	$\frac{1}{r^2}$	$\frac{1}{\sqrt{r}}$
Within the half-space	$\frac{1}{r}$	N/A
Surface line source (cylindrical spreading)		
Surface	$\frac{1}{r}$	1
Within the half-space	$\frac{1}{\sqrt{r}}$	N/A

As Rayleigh waves, being surface waves, only propagate along the surface of the elastic half-space, they are not present at monitoring locations located within the half-space, well below the surface. Also, for line sources monitored at the surface of the half-space, the geometric attenuation of Rayleigh waves is independent of the distance from the source, and in an ideal undamped elastic half-space, they would propagate away from the source with constant amplitude. (Gutowski & Dym, 1976)

The geometric attenuation associated with vibration sources located within an elastic half-space differs from those presented in Table 2. 3. For sources located sufficiently deep in an elastic half-space, such that a far-field can be developed, the geometric attenuation of body waves is presented in Table 2. 4, as stated in Gutowski & Dym (1976). Surface waves resulting from the interaction between body waves and the half-space free surface can also be generated by an underground vibration source. However, their amplitude would be negligible when compared to the amplitude of body waves, the exception to this being if the underground source is located close to the surface.

Table 2. 4 Geometrical attenuation for body waves generated by underground sources

Monitoring location	Geometrical attenuation of body wave vibration amplitude with distance r from a source in an elastic half-space
Underground point source (spherical spreading)	
Within the half-space	$\frac{1}{r}$
Underground line source (cylindrical spreading)	
Within the half-space	$\frac{1}{\sqrt{r}}$

When considering vibration propagation over large distances, damping can play a crucial part in the attenuation of vibrational energy in an elastic half-space. Attenuation of energy with distance due to damping in soil can be higher than that provided by geometrical attenuation. (ANC, 2012)

BS ISO 14387-1:2005 (BSI, 2005) recommends that careful consideration is given to damping. Elements such as water saturation of porous soils and layering can have significant effects on vibration attenuation through the ground due to damping.

Damping can be modelled in many ways. These are briefly discussed below (ANC, 2012):

- Viscous damping: this type of damping occurs where vibration forces liquid through an orifice. Friction caused by the viscosity of the liquid results in energy being converted into heat. Vibration transmission through fluids is affected by viscous damping.
- Radiation damping: the radiation of vibration from a finite structure into its surroundings is often regarded as an energy loss to the finite structure system. This can be referred to as radiation damping.
- Hysteretic damping: damping introduces a phase difference between an excitation force and the displacement response of the structure or medium under study. In the frequency domain, damping in a material is often represented as a complex modulus of elasticity. This is a hysteretic damping model. The use of this type of damping when predicting ground-borne vibration produces a complex vibration propagation velocity in the ground. The loss factor, which is widely used to describe damping in a medium, is given by the ratio of the imaginary part to the real part of the complex modulus of elasticity in hysteretic damping.

Gutowski & Dym (1976) discuss the damping properties of soils, based on work by Barkan (1962), Crandall (1974) and Ungar & Bender (1975), and state that the decrease in wave amplitude in soil due to damping can be represented by

$$A(x) = A_0 e^{-\alpha x} \qquad \text{Equation 2. 2}$$

where α is the absorption coefficient and x the distance from the source. To suitably quantify damping, the frequency dependence of the absorption coefficient needs to be understood.

Barkan (1962) modelled viscous damping with the absorption coefficient being dependent on the square of the frequency. In his work, he also presented frequency independent damping attenuation values, which were rather large. A frequency independent approach would mean that such large values of attenuation would be valid over all frequency ranges. However, this is unlikely to be the case.

An alternative approach was suggested by Crandall (1974) and Ungar & Bender (1975) in that the absorption coefficient is dependent on the loss factor η, frequency f and wave speed c for the wave type under consideration as follows.

$$\alpha = \frac{\pi \eta f}{c}$$ Equation 2. 3

The above yields more conservative values for damping attenuation, and shows that the lower the wave speed and the shorter the wavelength, the greater the attenuation of vibration due to damping. The above also shows that as the wave speed of shear waves is lower than that of pressure waves, shear waves are attenuated at a greater rate than pressure waves. Whilst the above provides a more conservative assessment of losses due to damping, for some types of soil and rock, studies have shown that damping at low frequencies is independent of frequency. Currently, theoretical data for the modelling of damping in the ground is limited and many studies rely on empirical data or field measurements to determine damping. (ANC, 2012)

In addition to geometric attenuation and damping, the presence of different layers in soil can have an impact on the vibrational energy in the ground. If layers with differing properties are present, phenomena such as reflection and refraction can occur within the soil. (Ewing, Jardetzky, & Press, 1957) For example, if an underground train tunnel is located above a rock stratum, vibration generated from the passage of trains in the tunnel will be reflected off the rock layer towards the surface. This principle is indicatively shown in Figure 2. 1.

A number of models have been developed to predict the losses through the ground. These typically include for geometrical attenuation, damping and changes of soil or rock along the propagation path. A good example of this is referred to in Chapter 16 of the Transportation Noise Reference Book (Remington, Kurzweil, & Towers, 1987) as the Ungar and Bender approach for underground trains. In Ungar and Bender's simple analysis model (1975), the total vibration attenuation A_r from a tunnel to a receiver location at a location x m from the source is given by Equation 2. 4.

$$A_r = A_s + A_d + A_i$$ Equation 2. 4

where

$$A_s = 10 \log_{10}\left(\frac{r_0 + x}{r_0}\right)$$ Equation 2. 5

$$A_d = 4.34 \frac{\omega \eta x}{c}$$ Equation 2. 6

$$A_i = 20 \log_{10}\left(\frac{1}{2}\left(1 + \frac{\rho_c c_c}{\rho_a c_a}\right)\right)$$ Equation 2. 7

A_s, given by Equation 2. 5, accounts for the geometrical attenuation through the soil, where r_0 is the tunnel radius. Equation 2. 6 and Equation 2. 7 account for the attenuation due to damping in the soil and rock and for the changes in soil or rock along the propagation path, respectively. Ungar and Bender's approach only considers compressional waves. Equation 2. 7 assumes that such waves travel from soil a to soil c, and ρ and c represent the density and compressional wave speed for each type of soil. This equation is only accurate where the thickness of each soil layer is several wavelengths wide.

2.4 Receiver

The third and final stage in Melke's (1988) vibration transmission line is the receiver. Ground-borne vibration from a given source can exhibit itself in two ways at a receiver location. The first of these is tactile or whole body vibration, i.e. vibration that can be felt in the form of vibrating structures. Structure-borne noise, a consequence of often imperceptible levels of vibration exciting walls, floors and ceilings in buildings causing them to radiate noise, is the other way in which vibration manifests itself. (BSI, 2005; BSI, 2008)

Ground-borne vibration and structure-borne noise can have negative effects on human occupants of buildings, by reducing their quality of life and / or work efficiency. The operation of sensitive equipment can be easily disrupted by ground-borne vibration, and this can also cause structural damage to buildings in extreme cases. (BSI, 2005)

The present section sets out the types of wave and mechanisms through which vibration and structure-borne noise propagate within a building.

2.4.1 Types of waves in building structures

Ground-borne vibration typically enters a building through its foundations. This is especially true for vibration generated by underground sources. Once in the building foundations, vibration propagates away from the point of entry through beams, columns, walls, floors and ceilings. The prediction of vibration propagation and losses through a building is a complex process, and it is often useful to simplify and group the various building components into beams and plates. For example, beams and columns in a building can be modelled as beams, while floors, walls and ceilings can be modelled as plates.

Vibrational energy within a building is carried through various wave types:

- (quasi-) Longitudinal or compressional waves;
- Transverse waves;
- Bending or flexural waves.

Pure longitudinal waves can only occur in solids with dimensions in all directions that are significantly larger than a longitudinal wavelength. Whilst they can occur in building structures, most beams and plates in buildings are too thin when compared to the longitudinal wavelength, across the frequency range of interest. Hence the term *quasi-longitudinal* is used to describe longitudinal waves in buildings. This type of wave causes longitudinal and lateral strains, and contraction of building structures. The extent of contraction is dependent on the Poisson's ratio for the material in question. The lateral strains caused by this type of wave result in rather small lateral displacements. Consequently, sound radiation from quasi-longitudinal waves is often negligible when compared to that of bending waves. This said, quasi-longitudinal waves contribute highly to the transmission of vibrational energy between interconnected structures. (Hopkins, 2007)

Transverse waves are generated as a result of solids opposing changes in volumes and shapes, through being capable of withstanding shear stresses. Transverse waves in plates are referred to as transverse plane waves, while in beams they are referred to as torsional waves. Transverse plane waves occur in plates due to shear stresses and cause the shape of a rectangular plate to be distorted into a parallelogram. (Cremer, Heckl, & Ungar, 1988) Hopkins (2007) refers to transverse plane waves as transverse shear waves, and states that the only motion of a plate surface in the presence of transverse shear waves is tangential to the adjacent air, and as a result these waves cannot radiate sound. However, as quasi-longitudinal waves, they play an important part on vibration transmission to other connected structures.

Torsional waves occur when a narrow beam is subjected to a time varying, torsional moment, i.e. a moment whose axis coincides with that of the beam, causing the cross-section of the beam to rotate about its axis. When this occurs, all points on the beam cross-section experience displacements. The further away the points on the cross-section of the beam are from its axis, the larger these displacements. (Cremer et al., 1988)

The other type of waves that can propagate in buildings are bending (or flexural) waves. These are the most significant for sound radiation, the reason for this being that bending waves generate substantial lateral displacements in a direction perpendicular to the direction of propagation. Some may consider bending waves to fall within the same category as transverse waves, given the large lateral displacements. However, this would be incorrect for the following reasons:

- The stresses and strains present in bending waves act on the longitudinal direction, rather than on a direction perpendicular to the longitudinal direction;
- The behaviour and underlying principles of bending waves are significantly different from that of transverse waves.

Therefore, bending waves fall in a category of their own. (Cremer et al., 1988 and Fahy & Gardonio, 2007)

The above paragraphs provide a brief overview of the types of waves that can propagate in building structures. The main characteristics and deformation patterns associated with each wave type are presented in Table 2. 5 and Figure 2. 3, respectively. Further details on each wave type can be found in Cremer et al. (1988), Fahy & Gardonio (2007) and Hopkins (2007).

Table 2. 5 Types of waves in building structures (Cremer et al., 1988; Fahy & Gardonio, 2007 and Hopkins, 2007)

Wave types	Sub-division	Particle motion in relation to propagation along x- axis	Characteristics
Longitudinal waves	Pure longitudinal	Parallel to direction of propagation.	Propagation velocity is given by $c_L = \sqrt{\frac{D}{\rho}}$. The propagation phase velocity of pure longitudinal waves is independent of frequency.
	Quasi-longitudinal	Parallel to direction of propagation.	The propagation phase velocity of quasi-longitudinal waves is different for plates and beams and is also independent of frequency. For beams, $c_{L,b} = \sqrt{\frac{E}{\rho}}$. For plates, $c_{L,p} = \sqrt{\frac{E}{\rho(1-\nu^2)}}$.
Transverse waves	Transverse plane waves	Perpendicular to direction of propagation.	Transverse plane waves occur in plates (walls, floors, etc.). Their propagation phase velocity is given by $c_{T,p} = \sqrt{\frac{G}{\rho}} = \sqrt{\frac{E}{2\rho(1-\nu)}}$. The propagation velocity of transverse plane waves is smaller than that of quasi-longitudinal waves, and is also independent of frequency.
	Torsional waves	Rotation about the x- axis, see Figure 2. 3 c).	Torsional waves occur in beams. Their propagation phase velocity is given by $c_{T,b} = \sqrt{\frac{T}{\rho I_\theta}}$. T and I_θ are different for beams of rectangular and circular cross-sections. For solid rectangular beams: $T = G\frac{h_z h_y^3}{3}\left[1 - \frac{192h_y}{\pi^5 h_z}\tanh\frac{\pi h_z}{2h_y}\right]$ and $I_\theta = \frac{(h_y h_z^3 + h_z h_y^3)}{12}$. h_y and h_z are the width and height of the beam, respectively.

Bending (or flexural) waves	-	Perpendicular to direction of propagation.	Bending waves cause both rotation and lateral displacement of a beam or plate. The propagation phase velocity of bending waves is different for plates and beams and is frequency dependent. For beams, $c_{B,b} = \sqrt[4]{\frac{\omega^2 B_b}{m'}}$, where $B_b = EI_b$. For beams of rectangular cross-section: $I_b = \frac{h_y h_z^3}{12}$ for lateral displacement in the z-direction and moment of inertia about the y-axis, and $I_b = \frac{h_z h_y^3}{12}$ for lateral displacement in the y-direction and moment of inertia about the z-axis. h_y and h_z are the width and height of the beam, respectively. For plates, $c_{B,p} = \sqrt[4]{\frac{\omega^2 B_p}{m''}}$, where $B_p = \frac{EI_p}{1-\nu^2}$ and $I_p = \frac{h^3}{12}$. h is the thickness of the plate.

The shear modulus, G, mentioned in Table 2. 5 can be calculated using Equation 2. 8.

$$G = \frac{E}{2(1+\nu)} \qquad \text{Equation 2. 8}$$

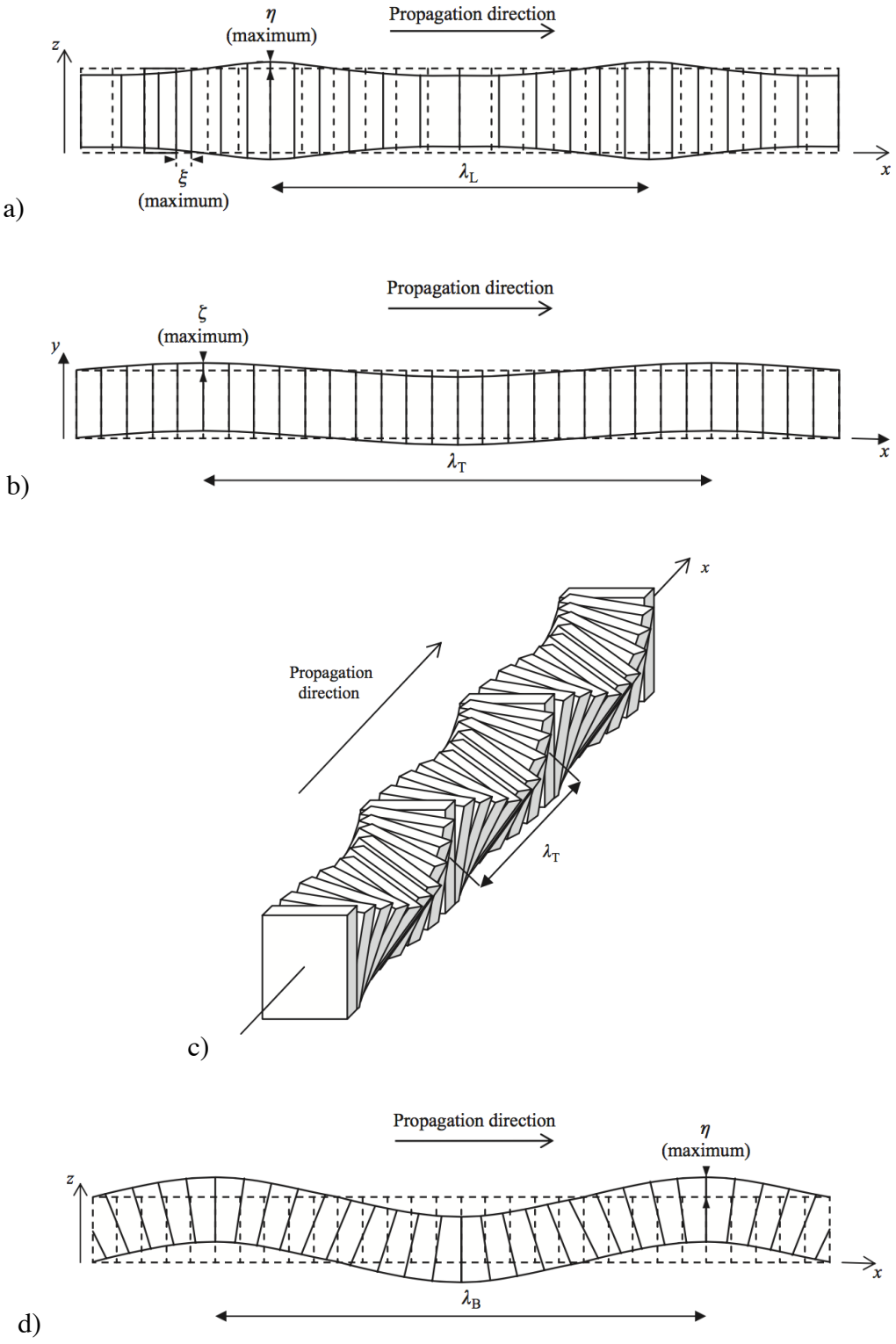

Figure 2. 3 Deformation patterns of wave types in beams and plates: a) quasi-longitudinal wave, b) transverse plane wave, c) torsional wave, d) bending wave (Hopkins, 2007)

2.4.2 Vibration transmission through buildings

The propagation of vibration through a building is a complex field, highly dependent on the response of the building structure, and of its walls, floors and ceilings. Nelson & Saurenman (1987) divide the response of buildings to vibration into three main components:

- Foundation coupling loss;
- Floor resonance amplification;
- And floor to floor attenuation.

As previously mentioned, building foundations typically represent the point of entry of vibrational energy into a building. The response of building foundations to vibration is characterised by their mass and geometry, the soil properties and the direction and type of incident vibration, and is described using a parameter called foundation coupling loss. (Nelson & Saurenman, 1987) Coupling losses are described in Cremer et al. (1988) as energy losses in a system that are a consequence of energy being reflected at discontinuities. In a building, these discontinuities can be structural connections between internal walls, beams and columns, change of medium between the building foundations and the soil, as well as between walls and the air in rooms. Kurzweil (1979) defines foundation coupling loss as the difference between the vibration levels in the soil and those in the building support structure. Nelson & Saurenman (1987) clarify that the levels of vibration in the soil should be considered without the presence of the foundations. The ANC Guidelines (2012) suggest that free-field vibration levels in the soil can reduce by up to 60 % when entering the foundations of a building, while the Federal Transit Administration (FTA; Hanson, Towers, & Meister, 2006) uses the following principle: "*The heavier the building foundation, the greater the coupling loss*".

Slab on grade, spread footings, piles founded in earth, and piles supported on rock are some of the most common building foundation types. For slab on grade floors, including most basement floors, excited by an underground vibration source, the large surface area of the slab is coupled with the soil underneath. This results in the vibration levels of the slab being similar to the levels that would be present in the soil without the slab. In these cases, the coupling loss between the soil and the building foundations is 0 dB at frequencies below the resonant frequency of the slab on grade. (Remington et al., 1987) A coupling loss of 0 dB is also experienced by lightweight frame buildings and buildings supported on rock. (Kurzweil, 1979)

In contrast with the above, the vibration levels entering a building through piled foundations can be significantly affected. In large cities with densely populated underground areas, such as London which has a total of eleven public underground train lines, in addition to underground lines to and from mainline train stations and significantly more service tunnels, building piles are often located within metres of the underground tunnel walls. The coupling losses associated with piled foundations are often high, except when the wavelength of the vibration in the soil matches that of the wave motion in the pile. For typical pile dimensions, this essentially means that bending waves cannot normally be excited between 25 Hz and 250 Hz, where most of the energy from underground trains occurs. Effective vibration transmission, i.e. minimal coupling losses, only occur significantly above the frequency range of interest. (ANC, 2012)

Saurenman et al. (1982) set out empirical curves for coupling losses provided by various types of foundations between the frequency range of 4 Hz to 500 Hz, based on measurements undertaken in various cities in the USA. These curves are also provided in Nelson & Saurenman (1983 and 1987) and Remington et al. (1987), and show foundation coupling losses varying from approximately -1 dB at 500 Hz for single family dwellings to -16 dB at 31.5 Hz for large masonry buildings on spread footings. Figure 2. 4 shows the curves as presented by Nelson & Saurenman (1983). Although these curves date back to the 1980s, they are still widely used to model foundation coupling losses. However, the typical constructions in the USA can be substantially different from those encountered in the UK, meaning the losses associated with the coupling between the building foundations and the ground can also be significantly different. Avillez (2013) proposes a different set of curves for typical UK dwellings, i.e. 2 to 3 storey terraced, semi-detached and detached residential buildings, on strip footings with a ground bearing slab. Avillez's curves follow the same trend as those presented in Figure 2. 4. However, the coupling losses vary from approximately +3 dB at 16 Hz to -9 dB at 40 – 63 Hz, suggesting the foundations of this type of buildings can in fact amplify vibration levels at certain frequencies.

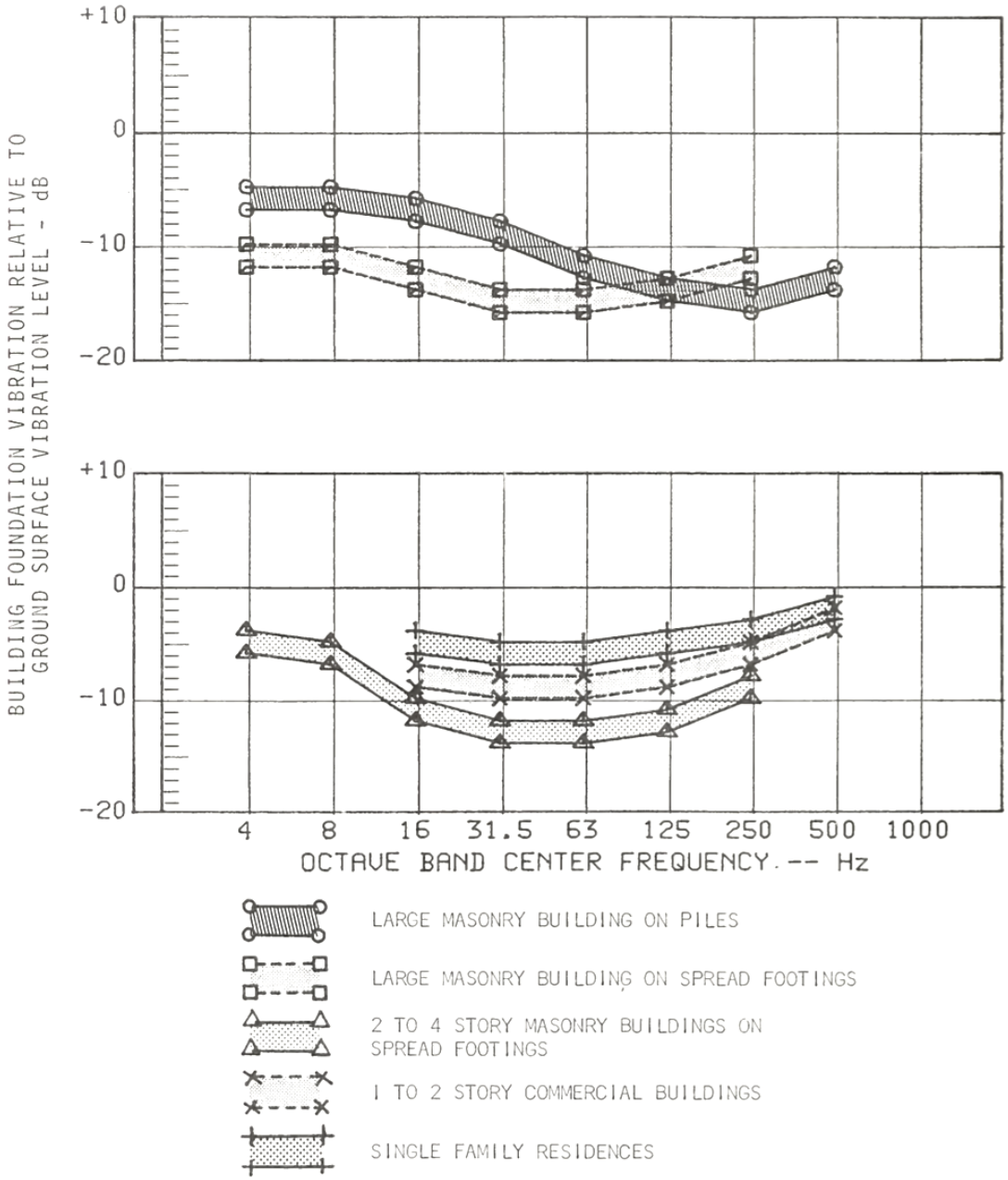

Figure 2. 4 Foundation coupling losses for different types of buildings (Nelson & Saurenman, 1983)

When peaks in the ground-borne vibration spectrum coincide with the resonances of the building structure, amplification of the vibration levels experienced within the building may occur. (ANC, 2012) Nelson & Saurenman (1987) state that little or no amplification typically occurs below the resonant frequency of the floors. However, above this frequency, the vibration levels may be amplified as a result of the greater number of modes that exist within structures at higher frequencies. This can be considered to some extent inversely analogous to the force transmissibility, i.e. the difference between the input and output forces, of a vibration isolator system. For a single degree of freedom system, amplification occurs at frequencies up until $\sqrt{2}f_0$,

where $f_0$is the resonant frequency of the system, with maximum amplification occurring when the exciting frequency matches the resonant frequency of the system. At frequencies above $\sqrt{2}f_0$, the isolator starts to attenuate the transmitted force instead of amplifying it. (Rajaram & Saurenman, 2013) The level of vibration amplification is highly dependent on the type of construction of the building, and tends to be lower near the junctions between walls and floors, and between walls and ceilings (Hanson et al., 2006), as the constructions at these locations are stiffer and therefore harder to excite.

Chapter 16 of the Transportation Noise Reference Book (Remington et al., 1987) provides typical vibration amplification factors for floor slabs supported on columns or shear walls. These are based on the estimates given by Nelson & Saurenman (1983), vary between 5 dB and 15 dB in the frequency range of 16 – 80 Hz, and are reproduced in Figure 2. 5. Whilst some amplification of vibrational energy is expected in building constructions, especially at mid-span locations of walls and floors, the extent of amplification is highly dependent on the characteristics of the vibration excitation, as well as on the damping of the constructions. For instance, for short transient vibration events, such as vibration from trains, the resonance of the construction will not have been fully excited, meaning that the maximum amplification will be less than if the construction was excited by a continuous vibration source. (ANC, 2012) Therefore, amplification values of up to 15 dB may not actually be realised in situations where train events are the main vibration source. The FTA (Hanson et al., 2006), on the other hand, suggest an adjustment to the vibration level of +6 dB for amplification due to resonances of floors, walls and ceilings, with the acknowledgement that the *"actual amplification will vary greatly depending on the type of construction"*. This single figure number should be applied to the frequency range of the resonant frequency.

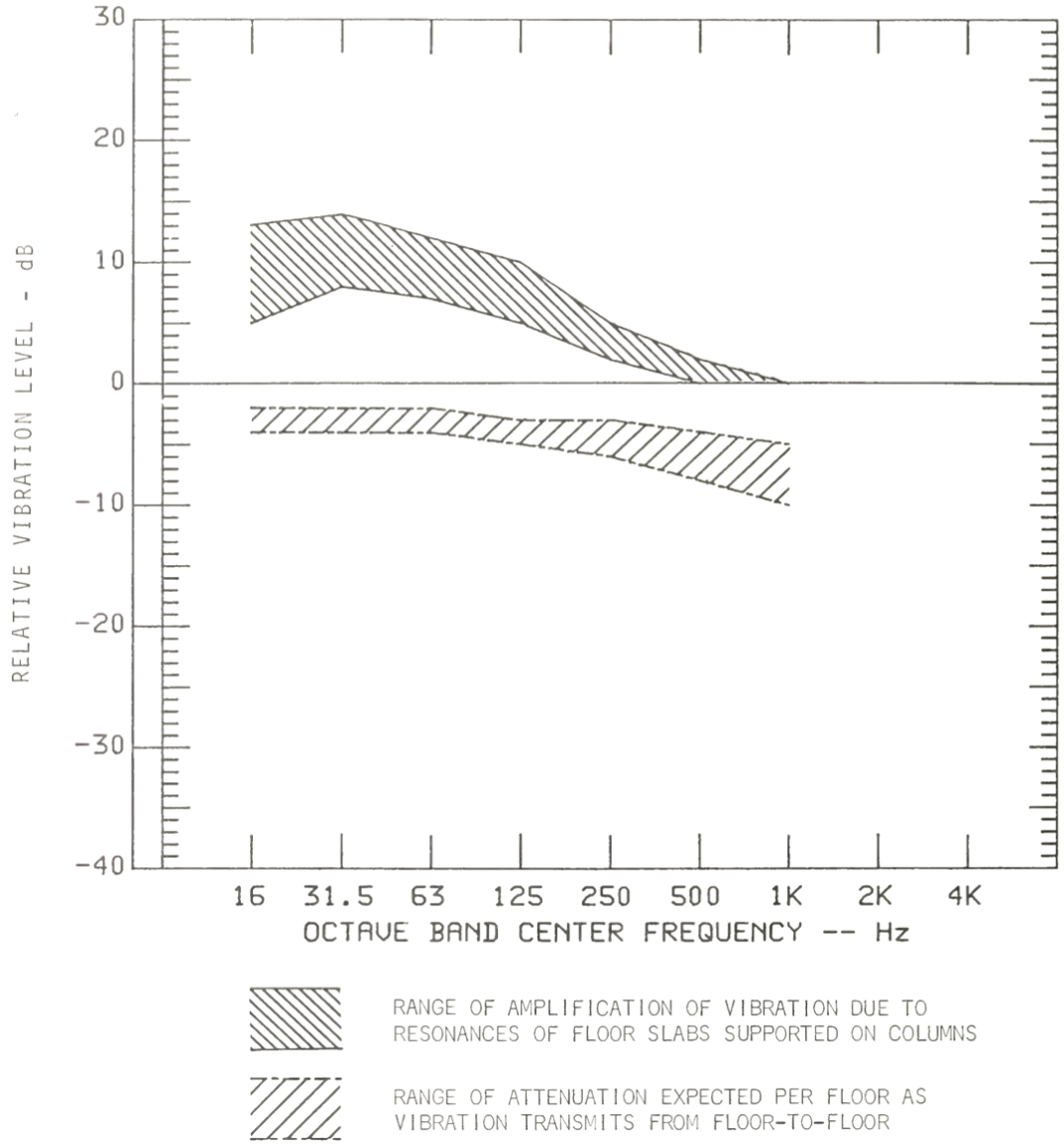

Figure 2. 5 Range of floor amplification due to floor resonances and attenuation per floor (Nelson & Saurenman, 1983)

The last component of the response of buildings to vibration mentioned in Nelson & Saurenman (1987) is floor to floor attenuation. Similarities can be drawn between this and airborne sound propagation in ductwork systems. In the latter, losses occur when sound encounters a discontinuity, such as a branch, and part of the sound energy will be reflected and the remaining energy will spread through the other duct branches. (Cremer et al., 1988) A similar attenuation mechanism is applicable for floor to floor vibration attenuation in buildings. Typical values of floor to floor attenuation in multi-storey buildings are provided in Figure 2. 5, based on Nelson & Saurenman's work. These show that the vibration attenuation from floor to floor is approximately -3 dB. Ishii & Tachibana's work (1978) showed that the level of attenuation per floor of a building is not constant throughout, reduces with the height of the building and is

dependent on the floor to floor distance. Table 2. 6 shows the levels of attenuation per floor as estimated by Ishii & Tachibana and reproduced by Remington et al. (1987). In addition to these, the FTA (Hanson et al., 2006) suggests that between levels 1 to 5 above grade, the levels of vibration within a building is attenuated by 2 dB per floor, while between levels 5 to 10 above grade this reduces to 1 dB per floor. The attenuation values advised by the FTA are frequency independent and can potentially lead to oversimplification of the actual losses per floor. However, the losses suggested are somewhat more conservative than those given by Ishii & Tachibana (1978).

Table 2. 6 Attenuation of acceleration level per floor in dB for a point source below a building (Remington et al., 1987)

Frequency (Hz)	Floor level above grade									
	1	2	3	4	5	6	7	8	9	10
Floor to floor distance: 3 m										
31	2	2	2	1	1	1	1	1	1	1
63	3	2	2	2	2	1	1	1	1	1
125	3	3	2	2	2	2	2	1	1	1
250	3	3	3	3	3	3	3	2	2	2
500	4	4	3	3	3	3	3	3	3	3
1k	5	5	4	4	4	4	4	3	3	3
Floor to floor distance: 3.7 m										
31	2	2	2	2	1	1	1	1	1	1
63	3	2	2	2	2	1	1	1	1	1
125	3	3	3	2	2	2	2	1	1	1
250	4	4	3	3	3	2	2	2	2	2
500	4	4	4	4	4	3	3	3	3	3
1k	5	5	5	4	4	4	4	4	4	4

The guidance provided in Chapter 16 of the Transportation Noise Reference Book (Remington et al., 1987), commonly used in the UK, and the US' *Transit noise and vibration assessment report* (Hanson et al., 2006) are based on the original work by Saurenman et al. (1982) and Nelson & Saurenman (1983 &1987), and provide reasonably similar guidance. A summary of the guidance on foundation coupling loss, floor resonance amplification and floor to floor attenuation given in both of these documents is provided in Table 2. 7 in terms of single number values.

Several methods, models and calculation tools have been developed for the prediction of structure-borne noise in buildings, some of which are based on the guidance set out in the present section. A review of these is provided in Section 3.

Table 2. 7 Summary of guidance on factors affecting the response of buildings to vibration

	Reference document	
Factors affecting the response of buildings to vibration	Transportation Noise Reference Book (Remington et al., 1987)	Federal Transit Administration (Hanson et al., 2006)
Foundation coupling loss	Slab on grade / lightweight frame buildings: 0 dB Other foundation types: -1 dB to -16 dB over 4 – 500 Hz (refer to Figure 2. 4)	Wood frame houses: -5 dB 1 – 2 storey masonry buildings: -7 dB 3 – 4 storey masonry buildings / large masonry buildings on piles: -10 dB Large masonry buildings on spread footings: -13 dB Foundation in rock: 0 dB
Floor resonance amplification	+5 to +15 dB over 16 – 80 Hz (refer to Figure 2. 5)	+6 dB
Floor to floor attenuation	-3 dB / floor (refer to Figure 2. 5)	1 to 5 floors above grade: -2 dB / floor 5 to 10 floors above grade: -1 dB / floor

2.4.3 Attenuation mechanisms through buildings

Whilst the guidance given in Remington et al. (1987) and by the FTA (Hanson et al., 2006) is useful and reasonably easy to apply, it is worth gaining a better understanding of how vibration is attenuated within buildings.

Once vibrational energy enters a building and propagates through it, it is bound to encounter discontinuities, such as changes in the type of material and / or structure. These reduce the amplitude of the wave transmitted past such discontinuities by reflecting some of the incident energy. For the amplitude of the transmitted wave to be significantly lower than that of the incident wave, i.e. for high levels of attenuation to occur, significant changes in the material densities and stiffnesses are required. In addition to a change in the material, a change in the cross-sectional area of beams and plates might also occur. This would result in reflections off the discontinuity and would also provide additional attenuation. (Cremer et al., 1988)

Other mechanisms through which the amplitude of vibration waves can be attenuated in buildings include corners and branches at right angles, elastic interlayers and blocking masses. These mechanisms and their effect are further described in the following paragraphs. However, as Craik (1988) and Cremer et al. (1988) note, there are several types of junctions and discontinuities encountered in buildings, such that it is not possible to analyse all the possible scenarios. Therefore, the following paragraphs only provide examples of the most basic situations that are typically found in buildings.

Changes in material and cross-sectional area affect quasi-longitudinal and bending waves in different ways. For instance, in the case of a beam, the transmission efficiency τ of quasi-longitudinal waves across the discontinuity, i.e. the ratio of transmitted to incident power at the discontinuity, is given by Equation 2. 9, where Z_1 and Z_2 are the wave impedances of the beam on both sides of the discontinuity. This equation relies on the following boundary conditions. (Cremer et al., 1988)

1. The velocity on both sides of the discontinuity must be equal ($v_1 = v_2$);
2. The longitudinal forces on both sides of the discontinuity and at a small distance from it must also be the same ($F_1 = -\sigma_1 S_1 = F_2 = -\sigma_2 S_2$). This boundary condition does not apply to arbitrary changes in cross-section, nor for very high frequencies.

$$\tau = \frac{4}{\left(\sqrt{\frac{Z_1}{Z_2}} + \sqrt{\frac{Z_2}{Z_1}}\right)^2}$$ Equation 2. 9

where

$$Z_1 = m'_1 c_{L,b1}$$ Equation 2. 10

$$Z_2 = m'_2 c_{L,b2}$$ Equation 2. 11

For bending waves, the transmission efficiency across the discontinuity is somewhat more complex and is given by Equation 2. 12. Cremer et al. (1988) state that this requires the following parameters to be continuous across the discontinuity: transverse velocities ($v_{y1} = v_{y2}$), shear forces ($F_{y1} = F_{y2}$), angular velocities ($w_{z1} = w_{z2}$), and moments ($M_{z1} = M_{z2}$).

$$\tau = \left[\frac{2\sqrt{\chi\psi}(1+\chi)(1+\psi)}{\chi(1+\psi)^2 + 2\psi(1+\chi)^2}\right]^2$$ Equation 2. 12

where

$$\chi = \sqrt[4]{\frac{m'_2 B_1}{m'_1 B_2}} = \frac{\lambda_1}{\lambda_2}$$ Equation 2. 13

$$\psi = \sqrt{\frac{m'_2 B_2}{m'_1 B_1}}$$ Equation 2. 14

Equation 2. 15 sets out the relationship between the transmission efficiency and the transmission loss across the discontinuity.

$$R = 10 \log \frac{1}{\tau}$$ Equation 2. 15

Substituting Equation 2. 9 and Equation 2. 12 into the above, the transmission losses for quasi-longitudinal and bending waves across a junction with different materials and / or cross-sectional areas can be found.

$$\text{Quasi-longitudinal waves: } R = 20\log_{10}\left[\frac{\sqrt{\frac{Z_1}{Z_2}}+\sqrt{\frac{Z_2}{Z_1}}}{2}\right] \qquad \text{Equation 2. 16}$$

$$\text{Bending waves: } R = 20\log_{10}\left[\frac{\chi(1+\psi)^2+2\psi(1+\chi)^2}{2\sqrt{\chi\psi}(1+\chi)(1+\psi)}\right] \qquad \text{Equation 2. 17}$$

Cremer et al. (1988) demonstrate the effect a change in thickness between two connected plates would have on the transmission loss across the discontinuity, by plotting the results of Equation 2. 16 and Equation 2. 17 for two plates of the same material. This is reproduced in Figure 2. 6. Essentially, the greater the difference between the cross-sectional area of the two plates, the greater the attenuation across the discontinuity. However, changes in cross-sectional areas between $0.2 > \frac{h_2}{h_1} > 5$ are not often encountered, and in reality attenuation due to changes in cross-sectional area are usually in the region of 3 dB for common building structures.

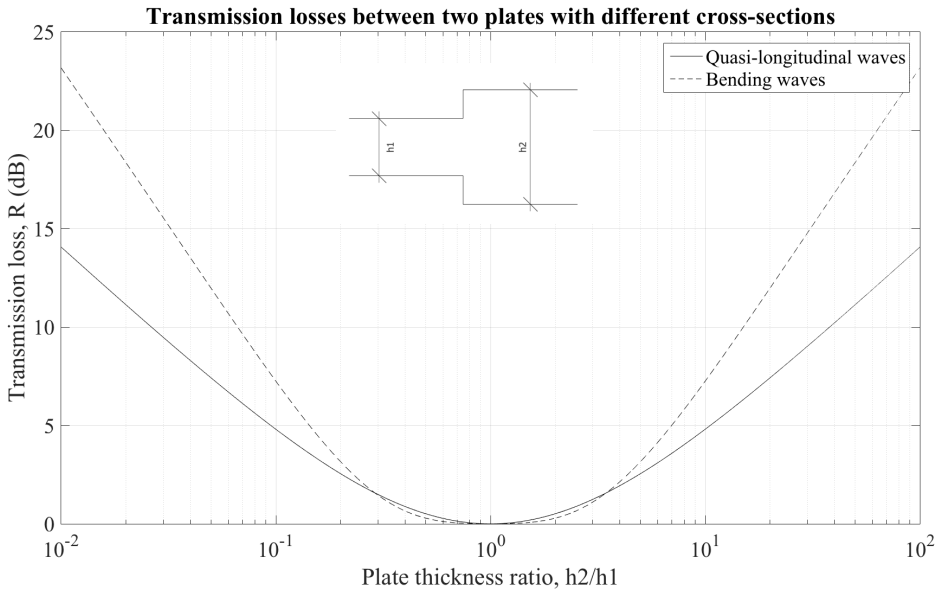

Figure 2. 6 Transmission losses between two plates with different cross-sections

The second and potentially more important vibration attenuation mechanism encountered in buildings occurs where structural elements, such as a wall and a floor or two beams, meet at right angles.

To rationalise the number and type of constructions, as well as the interface details between various elements within a building, a certain degree of symmetry often exists between adjacent areas in buildings, meaning that some beams and plates will have very similar, if not the same, properties (material and cross-sectional area). There are three main types of junctions where plates / beams meet at right angles: L-junctions, T-junctions and X-junctions. These types of junctions are shown in Figure 2. 7 a), b) and c), respectively. In line junctions, such as the junction between plates / beams 1 and 3 in Figure 2. 7, are also commonly found in buildings. For junctions between perpendicular beams or plates, the term *transmission around a corner* is useful to describe the energy propagation path. For in line junctions, the term *transmission across a straight section* is used. (Hopkins, 2007)

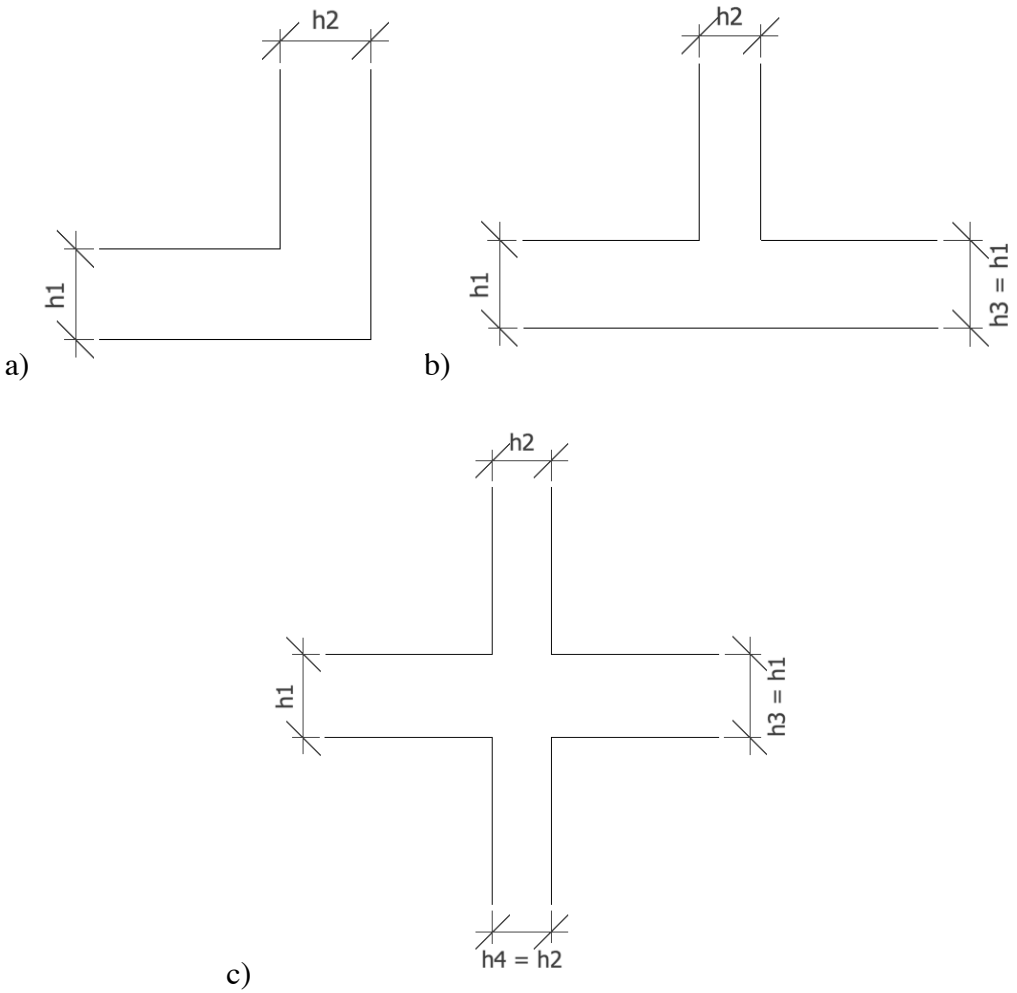

Figure 2. 7 Common beam / plate junctions encountered in buildings

An example of an L-junction between two beams is shown in Figure 2. 8, where the various force, linear velocity, moment and angular velocity components are given, as mentioned in Cremer et al. (1988).

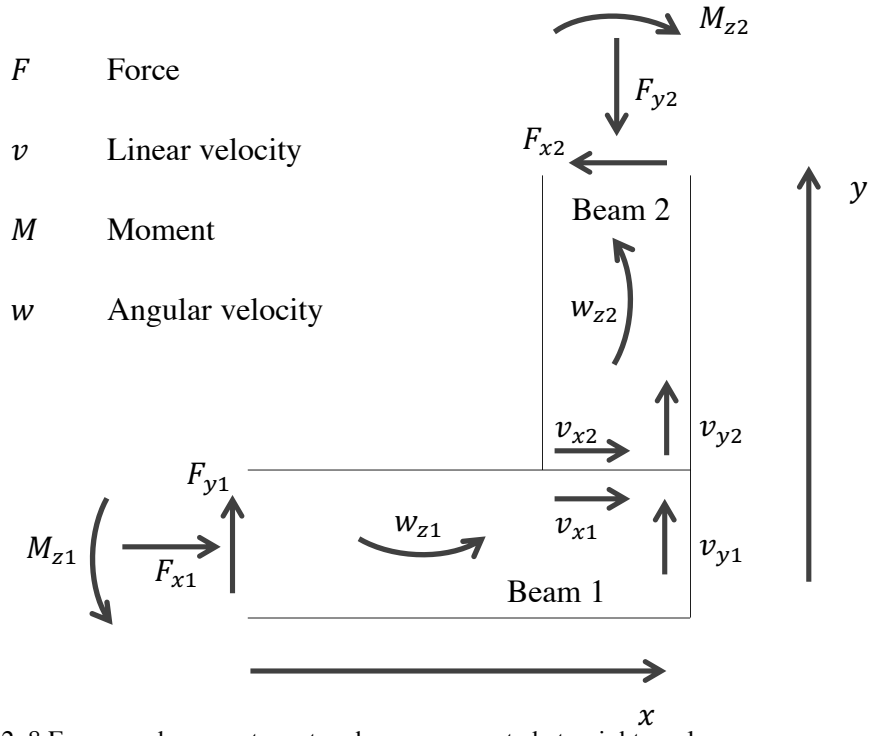

Figure 2. 8 Forces and moments on two beams connected at a right-angle corner

The above scenario requires the bending moments and the angular velocities on both sides of the corner to be the same, i.e. $M_{z1} = M_{z2}$ and $w_{z1} = w_{z2}$, respectively. These boundary conditions are as considered for the attenuation resulting from changes in material and cross-sectional areas. However, the remaining two boundary conditions are significantly different. For instance, whilst the shear force F_{y1} will have no impact on the bending wave in beam 2, it will produce a longitudinal force of the same magnitude in the second beam F_{y2}, such that $F_{y1} = F_{y2}$. From here, it follows that the amplitudes of the transverse velocity in beam 1 v_{y1} and of the longitudinal velocity in beam 2 v_{y2} will also be equal ($v_{y1} = v_{y2}$).

For the previous scenario of changes in material and cross-sectional areas, the magnitude of the reflected and transmitted waves at the discontinuity would add up to the magnitude of the incident wave. As a result, the reflection and transmission efficiencies would add up to 1. However, in the case of two beams (or two plates) at a 90° angle excited by a bending wave, this does not occur and consideration must be given to the fact that a reflected and transmitted longitudinal wave would be generated. Equation 2. 18 highlights the various reflection and transmission efficiency contributions to the beam arrangement shown in Figure 2. 8. (Cremer et al., 1988)

$$\varrho_{BB} + \varrho_{BL} + \tau_{BB} + \tau_{BL} = 1 \qquad \text{Equation 2. 18}$$

where

ϱ_{BB} is the reflection efficiency of a bending wave from an incident bending wave, $\varrho_{BB} = |r|^2$ — Equation 2. 19

ϱ_{BL} is the reflection efficiency of a longitudinal wave from an incident bending wave, $\varrho_{BL} = \frac{c_{L1}}{2c_{B1}}\left|t + t_j\right|^2$ — Equation 2. 20

τ_{BB} is the transmission efficiency of a bending wave from an incident bending wave, $\tau_{BB} = \chi\,\psi|t|^2$ — Equation 2. 21

τ_{BL} is the transmission efficiency of a longitudinal wave from an incident bending wave, $\tau_{BL} = \frac{1}{2\beta_2}\left|1 + r + r_j\right|^2$ — Equation 2. 22

The above equations for the reflection and transmission efficiencies show that these are dependent on the following parameters, as well as on χ and ψ given in Equation 2. 13 and Equation 2. 14, respectively.

$$\beta_1 = \frac{c_{B2}m'_2}{c_{L1}m'_1} \qquad \text{Equation 2. 23}$$

$$\beta_2 = \frac{c_{B1}m'_1}{c_{L2}m'_2} \qquad \text{Equation 2. 24}$$

$$r = \frac{\begin{matrix}[\psi(1-2\beta_2-\beta_1\beta_2)+\chi(1+2\beta_1-\beta_1\beta_2)] \\ +j[\psi(1+\beta_1-\beta_1\beta_2)+\chi(-1+\beta_2+\beta_1\beta_2)]\end{matrix}}{\begin{matrix}[\psi(-1-\beta_1-2\beta_2-\beta_1\beta_2)+\chi(-1-2\beta_1-\beta_2-\beta_1\beta_2)] \\ +j[(\psi+\chi)(1-\beta_1\beta_2)]\end{matrix}} \qquad \text{Equation 2. 25}$$

$$r_j = \frac{-1+\beta_2-r(1+\beta_2)}{1+j\beta_2} \qquad \text{Equation 2. 26}$$

$$t = \frac{2(\beta_1+\beta_2)-2j(1-\beta_1\beta_2)}{\begin{matrix}[\psi(-1-\beta_1-2\beta_2-\beta_1\beta_2)+\chi(-1-2\beta_1-\beta_2-\beta_1\beta_2)] \\ +j[(\psi+\chi)(1-\beta_1\beta_2)]\end{matrix}} \qquad \text{Equation 2. 27}$$

$$t_j = \frac{1+\beta_1}{-1-j\beta_1}t \qquad \text{Equation 2. 28}$$

The transmission losses across two beams (or plates) rigidly connected in an L-junction in bending are shown in Figure 2. 9, as a function of the ratio between the beam (or plate) thicknesses. These are as provided in Cremer et al. (1988) for two beams / plates of the same material, but with different cross-sectional areas. Figure 2. 9 shows that the highest transmission loss between two beams / plates of the same material and cross-sectional area $\left(\frac{h_2}{h_1} = 1\right)$ is approximately 4 dB.

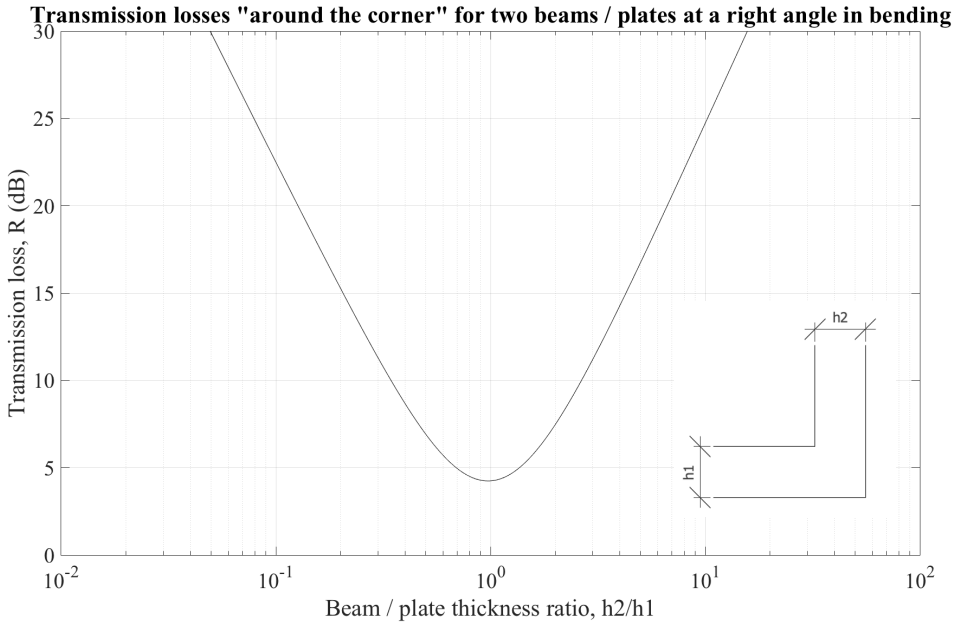

Figure 2. 9 Transmission losses between two beams at a right angle in bending (L-junction)

Whilst it is useful to understand how energy is transmitted across L-junctions, such type of junctions is not as common in buildings as branching junctions, where three or four plates or beams meet (T- and X-junctions). Cremer et al. (1988) have derived the transmission and reflection efficiencies for these scenarios from the equations provided for the two beams or plates in a corner arrangement.

The transmission losses associated with junctions between three and four plates as a function of their thickness ratio are provided in Figure 2. 10 and Figure 2. 11, respectively, as given in Cremer et al. (1988). Guidance on transmission losses for various types of junctions as a function of the ratio between the thickness of plates is also provided in Craik (1988) in tabulated form.

As a result of reciprocity and of the symmetry typically encountered in buildings, the transmission loss between plates 1 and 2 (R_{12}) is equal to the transmission loss between plates 2 and 1 (R_{21}) and between plates 2 and 3 (R_{23}).

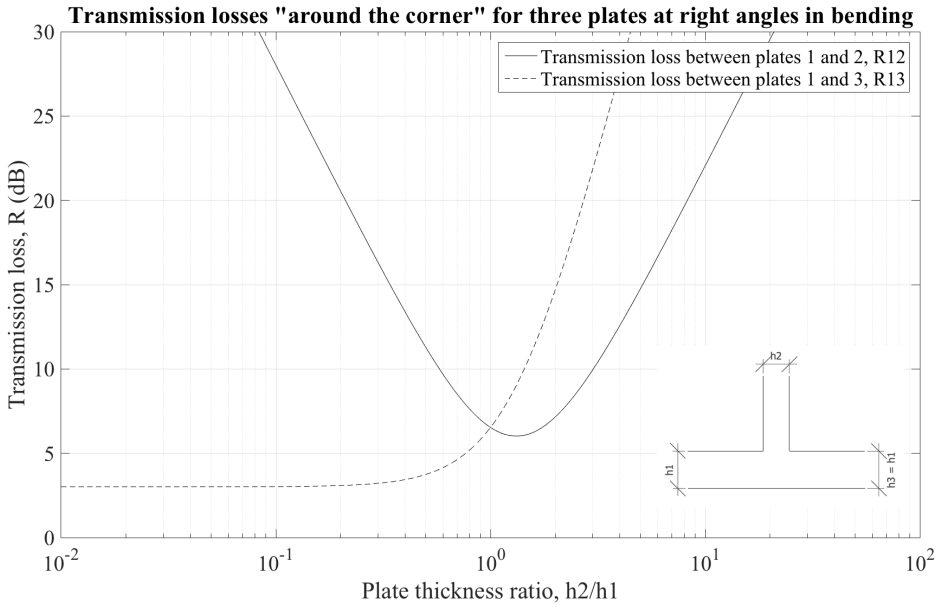

Figure 2. 10 Transmission losses between three plates at right angles in bending (T-junction)

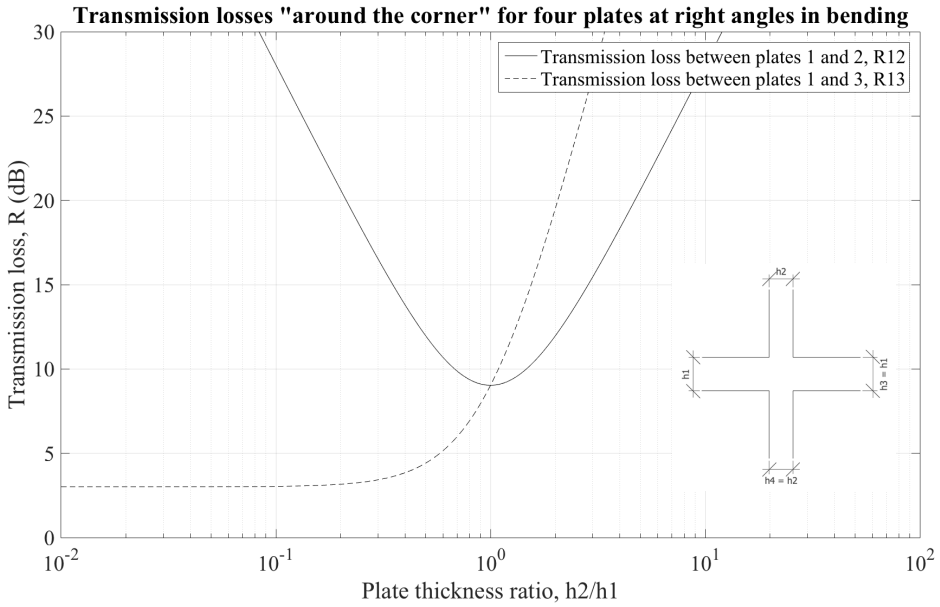

Figure 2. 11 Transmission losses between four plates at right angles in bending (X-junction)

Figure 2. 10 shows that the lowest transmission loss between plates 1 and 2 (R_{12}) of the same material and cross-section in a T-junction can be as low as approximately 6 dB. The transmission loss between plates 1 and 3 of identical properties in a T-junction (R_{13}) is approximately 6.5 dB and increases to 15 dB when plate 3 is twice as thick as plate 1.

For identical plates in an X-junction, as shown in Figure 2. 11, the lowest transmission loss between plates 1 and 2 (R_{12}) occurs when the thickness of the two plates is the same, and is approximately 9 dB. In this scenario, a 3 dB increase in the transmission loss (R_{12}) can occur when the thickness of the branching plate 2 is twice or half of the thickness of the primary plate 1. The transmission loss between plates 1 and 3 of identical properties in an X-junction (R_{13}) increases to a significant 20 dB when plate 3 is twice as thick as plate 1.

The relationships highlighted above between the transmission losses and the doubling or halving of the thickness of the plates are only valid for the transmitted power across the junctions. Cremer et al. (1988) state that these do not influence the velocities. Whilst these can be easily found from the transmission losses, they rely on the product of χ and ψ given in Equation 2. 13 and Equation 2. 14, rather than on their ratio, as is the case for the transmission losses.

The above analyses show that the losses obtained from changes in the material, cross-sectional area and changes of direction in structural elements typically found in buildings are often of limited benefit, unless these changes are rather significant. In the scenario of a building located in proximity to an underground train line, the losses associated with these mechanisms may not be sufficient to adequately control vibration and structure-borne noise within a building, and additional mitigation measures capable of providing higher transmission losses may be required.

Elastic interlayers, such as elastomeric bearings, are often used to reduce vibration and structure-borne noise transfer within buildings. The effectiveness of such materials relies on the introduction of a significant change of impedance into the system, which results in a large portion of the incident energy being reflected, rather than transmitted. Such layers are typically much softer when compared with the structure they are in. A good example of a material commonly used is cork, which has a characteristic impedance at least two orders of magnitude smaller than that of concrete. This means that even a thin layer of cork can have a significant effect on the transmission of energy through building structures. (Cremer et al., 1988) However, cork has a limited lifespan and its effectiveness decays severely with time, as it starts to crumble. Nowadays, elastomeric layers with longer life spans are more commonly used, especially for locations in buildings which will not be easily accessible for maintenance or replacement, such as the top of a pile or column.

The use of elastic interlayers falls outside of the remit of the present document, though further information can be found in Cremer et al. (1988), Craik & Osipov (1995) and Osipov & Vermeir (1996), to name a few.

The introduction of elastic interlayers in a building affects the transmission of longitudinal and bending waves differently, and can also have considerable effects on the structural stability of a building. As elastic interlayers are typically much "softer" than the surrounding structure, they cannot be relied upon to provide the shear-stiffening normally required. Often, in cases where this is overlooked in the design of a building, the on-site solution is to rigidly fix structural elements through the elastic interlayer, severely undermining its performance. Care must therefore be taken both during the design and construction of a building to ensure such problems do not occur. A measure that could be implemented during the design stages is the introduction of blocking masses, i.e. stiff structural elements that break the energy transmission path, reflecting some of the energy back, whilst providing the structural restraint necessary. Significant transmission losses can be obtained using such methods. Blocking masses are also encountered in ships. (Cremer et al., 1988)

2.4.4 Damping

Another mechanism which aids the reduction of vibrational energy in buildings by controlling the resonant response of the building and its elements is damping. Hopkins (2007) states that internal losses within a material are used to describe its damping properties. For instance, the internal losses of a beam or plate under deformation as a result of a wave excitation convert mechanical energy into heat. Damping is sometimes also referred to as dissipation. Even though it may help to reduce energy propagating through a building, the term damping (or dissipation) is not used to describe energy losses resulting from reflections at discontinuities. These are referred to as *"attenuation"* or *"coupling losses"* and fall under the mechanisms set out in Section 2.4.3 above. (Cremer et al., 1988)

The relationship between damping and the basic equations of elasticity for isotropic materials, such as Equation 2. 29 where σ is the stress, ε the strain and D the material stiffness, has interested physicists since the 1870s.

$$\sigma = D\varepsilon \qquad \text{Equation 2. 29}$$

O. E. Meyer, in 1874, proposed that a viscous friction force, proportional to the time derivative of the strain, acts in addition to the elastic forces in a material. With such force, the equation of elasticity would be re-written as per Equation 2. 30.

$$\sigma = D\left(\varepsilon + \vartheta\frac{d\varepsilon}{dt}\right) \quad \text{Equation 2. 30}$$

Applying a sinusoidal time variation $\varepsilon = \hat{\varepsilon}\cos(\omega t)$ to the above, Meyer's equation of elasticity becomes Equation 2. 31, where the strain and stress are out of phase with each other, implying the transformation of mechanical energy into heat. However, these equations are not sufficient to characterise damping.

$$\sigma = D\hat{\varepsilon}\big(\cos(\omega t) - \vartheta\omega\sin(\omega t)\big) \quad \text{Equation 2. 31}$$

Two years later, in 1876, Boltzmann proposed a different model for damping, in which the force that generates a strain is considered to be dependent on both the strain itself and on the "*strain history"*, i.e. the previous strains. The relationship between the stress and strain at different points in time, assuming the strain history is linearly superposed, can be written as shown in Equation 2. 32, where $\sigma(t)$ and $\varepsilon(t)$ are the stress and strain and at time t, and $\varepsilon(t-\Delta t)$ is the strain at an earlier time $(t-\Delta t)$. $\varphi(t)$ is the function that describes the after-effect of a strain and can take various forms. Of these, the "*relaxation function*" is important. For example, a material that has been subjected to a strain will experience processes at molecular level, including displacements, distortion and changes to its internal structure, that are excited and will decay gradually. Assuming the strain applied to such material causes its molecules to oscillate with an exponential decay, the after-effect function would take the form of Equation 2. 33, where D_2 is a constant and τ is the relaxation time, i.e. the time molecular oscillations take to decay. (Cremer et al., 1988)

$$\sigma(t) = D_1\varepsilon(t) - \int_0^\infty \varepsilon(t-\Delta t)\varphi(t)d(\Delta t) \quad \text{Equation 2. 32}$$

$$\varphi(t) = \frac{D_2}{\tau}e^{-\frac{\Delta t}{\tau}} \quad \text{Equation 2. 33}$$

Applying a periodic strain $\varepsilon = \hat{\varepsilon}\cos(\omega t)$ to the material and assuming the relaxation function is as given by Equation 2. 33, the expression for the stress would be given by Equation 2. 34. This equation shows that the relaxation function causes a phase shift between the stress and strain, which therefore leads to the dissipation of vibrational energy. The second term of Equation 2. 34, which is dependent on the frequency and relaxation time, determines how much of the vibrational energy is transformed into heat. Cremer et al. (1988) go on to state that all stress and strain relations can be derived from Equation 2. 32 and Equation 2. 33, if the various relaxation processes that occur simultaneously are accounted for, and consequently the *"relaxation model of after-effects may be taken as valid in general"*.

$$\sigma(t) = \left(D_1 - \frac{D_2}{\omega^2\tau^2 + 1}\right)\hat{\varepsilon}\cos(\omega t) - D_2\frac{\omega\tau}{\omega^2\tau^2 + 1}\hat{\varepsilon}\sin(\omega t) \qquad \text{Equation 2. 34}$$

However, the use of the above equations to account for the effect of damping leads to rather complicated expressions. Cremer et al. (1988) suggest that this can be avoided, if the problem is limited to periodic excitations and processes, and complex moduli are used. Equation 2. 31 and Equation 2. 34 both imply that the generation of a phase difference between the stress and strain is the main effect of damping. This can be expressed by Equation 2. 35.

$$\sigma(t) = Re\left(\underline{D}\hat{\varepsilon}e^{j\omega t}\right) = D^{\perp}\hat{\varepsilon}\cos(\omega t) - D^{\perp\perp}\hat{\varepsilon}\sin(\omega t) \qquad \text{Equation 2. 35}$$

where

$\underline{D} = D^{\perp} + jD^{\perp\perp} = D^{\perp}(1 + j\eta)$ is the complex modulus of elasticity (referred to in other sections of the present document as E), and — Equation 2. 36

$\eta = \frac{D^{\perp\perp}}{D^{\perp}}$ is the loss factor. — Equation 2. 37

Cremer et al. (1988) state that both Meyer's viscosity model and Boltzmann's relaxation model can be represented using a complex modulus of elasticity, as shown in Table 2. 8, allowing a simple representation of the complicated processes associated with damping for periodic excitations.

Table 2. 8 Modulus of elasticity and loss factor in different damping models (Cremer et al., 1988)

	Damping model	
	Meyer's viscosity model	Boltzmann's relaxation model
Modulus of elasticity	$D^{\perp} = D$	$D^{\perp} = D_1 - \frac{D_2}{\omega^2\tau^2 + 1}$ $D^{\perp\perp} = \frac{D_2\omega\tau}{\omega^2\tau^2 + 1}$
Loss factor	$\eta = \omega\vartheta$	$\eta = \frac{D^{\perp\perp}}{D^{\perp}}$

The loss factor η given in Table 2. 8 consists of the internal loss factor. As internal losses within a material can vary with frequency and type of wave, as well as with temperature, amplitude of vibration and manufacturing process, its internal loss factor is hard to quantify. This is typically done through measurements, though data is mainly available only for bending waves. Hopkins (2007) sets out two main methods for the measurement of the internal loss factor of a material for bending waves. For sheet materials, this involves the measurement of the structural reverberation time of the material. An alternative to this would be to form beams with short and narrow strips of the material, exciting them with a shaker and determining the loss factor at the various resonant frequency of the beams. The structural reverberation time can also be used to determine the total loss factor for plates over the frequency range of interest. Hopkins (2007) recommends that there should be a minimum of five bending modes in the relevant frequency bands, so as to minimise errors in the determination of the decay curves. The internal loss factor can be estimated, if the coupling losses between the plate and other elements, and sound radiation are negligible.

As internal loss factors only tend to be available for bending waves and there is a lack of information on internal loss factors for in-plane waves, Hopkins (2007) mentions that these are often assumed to be the same as for bending waves. Research and measurements by Kuhl & Kaiser (1952) show that this assumption is reasonable for materials such as concrete and bricks. Craik & Barry (1992) also undertook measurements of the internal loss factor of full sized walls, by using a test facility where the coupling losses between the test element and the frame are minimal. Their results show that the internal loss factor is somewhat frequency dependent, that plastering a wall can affect its performance, and that the type of construction and how it is built has an impact on the internal loss factor.

It is worth noting that, while internal losses of materials help convert mechanical energy into heat, damping provided by the coupling between structures in a building tends to be more significant. Craik (1981) states that the majority of the energy in a wall or floor in a building is not converted into heat within it, but it will propagate to another wall or floor somewhere else in the building where the conversion into heat will eventually happen. Even then, the reduction in vibration levels due to attenuation and / or coupling losses between the various elements in a building is higher than that provided by internal losses.

As alluded to in the previous paragraphs, the total damping (or total loss factor) of a building is a combination of the internal damping of the constructions, i.e. the internal losses within the construction that aid the conversion of mechanical energy into heat and which are characterised by the internal loss factor; the radiation damping, the losses that occur when energy is radiated into a room which are dependent on the radiation efficiency of the constructions; and the structural coupling between each element in a building, i.e. the losses that occur when energy is transferred from one part of the structure to another and which are described by coupling loss factors. (Craik, 1981; Hopkins, 2007)

In a typical low rise building in the UK, such as a masonry residential block, the total damping can vary between 0.02 to 0.10, with an average of approximately 0.05. In a tall building, however, the rate at which energy dissipates varies with the vibration mode being excited. Measurements in tall buildings where the coupling between the soil and structure is negligible have shown that the damping ratio can vary between 0.005 and 0.025 for the fundamental modes of vibration. Where the coupling between the soil and the building structure is significant at a particular mode, higher damping ratios would apply. Also, buildings with reinforced concrete frames tend to have higher damping values than those with steel frames. As previously mentioned, damping is affected by the method and type of construction of a building and its elements, the materials used, and workmanship. This essentially means that, during the design stage of a building, it is difficult to predict damping accurately and there often are significant errors associated with such predictions. (ANC, 2012)

The previous sections provide an overview of the vibration transmission line, from the source, through the propagation path and into the receiver, and of the various mechanisms through which vibrational energy is attenuated in each of these stages. As this document is to focus on the prediction of structure-borne noise in buildings, the following sections concentrate on the receiver stage of the vibration transmission line and on the various models currently available for the prediction of structure-borne noise in buildings.

3 Prediction of structure-borne noise in buildings

To determine the effect vibration sources, such as underground trains, have on buildings and their occupants, the prediction of ground-borne vibration and structure-borne noise in buildings is a necessary step, especially when either the source or the receiver are not yet in place and the levels of vibration and noise cannot be measured. BS ISO 14837-1 (BSI, 2005) acknowledges that the prediction of ground-borne vibration and structure-borne noise, especially that caused by railway systems, is a "*complex and developing technical field*". To aid the development of prediction models, this standard provides guidance on the many aspects that need to be considered and on the types of models that can be developed. The following are examples of the recommendations provided:

- Ground-borne noise and vibration should be determined as a function of frequency;
- The magnitude of ground-borne noise and vibration at the required location should be given as a function of the source, propagation path and receiver;
- The following parameters should be considered, depending on the stage of the assessment:
    - Source: route alignment, rolling stock, rail, track form, supporting infrastructure, construction tolerance, operation and maintenance;
    - Propagation path: type of ground and wave field;
    - Receiver: type of foundation and building structure.

The present chapter provides a summary of the different types of models currently available for the prediction of structure-borne noise in buildings, and relates to the second objective of this thesis.

3.1 Types of models

The detail required in a prediction model for a particular scheme or project varies with the stage at which it is. For instance, a project that is about to start construction requires a more accurate and detailed prediction model than one that is still in its feasibility study stage. BS ISO 14387-1 (BSI, 2005) defines three types of models for the prediction of ground-borne vibration and noise from new railway systems, and for new buildings near existing railways or for alterations to an existing rail system.

The characteristics and aims of each of these model types are somewhat different and are set out in Table 3. 1.

Table 3. 1 Summary of BS ISO 14387-1 prediction model types and their key points (BSI, 2005)

Type of model	Type of project	
	New rail system	Existing rail system / new building near existing railways
Scoping model	Used at very early stages of a scheme to ascertain whether ground-borne vibration and / or noise is a problem, and if so, where the main areas of concern are located.	Used to determine whether a new building may need to be isolated to control ground-borne vibration and noise from an existing railway. This model can also be used to determine whether an existing rail system needs to be modified.
Environmental assessment model	Uses the scoping model as a starting point and detail is added, to more accurately quantify the location and severity of the ground-borne vibration and noise problem. This type of model typically forms part of the planning process of a scheme, and highlights measures that are required to mitigate ground-borne vibration and noise from a new rail system.	This model is used to confirm how severe the ground-borne vibration and noise problem in a new building may be, and to define the type and extent of mitigation required. For modifications to existing rail systems, it will identify the type of modification needed.
Detailed design model	As the name suggests, this type of model supports the detailed design of a scheme. The mitigation measures highlighted with the environmental assessment model are developed and implemented during construction, focussing on the rolling stock and track design.	A detailed design model for a new building will contribute to the design of the foundations, floor and base isolation that may be required. It will also allow detailed design of any modifications to an existing rail system, such as changes to the rolling stock and tunnel.

A model for a new railway system is required to predict the absolute levels of ground-borne vibration and noise that will be generated. However, a model for a new building that is to be located near an existing railway only needs to predict the insertion gains or the transfer functions, i.e. the change that will occur in the ground-borne vibration and noise level with the new building in place. A similar principle is applicable when modifications are made to an existing railway scheme. Another difference between models for a new and for existing rail schemes is that the vibration level from an existing railway can and should be measured. This reduces the uncertainty associated with predicting the generation and propagation of vibration for new railway systems. The effect of constructing a new building near a railway, or modifying an existing railway, on the ground-borne vibration and noise levels can be assessed by correcting the measurement data with the insertion gains and transfer functions predicted. This will allow the calculation of the new levels of ground-borne vibration and noise that will be experienced by the new building or that will be generated by the modified existing railway. (BSI, 2005)

Whilst the above paragraphs discuss three types of prediction models, they only relate to how detailed a model is during different stages of a project and do not mention what methodology is used for the calculations. BS ISO 14837-1 (BSI, 2005) states that models for the prediction of ground-borne vibration and noise fall in two main categories: empirical and parametric (or theoretical). There are also models that are a combination of these two methods. As with any modelling, the quality and validity of the results obtained is only as good as the data that is input into it. Moreover, prediction models typically refer to and have been validated and calibrated to a specific situation. Care must therefore be taken when applying a model to a scenario that differs significantly from the calibrated and validated one. The following sections set out the main characteristics of empirical and parametric models.

3.1.1 Empirical models

Field measurement data form the basis of every empirical model, along with methods for extrapolating / interpolating predictions within the measurement dataset. BS ISO 14837-1 (BSI, 2005) sets out two main types of empirical models. These are single site models and multiple site models.

Single model sites are based on measurements obtained at a single site, as the name indicates. The extrapolation functions for this type of model are derived from other measurement databases, or from analytical models. This type of model should be used for single assessment sites, such as to determine whether mitigation measures are required for a new building at a single site.

Multiple site models, on the other hand, make use of measurements obtained at various sites, which are analysed by way of regression and trend analysis to develop the prediction model. In the case of a new rail system, the measurements should include variations in the parameters that will be present over the extent of the new system and will have an impact on the levels of ground-borne vibration and noise generated, such as soil properties, track system, vehicle type, measurement distances, etc. The number of sites that should be included in this type of model is dependent on the number of parameters that vary between the measurement and assessment sites, and on how significant that variation is. For instance, measurements at various distances from and / or along a railway track can be considered different sites on the basis that the distance and relative tunnel depth, and potentially soil properties, between measurement locations are different.

Empirical models rely on the derivation of transfer functions or insertion gains obtained from the field measurements undertaken. These transfer functions / insertion gains are then applied to the base vibration or noise level measured to assess the resulting level of ground-borne noise and vibration. Empirical models often require simplification of the scenario under study. The degree of simplification is dependent on the design stage of the assessment, and on how much variability there is between the measurement and assessment sites.

3.1.2 Theoretical models

Parametric models, also known as theoretical models, are normally deterministic and provide a solution for a specific set of input data. They require many input parameters, which often are not known to a sufficient degree of certainty. As previously mentioned, their results are only as good as the input data available. Therefore, BS ISO 14837-1 (BSI, 2005) recommends that care is taken when relying on a single set of input parameters, unless their origin and accuracy is fully known.

Theoretical models, comprising either analytical or numerical methods, are derived from first principles. In analytical models, the dynamics of the system under consideration are described using equations simplified through assumptions and approximations. This type of models requires a good understanding of the fundamental physical principles and are fast to run. However, even though the scenario modelled is simplified to some extent, the analytical equations needed are far from simple and straight forward, and numerical models are often preferred. Also, analytical models are often developed for rather specific problems and cannot normally be used for general vibration problems. An analytical approach is therefore more suitable to model simple structures and scenarios. (Jones, 2010; Lurcock & Thompson, 2014)

When sufficient information on the system properties is available, numerical models can be used to predict ground-borne noise and vibration with a reasonably high level of precision, depending of course on the accuracy of the input parameters. This type of models can be used for more complex structures, when compared to an analytical approach. Numerical models make use of three main calculation methods: finite element method (FEM), finite difference method (FDM) and boundary element method (BEM). (ANC, 2012)

In FEM, the system under consideration is divided into a number of finite, adjacent elements, whose extent are defined by a mesh, i.e. a grid of lines, and by discrete points (nodes) on the same mesh. An FEM model solves for the continuity across each element iteratively. (Fahy & Gardonio, 2007) FDM, on the other hand, involves the discretisation of a dynamic system with which calculations for each element are undertaken in the time domain, using differential equations with finite time intervals. This method can be used to provide advanced algebraic solutions to the wave equation. The third commonly used numerical method is BEM which only requires elements on the surface of a system to be modelled using an element mesh, such as that used in FEM. In ground-borne vibration, BEM is useful to model the semi-infinite characteristics of the ground. (BSI, 2005) The main advantages and disadvantages of FEM, FDM and BEM are summarised in Table 3. 2.

Table 3. 2 Advantages and disadvantages of FEM, FDM and BEM models (BSI, 2005; ANC, 2012)

Type of numerical model	Advantages	Disadvantages
Finite element method (FEM)	FEM software packages are widely available. Models are not limited to orthogonal grids.	Large computational costs.
Finite difference method (FDM)	FDM can be used to model a moving train easily. Less computationally expensive than FEM.	Not widely available. Models deal well with orthogonal grids, though they are not easily adaptable to other cases.
Boundary element method (BEM)	BEM only requires the boundary of any homogeneous element to be modelled. It can model wave propagation in an infinite homogeneous system without having to account for false boundary effects. BEM is often combined with FEM or FDM to provide hybrid prediction models.	BEM can be unstable. (Hargreaves & Cox, 2008)

The above numerical models all rely on the assumption that the structure and propagation media within each element are homogeneous and linear.

In addition, Lurcock & Thompson (2014) state that assumptions need to be made on the boundary conditions and connection restraints, and the material properties need to be appropriately specified, when using mathematical modelling methods.

3.1.3 Semi-empirical models

Semi-empirical models are a combination of the empirical models mentioned in Section 3.1.1 and the theoretical models in Section 3.1.2. In these models, one or more empirical components can be replaced with equivalent theoretical components, or a theoretical component can be substituted for measurements that have been undertaken on the partly completed works, for example measurements on a pile cap.

Semi-empirical models are often used to adapt an empirical model developed during the environmental assessment stage of a project to make them suitable for detailed design. The main areas that are often updated are source characteristics, such as the design of the tunnel, track and vehicles, and receiver parameters including foundation and building design. (BSI, 2005)

3.1.4 Model accuracy and validity

As previously mentioned, the prediction of ground-borne vibration and / or structure-borne noise is a complex field and all analyses have several unknowns and uncertainties. Therefore, when a prediction model is developed, it needs to be assessed and validated to provide confidence in its results. In general, the level of accuracy required of a model for a given scheme depends on the development stage at which it is. The more progressed the scheme is, the more accuracy is desired of the prediction model and the less error that can be tolerated. Also, knowing the limitations and accuracy of any prediction model is a powerful tool and will certainly help manage risk in the design of new schemes, such as railway systems or developments that are sensitive to ground-borne vibration and structure-borne noise.

The accuracy of a prediction model can be quantified through the following steps, as set out in BS ISO 14387-1 (BSI, 2005):

1. Development: during the development stages of a prediction model, a number of iterations are used to modify the model, with the aim of improving the agreement between its results and any measured data / test conditions. Such modifications should be based on theoretical and / or empirical knowledge of the fundamental physical processes involved. In the case of detailed and complex models with a requirement for high accuracy, each component of the vibration transmission line or sometimes even each parameter of the various transmission line stages may need to be developed individually. Wherever possible, the development and improvement of a prediction model for a specific site can and should make use of measurements at that site. For example, take an empirical model that accounts for the prediction of coupling losses between the soil and piled foundations of a building. Once the piles are in place, vibration measurements should be undertaken on the pile caps to confirm the levels that should be output by the model.

2. Calibration: with the model developed as much as possible, the next step is to calibrate its results. This is done by evaluating one or more calibration functions to assess the agreement between the model results and the measured data.
3. Validation: once the model is developed and calibrated, it needs to be validated, i.e. its results should be compared with independent measurement data that is not the same as that used during the calibration stage. If this is not available, models can also be validated against another validated model for a specific test case. However, care must be taken to ensure any differences in the input parameters, conditions and assumptions between the two models are noted and documented. When validating a prediction model, it is important that the input assumptions and parameters used in the validation are reported, along with the calculated accuracy and uncertainty of the model.
4. Verification: as models are often implemented through computer programs, a last step is required to verify the correctness of implementation of the model. For this stage, a test case is solved both by hand and by the computer program and the results are compared. The stability of the program should also be checked, by trying minimum to maximum values for each of the input parameters.

3.2 Existing empirical models

The following sections provide an overview of the different empirical models currently available for the prediction of structure-borne noise in buildings from railway systems. Most of the models found account for the complete vibration transmission line, i.e. they start with the source, predict the level of attenuation through the soil and calculate the structure-borne noise level in a building. Empirical and semi-empirical models were also found for the prediction solely of ground-borne vibration, such as EnVib 01, EnVib 02 and NGI, which acknowledge that structure-borne noise in buildings is associated with ground-borne vibration, but do not provide details on how to quantify this. Therefore, these models have not been included in the following sections. (Bahrekazemi, 2004; Madshus, Bessason, & Hårvik, 1996)

3.2.1 Kurzweil's model

One of the earliest empirical models for the prediction of structure-borne noise in buildings found is Kurzweil's model, which dates to 1979.

Kurzweil (1979) presented a method for the estimation of A-weighted noise levels in basement rooms located at 1 to 20 m from an underground train tunnel wall using the expression given in Equation 3. 1, where r is the distance in metres between the tunnel wall and the building wall, and r_0 is a reference distance of 1 m.

$$L_A = 59 - 20\log_{10}\left(\frac{r}{r_0}\right) \pm 10 \qquad \text{Equation 3. 1}$$

This equation is based on measurement data obtained by Lang (1971) for a range of different vehicle speeds, types and conditions, track types and conditions, type of building and tunnel constructions, and soil properties. Lang's measurements showed that higher levels of structure-borne sound in buildings were caused by systems with poor wheel and track conditions. The same was noted for stiff track designs and is corroborated by research undertaken by Cox et al. (2004) during the EC-Growth project CONVURT (CONtrol of Vibration from Underground Rail Traffic).

Despite the findings of Lang's measurements being validated by more recent work, Equation 3. 1 still offers a variation of $\pm$ 10 dB in the predicted A-weighted structure-borne noise level in buildings. While such variation may just be acceptable in a very early scoping model, during the detailed design stages of a project it may cause the structure-borne noise mitigation measures to be significantly over specified to a point that the project is no longer viable.

In the same paper, Kurzweil (1979) also provides a method for predicting noise and vibration spectral information from ground-borne vibration in buildings located near underground train tunnels, accounting for the dynamic properties of the tunnel and building structures, as well as the properties of the soil. This more detailed process allows the change in ground-borne vibration and structure-borne noise in buildings to be estimated. Kurzweil proposes that the vibration acceleration level in the floor of a room generated by the passage of a train in an underground tunnel in the vicinity of the building is given by Equation 3. 2.

$$L_{a,room} = L_{a,tunnel\ wall} - C_g - C_{gb} - C_b \ \left(\text{dB re } 10^{-6}\text{g(rms)}\right) \quad \text{Equation 3. 2}$$

where

$L_{a,tunnel\ wall}$ is the maximum octave band acceleration level on the tunnel wall during the passage of a train,

C_g is the vibration attenuation through the ground,

C_{gb} is the coupling loss between the ground and the building,

and C_b is the vibration attenuation through the building.

In Equation 3. 2, the octave band vibration acceleration level on the tunnel wall and in the room can be found from acceleration measurements using Equation 3. 3.

$$L_a = 20\log_{10}\left(\frac{rms\ octave\ band\ acceleration}{10^{-6}g(rms)}\right) \quad \text{Equation 3. 3}$$

where

$$g = 9.81 m/s^2$$

The mechanisms that affect the vibration propagation through tunnel structures, ground and building structures are as set out in Sections 2.2, 2.3 and 2.4 of this document, respectively. Kurzweil suggests that the relationship between the octave band floor acceleration level ($L_{a,room}$) and the resulting octave-band sound pressure level in the room ($L_{p,room}$) is given by Equation 3. 4, where f is the octave band centre frequency. Further details on the relationship between the floor acceleration level and the room sound pressure level can be found in research undertaken by the Toronto Transit Commission (1976), Manning et al. (1974) and others.

$$L_{p,room} = L_{a,room} - 20\log_{10} f + 37 \quad \text{Equation 3. 4}$$

The ANC Guidelines (2012) mentions that this relationship is still used nowadays and can also be used in 1/3 octave bands. Rewriting Equation 3. 4 in terms of velocity yields Equation 3. 5, where $L_{v,room}$ is the rms vibration velocity level on the floor of the room in dB with reference to $1\times10^{-9}\ m/s$.

$$L_{p,room} = L_{v,room} - 27 \quad \text{Equation 3. 5}$$

However, research by the FTA (Hanson et al., 2006) suggests that Equation 3. 5 over predicts the sound pressure level in the room by approximately 5 dB and that a correction of -32 (instead of -27) shows good agreement with their measurement data. The sound pressure level in the room would then be given by Equation 3. 6. Measurements undertaken in residences with the London Underground Central Line in operation revealed a similar overestimation by Equation 3. 5. (ANC, 2012) However, the development of Crossrail in London still uses Equation 3. 5. (Crossrail Ltd, 2016)

$$L_{p,room} = L_{v,room} - 32 \qquad \text{Equation 3. 6}$$

3.2.2 Nelson & Saurenman's model

The guidance provided in Chapter 16 of the Transportation Noise Reference Book (Remington et al., 1987) is based on Kurzweil's model above and makes use of the research undertaken by Saurenman et al. (1982) and Nelson & Saurenman (1983) on building response. However, in 1987, Nelson & Saurenman proposed a new model for the prediction of structure-borne noise in buildings encompassing the following stages:

1. Select the trackbed force density;
2. Determine the line source response;
3. Calculate the building response;
4. Calculate the structure-borne noise level in a room.

The trackbed force density in this model is estimated from measurements undertaken at a number of sites. If the track being modelled differs from that in the measurements, adjustments need to be made to the force density, as necessary. The next step in this model is to apply a line source response, which is done by determining the ground-borne vibration velocity level at the receiver location relative to the vibration force density in the tunnel. As a result of the shape of an underground tunnel and train, the energy generated by the passage of a train in the tunnel will spread cylindrically through the soil. Therefore, modelling the geometric attenuation through the ground using a line source approach is considered appropriate. However, the rate of attenuation will still be dependent on the location of the tunnel in relation to the surface and to the measurement location, as described in Section 2.3.2. Nelson & Saurenman (1987) developed a procedure to determine the line source responses through the measurement of the transfer mobilities between the tunnel and the ground,

or between the bottom of a borehole and the surface of the ground, and then using numerical regression and integration methods to convert the transfer mobilities into a line source response. This step equates to the effect of propagation through the ground on the vibration levels.

Step 3 of this model makes use of the research published by Saurenman, Nelson, & Wilson in 1982, and by Nelson & Saurenman in 1983 on the response of buildings to vibration. A summary of the foundation coupling losses, floor resonance amplification and floor-to-floor attenuation presented in these references is provided in Section 2.4.2 of this document. The final stage of Nelson & Saurenman's model is the prediction of structure-borne noise in a room. For this, they state that Equation 3. 7 can be used to convert 1/3 or 1/1 octave band vibration levels into noise levels.

$$L_p = L_v - 10\log_{10}(a) - 1 \qquad \text{Equation 3. 7}$$

where

L_p is the sound pressure level in the room (dB re 20 μPa),

L_v is the vibration velocity level (dB re 1 μin/s),

and a is the absorption coefficient in the room.

Nelson & Saurenman (1987) mention that the predicted structure-borne noise levels are only *"best estimates"* of the 1/3 octave band levels. The authors go on to state that the procedure does not include any margin of error and recommend that safety factor of 5 – 10 dB is added to the predicted noise levels *"to protect the major part of the potential receivers"*. This prediction model is noted to be most accurate in the resonance region of the rail system's primary suspension and where soil attenuation is at its lowest, i.e. at frequencies between 8 to 30 Hz. However, energy from rail systems is typically present at frequencies of up to 80 Hz, as stated in BS 7385-1 (BSI, 1990), with some train systems exciting frequencies up to 100 Hz. This essentially means that Nelson & Saurenman's model may not yield the most accurate results for underground rail systems.

3.2.3 FTA / FRA model

Another empirical prediction method that is largely based on the work of Saurenman et al. (1982) and Nelson & Saurenman (1983) is the FTA's ground-borne vibration and structure-borne noise prediction model.

The FTA (Hanson et al., 2006) provides guidance on three assessment methods that can be used for the prediction of ground-borne vibration and structure-borne noise from new transportation systems. The first of these is the screening model used during the very early stages of design of a project to determine whether ground-borne vibration and noise from it are likely to have an impact on nearby noise and vibration sensitive uses and how severe this impact may be. The screening model can then be developed into a general assessment model, which uses measurement data as the basis to predict the ground-borne vibration level at a receiver location. Should the measurement data available not match the scenario being modelled, the FTA provide a number of corrections for items, such as vehicle speed, track and wheel condition and track support system in the case of a new railway system. However, the general assessment model does not take into account the frequency spectrum of the ground-borne vibration and noise. For this, a detailed analysis model, which is the most complex and accurate prediction model of the three, is required. This type of model makes use of site-specific measurements to establish how ground-borne vibration propagates in the soil. It can be assumed that a similar principle would apply to the prediction of vibration transfer in an existing building. Unless a building, such as a recording studio or concert hall, is particularly sensitive to ground-borne vibration and noise, a general assessment model tends to provide a sufficient level of detail. However, where the levels of vibration and noise are very high or a building is very sensitive, a detailed analysis model is more suitable. Similarities can be drawn between the FTA's three assessment methods and the various types of models described in BS ISO 14387-1 (BSI, 2005), namely the scoping model, environmental assessment model and the detailed design model.

The starting point of FTA's general assessment model is the definition of a base curve, or set of curves, that model the vibration levels on the ground surface generated by a proposed transportation system at a certain distance from the source. The FTA (Hanson et al., 2006) provide base curves for rubber-tired vehicles, locomotive powered passenger or freight trains and for rapid transit or light rail vehicles. The levels of ground-borne vibration and noise in a receiving building is then calculated by correcting the base curves for aspects such as the speed of the vehicles, type of building foundation and construction, and the receiver location in the building. Such corrections are given as single number values, i.e. they do not account for the frequency dependence of parameters such as foundation coupling loss, floor resonance amplification and losses with height / floors within a building. For this, a detailed analysis model would be required, based on site specific measurements.

The corrections for foundation coupling loss, floor resonance amplification and floor-to-floor attenuation within a building in a general assessment and in a detailed analysis model are the same, and are as set out in Table 2. 7 in Section 2.4.2.

The above empirical model is also used by the US Federal Railroad Association (FRA) for the prediction of ground-borne vibration and structure-borne noise in buildings from high-speed ground transportation, as per the information available in Hanson, Ross & Towers (2012).

The FTA / FRA detailed analysis models have been validated against a hybrid finite element – boundary element (FE-BE) model for ground-borne vibration generated by underground trains. Good agreement was found between the two models, especially at higher frequencies. (Verbraken, Lombaert, & Degrande, 2011)

3.2.4 Melke's model

Melke (1988) developed a simple model for the prediction of ground-borne vibration and structure-borne noise in buildings employing empirical and analytical techniques. The purpose of the model was to investigate the effectiveness of a number of low cost isolated track designs. With this model, the sound pressure level within a building is given by Equation 3. 8.

$$L_B = L_r + R_{tr} + R_{tu} + R_g + R_b \qquad \text{Equation 3. 8}$$

where

L_r is the rail velocity level (dB re 50 nm/s),

R_{tr} is the track transmission loss (dB),

R_{tu} is the tunnel transmission loss (dB),

R_g is the ground transmission loss (dB),

R_b is the building transmission loss (dB)

and L_B is the velocity level (dB re 50 nm/s) or sound pressure level in the building (dB re 20 μPa).

The reverberant sound pressure level in a room resulting from the vibration of walls and floors can be estimated from Equation 3. 9.

$$L_p = L_v + 10\log_{10}(\sigma) + 10\log_{10}\left(\frac{4S}{A}\right) \qquad \text{Equation 3. 9}$$

where

L_v is the vibration velocity level of the surface (dB re 50 nm/s),

σ is the radiation efficiency of the vibrating surface (no units),

S is the area of the vibrating surface (m^2),

A is the absorption area in the room (m^2),

and L_p is the sound pressure level in the room (dB re 20 μPa).

The above equation can be used to calculate 1/3 and 1/1 octave band levels and transmission losses, as well as narrow bandwidth and frequency-weighted single number values. The model also assumes that the levels predicted are averaged over the duration of the train event, while the transmission losses are linear and constant with time. Melke's model relies on estimates and / or measurements of the parameters given in Table 3. 3, as a minimum, to allow it to be completed.

Table 3. 3 Parameters necessary to solve Melke's prediction model (Melke, 1988)

Parameter	Melke's approach
Track impedance	Modelled as a lumped parameter electric circuit analogy.
Rail velocity level, L_r	Determined either through measurements or predictions based on the train, track and operating parameters.
Track transmission loss, R_{tr}	Dependent on the localised track stiffness impedance Z_{rs} and mass impedance Z_{rm}. Z_{rs} can be obtained from laboratory measurements or from the dynamic stiffness and loss factor of the track. Z_{rm} can be calculated using a mass-spring (or a beam-spring) model.
Tunnel transmission loss, R_{tu}	Dependent on the tunnel design and parameters, such as tunnel floor impedance and bending wave attenuation with distance and by reflection.
Ground transmission loss, R_g	Dependent on the soil properties. Calculated from geometrical spreading and damping within the ground. At short distances from the tunnel, the ground transmission loss is affected only by damping and can be approximated by $R_d \approx \frac{\eta f r}{c}$, where η is the soil loss factor, f is the frequency, r the distance from the source and c the wave velocity.
Building transmission loss, R_b	Dependent on the building design. At low frequencies, suspended floors in buildings can be modelled as a lumped parameter mass-spring system.

Validation of the Melke's model revealed the following (Melke, 1988):

- A similar trend was present between the calculated model results and measured values;
- The model is appropriate to provide a rough estimate of the structure-borne noise levels experienced within a building.

3.2.5 Jakobsen's model

Two years later, Jakobsen (1989) developed an empirical model based on vibration measurements at six different residential sites in Denmark affected by nearby surface railway lines. At each site, measurements were undertaken outside and inside the buildings, and transfer functions between the ground and the building determined by subtracting the vibration level measured at the reference point outside from the vibration levels measured inside the building. The sample of buildings used consisted of two blocks of flats and four single family dwellings.

The transfer functions obtained from the above measurements are summarised in Table 3. 4, where a is the horizontal distance between the centre of the train track and the edge of the track bed, and b is the distance between the edge of the track bed and the reference measurement position outside the building. The expressions for the losses through the soil were derived from measurements undertaken at eight sites, presented in Jakobsen (1987).

Jakobsen's prediction model itself comprises the following stages (1989):

1. The vibration levels from a train pass-by should be measured at a short distance from the railway line, such as at the edge of the track bed.
2. If the vibration level cannot be measured outside the building, this should be estimated by applying the losses through the soil given in Table 3. 4.
3. The vibration level within the building is then found by applying the corrections in Table 3. 4 for the transfer of energy between the soil and the foundation and between the foundation and the relevant floor.

Noting that empirical prediction models are often inaccurate, Jakobsen (1989) states that there may be a variation in the predicted levels by up to approximately 10 dB. It is also noted that the transfer functions between floors should only be used as *"crude estimates"*, given the small amount of data they are based on.

Table 3. 4 Transfer functions used in Jakobsen's prediction model as given in Jakobsen (1989) with the addition of clarifications on building components

Transfer function	Building components	Transfer functions (dB) at 1/1 octave band centre frequencies					Overall (dB)
		4 Hz	8 Hz	16 Hz	31.5 Hz	63 Hz	
Propagation in soil from a to b (m)	(Jakobsen, 1987)	$-3-9.2\log_{10}\left(\frac{b}{a}\right)$	$-8.5\log_{10}\left(\frac{b}{a}\right)$	$-1-12.1\log_{10}\left(\frac{b}{a}\right)$	$-24.3\log_{10}\left(\frac{b}{a}\right)$	$-28.7\log_{10}\left(\frac{b}{a}\right)$	$-17.1\log_{10}\left(\frac{b}{a}\right)$
Transfer between soil and foundation, vertical component	Frame type foundation	-4	-2	-2	-2	-2	-2
	Basement foundation	-3	-4	-10	-9	-6	-8
Transfer between foundation and floors, vertical component	1-storey building (or ground floor of 2-storey building) with wooden floor	+12	+15	+14	+10	+10	+12
	Upper floor of 2-storey building with wooden floor	+10	+20	+23	+22	+8	+20
	Multi-storey building with concrete deck, with / without wooden floors	0	+2	+7	+9	+11	+9
Transfer between foundation and floors, horizontal component	1-storey building (or ground floor of 2-storey building) with wooden floor	+10	+12	+5	+4	+4	+5
	Upper floor of 2-storey building with wooden floor	+11	+23	+20	+23	+7	+20
	Multi-storey building with concrete deck, with / without wooden floors	+2	+3	+2	0	+1	+1

3.2.6 VIBRA 1-2-3

In an attempt to reduce the costs associated with ground-borne vibration and structure-borne noise measurements and calculations, Swiss Federal Railways (SBB), in conjunction with vibration specialists Ziegler Consultants, developed a three-part computer model to help predict vibration and structure-borne noise in buildings from railways in a more cost effective and time efficient manner. This computer model is known as VIBRA 1-2-3 and comprises the following packages (Kuppelwieser & Ziegler, 1996):

- VIBRA-1: simple, semi-empirical calculation tool to provide rough estimates of ground-borne vibration and structure-borne noise levels in buildings, and allow problem areas of a development to be identified;
- VIBRA-2: a more complex and detailed tool to help model the various factors that affect ground-borne vibration and structure-borne sound radiation in buildings;
- VIBRA-3: database comprising all the results obtained from ground-borne vibration, and from structure-borne and airborne noise measurements of railway systems. The data in VIBRA-3 feeds into VIBRA -1 and VIBRA-2.

VIBRA-1 uses Equation 3. 10 to calculate the vibration velocity level v and Equation 3. 11 to predict the level of structure-borne noise in the centre of a room in a building from a nearby railway system. The calculation of structure-borne noise from Equation 3. 11 accounts for the vibration velocity levels between 40 Hz and 100 Hz, with emphasis on the 63 Hz 1/3 octave band, where most of the energy from train events is. However, frequency dependence is not accounted for in Equation 3. 10. The variables in the following equations are based on statistical analysis of the data available in VIBRA-3. (Ziegler Consultants, 2009)

$$v = v_0 F_s \left(\frac{r_0}{r}\right)^m F_a F_e \qquad \text{Equation 3. 10}$$

where

v_0 is the overall vibration level at the reference distance r_0 from the track;

F_s is the rail factor to account for the effect of rail switches on the vibration levels;

r is the distance between the centre of the track and the receiving building;

m is a correction for geometrical and material damping;

F_a is the foundation coupling loss factor;

and F_e is the amplification factor of the floor slabs.

$$L_{eq} = v_{63} - A(f) + \Delta SP + \sigma + 10 \log_{10}\left(\frac{Z t_{vorb}}{3600}\right) \qquad \text{Equation 3. 11}$$

where

v_{63} is the vibration level of the floor in the 63 Hz 1/3 octave band;

$A(f)$ is the A-weighting correction at the relevant 1/3 octave band centre frequency (-26 dB at 63 Hz);

ΔSP is a 3 dB correction for summation (it is not entirely clear what this correction relates to);

σ is the radiation efficiency of the floor;

Z is the number of train events per hour;

and t_{vorb} is the duration of a train event.

The calculation procedure in VIBRA-2 differs from that used for the high-level predictions of VIBRA-1. For the second component of this prediction model, SBB and Ziegler Consultants developed an open system, frequency dependent attenuation model, which contains partial prediction models for rail – track interaction, propagation of vibration between the track and a receiver location in the soil, attenuation due to the coupling of the building foundations to the soil, vibration of the outer walls / shell of the building, vibration of the internal floor slabs, and the re-radiation of vibration as structure-borne noise in a room. The vibration and / or structure-borne noise level in a room is obtained from a step-by-step multiplication of a base vibration level with spectral transfer functions. These are either based on statistical analysis of the data available in VIBRA-3 or they can be user defined. (Kuppelwieser & Ziegler, 1996)

With regard to accuracy, Ziegler Consultants (2009) state that the uncertainty associated with the prediction of structure-borne noise levels by VIBRA 1-2-3 is approximately $\pm$ 6.5 dB. For vibration levels, they state that an uncertainty factor of approximately 2 should be considered.

3.2.7 High Speed 1 & High Speed 2

At the time of the design and construction of the Channel Tunnel Rail Link (CTRL) that connects London to the Channel Tunnel, also known as High Speed 1 (HS1), an empirical model for the prediction of ground-borne vibration and structure-borne noise in buildings from high speed trains was developed, to allow the future impact of the operation of the CTRL on existing noise and vibration sensitive uses to be assessed, and mitigation measures determined. The model covers the prediction of tactile vibration and structure-borne noise from trains on the surface, in bored tunnels, and in cut and cover tunnels. At the origin of this model is a database of more than 3000 measurements of TGV (France's high speed rail service) train events.

As Hood, Greer, Breslin & Williams (1996) mention, their model is divided into three stages: source, propagation and building response, much like the other prediction methods previously discussed. The source is modelled based on the TGV measurements performed at 10 m from the nearest rail on the surface for various soil types. To allow for different types of trains, such as the Eurostar, corrections were applied to the vibration levels measured on the surface. Further adjustments were made to these levels to account for sections of bored tunnels, based on measurements

at Stansted Tunnel in the UK, and for cut and cover tunnels, from measurements undertaken by Deutsche Bahn.

For the second stage of the model, the attenuation through the soil was calculated from the statistical analysis of the ground-borne noise and vibration measurement results for a number of train types in tunnels. Factors such as the absorption and geometric dispersion of body waves between the tunnel and the surface, the absorption and dispersion of surface waves and the effect the width of the tunnel has on the vibration levels were accounted for. Hood et al.'s (1996) measurement data suggested that the propagation characteristics of body and surface waves did not change significantly with different types of soil, meaning their models do not account for changes in soil.

The structure-borne noise levels near the centre of a room in a building are calculated from the 1/3 octave band rms vertical particle velocities measured outside the building during a train pass-by. Hood et al.'s (1996) model uses the equations given by Kurzweil (1979) to convert the external vibration levels into internal structure-borne noise levels, albeit validated and corrected through the analysis of additional measurements. The relevant equations are Equation 3. 2 to Equation 3. 4, given in Section 3.2.1. Another difference between Kurzweil's and the HS1 models is that a conservative assumption has been made on the floor-to-floor attenuation in high rise buildings. For instance, Kurzweil (1979) notes that a reduction of 3 dB / floor is a typical value for floor-to-floor attenuation. However, for HS1, this was only assumed to be 1 dB / floor irrespective of building constructions.

In terms of model accuracy, Hood et al. (1996) have compared their predictions with pseudo-measurements (calculated from applying the soil to building transfer function to the vibration levels measured), and noted that there is significant variation of structure-borne noise levels between different types of trains and sites. This comparison also revealed that the calculation model seems to over predict structure-borne noise levels from low vibration levels, i.e. at distances far from the source, but underestimates noise levels calculated from high levels of vibration, which typically occur near the source.

With HS1 complete, works have started on High Speed 2 (HS2) to connect London to the West Midlands and beyond. The assessment method described above for HS1 is also being used to predict ground-borne vibration and structure-borne noise from the new rail system. (High Speed 2 (HS2) Limited, 2013; ARUP & ERM, 2017)

3.2.8 RIVAS

Under the Railway Induced Vibration Abatement Solutions (RIVAS) project, a joint research project co-funded by the European Commission within the 7th European Framework Programme, various existing models for the prediction of ground-borne vibration and noise in buildings were reviewed, with a view to estimate annoyance caused to building occupants. The main aim of the project was to develop control measures at source, track, propagation path and in the building that can be used to reduce annoyance. RIVAS looks at ground-borne vibration and noise propagation in three stages: emission, propagation and immission. These relate to the source, propagation path and receiver stages of the vibration transmission line described in Chapter 2, respectively. RIVAS uses the transfer functions shown in Table 3. 5 to describe the vibration attenuation between these stages, where the relevant variables necessary are as follows (Villot, Guigou, Jean, & Picard, 2012):

- L_{v1} are the ground vibration levels at a reference distance of 8 m from the train track;
- L_{v2} are the free-field ground vibration levels at the distance of the building from the track, but without the building in place;
- L_{v3} are the foundation vibration levels;
- L_{v4} are the floor vibration levels;
- and L_p are the sound pressure levels in the room.

Table 3. 5 Transfer functions used by RIVAS (a similar table is provided in Villot et al. (2012), though additional information is included in the second column below for clarity)

Transfer function	Description	Input variable	Output variable
TF1	Attenuation of vibration levels through the soil from a location 8 m away from the track to the building location (without the building in place)	L_{v1}	L_{v2}
TF2	Coupling losses provided by the interaction between the building foundations and the ground	L_{v2}	L_{v3}
TF3	Amplification due to floor slab resonances	L_{v3}	L_{v4}
TF4	Conversion of floor vibration levels into structure-borne noise levels in a room	L_{v4}	L_p

RIVAS makes use of numerous models to ascertain TF1 to TF4. However, only two of the models considered provide guidance on the prediction of ground-borne vibration and noise from the source through to the receiver. These are the empirical VIBRA-1-2-3 model, described in Section 3.2.6, and the theoretical BAM prognosis tool mentioned in Section 3.3.6. Of the four transfer functions used by RIVAS, TF1 is the only one that can be more accurately known using measurement data available from VIBRA-1-2-3 (Kuppelwieser & Ziegler, 1996; Ziegler Consultants, 2009), and DB & Obermeyer (2003), which includes statistical data at various distances from train tracks for different types of trains, soils, etc. For instance, with measurement data available at two reference distances from the train track, such as 8 m and 16 m, and if the building is to be built at the farther reference distance from the track, TF1 can be determined from the difference between the vibration levels measured at each location. TF2 and TF4, on the other hand, need to be estimated statistically. Guidance on how these are calculated is provided in Villot et al. (2012).

With regard to the accuracy of the calculation of TF2 to TF4, Villot et al. (2012) state that the standard deviation of the predictions is *"of the order"* of 5 dB.

3.3 Existing theoretical models

The following sections provide an overview of the various theoretical models currently available for the prediction of ground-borne vibration and structure-borne noise in buildings from railway systems. Great part of the models found, such as the Pipe-in-Pipe model (Kuo, Jones, Hussein, & Hunt, 2013) and others, deal only with the prediction of ground-borne vibration between the source and the soil, and do not look at vibration or structure-borne noise levels in buildings. The following sections provide a summary of the various theoretical models that account for the complete vibration transmission line, i.e. they start with the source, predict the level of attenuation through the soil and calculate the ground-borne vibration and structure-borne noise levels in a building.

3.3.1 CATdBTren model

The CATdBTren project is a collaborative Catalonian research project with the aim of developing a model for the prediction of ground-borne vibration and structure-borne noise from train sources to a receiver using limited computational resources. With this requirement in mind, numerical techniques were discarded and a semi-analytical model was developed. The model contains three main block components, as set out below, and provides 1/3 octave band vibration levels inside a building $V_r(\omega)$. The relationship between the three components is given by Equation 3. 12. (Romeu, et al., 2009)

- Source model: represented by $V_s(\omega)$;
- Ground propagation model: represented by $T(\omega)$;
- Building model: represented by $F(\omega) \cdot S(\omega)$, where $F(\omega)$ relates to the foundations of a building and $S(\omega)$ to its structure.

$$V_r(\omega) = V_s(\omega) \cdot T(\omega) \cdot F(\omega) \cdot S(\omega) \qquad \text{Equation 3. 12}$$

The output of the source model component is the ground vibration level at the location of the train track $V(\omega)$, which requires consideration to be given to track characteristics, as well as the wheel-rail interface. Further information on how source vibration is modelled is provided in Palacios, Arcos, Prat, & Balastegui (2009).

The propagation of vibration through the ground in this model can be divided into two categories. The first consists of propagation of vibration along the ground surface. The vibration amplitude at a point b from a given vibration amplitude at point a is modelled with Equation 3. 13, developed by Lamb (1904) and subsequently used by Barkan (1962). In the CATdBTren model for surface trains, a train is considered to be a moving multipoint source. The total vibration amplitude at a given point consists of the sum of the vibration amplitudes (given by Equation 3. 13) for all the train point sources, with a geometric attenuation coefficient γ of 0.5. For underground vibration sources, the vibration amplitude on the surface of the ground is obtained using a 2D finite element method (FEM) model. (Romeu, et al., 2009)

$$v_b = v_a \left(\frac{r_a}{r_b}\right)^{\gamma} e^{\alpha(r_a - r_b)} \qquad \text{Equation 3. 13}$$

where

v_a and v_b are the vibration velocity amplitudes at points a and b;

r_a and r_b are the distances of points a and b from the vibration source;

γ is a coefficient for geometric attenuation in the soil, varying between 0.5, 1 and 2 depending on the type of source and wave (Gutowski & Dym, 1976);

and α is the frequency dependent material damping coefficient for the soil in question.

The coupling between the ground and the building foundations, as well as the vibration response of the building, can also be modelled with FEM. However, Romeu et al. (2009) state that a more appropriate method for this would be to use a coupled FEM-SEA (statistical energy analysis) approach, as this would reduce the dimensions and computational cost of the model.

CATdBTren model seems to have been validated against measurements undertaken on the ground, but not in buildings. Despite this, good agreement was found between the predicted and measured vibration levels for rail systems at grade. (Cardona, Romeu, Arcos, & Balastegui, 2010) Whilst the prediction model deals with the receiver, its results only relate to ground-borne vibration velocity levels. Structure-borne noise levels can be calculated from these, though Romeu et al. (2009) do not provide guidance on the conversion.

3.3.2 Impedance / dynamic stiffness model

Another prediction model that looks at vibration propagation within buildings, but does not provide guidance on structure-borne noise as such is Sanayei, Zhao, Maurya, Moore, Zapfe & Hines's (2011) impedance-based model. This type of model is a less computationally expensive alternative to FEM models, which achieves equally (if not more) accurate results for the prediction of floor vibration in a building.

Although Sanayei et al.'s prediction model (2011) deals with train-induced floor vibrations, it focuses solely on the propagation of vibration within a building and does not consider train vibration propagating through the ground. Sanayei et al. (2011) acknowledge that predicting the coupling losses between the soil and the building foundations is a complex process, and that although horizontal vibration components exist, the vibration experienced by the foundations of a building are mainly in the vertical direction. Once vibration enters a building, it is transmitted to the upper floors by quasi-longitudinal waves through the columns. The model also assumes that the vibration force excitation is applied at the base of the columns in the vertical direction.

Sanayei et al.'s model (2011) can be divided into two main components, relating to how columns / beams and slabs are modelled. The dynamic stiffness method is used to calculate the response of the columns in a building to the excitation force, using the relationship between the force f, stiffness k_{col} and displacement u given in Equation 3. 14.

$$\{f\} = [k_{col}]\{u\} \qquad \text{Equation 3. 14}$$

Sanayei et al. (2011) solve the above model for the columns, for two boundary conditions: one end of the column is fixed and the excitation force is applied to the free end; and one end of the column is fixed and the excitation force is applied to the fixed end. The response of the columns to the excitation force with these boundary conditions in place is given by the dynamic stiffness matrix set out in Equation 3. 15.

$$[k_{col}] = \frac{E_c A\beta}{\sin \beta L}\begin{bmatrix}\cos \beta L & -1 \\ -1 & \cos \beta L\end{bmatrix} \quad \text{Equation 3. 15}$$

where

E_c is the complex modulus of elasticity accounting for energy dissipation within the column and is given by $E_c = E(1 + j\eta)$;

A is the cross-sectional area of the column;

β is the quasi-longitudinal wavenumber, which is dependent on the angular frequency ω, complex modulus of elasticity E_c and density ρ of the column, and is given by $\beta = \omega\sqrt{\frac{\rho}{E_c}}$;

and L is the length of the column.

As the floor slabs are attached to the columns, they can be considered energy dissipating floor slabs and be modelled as thin plates in bending. The response of a floor slab / plate of thickness h and density ρ is given by Equation 3. 16, in terms of its dynamic effective mass m_{eff} with respect to angular frequency ω.

$$m_{eff} = \frac{Z}{j\omega} = -\frac{j}{\omega} 8\sqrt{D}\sqrt{\rho h} \quad \text{Equation 3. 16}$$

where

Z is the point force impedance of the plate, which is given by $Z = 8\sqrt{D}\sqrt{\rho h}$;

and D is the dynamic bending stiffness of a plate given by $D = \frac{Eh^3}{12(1-\nu^2)}$ (ν is the plate's Poisson's ratio).

The dynamic stiffness matrices k_{col} and the dynamic effective mass m_{eff} of the columns and slabs, respectively, are then assembled into global matrices for the system, $[K_{col}]$ and $[M_{slab}]$. The steady state response of the system $\{U\}$ subjected to a harmonic force excitation $\{F\}$ is given by Equation 3. 18, and the vibration velocity level for all floors can be found from Equation 3. 18 and Equation 3. 19. The structure-borne noise level in a room in the building can then be estimated from Equation 3. 20 in line with Kurzweil's work (1979) or Equation 3. 21 based on subsequent recommendations by the FTA (Hanson et al., 2006).

$$\{U\} = \frac{\{F\}}{[K_{col} - \omega^2 M_{slab}]} \quad \text{Equation 3. 17}$$

$$\{V\} = j\omega\{U\} \quad \text{Equation 3. 18}$$

$$L_v = 20 \log_{10}\left(\frac{v}{v_{ref}}\right) \text{(dB re } 10^{-8} \text{ m/s)} \quad \text{Equation 3. 19}$$

where

$$v_{ref} = 1{\times}10^{-8}\, m/s$$

$$L_p = L_v - 27 \text{ (dB re 20 µPa)} \quad \text{Equation 3. 20}$$

$$L_p = L_v - 32 \text{ (dB re 20 µPa)} \quad \text{Equation 3. 21}$$

The above equations are for a four-storey high building, and only account for one column being excited at the base, which runs through the centre of four slabs on the top of each other. Therefore, $\{U\}$ is a 5 x 5 matrix allowing for only 5 degrees of freedom (one for the column subjected to longitudinal forces, and one for each of the floor slabs in bending). (Sanayei, Maurya, Zhao, & Moore, 2012)

The above model has been validated against an FEM model by Sanayei et al. (2012), a scale model of a building by Sanayei et al. (2011) and against an actual full size building (Sanayei, Anish, Moore, & Brett, 2014).

For the FEM validation, three models of the same four-storey building were built to various degrees of detail. These models took between 12 minutes and just over 6 hours to run, depending on the level of detail, compared to only 20 seconds of the impedance model, making the latter significantly more efficient especially when the need to model large buildings arises. Sanayei et al. (2012) state that *"Compared to FE models, it [impedance modelling] provides much higher accuracy with a method that is far more computationally efficient."* This can be atributed to the fact that their impedance / dynamic stiffness model is based on closed-form analytical expressions for known elements, such as beams and plates, and no additional assumptions on the structures being modelled are needed. However, the impedance approach is only applicable where analytical expressions are available, and for more complex elements FE modelling may be the only option.

A comparison between the measurements undertaken in a full-scale four-storey building and the results of this prediction model revealed that, below 50 Hz, there is good agreement between the measured and predicted vibration levels. However, above 50 Hz, the differences between the predicted and measured values become more noticeable. (Sanayei et al., 2014)

Li, Wu & Yin (2017) developed a similar dynamic stiffness formulation to model the response of a double-bottom cabin in a ship. However, their model accounts for both bending and in-plane waves in plates that are simply supported along two edges, rather than just one type of wave per component as considered in Sanayei's et al.'s (2011) model. The assembly of the global dynamic stiffness matrix for the system and the coupling between each element in Li, Wu & Yin's (2017) model follow the same procedure as that used in FEM, with the exception that the degrees of freedom for the plates under consideration are modelled as lines instead of nodes. The results of this model were validated against two FEM models with different element sizes. A comparison between the models for bending waves revealed that discrepancies are present in the results at the resonant frequencies of the system. Also, as the accuracy of FEM reduces at higher frequencies, more variation between the FEM and dynamic stiffness models at such frequencies is evident. This said, the results of the two model types follow the same trend. For in-plane waves, good agreement was found between the dynamic stiffness and FEM models, especially when the element sizes in the FEM model are smaller. In terms of computation time, the FEM models took up to 1.5 hours to compute the results up to 10 kHz, while Li, Wu & Yin's model only required 10 minutes to calculate the results for the same frequency range.

3.3.3 Finite difference time domain model

A calculation method that can be used to provide reasonably accurate predictions of ground-borne vibration and structure-borne noise in buildings is finite difference time domain (FDTD) modelling. This method allows moving sources to be modelled numerically in 3D. In addition to this, when combined with the boundary element method (BEM), it can be used to model radiation of noise through air to the far field. FDTD is also useful as it can accommodate propagation through anisotropic media, such as soils and other materials. Another advantage of FDTD is that the output of the model is a time domain plot, which can be converted into a .wav file and then played through loudspeakers. (Thornely-Taylor, 2004a & 2004b)

An example of a commercial FDTD numerical modelling package is FINDWAVE authored by Rupert Taylor Ltd. While it is mainly used to model railway noise and vibration, FINDWAVE can also solve any acoustic or 3D wave propagation problem. With regard to railway systems, it can be used to predict ground-borne vibration and structure-borne noise from a source (either underground or on the surface) propagating through the soil and into buildings. In this field, FINDWAVE contains two main modules (RPS, 2005):

- The train module, in which the rail vehicle is modelled as a number of damped masses and springs on top of each other;
- And the track / structure / environment module, which is used to model the dynamic response of the track and other structure supporting the vehicle, the medium surrounding it and any structures below or above ground. These structures are modelled as cells in a 3D orthogonal grid. Each cell is assigned a density, loss factor and Lamé constants.

One of the largest applications of FINDWAVE is Crossrail in London, in which it was largely used to predict the future levels of structure-borne noise that will be experienced by existing buildings from the passage of trains in the new underground tunnels. Three types of assessment were required, the first of which comprised the production of structure-borne noise contours, based on assumptions on the building constructions and foundations (no deep or piled foundations), as well as simplified assumptions for the soil. For the second type of model, buildings with deep or piled foundations were assessed individually. The third assessment type consists of the assembly of full numerical models of significant buildings that are particularly sensitive to ground-borne vibration and noise. This type of assessment was only undertaken at the detailed design stage. (RPS, 2005)

As with any other prediction model, the accuracy of an FDTD model and of FINDWAVE itself is highly dependent on the quality of the parameters entered in the model. FINDWAVE has been validated for Crossrail against field measurements above one of the tunnels of the Docklands Light Railway (DLR) Lewisham Extension in London, which was chosen for its multitude of soil layers. (RPS, 2005) The predicted levels of structure-borne noise were within 3 dB(A) of the measured values when modelled without a building structure, but with measured rail roughness. This parameter varies significantly with time, distance and between trains passing through the same location. With uncontrolled variations in the rail roughness, the levels of

structure-borne noise can vary by up to 20 dB(A). For Crossrail, it was assumed that the rails and train wheels will undergo maintenance when the roughness approaches a certain limit. Such rail roughness limit has been used in the FINDWAVE model to allow a worst-case assessment. Based on this, the uncertainties associated with the dynamic properties of soil and of track components result in a variation of up to 3 dB(A) between the FINDWAVE and measurement results. When the results of the validation studies are combined and the uncertainties associated with the existing building structures are accounted for, RPS (2004) states that the *"measured levels are unlikely to exceed predicted levels by more than 5 dB(A)"*.

3.3.4 Finite element method models

One of the most commonly used numerical techniques to model the response of a building to vibration excitation is FEM. In contrast with empirical models and potentially some other theoretical models, it allows design changes to buildings, such as the introduction of mitigation measures, to be modelled and their impact assessed.

Lurcock & Thompson (2014) have investigated the accuracy of FEM models with varying degrees of detail against historical measurement data for 12 concrete frame buildings in London, affected by existing underground train lines. The time domain recordings obtained for each train event were post-processed to obtain slow weighted, 1/3 octave band vibration levels and the A-weighted sound pressure levels on each floor level. The measurement results were compared with 1D, 2D and 3D FEM models developed using COMSOL Multiphysics. Three 3D models were assembled from as simple as a single 1 x 1 portal frame to a full building model with structural shafts. The 2D models included a four-bay and single-bay model. Two 1D models were also developed. In the first model, the floors were represented by a number of point masses, connected by rods representing the columns in a building. Such representation cannot consider any amplification that occurs at mid-span slab locations. For this, a simply supported plate was assumed to be weakly coupled to the 1D plate and rod representation.

A summary of Lurcock & Thompson's (2014) findings is provided in Table 3. 6. It is worth noting that the measurement data used for the comparisons consists of the average of the measured vibration levels on each floor across all buildings. One of the main conclusions of this study is that care must be taken when analysing measurement data from buildings with different floor spans and column designs, as the averaging of the data undertaken seems to have masked the effect of floor resonances, which was clear in the 2D and 3D FEM models. Also, the 2D and 3D FEM models resulted in vibration levels closest to the average of the measured A-weighted vibration levels. For spectral analysis, there is benefit in using a full 3D FEM model of a building with structural shafts. In addition to this, both the measurements and the model results have shown an attenuation of 1 dB(A) per floor. Similar results were previously obtained by Lurcock, Thompson & Bewes (2013).

Table 3. 6 Comparison between FEM models and measurement data in 12 buildings over 6 floors, based on Lurcock & Thompson's research (2014)

	FEM models		
	1D	2D	3D
Degrees of freedom	87 – 2,910	612 – 1,011	21,642 – 224,250
Model calculation time	15 seconds – 25 minutes	~ 1 minute	2 hours – 18 hours
Comparison with vibration levels measured on different floors within the buildings	Good agreement with A-weighted levels measured in the basement. However, such agreement reduces significantly in the higher floors of the building.	Similar results were obtained with the 2D and 3D models for A-weighted vibration levels. The results of the 2D and 3D models follow the same trend as the measured results, with an approximate reduction of 1 dB(A) per floor.	
Comparison with 1/3 octave band vibration levels on level 3 of the buildings	The model results do not follow the spectral shape of the measurements nor of the other FEM models considered.	Similar results were obtained with the 2D and 3D models. The effect of the natural frequencies of the floor (8 Hz to 10 Hz) are more noticeable than in the averaged measurement data. The more detailed the model, the less pronounced this effect is.	

As highlighted in Table 3. 6, FEM has large computational requirements when compared to other prediction models, such as the impedance model described in Section 3.3.2. Another of its limitations is related to the fact that the higher the frequencies being modelled (small wavelengths), the higher the number of degrees of freedom required to model them accurately. This has further implications on the calculation times of the models. FEM is therefore best suited to model low frequency vibration. (Cotoni, Shorter, & Langley, 2007) To get around this and other limitations of FEM, several hybrid models have been developed using other numerical techniques such as energy FEM (Hong, Wang, & Vlahopoulos, 2006), BEM (discussed in Section 3.3.6) and SEA (discussed in Section 3.3.8).

3.3.5 Boundary element method models

The boundary element method (BEM) is another commonly used method for the prediction of vibration propagation through the soil and in buildings. Some authors, such as Nagy, Fiala, Márki, Augusztinovicz, Degrande, Jacobs & Brassenx (2004 & 2006), go as far as stating that BEM is the most accurate way of predicting structure-borne noise from vibration velocities. Its main advantages are that it can model random shaped rooms and can be easily coupled with an FE model. On the other hand, it has the same disadvantage as FEM, i.e. it is a low-frequency prediction method. To model a typical room with BEM in the mid-frequency range, Nagy et al. (2006) state that the density of the boundary mesh should be increased, which would result in the need to solve several linear equations, increasing the computational cost of the model. As a result, BEM is also often coupled with other predictions methods, as can be seen in Section 3.3.6.

3.3.6 Hybrid finite element – boundary element method models

Given the versatility of FEM and BEM, there are various models for the prediction of ground-borne vibration and structure-borne noise from trains that have combined these two methods together. Examples of this include the BAM prognosis tool developed by Rücker & Auersch (2007), the EC-Growth project CONVURT (CONtrol of Vibration from Underground Railway Traffic) and CSTB's MEFISSTO tool. Whilst the above all use FEM and BEM coupled together, they do not apply such coupling in the same way. For instance, the BAM prognosis tool and some of the work undertaken on CONVURT both use a hybrid FEM-BEM method to model the source of vibration. However, MEFISSTO uses BEM to model the propagation of vibration through the ground and FEM to model the receiving building. A comparison

between these three prediction models is provided in Table 3. 7, based on the literature available. From this, it seems most modelling packages focus on the prediction of ground-borne vibration. The levels of structure-borne noise are often calculated as an extension to the original models.

Even though MEFISSTO is a numerical model, it features in the semi-empirical RIVAS model described in Section 3.2.8, to help predict the effect changes in the soil parameters would have on the vibration levels and to better understand the building response with regard to foundation and floor vibration, and structure-borne noise. (Villot et al., 2012)

Table 3. 7 Comparison between FEM-BEM models used for the prediction of structure-borne noise in buildings

Model reference / project	Key papers	Technique used to model vibration transmission line stages			Accuracy of structure-borne noise prediction	Notes
		Source	Propagation path	Receiver		
BAM prognosis tool	Rücker & Auersch (2007) Villot et al. (2012)	Vehicle is modelled as a multi-body and the tracks (including ground stiffness) are modelled as a beam-on-support. For complex vehicle-track interaction scenarios, a coupled FEM-BEM model is used.	Transmission through the ground is modelled using a transfer function for a homogeneous half space. To model layered soils, the response of the soil layers is approximated by adjusting the frequency dependent material properties.	Vibration velocity is estimated from a wall-floor model, accounting for the presence of the ground as spring-damper elements.	Not validated as of 2012. No additional information found.	The receiver stage is based on measurement data. The model is given in one main module (emission, transmission and immission). However, an additional module is available for the prediction of structure-borne noise.
CONVURT	Clouteau et al. (2004) Nagy et al. (2004) Nagy et al. (2006) Fiala et al. (2007)	Source and propagation path modelled with either the Pipe-in-Pipe modelling software (originally developed as part of the CONVURT project) or a coupled FEM-BEM model. In the latter approach, FEM is used to model the vehicle-track interaction, while BEM is used to model the soil propagation.		Receiver modelled either using Rayleigh radiation integral & modified BEM model, or FEM model.	Rayleigh radiation integral model: ± 10 dB in 1/3 octave bands and ± 3 dB A-weighted. FEM model: not specified.	Structure-borne noise validated against BEM model and measurement data.

Model reference / project	Key papers	Technique used to model vibration transmission line stages			Accuracy of structure-borne noise prediction	Notes
		Source	Propagation path	Receiver		
MEFISSTO	Jean et al. (2004) Villot et al. (2011) Villot et al. (2012)	Source vibration levels are measured.	Transmission path between measurement location and receiver is modelled with BEM.	Receiver is modelled with FEM.	Validated against measurements. $\pm$ 3 dB(A) for vibration levels.	The standard MEFISSTO package is a 2D BEM-FEM model. However, to calibrate the train excitation from the measured free field ground vibration levels correctly and to better model attenuation through the ground, a 2.5D version of MEFISSTO should be used. Structure-borne noise is calculated from the average floor vibration velocity level in a separate module.*

* The average structure-borne noise level in a room is given by $L_p = L_v + 10\log_{10}\sigma + 10\log_{10}\left(\frac{4S}{A}\right)$, where L_v is the average floor vibration velocity level with reference 5×10^{-8} m/s, σ and S are the radiation efficiency and density of the floor, and A is the absorption area of the room.

3.3.7 Statistical energy analysis

Statistical energy analysis (SEA) is a calculation method frequently used for the prediction of sound transmission in buildings. It was first developed in the 1960s to aid the design of space craft, but has since found its way into other areas of engineering, namely buildings and rail vehicles. As its name indicates, SEA is a statistical approach to model energy transmission (also often referred to in terms of power flow) between sub-systems that form a larger system, such as walls and floors in a building. The response of a system when modelled using SEA is determined by the presence of resonant modes at a given frequency and how these modes are coupled together. Each of the sub-systems considered in SEA can therefore store modal energy. Damping of the modes and modal overlap, i.e. the portion of the frequency spectrum that is governed by resonant modes, also play an important part in SEA prediction models. In contrast with numerical models, such as FEM or BEM, SEA does not require all parameters of a specific sub-system to be exactly known, which allows the sub-systems under consideration to be simplified. (Craik, 1988; Fahy & Gardonio, 2007; Hopkins, 2007; Robinson, 2012)

As previously mentioned, FEM and BEM are both low frequency methods and are not typically used to model high frequencies for a number of reasons. At high frequencies, the number of modes in a system increases significantly and to model them with a numerical method would require all the modes to be known precisely and accounted for. Also, the modes at such frequencies are very sensitive to geometrical imperfections, such that it is significantly harder to predict them with any level of accuracy. Increasing the level of detail in a numerical model, even if accurate predictions can be obtained, can have a significant impact on the calculation time and overall computational cost of the model, as can be seen from Table 3. 6 in Section 3.3.4. (Woodhouse, 1981) Being a statistical method, SEA can be used to calculate the response of a system at high frequencies without needing the same level of detail a numerical model would, and therefore it is considered a high frequency modelling method. Extensive work on SEA and on how it can be used to model sound transmission through buildings has been carried out by Craik (1988) and Hopkins (2007).

In its standard form, i.e. with a steady-state power input into the sub-systems under consideration, SEA can only be used to predict steady-state sound pressure levels and vibration levels. However, variations to the standard SEA method have been developed to allow systems with lower modal count and indirect coupling between subsystems to be modelled, as well as the prediction of parameters other than steady-state sound pressure and vibration levels and the use of transient sources. For instance, advanced statistical energy analysis (ASEA) is a high-frequency method which uses a combination of standard SEA and ray tracing techniques. ASEA was originally developed by Heron (1994) to allow indirect coupling between sub-systems to be considered when calculating the power transmission between coupled sub-systems. Wang & Hopkins (2016) have used ASEA to model the coupling between rectangular beams in an L-junction with bending and longitudinal, or bending and torsional wave motion. The model switches between Euler-Bernoulli and Timoshenko's beam theories when there is a difference of at least 1 dB in the resulting coupling loss factors. This corresponds to a difference of 26% between the group velocities of both beam theories. The results of the model were compared against a standard SEA model, FEM and measurements, and have shown that ASEA is capable of predicting high propagation losses, which are more significant at high frequencies and are not accounted for with SEA. Such losses can occur in different wave types.

Experimental statistical energy analysis (ESEA) is another of the variants of SEA, which can be used to establish the *in situ* coupling loss factors for a set of sub-systems with low modal density and low modal overlap. These can then be input into a standard SEA model. (Hopkins, 2002; Hopkins, 2009; Robinson, 2012) Transient statistical energy analysis (TSEA) is also a variation of SEA, which allows the effect of transient noise and vibration sources, such as trains, doors closing in a building, etc., on the energy and power flows of a sub-system to be determined. Further information on TSEA can be found in sources such as King & Scholl (2011) and Robinson (2012).

As ground-borne vibration and structure-borne noise from trains, or other sources, occur mainly at low frequencies, SEA is not commonly used in prediction models for such parameters. This said, Trochides (1991) proposed a simple method to estimate structure-borne noise levels in buildings caused by ground-borne vibration from nearby underground train tunnels, in which the vibration levels from the source to the receiver were estimated using impedance formulae, while SEA was used to model the

structural response of the building. The results of Trochides' (1991) model were validated against measurements undertaken on a 1:10 scale model of the system under consideration, over a frequency range of 500 Hz to 5000 Hz (equivalent to 50 Hz to 500 Hz in a full scale model). The results of the validation were limited, though a comparison between the predicted and measured values shows that the model underestimates the response of the building structure at resonant frequencies.

3.3.8 Hybrid finite element – statistical energy analysis method

As mentioned in the previous section, SEA is a method commonly used to predict energy transmission between complex systems and sub-systems, as it does not require the full properties of the elements being modelled to be fully known. Instead, as its name indicates, the energy / power flow between sub-systems can be estimated from statistical analysis of the number of modes and modal overlap of a sub-system at a given frequency. The larger the number of modes present, i.e. the higher the frequency, the higher the accuracy of SEA. However, the number of modes in a sub-system, and hence the reliability of the model, reduce with frequency. Numerous studies have been undertaken on the lowest number of modes needed to allow reasonably accurate SEA results, some suggesting a minimum of 2 – 30 modes per frequency band. However, information on damping and modal overlap is also needed to better determine a lower frequency limit for SEA predictions. (Craik, 1988)

FE, on the other hand, relies on the details of each element under consideration, such as degrees of freedom and number of modes, being precisely known at all frequencies. At high frequencies, where the wavelength is significantly smaller than the dimensions of the element being modelled, the number of modes increases significantly. At the same time, the response of an element can be highly affected by small imperfections within it, such as those from a manufacturing or construction process, which at smaller wavelengths would become more noticeable and their impact on the response of the element more substantial. A good example of the impact of these on the accuracy of FE is often encountered in the automotive industry, where cars in a production line are modelled using very detailed FE models with millions of degrees of freedom and intensive computation costs. Even with such detailed models, measurements on successive cars on the production line have shown significantly different responses. A statistical analysis method, such as SEA, is therefore preferable to model high frequencies. (Cotoni, Shorter, & Langley, 2007; Kompella & Bernhard, 1993; Cornish, 2000)

With the above limitations in mind, there are some theoretical prediction models that combine statistical and numerical methods to model ground-borne vibration and structure-borne noise in buildings more accurately and over a larger frequency range. A good example of this is Shorter & Langley's (2005) hybrid deterministic-statistical method to model complex vibro-acoustic systems, which was implemented in collaboration with Vibro-Acoustic Sciences Inc. (VASci), later incorporated within the ESI Group. The model is based on work carried out by Langley & Bremner (1999) and in 2005, the model was developed into the vibro-acoustics analysis software package VA One. (University of Cambridge, 2014) Although this model is not specific to ground-borne vibration and structure-borne noise from trains, it can be used to model the receiver stage of the vibration transmission line.

Shorter & Langley's (2005) hybrid model uses FEM to model low frequencies, and SEA for the high frequencies. However, the mid-frequency zone, i.e. the division between low and high frequencies, does not fall entirely within the domain of FEM or SEA. The output of the model is the ensemble average response of the system and takes into account the contribution of the direct and reverberant fields within the system. The model has been validated against various FEM models, and the results of the two techniques are in good agreement. (Cotoni, Shorter, & Langley, 2007)

A very similar prediction model was developed by Maksimov & Tanner (2011). This model also uses FEM to model low frequencies and SEA to model high frequencies. The main difference between this and Shorter & Langley's (2005) model seems to be related to whether the models account for the reciprocity relationship between the direct and reverberant fields.

3.4 Summary of existing models and their limitations

The main characteristics of the various empirical and theoretical models for the prediction of ground-borne vibration and structure-borne noise in buildings, reviewed in Sections 3.2 and 3.3 of the present document, are summarised in Table 3. 8 and Table 3. 9, respectively. These tables follow the same format as those presented by Lotinga (2014) for the prediction of ground-borne noise and vibration in the soil, though the information in them only relates to models that deal with ground-borne vibration and structure-borne noise in buildings.

Table 3. 8 Summary of existing empirical models for the prediction of structure-borne noise in buildings

Model / project	Key papers	Description	Accuracy in the prediction of structure-borne noise	Notes
	Kurzweil (1979) Lang (1971)	Empirical	± 10 dB variation	Simplified model for A-weighted noise levels.
	Kurzweil (1979)	Empirical	Not disclosed	Prediction of structure-borne noise in a room in one octave bands. Potentially over predicts structure-borne noise.
	Nelson & Saurenman (1987)	Empirical	Not disclosed	The authors recommend that a safety factor of 5 – 10 dB is added to the predictions, and that the model is most accurate between 8 – 30 Hz.
FTA / FRA general	Hanson et al. (2006) Hanson et al. (2012)	Empirical	Not disclosed	
FTA / FRA detailed	Hanson et al. (2006) Hanson et al. (2012)	Empirical	Prediction of ground-borne vibration validated against FE-BE model. Good agreement was found between the results of the two models.	
	Melke (1988)	Semi-empirical / analytical	Not disclosed	Based on analytical techniques, and on laboratory and field measurements. Appropriate for a rough estimate of structure-borne noise levels in a building.
	Jakobsen (1987 &1989)	Empirical	± 10 dB variation	Based on a small number of measurements.
VIBRA 1-2-3	Kuppelwieser & Ziegler (1996) Ziegler Consultants (2009)	Semi-empirical	± 6.5 dB variation	

Model / project	Key papers	Description	Accuracy in the prediction of structure-borne noise	Notes
HS1 & HS2	Hood et al. (1996) High Speed (HS2) Limited (2013) ARUP & ERM (2017)	Empirical	Overestimates structure-borne noise from low levels of vibration, but under predicts noise levels from high levels of vibration.	Large variation between sites and types of trains. However, the prediction model has gone through numerous peer reviews and is still being used on HS2.
RIVAS	Villot et al. (2012)	Empirical	Estimated ± 5 dB variation	Uses VIBRA-1-2-3 and other models.

Table 3. 9 Summary of existing theoretical models for the prediction of structure-borne noise in buildings

Model / project	Key papers	Description	Accuracy in the prediction of structure-borne noise	Notes
CATdBTren	Romeu et al. (2009) Cardona et al. (2010)	Analytical with FEM		Model outputs ground-borne vibration velocity levels in a building, though no conversion into structure-borne noise is given.
	Sanayei et al. (2011) Sanayei et al. (2012) Sanayei et al. (2014)	Analytical, impedance based		Model outputs vibration velocity levels in a building, though there is good agreement between predicted and measured data.
	Li, Wu & Yin (2017)	Analytical, dynamic stiffness		Developed to model the response of a double-bottom cabin in a ship. More detailed than Sanayei et al.'s (2011) model. This model can potentially be extended to buildings.
FINDWAVE	Thornely-Taylor (2004a & 2004b) RPS (2004 & 2005)	Numerical, FDTD	± 3 dB(A) variation	RPS (2004) states that measured levels are unlikely to exceed the predicted levels by more than 5 dB.

Model / project	Key papers	Description	Accuracy in the prediction of structure-borne noise	Notes
	Lurcock & Thompson (2014) Lurcock, Thompson & Bewes (2013)	Numerical, FEM		Results presented in terms of floor vibration levels. 2D and 3D FEM models are adequate to predict A-weighted vibration levels. However, for spectral analysis, full detailed 3D models are more accurate.
BAM prognosis tool	Rücker & Auersch (2007) Villot et al. (2012)	Numerical / analytical adjusted with measurement data	Not validated as of 2012. No additional information found	Receiver stage is based on measurement data. The model is given in one main module (emission, transmission and immission). An additional module is available for structure-borne noise.
CONVURT Rayleigh integral	Nagy et al. (2004) Nagy et al. (2006)	Analytical	± 10 dB in 1/3 octave bands and ± 3 dB A-weighted	FEM-BEM or Pipe-in-Pipe software can be used to model source and transmission path.
CONVURT FEM	Fiala et al. (2007)	Numerical, FEM	Not disclosed	FEM-BEM or Pipe-in-Pipe software can be used to model source and transmission path.
MEFISSTO	Jean et al. (2004) Villot et al. (2011) Villot et al. (2012)	Numerical, FEM-BEM	Validated against measurements. ± 3 dB(A) for vibration levels	The standard MEFISSTO package is a 2D BEM-FEM model. However, the 2.5D version of MEFISSTO should be used to model train vibration. Structure-borne noise is calculated from the average floor vibration velocity level in a separate module.
Hybrid FE-SEA	Shorter & Langley (2005) Cotoni, Shorter & Langley (2007)	Numerical, FEM-SEA	Validated against other FEM models. Results are in good agreement.	

3.5 Proposal for a new simplified hybrid model

The review of the existing models presented in the previous sections shows that detailed calculation models tend to be more accurate than simplified models. This is especially true where two types of calculation methods, such as FEM-SEA or FEM-BEM, have been combined. However, there is an inherent computational cost associated with detailed models. Take, for instance, the example of the FEM models presented in Section 3.3.4. Good agreement was obtained between measurement data and the results of the 2D and 3D FEM models used. The model that best represented the measured data was the full 3D model of a building with structural shafts. However, the computational time to solve this model was approximately 18 hours, compared to 2 hours for a somewhat simpler 3D FEM model.

The results of Sanayei et al.'s (2011 & 2012) impedance-based model presented in Section 3.3.2 suggest that there may be some merit in using a simplified approach to FEM, whilst still obtaining reasonably similar results and significantly reducing computation time. Sanayei et al's model is a rather simplified approach, which models quasi-longitudinal waves propagating in a single column that runs through four floor slabs on top of each other, to simulate a four-storey building. The floor slabs themselves are modelled as thin plates in bending, and in-plane waves are not taken into account. The accuracy of this type of prediction model can be improved by increasing the number of degrees of freedom considered.

In addition to the above, most of the prediction models reviewed included the prediction of ground-borne vibration and structure-borne noise from the source to the receiver, modelling the ground through various means. As the properties of the source (wheel-track interaction, rail roughness, etc.) and of the soil (type(s) of soil, damping characteristics, etc.) are not always known precisely, modelling these components can and does introduce uncertainties into the prediction model, reducing its accuracy. Ideally, the starting point of all models would be to measure the vibration levels generated by the source under consideration at the location of the receiver. However, this would only be possible for existing railway systems. New railway projects would still have to rely on predictions to model source vibration. For vibration propagation through the ground, the transfer function between the source and receiver location for the specific site of the project can be determined from measurements, helping to reduce the uncertainties of the model.

A better alternative to this would be to consider ground-borne vibration and structure-borne noise from the point of entry into the building only. From this point, the materials and their properties, as well as the type of construction used, are known either from design development or historic construction drawings. Although this approach would remove uncertainties related to the source and propagation path altogether, it would rely on vibration measurements at the point of entry into the building. If the building foundations are a ground bearing slab or a raft, this approach would be reasonably straightforward. However, for buildings with piled foundations, either a borehole would be necessary to ascertain the vibration levels that will enter the future building, or measurements can only be undertaken once the piles are in place. In sites where ground-borne vibration and / or structure-borne noise is a concern, waiting to undertake measurements on a pile cap to determine whether vibration isolation measures are required might be too late in the design, and can have severe cost implications and cause delays to the project. This approach would be better suited as a detailed design stage validation tool for assessments carried out in the early stages of a project.

With the above paragraphs in mind, a simplification to Shorter & Langley's (2005) hybrid deterministic-statistical model is proposed for the prediction of structure-borne noise in buildings. The deterministic elements (beams and columns) in the model are proposed to be represented through simple, analytical, mobility / dynamic stiffness beam functions with six degrees of freedom each, while the statistical systems, such as walls and floors, would be modelled with SEA as per Shorter & Langley's (2005) model. This is expected to provide a better representation of the structural frame of a building and its effect on vibration transmission to other elements, compared to Sanayei et al.'s (2011 & 2012) model. In addition to this, modelling walls and floors using SEA will allow their resonant behaviour to be accounted for in contrast with Sanayei et al.'s model. Such approach is also expected to yield more accurate predictions, while keeping the calculation time to a minimum. The model is only proposed to consider vibration from the entry point to a building.

The following chapters provide further details on the stages of the proposed simplified model. Chapter 4 sets out the process for deriving the analytical beam functions used in the proposed model, while the coupling between deterministic elements is discussed in Chapter 5. The results of the proposed deterministic part of the model are validated against FEM in each chapter. Chapter 6 provides a comparison between the various stages of the proposed simplified model and Shorter & Langley's (2005) model.

4 Modelling beams using the dynamic stiffness method

Following the proposal for a simplified hybrid deterministic-statistical model for the prediction of structure-borne noise in buildings in Section 3.5, the present chapter sets out the process through which the modelling of the deterministic elements in Shorter & Langley's (2005) model can be simplified. It includes additional information on the dynamic stiffness approach to modelling deterministic elements, such as beams and columns, along with derivations of the relevant analytical beam mobility functions. In addition to this, the results of the derived functions are validated against a FE model. This chapter relates directly to objective 3 of this thesis.

Beams (and columns) form the base structure of a building. The response of beams to vibration excitation has interested researchers for quite some time, such that plenty of guidance is available. Examples of relevant sources include Graff (1975 / 1991), Cremer et al. (1988) and Fahy & Gardonio (2007), to name a few. Where the term beam is used in the following sections, it refers to beams and columns in buildings.

4.1 Impedance, mobility and dynamic stiffness

The term *impedance* first came into use in the 1880s. This was introduced by Oliver Heaviside and in its early years related mainly to the fields of electricity and electromagnetism. Only in the 1910s, the concept of using impedance to describe vibrating mechanical systems was developed, when Professor Arthur G. Webster realised its potential. (Gardonio & Brennan, 2002)

The mechanical impedance as a function of frequency $Z(\omega)$ of a system is given by Equation 4. 1. This describes how a system resists motion when a force $F(\omega)$ is applied through it.

$$Z(\omega) = \frac{F(\omega)}{v(\omega)} \qquad \text{Equation 4. 1}$$

where

$v(\omega)$ is the resultant velocity across the system.

The inverse of mechanical impedance is mobility, also known as admittance. The mobility as a function of frequency $Y(\omega)$ of a system is defined in Equation 4. 2 and is a representation of how easy it is for a system to admit motion. The relationship between impedance and mobility is given in Equation 4. 3. (Gardonio & Brennan, 2002)

$$Y(\omega) = \frac{v(\omega)}{F(\omega)} \qquad \text{Equation 4. 2}$$

where

$v(\omega)$ is the resultant velocity across the system;

and $F(\omega)$ is the resultant force through the system.

$$Z(\omega) = \frac{1}{Y(\omega)} \qquad \text{Equation 4. 3}$$

For the simple case of a beam on which a shear force and bending moment are applied, as shown in Figure 4. 1, the response of the beam as a function of frequency can be modelled using Equation 4. 4 in terms of impedance, and Equation 4. 5 in terms of mobility, where the numbers shown refer to the relevant points on the beam. (Rubin, 1967; Fahy & Gardonio, 2007) The frequency term (ω) is not shown for simplicity, but it is still included. The concepts and sign convention are illustrated in this section using the example of a beam in bending with two degrees of freedom. The partitioning shown in Equation 4. 4 and Equation 4. 5 helps to identify the excitation and response points on the beam. Different degrees of freedom are included within each partition. Closed form expressions for bending and other degrees of freedom are derived in Section 4.3.

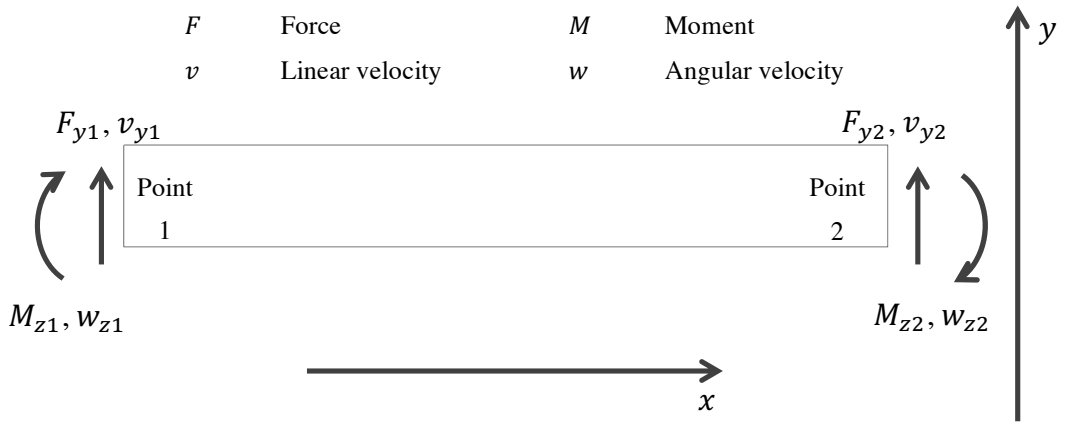

Figure 4. 1 Beam being excited by a shear force and bending moment

$$\begin{bmatrix} F_{y1} \\ M_{z1} \\ F_{y2} \\ M_{z2} \end{bmatrix} = \left[\begin{array}{cc:cc} Z_{F_y1v_y1} & Z_{M_z1v_y1} & Z_{F_y1v_y2} & Z_{M_z1v_y2} \\ Z_{F_y1w_z1} & Z_{M_z1w_z1} & Z_{F_y1w_z2} & Z_{M_z1w_z2} \\ \hdashline Z_{F_y2v_y1} & Z_{M_z2v_y1} & Z_{F_y2v_y2} & Z_{M_z2v_y2} \\ Z_{F_y2w_z1} & Z_{M_z2w_z1} & Z_{F_y2w_z2} & Z_{M_z2w_z2} \end{array}\right] \begin{bmatrix} v_{y1} \\ w_{z1} \\ v_{y2} \\ w_{z2} \end{bmatrix} \quad \text{Equation 4. 4}$$

$$\begin{bmatrix} v_{y1} \\ w_{z1} \\ v_{y2} \\ w_{z2} \end{bmatrix} = \left[\begin{array}{cc:cc} Y_{v_y1F_y1} & Y_{v_y1M_z1} & Y_{v_y1F_y2} & Y_{v_y1M_z2} \\ Y_{w_z1F_y1} & Y_{w_z1M_z1} & Y_{w_z1F_y2} & Y_{w_z1M_z2} \\ \hdashline Y_{v_y2F_y1} & Y_{v_y2M_z1} & Y_{v_y2F_y2} & Y_{v_y2M_z2} \\ Y_{w_z2F_y1} & Y_{w_z2M_z1} & Y_{w_z2F_y2} & Y_{w_z2M_z2} \end{array}\right] \begin{bmatrix} F_{y1} \\ M_{z1} \\ F_{y2} \\ M_{z2} \end{bmatrix} \quad \text{Equation 4. 5}$$

The above equations show a matrix for the impedances and mobilities. These are known as transmission matrices, and they are used to relate the input forces, moments and velocities at one end of the beam to the output at the other end. For instance, $\mathbf{Z}_{12}$ is the impedance at point 1 on the beam from excitation at point 2, while $\mathbf{Z}_{21}$ is the impedance at point 2 on the beam from excitation at point 1. The references to the forces and moments, as well as to the linear and angular velocities have been omitted here for simplicity. From these relations, the following types of impedances and mobilities can be defined (Rubin, 1967):

- **Driving-point, direct or self impedances / mobilities:** impedances and mobilities at an arbitrary point x on a beam from an excitation at point x ($\mathbf{Z}_{11}$, $\mathbf{Z}_{22}$, $\mathbf{Y}_{11}$ and $\mathbf{Y}_{22}$ in the above equations);
- **Transfer, cross or mutual impedances / mobilities:** Impedances and mobilities at an arbitrary point x on a beam from an excitation at point y ($\mathbf{Z}_{12}$, $\mathbf{Z}_{21}$, $\mathbf{Y}_{12}$ and $\mathbf{Y}_{21}$ in the above equations).

When modelling linear, elastic and dissipative structures, as is the case of beams in a building, the impedance and mobility matrices are symmetric. This is a result of the *principle of reciprocity*. Rubin (1967) states that if the total work performed during a given displacement is equal to the product of that displacement with the respective force / moment, reciprocity is true. The effect of reciprocity on the impedance and mobility transmission matrices is highlighted in Equation 4. 6 and Equation 4. 7, respectively.

$$\mathbf{Z}(\omega) = \mathbf{Z}^T(\omega)$$

$$\begin{bmatrix} \mathbf{Z}_{11} & \mathbf{Z}_{12} \\ \mathbf{Z}_{21} & \mathbf{Z}_{22} \end{bmatrix} = \begin{bmatrix} \mathbf{Z}_{11} & \mathbf{Z}_{21} \\ \mathbf{Z}_{12} & \mathbf{Z}_{22} \end{bmatrix}$$

Equation 4. 6

$$\mathbf{Y}(\omega) = \mathbf{Y}^T(\omega)$$

$$\begin{bmatrix} \mathbf{Y}_{11} & \mathbf{Y}_{12} \\ \mathbf{Y}_{21} & \mathbf{Y}_{22} \end{bmatrix} = \begin{bmatrix} \mathbf{Y}_{11} & \mathbf{Y}_{21} \\ \mathbf{Y}_{12} & \mathbf{Y}_{22} \end{bmatrix}$$

Equation 4. 7

In addition to impedance and mobility, the response of a system can also be described in terms of its dynamic stiffness, which in contrast with the previous approaches uses displacement instead of velocity as its starting point. The dynamic stiffness method, also known as the displacement method, looks to determine the overall stiffness matrix for a system based on the stiffness matrix from each individual element of the system. (Rubin, 1967) Shorter & Langley's (2005) model makes use of dynamic stiffness matrices $\mathbf{D}(\omega)$ for both the deterministic and statistical sub-systems. The relationship between these and the impedance and mobility matrices is given by Equation 4. 8. (Fahy & Gardonio, 2007)

$$\mathbf{D}(\omega) = j\omega\, \mathbf{Z}(\omega) = j\omega\, \mathbf{Y}(\omega)^{-\mathbf{1}}$$

Equation 4. 8

The input into the simplified prediction model proposed in this thesis is intended to be the velocity measured at the entry point to the building. The force excitation can then be calculated from the measured velocity levels and the mobility matrix for the whole building.

4.2 Degrees of freedom for free-free beams

As mentioned in Section 2.4.1, there are three main types of waves that propagate through building structures. In beams, these are quasi-longitudinal, torsional and bending waves. Each of these waves and their sub-components consist of a degree of freedom that needs to be considered. Each free end of a beam has six degrees of freedom, three translations and three rotations. These are shown in Figure 4. 2 and Table 4. 1 for clarity.

Whilst it is acknowledged that beams in buildings are not free-free beams, i.e. they are coupled to other elements, free-free finite beams form a suitable building block for the proposed simplified model. Their response can be easily determined from closed form expressions and the effect of coupling them to other beams and elements can be modelled. For instance, when coupling two free-free beams together, the total impedance at the location where the two beams meet will consist of the sum of the impedances at the respective free end of each beam, thus allowing the coupling between elements to be accounted for. (Rubin, 1967) Further details on the effects of coupling free-free beams on their response are provided in Chapter 5.

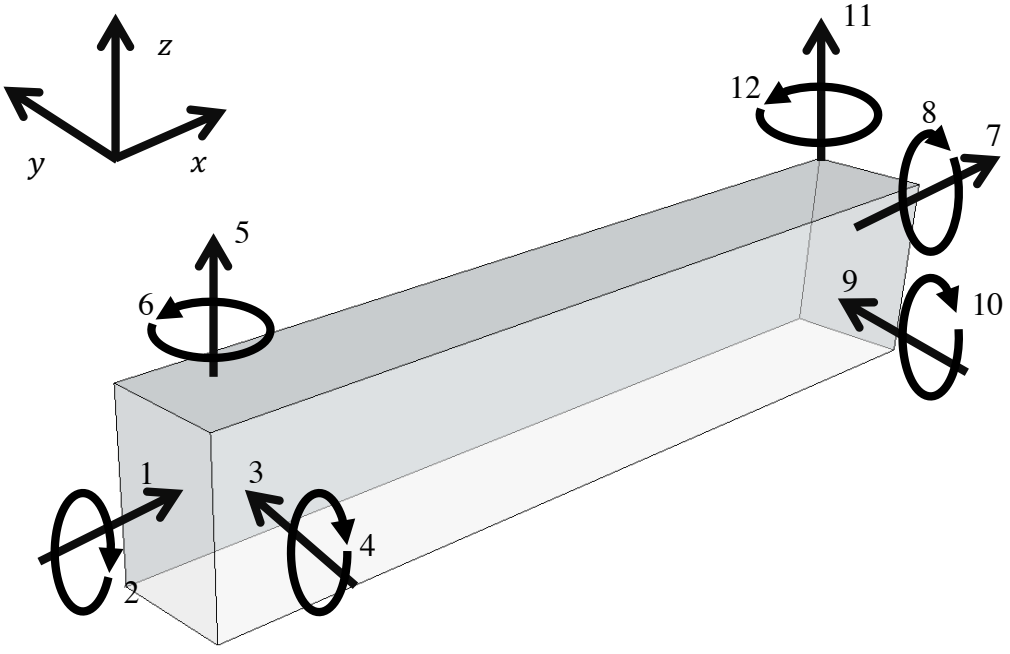

Figure 4. 2 Degrees of freedom at both ends of a free-free beam (refer to Table 4. 1)

Table 4. 1 Degrees of freedom at both ends of a free-free beam (refer to Figure 4. 2)

Reference	Degrees of freedom at both ends of a free-free beam corresponding to Figure 4. 2	
	Translations	Rotations
Quasi-longitudinal waves	1, 7	-
Torsional waves	-	2, 8
Bending waves, y direction	3, 9	4, 10
Bending waves, z direction	5, 11	6, 12

4.3 Free-free beam mobilities

The governing mobility equations for each of the degrees of freedom mentioned above have been derived to allow the beams, and energy transfer between them, to be modelled in the proposed simplified prediction tool. These are set out in the following sections for a beam of finite length. Although quasi-longitudinal and torsional waves may not contribute significantly to direct structure-borne noise radiation into a room, they will propagate to other areas within a building where they may be coupled with bending waves, which will then radiate structure-borne noise as a result of the energy transmitted by quasi-longitudinal and torsional waves. Therefore, the three wave types above have been considered in the analysis that follows.

4.3.1 Quasi-longitudinal waves

The mobilities for a beam subjected to a longitudinal harmonic excitation can be derived from first principles. The procedure used to derive these is described in the following paragraphs, in line with guidance provided by Cremer et al. (1988).

The first step to develop the quasi-longitudinal mobilities for a free-free beam is to determine the displacement caused by the excitation. Assuming the velocity $v(x,t)$ is given by Equation 4. 9, the displacement $\xi(x,t)$ can be found by integrating the velocity with respect to time. A and B are constants that will be determined by the boundary conditions to be applied. c is the constant of integration.

$$v(x,t) = Ae^{j(\omega t - kx)} + Be^{j(\omega t + kx)} \qquad \text{Equation 4. 9}$$

$$\xi(x,t) = \int v(x,t)\,dt = \frac{1}{j\omega}Ae^{j(\omega t - kx)} + \frac{1}{j\omega}Be^{j(\omega t + kx)} + c \qquad \text{Equation 4. 10}$$

The strain ε_x on the beam can be calculated from the displacement with the expression in Equation 4. 11. This can then be used to determine the stress σ_x using the relationship in Equation 4. 12.

$$\varepsilon_x = \frac{\partial \xi}{\partial x} = -\frac{1}{c_L} A e^{j(\omega t - kx)} + \frac{1}{c_L} B e^{j(\omega t + kx)} \quad \text{Equation 4. 11}$$

$$\sigma_x = D\varepsilon_x = -\frac{D}{c_L}\left(A e^{j(\omega t - kx)} - B e^{j(\omega t + kx)}\right) \quad \text{Equation 4. 12}$$

where

c_L is the quasi-longitudinal wave speed in beams (refer to Table 2. 5);

and D is the longitudinal stiffness given by $D = \frac{E(1-\nu)}{(1+\nu)(1-2\nu)}$, where E is the Young's modulus and ν is the Poisson's ratio for the beam.

The stress σ_x is directly proportional to the longitudinal force F. The relation between these two parameters is set out below, where S is the cross-sectional area of the beam.

$$F = -S\sigma_x = \frac{SD}{c_L}\left(A e^{j(\omega t - kx)} - B e^{j(\omega t + kx)}\right) \quad \text{Equation 4. 13}$$

Of the variables given in Equation 4. 9 and Equation 4. 13, A and B are the only unknowns. However, these can be determined following application of the relevant boundary conditions below.

If the beam is excited at $x_0 = 0$, the stresses $\sigma_x(x)$ at both ends of the free-free beam will be as per Equation 4. 14 and Equation 4. 15. Solving the stress equations for F simultaneously (using Equation 4. 13) reveals that the relationship between constants A and B is given by Equation 4. 16, where l is the length of the beam.

$$\sigma_x(0) = -\frac{F}{S} \quad \text{Equation 4. 14}$$

$$\sigma_x(l) = 0 \quad \text{Equation 4. 15}$$

$$B = A\frac{e^{-jkl}}{e^{jkl}} = \frac{A}{\cos 2kl + 2j\cos kl \sin kl} \quad \text{Equation 4. 16}$$

If the beam is excited at $x_0 = l$ instead, the stresses $\sigma_x(x)$ at both ends of the free-free beam will be as per Equation 4. 17 and Equation 4. 18. Solving the stress equations for F simultaneously (using Equation 4. 13 as before) reveals that $A = B$.

$$\sigma_x(0) = 0 \qquad \text{Equation 4. 17}$$

$$\sigma_x(l) = -\frac{F}{S} \qquad \text{Equation 4. 18}$$

Incorporating the expressions for A and B in Equation 4. 9 and Equation 4. 13 and representing these in trigonometric form yields the following mobility expressions, where numbers 1 and 2 represent the two ends of the beam.

$$Y_{L11} = \frac{v_1}{F_1} = \frac{c_L}{jSD}\frac{\cos kl}{\sin kl} \qquad \text{Equation 4. 19}$$

$$Y_{L12} = \frac{v_1}{F_2} = \frac{c_L}{jSD}\frac{1}{\sin kl} \qquad \text{Equation 4. 20}$$

$$Y_{L21} = \frac{v_2}{F_1} = \frac{c_L}{jSD}\frac{1}{\sin kl} \qquad \text{Equation 4. 21}$$

$$Y_{L22} = \frac{v_2}{F_2} = \frac{c_L}{jSD}\frac{\cos kl}{\sin kl} \qquad \text{Equation 4. 22}$$

The mobilities derived above can be arranged in a 2 x 2 matrix, as given by Equation 4. 23, which will feed into the overall mobility matrix for the beam. The subscript L is to indicate that these mobilities are quasi-longitudinal mobilities. While no axis descriptor has been included here, when assembling the overall mobility matrix for the beam, this will need to be included to differentiate between quasi-longitudinal and bending translations.

$$\mathbf{Y}_L = \begin{bmatrix} Y_{L11} & Y_{L12} \\ Y_{L21} & Y_{L22} \end{bmatrix} \qquad \text{Equation 4. 23}$$

4.3.2 Torsional waves

The torsional beam mobilities can be derived in a similar manner to the quasi-longitudinal mobilities above. The main difference between the two derivations is that instead of using linear velocity and force, the angular velocity and moment should be used instead. The following paragraphs are based on the guidance provided in Cremer et al. (1988).

Assuming the angular velocity $w(x,t)$ is given by Equation 4. 24, the angular displacement $\chi(x,t)$ can be found by integrating the angular velocity with respect to time. As before, A and B are constants that will be determined by the boundary conditions to be applied, and c is the constant of integration.

$$w(x,t) = \frac{A}{r}e^{j(\omega t - kx)} + \frac{B}{r}e^{j(\omega t + kx)} \qquad \text{Equation 4. 24}$$

$$\chi(x,t) = \int w(x,t)\,dt = \frac{1}{j\omega r}Ae^{j(\omega t - kx)} + \frac{1}{j\omega r}Be^{j(\omega t + kx)} + c \qquad \text{Equation 4. 25}$$

where

r is the radius of gyration of the beam.

The shear stresses τ and torsional moment M_x on the beam can be calculated from the angular displacement using Equation 4. 26 and Equation 4. 27, respectively.

$$\tau = Gr\frac{\partial \chi}{\partial x} = -\frac{G}{c_T}Ae^{j(\omega t - kx)} + \frac{G}{c_T}Be^{j(\omega t + kx)} \qquad \text{Equation 4. 26}$$

$$M_x = T\frac{\partial \chi}{\partial x} = \frac{T}{G}\tau = -\frac{T}{c_T}Ae^{j(\omega t - kx)} + \frac{T}{c_T}Be^{j(\omega t + kx)} \qquad \text{Equation 4. 27}$$

where

c_T is the torsional wave speed in beams (refer to Table 2. 5 for c_T for rectangular beams);

G is the shear modulus given by $G = \frac{E}{2(1+\nu)}$, where E is the Young's modulus and ν is the Poisson's ratio for the beam;

and T is the torsional stiffness (refer to Table 2. 5 for T for rectangular beams).

A and B are the only unknowns in Equation 4. 26 and Equation 4. 27, which can be determined following application of the relevant boundary conditions below.

If the beam is excited at $x_0 = 0$, the stresses $\tau(x)$ at both ends of the free-free beam will be as per Equation 4. 28 and Equation 4. 29, where l is the length of the beam. Solving the stress equations for M_x simultaneously (using Equation 4. 56) reveals that the relationship between constants A and B is given by Equation 4. 30.

$$\tau(0) = \frac{G}{T} M_x \qquad \text{Equation 4. 28}$$

$$\tau(l) = 0 \qquad \text{Equation 4. 29}$$

$$B = A\frac{e^{-jkl}}{e^{jkl}} = \frac{A}{\cos 2kl + 2j\cos kl \sin kl} \qquad \text{Equation 4. 30}$$

If the beam is excited at $x_0 = l$ instead, the stresses $\tau(x)$ at both ends of the free-free beam will be as per Equation 4. 31 and Equation 4. 32. Solving the stress equations for M_x simultaneously (using Equation 4. 56) reveals that $A = B$.

$$\tau(0) = 0 \qquad \text{Equation 4. 31}$$

$$\tau(l) = \frac{G}{T} M_x \qquad \text{Equation 4. 32}$$

Incorporating the expressions for A and B in Equation 4. 26 and Equation 4. 27 and representing these in trigonometric form yields the following mobility expressions.

$$Y_{T11} = \frac{w_1}{M_1} = \frac{c_T}{jT}\frac{\cos kl}{-\sin kl} \qquad \text{Equation 4. 33}$$

$$Y_{T12} = \frac{w_1}{M_2} = \frac{c_T}{jT}\frac{1}{-\sin kl} \qquad \text{Equation 4. 34}$$

$$Y_{T21} = \frac{w_2}{M_1} = \frac{c_T}{jT}\frac{1}{-\sin kl} \qquad \text{Equation 4. 35}$$

$$Y_{T22} = \frac{w_2}{M_2} = \frac{c_T}{jT}\frac{\cos kl}{-\sin kl} \qquad \text{Equation 4. 36}$$

The mobilities derived above can be arranged in a 2 x 2 matrix, as given by Equation 4. 37, which will feed into the overall mobility matrix for the beam. The subscript T is to indicate that these mobilities are torsional mobilities. While no axis descriptor has been included here, when assembling the overall mobility matrix for the beam, this will need to be included to differentiate between torsional and bending rotations.

$$\mathbf{Y}_T = \begin{bmatrix} Y_{T11} & Y_{T12} \\ Y_{T21} & Y_{T22} \end{bmatrix} \quad \text{Equation 4. 37}$$

4.3.3 Bending waves

Unlike quasi-longitudinal and torsional waves, two degrees of freedom are associated with each bending wave: a translation and a rotation. The translation is represented by a transverse force, i.e. a force perpendicular to the direction of propagation of the wave, while the rotation is represented by a bending moment. The bending translation and rotation are therefore characterised by four parameters. These are the angular velocity w, the bending moment M, transverse force F and linear velocity v. They are related by Equation 4. 38 to Equation 4. 41, as set out by Cremer et al. (1988). As previously noted, bending in a rectangular beam occurs in two directions perpendicular to the direction of propagation. Whilst the orientation changes, the governing equations are the same. In the following equations, x represents the direction of propagation along the length of the beam, y is the horizontal coordinate perpendicular to the direction of propagation and z is the vertical coordinate. These are as shown in Figure 4. 2 for information. ω is the angular frequency, m' is the mass per unit length of the beam and B is its bending stiffness (refer to Table 2. 5 in Section 2.4.1).

$$w_z = \frac{\partial v}{\partial x} \quad \text{Equation 4. 38}$$

$$M_z = -\frac{B}{j\omega}\frac{\partial w}{\partial x} \quad \text{Equation 4. 39}$$

$$F_y = -\frac{\partial M_z}{\partial x} \quad \text{Equation 4. 40}$$

$$v_y = -\frac{1}{j\omega m'}\frac{\partial F_y}{\partial x} \quad \text{Equation 4. 41}$$

The above relations can be used to determine the force, transfer and moment mobilities for a beam in bending. Equation 4. 42 to Equation 4. 45 show how this can be achieved, based on guidance provided by Cremer et al. (1988), Fahy & Gardonio (2007) and Hopkins (2007). The subscripts v, F, w and M on the left hand side of the equations allows the parameters involved in the calculation (linear / angular velocities, force or moment) to be easily recognised. The y and z subscripts relate to the axis on which these parameters act.

Force mobility $$Y_{v_y F_y} = \frac{v_y}{F_y}$$ Equation 4. 42

Transfer mobility $$Y_{v_y M_z} = \frac{v_y}{M_z}$$ Equation 4. 43

Transfer mobility $$Y_{w_z F_y} = \frac{w_z}{F_y}$$ Equation 4. 44

Moment mobility $$Y_{w_z M_z} = \frac{w_z}{M_z}$$ Equation 4. 45

Substituting Equation 4. 38 to Equation 4. 41 into the above, considering a velocity of $v = Ae^{j(\omega t - kx)} + Be^{j(\omega t + kx)}$ where A and B are determined by the boundary conditions of the beam, and solving for $Y_{v_y F_y}$ yields the following relationships between mobilities. As $Y_{v_y F_y}$ is a function of the response position x and the excitation position x_0 on the beam, as well as of the frequency ω, x and x_0 are variables until the response and excitation positions have been fixed. Therefore, derivation with respect to x and x_0 is possible. (Moorhouse, Evans, & Elliott, 2011; Su, 2003) It is worth noting that B in the velocity expression does not refer to the bending stiffness of the beam, but to a variable to be determined by the boundary conditions.

Transfer mobility $$Y_{v_y M_z} = \frac{dY_{v_y F_y}}{dx_0}$$ Equation 4. 46

Transfer mobility $$Y_{w_z F_y} = \frac{dY_{v_y F_y}}{dx}$$ Equation 4. 47

Moment mobility $$Y_{w_z M_z} = \frac{d^2 Y_{v_y F_y}}{dx dx_0}$$ Equation 4. 48

The force mobility for a free-free beam varies depending on where the excitation and response / receiving points (x_0 and x, respectively) are on the beam in relation to its length l. Su (2003) sets out the closed form solutions for the force mobility for a free-free beam. These are provided in Equation 4. 49 and Equation 4. 50, as presented by Su (2003). ω, B and k are the angular frequency, bending stiffness and bending wavenumber.

$$0 \leq x \leq x_0 \qquad Y_{v_y F_y} = \frac{j\omega}{2Bk^3}\left(f_1(x_0)g_1(x) + f_2(x_0)g_2(x)\right) \qquad \text{Equation 4. 49}$$

$$x_0 \leq x \leq l \qquad Y_{v_y F_y} = \frac{j\omega}{2Bk^3}\left(f_1(x)g_1(x_0) + f_2(x)g_2(x_0)\right) \qquad \text{Equation 4. 50}$$

where

$$\begin{aligned} f_1(x) = {} & \cosh kx - \cosh k(l-x)\cos kl \\ & - \sinh k(l-x)\sin kl - \cos kx \\ & + \cos k(l-x)\cosh kl \\ & - \sinh kl \sin k(l-x) \end{aligned} \qquad \text{Equation 4. 51}$$

$$\begin{aligned} f_2(x) = {} & \sinh kx + \sinh k(l-x)\cos kl \\ & - \sin kl \cosh k(l-x) - \sin kx \\ & + \sinh kl \cos k(l-x) \\ & - \cosh kl \sin k(l-x) \end{aligned} \qquad \text{Equation 4. 52}$$

$$g_1(x) = -\frac{\sin kx + \sinh kx}{2(1 - \cosh kl \cos kl)} \qquad \text{Equation 4. 53}$$

$$g_2(x) = \frac{\cos kx + \cosh kx}{2(1 - \cosh kl \cos kl)} \qquad \text{Equation 4. 54}$$

As the prediction model will require beams to be coupled together so that energy transfer across them can be assessed, the response at the two ends of the beam from an excitation at each end needs to be determined. For ease of reference in the following paragraphs, functions $f_1(x)$, $f_2(x)$, $g_1(x)$ and $g_2(x)$ have been simplified to the expressions presented in Table 4. 2.

Table 4. 2 Simplified $f_1(x), f_2(x), g_1(x)$ and $g_2(x)$ functions at each end of the beam

Simplified $f_1(x), f_2(x), g_1(x)$ and $g_2(x)$ functions (refer to Equation 4. 49 and Equation 4. 50)	
$x = 0$	$x = l$
$f_1(0) = -2\sinh kl \sin kl$	$f_1(l) = 2\cosh kl - 2\cos kl$
$f_2(0) = 2\sinh kl \cos kl - 2\sin kl \cosh kl$	$f_2(l) = 2\sinh kl - 2\sin kl$
$g_1(0) = 0$	$g_1(l) = -\dfrac{\sin kl + \sinh kl}{2(1 - \cosh kl \cos kl)}$
$g_2(0) = \dfrac{1}{1 - \cosh kl \cos kl}$	$g_2(l) = \dfrac{\cos kl + \cosh kl}{2(1 - \cosh kl \cos kl)}$

The force mobility at each end of the beam can be found by substituting the simplified expressions given above into Equation 4. 49 and Equation 4. 50. The transfer and moment mobilities at each end can then be derived from the force mobility using the relationships given in Equation 4. 46 to Equation 4. 48. Table 4. 3 and Table 4. 4 present the simplified transfer and moment mobilities for a free-free beam with excitation at $x_0 = 0$ and at $x_0 = l$, respectively.

Table 4. 3 Transfer and moment mobilities for a free-free beam with excitation at $x_0 = 0$ (refer to Equation 4. 50 and Table 4. 4)

Transfer and moment mobilities for a free-free beam with excitation at $x_0 = 0$	
$Y_{v_y M_z} = \dfrac{dY_{v_y F_y}}{dx_0} = \dfrac{d}{dx}\left(\dfrac{j\omega}{2Bk^3}\left(f_1(x)g_1(0) + f_2(x)g_2(0)\right)\right)$ $= -\dfrac{j\omega}{2Bk^2}\dfrac{1}{(1 - \cosh kl \cos kl)}(\cosh kx - \cosh k(l-x)\cos kl$ $- \sinh k(l-x)\sin kl - \cos kx + \cos k(l-x)\cosh kl$ $- \sinh kl \sin k(l-x))$	Equation 4. 55
$Y_{w_z F_y} = \dfrac{dY_{v_y F_y}}{dx} = \dfrac{d}{dx}\left(\dfrac{j\omega}{2Bk^3}\left(f_1(x)g_1(0) + f_2(x)g_2(0)\right)\right)$ $= \dfrac{j\omega}{2Bk^2}\dfrac{1}{(1 - \cosh kl \cos kl)}(\cosh kx - \cosh k(l-x)\cos kl$ $+ \sin kl \sinh k(l-x) - \cos kx + \sinh kl \sin k(l-x)$ $+ \cosh kl \cos k(l-x))$	Equation 4. 56

Transfer and moment mobilities for a free-free beam with excitation at $x_0 = 0$

$$Y_{w_z M_z} = \frac{d^2}{dx dx_0}\left(\frac{j\omega}{2Bk^3}\left(f_1(x)g_1(0) + f_2(x)g_2(0)\right)\right)$$
$$= -\frac{j\omega}{2Bk}\frac{1}{(1-\cosh kl\cos kl)}(\sinh kx + \sinh k(l-x)\cos kl$$
$$+ \cosh k(l-x)\sin kl + \sin kx + \sin k(l-x)\cosh kl$$
$$+ k\sinh kl\cos k(l-x))$$

Equation 4. 57

Table 4. 4 Transfer and moment mobilities for a free-free beam with excitation at $x_0 = l$ (refer to Equation 4. 49 and Table 4. 4)

Transfer and moment mobilities for a free-free beam with excitation at $x_0 = l$

$$Y_{v_y M_z} = \frac{dY_{v_y F_y}}{dx_0} = \frac{d}{dx}\left(\frac{j\omega}{2Bk^3}\left(f_1(l)g_1(x) + f_2(l)g_2(x)\right)\right)$$
$$= \frac{j\omega}{2Bk^3}\frac{1}{2(1-\cosh kl\cos kl)}\big((-\sin kx - \sinh kx)(2k\sinh kl$$
$$+ 2k\sin kl) + (\cos kx + \cosh kx)(2k\cosh kl - 2k\cos kl)\big)$$

Equation 4. 58

$$Y_{w_z F_y} = \frac{dY_{v_y F_y}}{dx} = \frac{d}{dx}\left(\frac{j\omega}{2Bk^3}\left(f_1(l)g_1(x) + f_2(l)g_2(x)\right)\right)$$
$$= \frac{j\omega}{2Bk^3}\frac{1}{2(1-\cosh kl\cos kl)}\big(f_1(l)(-k\cos kx - k\cosh kx)$$
$$+ f_2(l)(-k\sin kx + k\sinh kx)\big)$$

Equation 4. 59

$$Y_{w_z M_z} = \frac{d^2}{dx dx_0}\left(\frac{j\omega}{2Bk^3}\left(f_1(l)g_1(x) + f_2(l)g_2(x)\right)\right)$$
$$= \frac{j\omega}{2Bk^3}\frac{1}{2(1-\cosh kl\cos kl)}\big((-k\cos kx - k\cosh kx)(2k\sinh kl$$
$$+ 2k\sin kl) + (-k\sin kx + k\sinh kx)(2k\cosh kl - 2k\cos kl)\big)$$

Equation 4. 60

The mobilities derived above can be arranged in a 2 x 2 matrix, as given by Equation 4. 61, which will feed into the overall mobility matrix of the beam. Additional information can be added to the matrix by including the excitation and response points as shown in Equation 4. 62. The subscript *B* indicates that these mobilities are bending mobilities. As opposed to the quasi-longitudinal and torsional mobilities derived, the bending mobilities require reference to the coordinate system to be included in the nomenclature, so as to identify which axis the translations and rotations refer to.

$$\mathbf{Y}_B = \begin{bmatrix} \mathbf{Y}_{v_y F_y} & \mathbf{Y}_{v_y M_z} \\ \mathbf{Y}_{w_z F_y} & \mathbf{Y}_{w_z M_z} \end{bmatrix} \qquad \text{Equation 4. 61}$$

$$\mathbf{Y}_B = \begin{bmatrix} Y_{v_y 1 F_y 1} & Y_{v_y 1 F_y 2} & Y_{v_y 1 M_z 1} & Y_{v_y 1 M_z 2} \\ Y_{v_y 2 F_y 1} & Y_{v_y 2 F_y 2} & Y_{v_y 2 M_z 1} & Y_{v_y 2 M_z 2} \\ Y_{w_z 1 F_y 1} & Y_{w_z 1 F_y 2} & Y_{w_z 1 M_z 1} & Y_{w_z 1 M_z 2} \\ Y_{w_z 2 F_y 1} & Y_{w_z 2 F_y 2} & Y_{w_z 2 M_z 1} & Y_{w_z 2 M_z 2} \end{bmatrix} \qquad \text{Equation 4. 62}$$

The results of the mobility formulations for quasi-longitudinal, torsional and bending waves in beams are presented in Section 4.4.

4.4 Results and validation of beam mobilities

The mobilities for a finite beam free at both ends derived in Section 4.3 have been modelled in MATLAB and compared against known expressions for infinite beams. In addition to this, a finite element (FE) model has also been built in COMSOL and its results compared with those from the derived mobilities. The following sections provide a summary of the parameters used in each model, as well as a comparison of their results.

The code used to model the beam mobilities in MATLAB is provided in Appendix C.

4.4.1 Model parameters

Concrete is one of the most common construction materials found in buildings, and was the material chosen for the beam being modelled. Its density and other properties are highly dependent on the mix of materials used during the manufacturing process and can vary significantly. It is therefore important to clarify the material properties used in the MATLAB and COMSOL models. These are summarised in Table 4. 5.

It is also worth confirming the notation used for the mobilities in the following sections. Whilst the present chapter is only concerned with the mobilities for a single beam, Chapter 5 will include the response of various beams in the same calculation and therefore details such as the beam reference and the number of nodes on the beam will need to be included in the mobility subscripts. For consistency with Chapter 5, the same approach has been followed here, where the response of a beam A has been modelled at points 1A and 2A, as shown in Figure 4. 3.

Table 4. 5 Beam parameters used in MATLAB and COMSOL models (Hopkins, 2007)

Parameter	Value
Beam dimensions (L x W x H)	4 m x 0.2 m x 0.3 m
Density, ρ [1]	2200 kg/m^3
Young's modulus, E (refer to Section 4.4.1.1) [1]	27×10^{-9} Pa
Poisson's ratio, ν [1]	0.2
Internal loss factor, η [2]	0.05
Frequency range	1 – 5000 Hz

[1] Values for density and Poisson's ratio are as provided in Hopkins (2007). The base value for the Young's modulus is as given in BS EN 1992-1-1:2004 *Eurocode 2: Design of concrete structures – Part 1-1: general rules and rules for buildings* (CEN, 2004).

[2] Although Hopkins (2007) states that dense concrete has an internal loss factor of 0.005, beams in buildings will be coupled to other elements and the damping of these elements will be much greater. A higher internal loss factor has therefore been used to represent these additional coupling losses.

The shear modulus used in the models was calculated using Equation 2. 8.

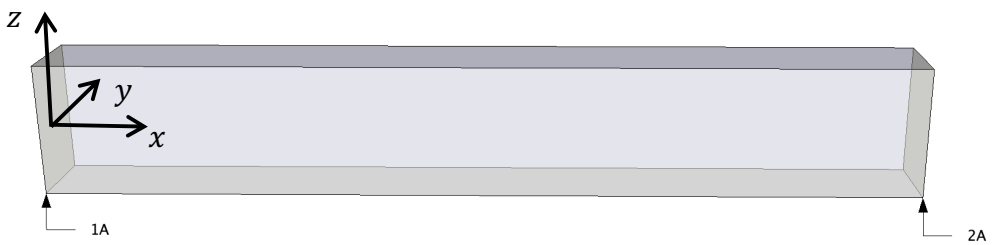

Figure 4. 3 Sketch showing reference points in the beam and coordinate axes

4.4.1.1 Damping

As mentioned in Section 2.4.4, the effect of damping in a structure can be accounted for by applying a hysteretic damping model to the calculations. This uses a complex modulus of elasticity which accounts for the internal loss factors of the materials used and allows the model to be simplified when working in the frequency domain. (ANC, 2012; Cremer et al., 1988)

The complex modulus of elasticity in the analytical and FE models has been taken as $27 \times 10^{-9}(1 + j0.05)$ Pa. The use of such parameter will allow the decay of energy with frequency in the beam to be evaluated.

The use of damping as part of the models will also aid with the validation of the mobility functions derived. The predicted mobilities with damping included will converge towards the mobilities of an infinite beam, allowing conclusions to be drawn on whether the results of the analytical model are as would be expected.

4.4.1.2 FEM assumptions

In addition to the parameters described above, a number of assumptions were made in the FE model to allow the beam to be modelled. These are described in the following paragraphs.

Numerous theories for the response of beams in bending are available, the most common of which are Euler-Bernoulli's and Timoshenko's theories. COMSOL offers both of these as options to model a beam. The main assumptions of Euler-Bernoulli's beam theory are that the cross-section of the beam is infinitely rigid in its plane, and that when a transverse force is applied to a beam, the cross-section of the beam will remain plane and perpendicular to the central axis of the beam at any given point. (Bauchau & Craig, 2009) Timoshenko's beam theory, on the other hand, assumes that the cross-section of the beam rotates in relation to its central axis when a transverse force is applied to it, i.e. the cross-section remains perpendicular to the original central axis of the beam before a transverse force was applied. This rotation is a result of the shear deformation that occurs when a transverse force is applied to the beam. (Han, Benaroya, & Wei, 1999) Both theories have their own limitations and are used to model different scenarios. While Euler-Bernoulli's theory does not take rotation of the beam cross-section into account, such rotation will only be significant under severe bending. In addition to this, when choosing between Euler-Bernoulli's and Timoshenko's beam theories consideration also needs to be given to the frequency

dependency of the two theories and of their group velocities. Wang & Hopkins (2016) have shown that as frequency increases, so do the differences between Euler-Bernoulli and Timoshenko group velocities. The effects of rotatory inertia and shear deformation become significant with increased frequency, causing the Timoshenko group velocities to be lower than those of Euler-Bernoulli theory. The latter tend to increase continuously with frequency, while the Timoshenko group velocities flatten out. However, as the mobility matrices have been derived based on Euler-Bernoulli's theory, this was used in the FE model. Additional information on these and other beam theories can be found in works such as Timoshenko & Goodier (1970), Han et al. (1999) and Bauchau & Craig (2009).

In addition to this, the geometry of the beam was modelled using a Bézier polygon, which allows the beam to be modelled as a sequence of connected line segments with cross-section dimensions added later in the calculation process. (COMSOL Multiphysics, 2018) The beam was modelled using 1D elements with excitation and response points along the central axis of the beam.

An extra fine mesh was used to model the beam. As the purpose of the FE model is to validate the results of the predicted mobilities at each end of the beam at low frequencies, rather than to predict the response at multiple points in the centre of the beam, the number of elements used in the calculation was limited to 20. Based on a beam length of 4 m, as mentioned in Table 4. 5, each element on the beam is 0.2 m long.

The accuracy of FE models is dictated by the size of the finite elements in relation to frequency. Suitable element sizes can be determined through an iterative process in which their size is reduced until a suitable level of convergence towards a solution is found. Hopkins (2007) states that suitable element sizes typically vary between $\frac{\lambda}{3}$ and $\frac{\lambda}{6}$. At frequencies above which the element sizes are greater than $\frac{\lambda}{6}$, discretisation errors may occur in the FE model and as such, the results at these frequencies may not be as accurate. As the wave speeds for longitudinal, torsional and the two bending degrees of freedom considered are different, and as the bending wave speeds are frequency dependent, the cut-off frequencies for each wave type vary. The cut-off frequencies for each wave type, along with the approximate element size in relation to the wavelength at the lowest cut-off frequency for 0.2 m long elements are shown in Table 4. 6. Based on these, element sizes of 0.2 m allowed the response at each end of

the beam to be accurately predicted at the frequencies of interest without significantly increasing the calculation time of the model. However, it is worth noting that the results in the sections that follow are presented up to 5000 Hz to allow consistency in the display of the results despite the various cut-off frequencies. It should be noted that the results above the cut-off frequencies shown in Table 4. 6 for the FE model may not be accurate as the element size exceeds $\frac{\lambda}{6}$.

Table 4. 6 Approximate element size in relation to wavelength

Degree of freedom	Frequency at which element size corresponds to $\frac{\lambda}{6}$ (Hz)	Approximate element size in relation to wavelength at lowest cut-off frequency (883 Hz)
Quasi-longitudinal	2922	0.05λ
Torsional	1606	0.09λ
Bending along the y-axis	883	$0.17\lambda \approx \frac{\lambda}{6}$
Bending along the z-axis	1325	0.14λ

As the mobilities in Section 4.3 were derived in the frequency domain, the FE model has also been built in the frequency domain. Both ends of the beam were modelled as free to match the assumptions of the derived analytical mobility functions. The various mobilities were calculated in the FE model by applying a 1 N force or 1 Nm moment harmonic excitation to the relevant end of the beam and using the relationship between mobility, force, moment, and linear and angular velocity given in Equation 4. 63 to Equation 4. 66.

$$Y_{vF}(\omega) = \frac{v(\omega)}{F(\omega)} \qquad \text{Equation 4. 63}$$

$$\text{when } F(\omega) = 1N, Y_{vF}(\omega) = v(\omega)$$

$$Y_{vM}(\omega) = \frac{v(\omega)}{M(\omega)} \qquad \text{Equation 4. 64}$$

$$\text{when } M(\omega) = 1Nm, Y_{vM}(\omega) = v(\omega)$$

$$Y_{wF}(\omega) = \frac{w(\omega)}{F(\omega)} \qquad \text{Equation 4. 65}$$

$$\text{when } F(\omega) = 1N, Y_{wF}(\omega) = w(\omega)$$

$$Y_{wM}(\omega) = \frac{w(\omega)}{M(\omega)} \qquad \text{Equation 4. 66}$$

$$\text{when } M(\omega) = 1Nm, Y_{wM}(\omega) = w(\omega)$$

The results of the analytical mobility function and FE models for quasi-longitudinal, torsional and bending waves are presented in the following sections.

4.4.2 Quasi-longitudinal mobilities

The quasi-longitudinal driving point and transfer force mobilities predicted at both ends of the free-free beam described in Section 4.4.1 are shown in Figure 4. 4 and Figure 4. 5, respectively, where:

- Y_{L1A1A} is the driving point mobility at point 1A from excitation at point 1A. As the beam is symmetric, the driving point mobility at point 2A from excitation at point 2A (Y_{L2A2A}) is equal to Y_{L1A1A};
- Y_{L1A2A}. is the transfer mobility at point 1A from excitation at point 2A. As the beam is symmetric, the transfer mobility at point 2A from excitation at point 1A (Y_{L2A1A}) is equal to Y_{L1A2A}.

The results of the FE model and a comparison with the quasi-longitudinal driving point mobility for a semi-infinite beam are also provided.

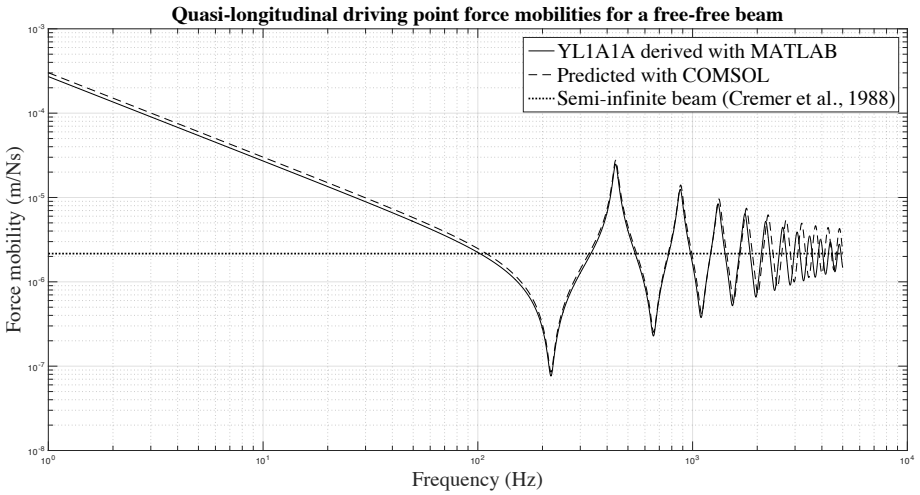

Figure 4. 4 Quasi-longitudinal driving point force mobilities at one end of a free-free beam

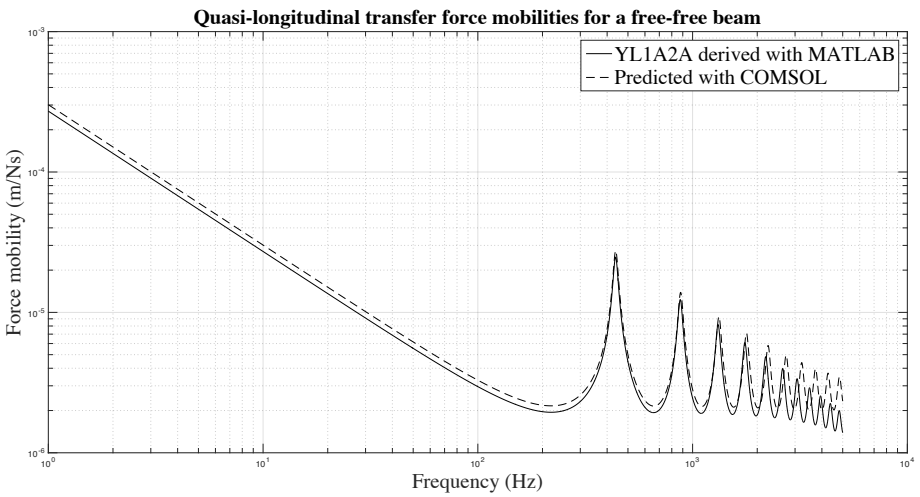

Figure 4. 5 Quasi-longitudinal transfer force mobilities at one end of a free-free beam

Figure 4. 4 shows that at frequencies of up to approximately 220 Hz, the response of the beam is controlled by its mass and energy decays at a rate of 6 dB per octave. As frequency increases, however, the behaviour of the beam starts to be affected by its damping. The latter causes the amplitude of the resonant and anti-resonant peaks to reduce with frequency.

Cremer et al. (1988) provide closed form expressions for the driving point impedance of infinite and semi-infinite beams excited by various wave types. The quasi-longitudinal impedance for a semi-infinite beam with excitation at one end has been converted into mobility and plotted against the results of the MATLAB model given in Figure 4. 4. As the frequency increases and the response of the beam is affected by damping, the mobility of the finite beam converges to that of the semi-infinite beam as would be expected.

Good agreement was also found between the analytical and FE models. The results of the latter follow the outline of the analytical model, albeit with small differences as can be seen in Figure 4. 4 and Figure 4. 5. The resonant and anti-resonant peaks of both models are congruent in both frequency and magnitude. However, as frequency increases, the discrepancies between the analytical and FE models become more apparent. The use of a finer mesh in the FE model would likely be required to reduce these discrepancies.

The quasi-longitudinal transfer mobilities shown in Figure 4. 5 indicate a similar beam behaviour as noted for the driving point mobilities at low frequencies. At mid to high frequencies, a notable difference between the driving point and transfer mobilities is the lack of anti-resonant peaks. Also, as frequency increases, so does the difference between the results of the FE and analytical models.

Another point worth noting is the confirmation of the principle of reciprocity in the mobility matrices, as mentioned by Rubin (1967). While not shown in Figure 4. 5, reciprocity was found between the derived transfer mobilities from excitation at the opposite ends of the beam, i.e. $Y_{L1A2A} = Y_{L2A1A}$.

4.4.3 Torsional mobilities

Similarly to the quasi-longitudinal mobilities, the torsional driving point and transfer moment mobilities predicted at both ends of the free-free beam are shown in Figure 4. 6 and Figure 4. 7, respectively, where:

- Y_{T1A1A} is the driving point mobility at point 1A from excitation at point 1A;
- Y_{T2A2A}. is the driving point mobility at point 2A from excitation at point 2A;
- Y_{T1A2A}. is the transfer mobility at point 1A from excitation at point 2A;
- Y_{T2A1A}. is the transfer mobility at point 2A from excitation at point 1A.

The results of the FE model and a comparison with the torsional driving point mobility for a semi-infinite beam are also provided.

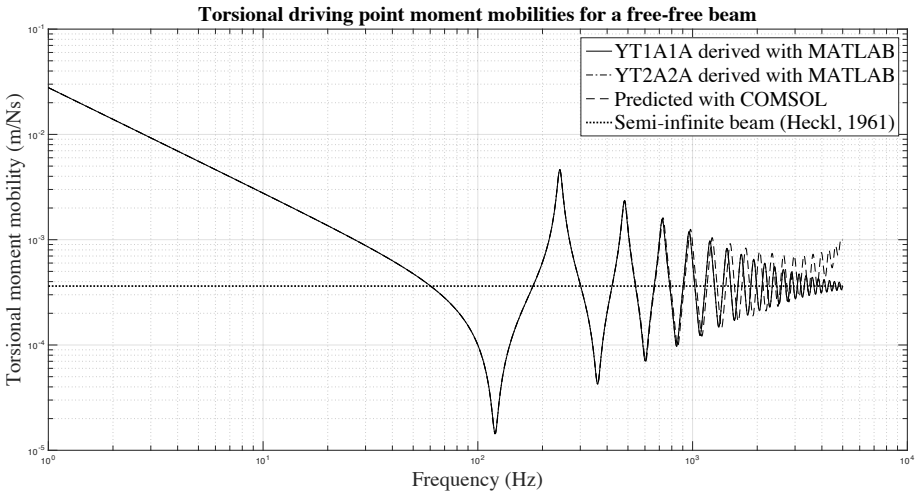

Figure 4. 6 Torsional driving point moment mobilities at the two ends of a free-free beam

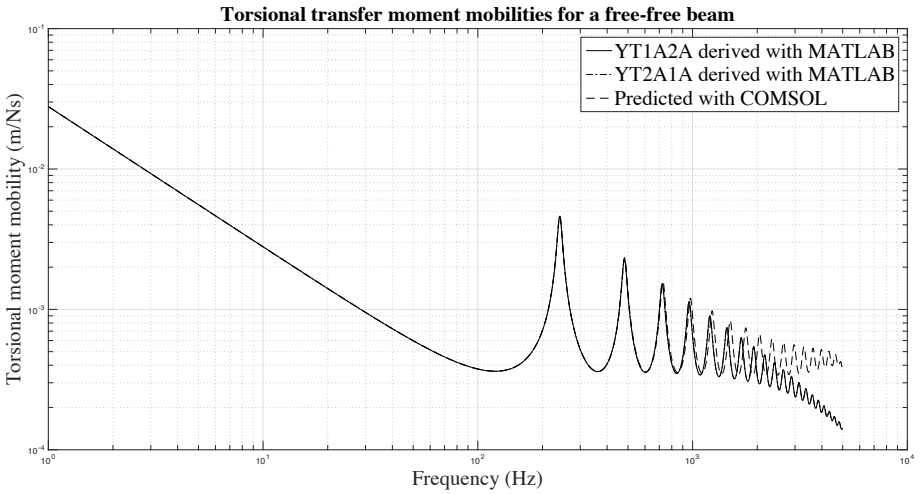

Figure 4. 7 Torsional transfer moment mobilities at the two ends of a free-free beam

The response of the beam when excited by a torsional moment differs from when it is excited by a longitudinal force, as can be seen when comparing Figure 4. 4 and Figure 4. 6. In the latter, the mass controlled region seems to have reduced to frequencies up to approximately 140 Hz where the first resonance occurs. A similar decay of 6 dB per doubling of frequency, as for the quasi-longitudinal driving point mobilities, is present in the torsional driving point mobilities.

Comparing the predicted torsional driving point mobilities for a finite beam given in Figure 4. 6 with that calculated for a semi-infinite beam with excitation at one end based on Heckl (1961) reveals the effect of damping on the response of the beam. As before, the torsional driving point mobilities for the finite beam show the expected trend by tending to the driving point mobility for the semi-infinite beam as the frequency increases.

A comparison between the FE model results and the analytical mobilities shows good agreement between the two models at low and mid frequencies. However, at high frequencies, the differences between the analytical and FE models become more apparent. For the driving point mobilities, the FE model predicts an increase in mobility at high frequencies which is not matched by the predictions from the analytical model. This discrepancy can potentially be attributed to the fact that a finer mesh may be needed in the FE model to calculate the system response at high frequencies with a minimum degree of certainty. A similar scenario can be seen in the transfer mobilities shown in Figure 4. 7, where the mobilities calculated with the analytical model decay significantly at high frequencies when compared to the FE

model. A combination of the level of detail in the FE model used and potential numerical errors in the analytical solution may be the cause of these discrepancies.

The principle of reciprocity in the mobility matrices can also be seen in Figure 4. 7, the derived transfer mobilities from excitation at the opposite ends of the beam yield the same results, i.e. $Y_{T1A2A} = Y_{T2A1A}$.

4.4.4 Bending mobilities – bending along the y-axis

As mentioned in Sections 2.4 and 4.3, bending in beams can occur in two directions perpendicular to the longitudinal axis of the beam. The driving point and transfer force and moment mobilities predicted at both ends of the free-free beam in bending along the y-axis are shown in Figure 4. 8 to Figure 4. 11 where:

- $Y_{vy1AFy1A}$ is the driving point force mobility at point 1A from excitation at point 1A;
- $Y_{vy2AFy2A}$ is the driving point force mobility at point 2A from excitation at point 2A;
- $Y_{vy1AFy2A}$ and $Y_{vy2AFy1A}$ are the transfer force mobilities at point 1A from excitation at point 2A and vice-versa;
- $Y_{wz1AMz1A}$ is the driving point moment mobility at point 1A from excitation at point 1A;
- $Y_{wz2AMz2A}$ is the driving point moment mobility at point 2A from excitation at point 2A;
- $Y_{wz1AMz2A}$ and $Y_{wz2AMz1A}$ are the transfer moment mobilities at point 1A from excitation at point 2A and vice-versa.

The results of the FE model and a comparison with the bending driving point mobility for a semi-infinite beam are also provided.

The results of the analytical and FE models for a free-free beam in bending along the z-axis are included in Appendix A for completeness. However, as the results are very similar to those along the y-axis, no discussion has been included in the appendix. Reference should be made to the discussion in this section instead.

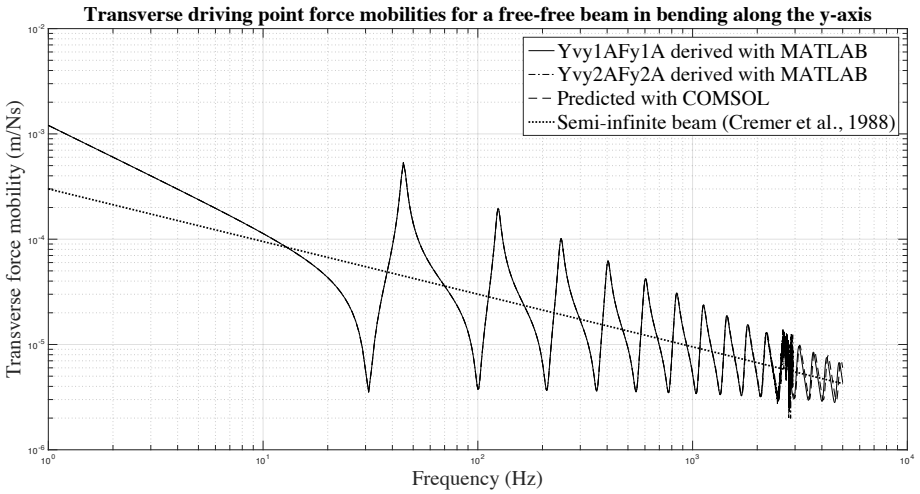

Figure 4. 8 Transverse driving point force mobilities for a free-free beam in bending along the y-axis

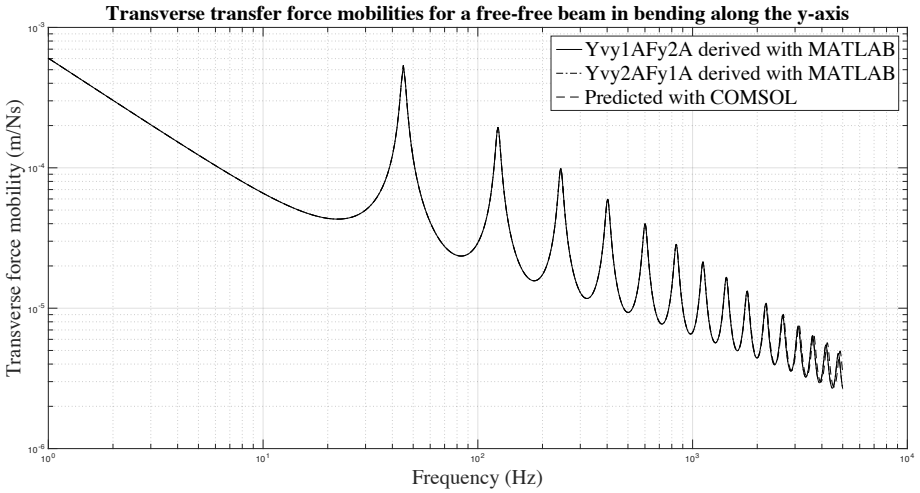

Figure 4. 9 Transverse transfer force mobilities for a free-free beam in bending along the y-axis

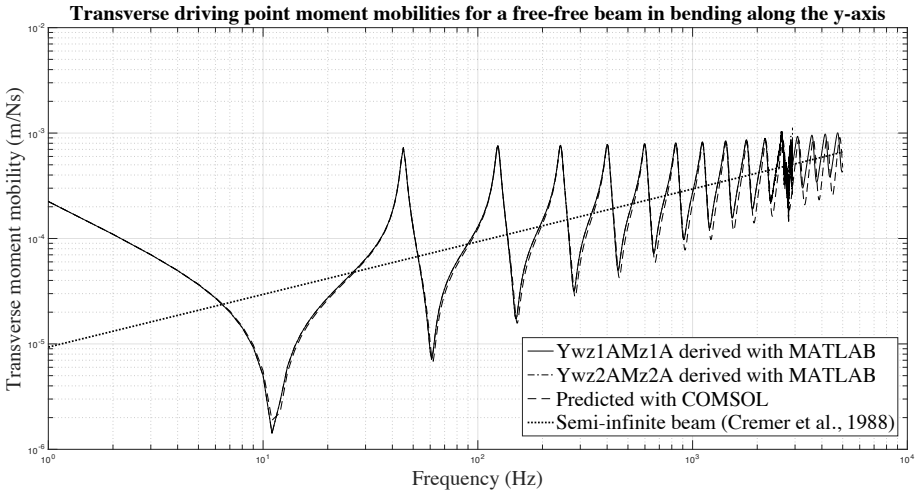

Figure 4. 10 Transverse driving point moment mobilities for a free-free beam in bending along the y-axis

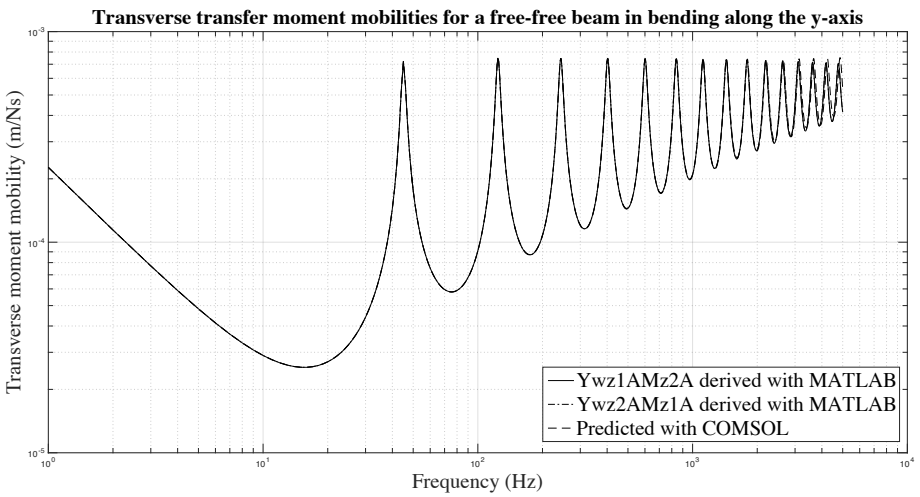

Figure 4. 11 Transverse transfer moment mobilities for a free-free beam in bending along the y-axis

The conclusions to be drawn from the results of the bending mobilities are similar to those for the quasi-longitudinal and torsional beam mobilities. The behaviour of the beam at low frequencies is controlled by its mass up until the first resonance. The frequency of this resonance varies depending on which beam dimension and degree of freedom is considered.

The effect of damping on the response of the beam becomes evident as the frequency increases and the driving point force and moment mobilities shown in Figure 4. 8 and Figure 4. 10 converge towards the driving point force and moment mobilities of a semi-infinite beam excited at one end. These were calculated based on the impedances given in Cremer et al. (1988).

In addition to the above, good agreement was found between the driving point and transfer bending mobilities in the analytical and FE models. The results of the latter follow the contours of the analytical model reasonably accurately as can be seen in Figure 4. 8 to Figure 4. 11. At high frequencies, the differences between the results of the FE and analytical models become somewhat more noticeable. Assembling a more detailed FE model would likely limit the small differences at high frequencies.

The driving point force and moment mobilities in Figure 4. 8 and Figure 4. 10 predicted using the analytical model exhibit what seems to be a numerical error at high frequencies. Such errors are often small and, in the frequency range in which they occur, of little interest. As good agreement was found between the analytical and FE models at the frequencies of interest, as well as between these and the mobility matrix for a semi-infinite beam in bending, the numerical errors shown (maximum

normalized error of 6 dB for the driving point force mobilities and 4 dB for the driving point moment mobilities) are considered to be acceptable.

As with the quasi-longitudinal and torsional transfer mobilities, the symmetry of the mobility matrices is clear such that the derived transfer mobilities from excitation at the opposite ends of the beam yield the same results, i.e. $Y_{vy1AFy2A} = Y_{vy2AFy1A}$ and $Y_{wz1AMz2A} = Y_{wz2AMz1A}$. Similar relationships were found between the transfer mobilities $Y_{vy1AMz1A} = Y_{wz1AFy1A}$, $Y_{vy1AMz2A} = Y_{wz1AFy2A}$, $Y_{vy2AMz1A} = Y_{wz2AFy1A}$ and $Y_{vy2AMz2A} = Y_{wz2AFy2A}$.

4.4.5 Computation time

Part of the reason for the proposal to simplify Shorter & Langley's FE-SEA structure-borne noise prediction model (2005) relates to the often high computation costs associated with FE models. It is therefore considered appropriate to present a comparison of the computation time taken for analytical and FE models to run. This can be found in Table 4. 7.

Table 4. 7 Comparison of computation times of the analytical and FE models

	Computation time of each model	
	Analytical beam functions (MATLAB)	FE model (COMSOL)
Quasi-longitudinal mobilities	14 seconds	1 minute 17 seconds
Torsional mobilities	15 seconds	1 minute 23 seconds
Bending mobilities along the y- and z-axes	20 seconds	5 minutes 28 seconds

While the difference in time taken to run the models is clear from the table, it should also be noted that the set up of the FE model plays an important part on the computation time. For instance, if the number of elements on the beam and the mesh size were optimised, the times shown in Table 4. 7 for the FE model would likely be shorter and more in line with the analytical model. However, as the larger differences between the results of the analytical and FE models were noted to be at high frequencies, reducing the detail of the FE model might also impact on the overall accuracy at low and mid frequencies.

4.5 Combined mobility matrix for a free-free beam

The mobility matrices derived in Section 4.3 and validated in Section 4.4 have been assembled into one large matrix that contains the driving point and transfer force and moment mobilities for the two ends of a free-free beam. The assembled matrix is provided in Equation 4. 67 and is a result of numerous iterations to allow the various degrees of freedom of the beams to be coupled correctly in Chapter 5. This matrix includes the mobilities for the beam in bending along the y- and z-axes.

$$\mathbf{Y} = \begin{bmatrix} \mathbf{Y}_{1A1A} & \mathbf{Y}_{1A2A} \\ \mathbf{Y}_{2A1A} & \mathbf{Y}_{2A2A} \end{bmatrix} \quad \text{Equation 4. 67}$$

$$\mathbf{Y}_{1A1A} = \begin{bmatrix} Y_{Lx1A1A} & 0 & 0 & 0 & 0 & 0 \\ 0 & Y_{Tx1A1A} & 0 & 0 & 0 & 0 \\ 0 & 0 & Y_{v_y1AF_y1A} & Y_{v_y1AM_z1A} & 0 & 0 \\ 0 & 0 & Y_{w_z1AF_y1A} & Y_{w_z1AM_z1A} & 0 & 0 \\ 0 & 0 & 0 & 0 & Y_{v_z1AF_z1A} & Y_{v_z1AM_y1A} \\ 0 & 0 & 0 & 0 & Y_{w_y1AF_z1A} & Y_{v_y1AF_y1A} \end{bmatrix} \quad \text{Equation 4. 68}$$

$$\mathbf{Y}_{1A2A} = \begin{bmatrix} Y_{Lx1A2A} & 0 & 0 & 0 & 0 & 0 \\ 0 & Y_{Tx1A2A} & 0 & 0 & 0 & 0 \\ 0 & 0 & Y_{v_y1AF_y2A} & Y_{v_y1AM_z2A} & 0 & 0 \\ 0 & 0 & Y_{w_z1AF_y2A} & Y_{w_z1AM_z2A} & 0 & 0 \\ 0 & 0 & 0 & 0 & Y_{v_z1AF_z2A} & Y_{v_z1AM_y2A} \\ 0 & 0 & 0 & 0 & Y_{w_y1F_z2} & Y_{v_y1AF_y2A} \end{bmatrix} \quad \text{Equation 4. 69}$$

$$\mathbf{Y}_{2A1A} = \begin{bmatrix} Y_{Lx2A1A} & 0 & 0 & 0 & 0 & 0 \\ 0 & Y_{Tx2A1A} & 0 & 0 & 0 & 0 \\ 0 & 0 & Y_{v_y2AF_y1A} & Y_{v_y2AM_z1A} & 0 & 0 \\ 0 & 0 & Y_{w_z2AF_y1A} & Y_{w_z2AM_z1A} & 0 & 0 \\ 0 & 0 & 0 & 0 & Y_{v_z2AF_z1A} & Y_{v_z2AM_y1A} \\ 0 & 0 & 0 & 0 & Y_{w_y2AF_z1A} & Y_{v_y2AF_y1A} \end{bmatrix} \quad \text{Equation 4. 70}$$

$$\mathbf{Y}_{2A2A} = \begin{bmatrix} Y_{Lx2A2A} & 0 & 0 & 0 & 0 & 0 \\ 0 & Y_{Tx2A2A} & 0 & 0 & 0 & 0 \\ 0 & 0 & Y_{v_y2AF_y2A} & Y_{v_y2AM_z2A} & 0 & 0 \\ 0 & 0 & Y_{w_z2AF_y2A} & Y_{w_z2AM_z2A} & 0 & 0 \\ 0 & 0 & 0 & 0 & Y_{v_z2AF_z2A} & Y_{v_z2AM_y2A} \\ 0 & 0 & 0 & 0 & Y_{w_y2AF_z2A} & Y_{v_y2AF_y2A} \end{bmatrix} \quad \text{Equation 4. 71}$$

With the quasi-longitudinal, torsional and bending mobilities for a free-free beam derived and validated, and with the overall mobility matrix for the beam assembled, the next step in simplifying Shorter & Langley's (2005) model is to couple the deterministic elements of the system together using the derived mobility matrices. The following chapter discusses the coupling of beams further.

5 Coupling of beams using mobility functions

With the analytical beam mobilities derived in Chapter 4, the next step in the assembly of the simplified model is to couple the deterministic elements together. The process through which beams can be coupled using the derived mobility functions is set out in this chapter. This includes a description of the required coordinate system, the methodology for coupling beams, a summary of the results obtained and validation of these against a FE model. This chapter relates directly to objective 4 of this thesis.

5.1 Coordinate system

When coupling structures and degrees of freedom together, care must be taken to ensure the correct system coordinates are used. This is especially important when the structures to be connected are at different orientations to each other and multiple degrees of freedom are being modelled. It is often useful to develop global and local coordinate systems. For instance, when considering a building with a large number of beams at different angles to each other, a local coordinate system would help with calculations within that system and would avoid the need to identify the location of a particular component in a large global coordinate system. The following paragraphs provide details of the coordinate system and notation used when coupling beams together.

Clearly defining the global and local axes to be used is key to set up the coordinate system correctly. Global axes relate to the overarching coordinates and orientation of the system. In the case of a building with a rectangular footprint, the horizontal axes X and Y would typically relate to the length and width of the building, while the Z axis would relate to its height. A similar principle can be applied to the local coordinate axes, but instead of relating them to the building, they would refer to the axes of each element. For example, for a beam, the x and y axes typically refer to the beam's length and width, while the z axis often refers to its height. As beams and columns in buildings are characteristically at different orientations, the local axes for a beam would differ from those of a column. However, the global axes would be the same for both elements.

To distinguish between global and local axes, different notation is needed. In the sections that follow, the global axes are shown and referred to in upper case letters X, Y and Z, while the local axes make use of lower case letters x, y and z. This notation has been adopted in the following sections to couple beams together.

Figure 5. 1 illustrates the global and local axes for beams A and B in an L-junction, i.e. at 90° to each other. It can be seen that the local x axis in beam A is equivalent to the $-z$ axis in beam B, and that the z axis in beam A is equivalent to the x axis in beam B. However, as beam B is only rotated by 90° in relation to beam A on the XZ plane, the orientation of the local y axes of both beams coincides.

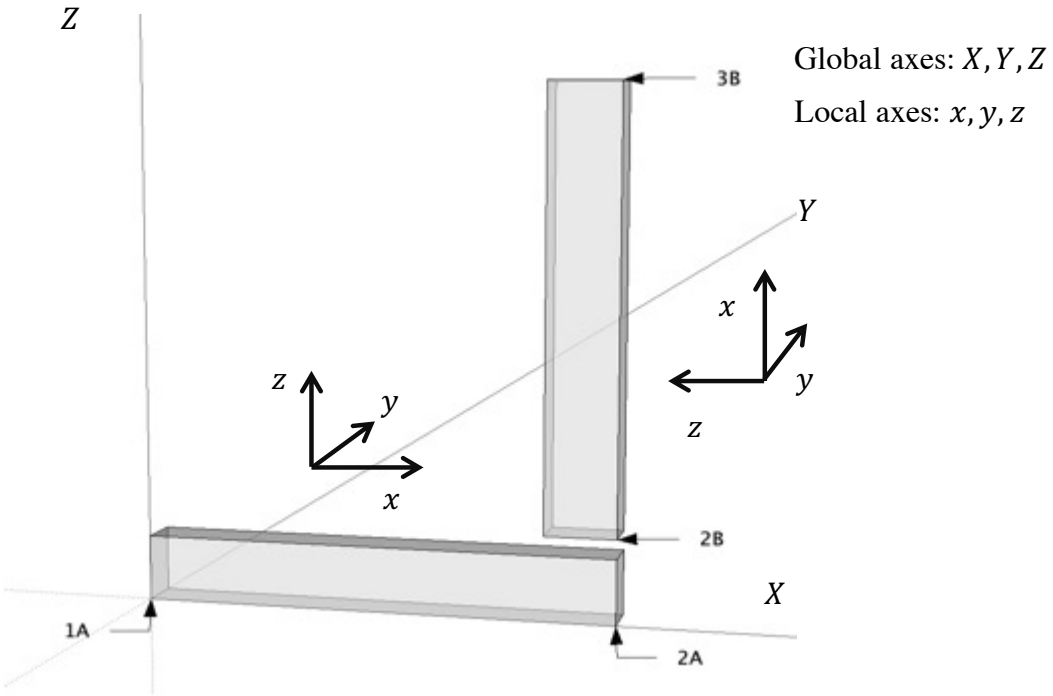

Figure 5. 1 Sketch showing an example of the local and global coordinate systems for two beams at 90° to each other

With the global and local axes and their notation defined above, the next step in the simplification of Shorter & Langley's model is to develop a strategy to couple the deterministic elements of a building together. This is set out in the following sections.

5.2 Methodology for coupling beams

The coupling between beams, columns and plates in buildings is key to maintain their structural integrity. When modelling buildings, such coupling can be accounted for in different ways, depending on the modelling method being used. The proposed simplified model makes use of a dynamic stiffness approach to model beams and columns within a building and their response has been derived in terms of mobility. However, mobilities are often used to describe the overall response of a system, and when considering the connection between structures and small segments, the use of impedances may be more suitable. (O'Hara, 1967) It is therefore considered appropriate to use impedance addition to model the coupling between these elements. The following paragraphs set out the method used to couple beams together.

Rubin (1967) provides guidance on how to couple various elements together using the impedance addition method. The main assumption needed to model the coupling between two (or more) elements is that the velocities at the interface between the elements must be the same, and the forces must be in equilibrium. In the case of two beams A and B coupled in a straight line at point 2, as shown in Figure 5. 1, the following conditions need to be realised at the connection point / junction between elements for the system to be in equilibrium.

$$\mathbf{v} = \mathbf{v}_{2A} = \mathbf{v}_{2B} \qquad \text{Equation 5. 1}$$

$$\mathbf{F} = \mathbf{F}_{2A} + \mathbf{F}_{2B} \qquad \text{Equation 5. 2}$$

The impedances on both sides of the junction can be calculated from $\mathbf{F}_{2A} = \mathbf{Z}_{2A}\mathbf{v}_{2A}$ and $\mathbf{F}_{2B} = \mathbf{Z}_{2B}\mathbf{v}_{2B}$. Substituting the conditions in Equation 5. 1 and Equation 5. 2 into these expressions yields the relationship given in Equation 5. 3. This shows that the impedance at a junction between two beams is given by the sum of the impedances of each of the beams at the connection point.

$$\mathbf{F} = (\mathbf{Z}_{2A} + \mathbf{Z}_{2B})\mathbf{v} \qquad \text{Equation 5. 3}$$

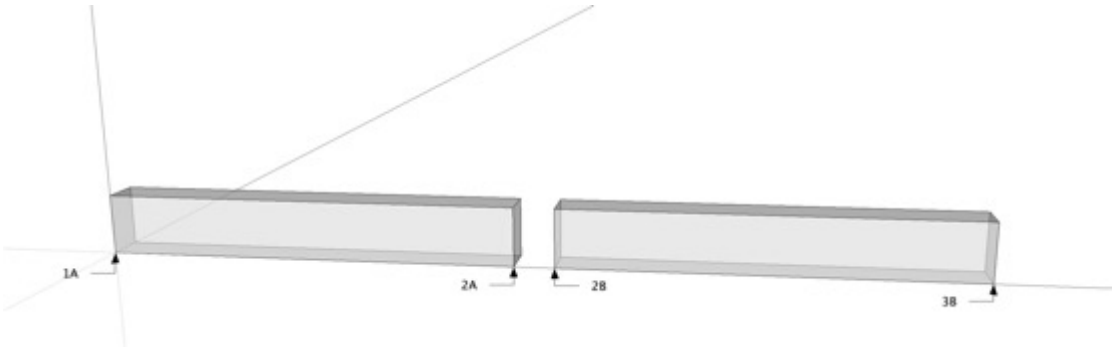

Figure 5. 2 Sketch illustrating two beams to be coupled in-line

Equation 5. 4 shows the impedance matrix for the above beams coupled in line as given by Rubin (1967). For consistency with the subscripts used in the mobility matrices derived in the previous chapter and in the sections that follow, the expression on the right-hand side includes a reference to which beam points 1, 2 and 3 refer to. When assembling the impedance and mobility matrices with numerous degrees of freedom, the relevant local axes coordinates of each element will also be shown.

$$\mathbf{Z} = \begin{bmatrix} Z_{11} & Z_{12} & Z_{13} \\ Z_{21} & Z_{22} & Z_{23} \\ Z_{31} & Z_{23} & Z_{33} \end{bmatrix} = \begin{bmatrix} Z_{1A1A} & Z_{1A2A} & 0 \\ Z_{2A1A} & Z_{2A2A} + Z_{2B2B} & Z_{2B3B} \\ 0 & Z_{2B3B} & Z_{3B3B} \end{bmatrix} \qquad \text{Equation 5. 4}$$

The coupling between beams in the proposed simplified prediction model is intended to follow the same principle as shown above. However, as the response of the beams has been modelled in terms of mobilities and as the above makes use of impedances to couple beams together, the first step in the coupling process will be to convert the mobilities into impedances. In addition to this, the mobility matrices derived in Chapter 4 for a free-free beam take in account six degrees of freedom at each end which will be coupled to six other degrees of freedom in another beam, depending on the arrangement being modelled. Equation 5. 4 will need to reflect the additional degrees of freedom being considered. As such, an intermediate matrix (referred to as a coupling matrix) has been developed to allow the selection of which degree of freedom in a beam connects to which degree of freedom in other beams. Increasing the number of degrees of freedom and the number of beams being modelled will inherently increase the size of the resultant impedance and mobility matrices for the coupled system.

The procedure used to derive the resultant impedance / mobility matrix for beams coupled together is summarised in steps 1 to 6 below. It is worth noting that the simple scenario of two beams coupled in line as shown in Figure 5. 2 has been used in the following steps. For simplicity and clarity in setting out the methodology used for coupling beams together, the various degrees of freedom considered in the mobility matrices have been excluded here. However, a more detailed look into the coupling matrix used and the resultant impedance matrix for two beams coupled in line is provided in Section 5.3.2.

1. Assemble the mobility matrices for the beams to be coupled as follows, taking into account the required degrees of freedom.

$$\mathbf{Y} = \begin{bmatrix} \mathbf{Y}_{1A1A} & \mathbf{Y}_{1A2A} & 0 & 0 \\ \mathbf{Y}_{2A1A} & \mathbf{Y}_{2A2A} & 0 & 0 \\ 0 & 0 & \mathbf{Y}_{2B2B} & \mathbf{Y}_{2B3B} \\ 0 & 0 & \mathbf{Y}_{3B2B} & \mathbf{Y}_{3B3B} \end{bmatrix} \qquad \text{Equation 5. 5}$$

2. Invert the mobility matrix in Equation 5. 5 to obtain the equivalent impedance matrix.

$$\mathbf{Z} = \mathbf{Y}^{-1} = \begin{bmatrix} \mathbf{Z}_{1A1A} & \mathbf{Z}_{1A2A} & 0 & 0 \\ \mathbf{Z}_{2A1A} & \mathbf{Z}_{2A2A} & 0 & 0 \\ 0 & 0 & \mathbf{Z}_{2B2B} & \mathbf{Z}_{2B3B} \\ 0 & 0 & \mathbf{Z}_{3B2B} & \mathbf{Z}_{3B3B} \end{bmatrix} \qquad \text{Equation 5. 6}$$

3. Assemble a matrix of 1s and 0s with the same number of rows as the impedance matrix given in Equation 5. 6. The number of columns in the new matrix should be equivalent to the number of columns in the impedance matrix in Equation 5. 6 minus the number of degrees of freedom / points that will be coupled together. Each non-zero element in Equation 5. 6 would relate to a 1 in Equation 5. 7, all other elements should be set to 0. Where degrees of freedom / points on the beam are to be coupled together, such as $\mathbf{Z}_{2A2A}$ and $\mathbf{Z}_{2B2B}$ in the present scenario, and as the coupling matrix has one less column than the impedance matrix, there will be a second 1 in the same column as shown below.

$$\mathbf{coupling} = \begin{bmatrix} 1 & 0 & 0 \\ 0 & 1 & 0 \\ 0 & 1 & 0 \\ 0 & 0 & 1 \end{bmatrix} \qquad \text{Equation 5. 7}$$

4. Multiply the impedance and coupling matrices to merge columns 2 and 3 of Equation 5. 6 into a single column.

$$\mathbf{Z}\times\mathbf{coupling} = \begin{bmatrix} \mathbf{Z}_{1A1A} & \mathbf{Z}_{1A2A} & 0 \\ \mathbf{Z}_{2A1A} & \mathbf{Z}_{2A2A} & 0 \\ 0 & \mathbf{Z}_{2B2B} & \mathbf{Z}_{2B3B} \\ 0 & \mathbf{Z}_{3B2B} & \mathbf{Z}_{3B3B} \end{bmatrix} \quad \text{Equation 5. 8}$$

5. Multiply the transpose of the coupling matrix given in Equation 5. 7 by Equation 5. 8 to add $\mathbf{Z}_{2A2A}$ and $\mathbf{Z}_{2B2B}$ together.

$$\mathbf{coupling}^{\mathrm{T}}\times(\mathbf{Z}\times\mathbf{coupling}) = \begin{bmatrix} 1 & 0 & 0 & 0 \\ 0 & 1 & 1 & 0 \\ 0 & 0 & 0 & 1 \end{bmatrix} \times \begin{bmatrix} \mathbf{Z}_{1A1A} & \mathbf{Z}_{1A2A} & 0 \\ \mathbf{Z}_{2A1A} & \mathbf{Z}_{2A2A} & 0 \\ 0 & \mathbf{Z}_{2B2B} & \mathbf{Z}_{2B3B} \\ 0 & \mathbf{Z}_{3B2B} & \mathbf{Z}_{3B3B} \end{bmatrix} \quad \text{Equation 5. 9}$$

$$\mathbf{Z}_{coupled} = \mathbf{coupling}^{\mathrm{T}}\times(\mathbf{Z}\times\mathbf{coupling}) = \begin{bmatrix} Z_{1A1A} & Z_{1A2A} & 0 \\ Z_{2A1A} & Z_{2A2A} + Z_{2B2B} & Z_{2B3B} \\ 0 & Z_{2B3B} & Z_{3B3B} \end{bmatrix} \quad \text{Equation 5. 10}$$

6. Invert $\mathbf{Z}_{coupled}$ to obtain the mobility matrix for the coupled system.

$$\mathbf{Y}_{coupled} = \mathbf{Z}_{coupled}^{-1} \quad \text{Equation 5. 11}$$

As previously mentioned, the above methodology was simplified to allow a clearer statement of the various steps needed to couple beams together. Also, as the overarching aim of this thesis is only to investigate the feasibility of replacing FEM with analytical beam functions in an existing prediction model, the coupling matrix given in Equation 5. 7 is created by hand. However, once the six degrees of freedom at each end of each beam being modelled are included in the above matrices, these will become rather large and hard to handle manually. As such, when modelling complex systems, for example the full frame of a building, it would be appropriate to automate the assembly of the coupling matrices for the system.

The process for coupling beams together has been set out above for a simple scenario of two beams coupled in line. Beams and columns in buildings, however, are often at different orientations to each other to form a frame. Although the principles given above would also apply to more complex arrangements, the coupling matrices would be specific to each scenario. The following section sets out the various scenarios analysed, along with the coupling matrices derived for each.

5.3 Beam arrangements modelled and their coupling matrices

Four beam interfaces commonly encountered in buildings have been modelled using the mobilities derived in Chapter 4 and the procedure for coupling beams set out in Section 5.2. The first scenario modelled is that of two beams in a straight line briefly discussed in the previous section. Beams in an L-junction arrangement have also been modelled along with a beam frame, i.e. four beams in L-junctions to each other forming a frame. The following sections provide additional details on how to interpret coupling matrices, along with a summary of the beam arrangements modelled, the coupling matrices used and the resultant impedance matrices at the connection points accounting for the six degrees of freedom described in Chapter 4 at each end of the beams.

As the full resultant impedance matrices for beams coupled together are rather large, they have been included in Appendix B. However, the derived impedance sub-matrices at the connection points of each beam are provided in the following sections for ease of reference.

5.3.1 Interpreting coupling matrices

Assembling the coupling matrices for a simple system such as two beams coupled in line with two degrees of freedom at each end of each beam is reasonably straightforward. However, assembling these matrices for more complex systems is trickier and more time consuming. It is therefore important to clarify what the various elements in the coupling matrix refer to, to help speed up the process. A summary of these is provided in the following paragraphs.

Taking the example of two beams A and B, each with six degrees of freedom at each end and coupled together at a given point, the combined impedance matrix for the two beams (Equation 5. 6) would have 24 rows and 24 columns. The coupling matrix, on the other hand, would have 24 rows and only 18 columns to allow for the addition of the impedances of the six degrees of freedom being coupled.

Each row of the coupling matrix therefore represents a local degree of freedom at each point on the beam, while the columns refer to the global degrees of freedom of the system.

5.3.2 Two beams in-line

While two beams in line on their own are not often found in buildings, it is useful to model this scenario to cement the processes described in Sections 5.1 and 5.2. The coordinate system, coupling matrices and resultant impedance matrices for this scenario are set out below.

One of the properties of two beams coupled in a straight line is the fact that the local x, y and z coordinates for each of the beams are the same as they have the same orientation. This can be clearly seen in Figure 5. 3, where beams A and B are to be coupled at point 2. The global coordinate system (axes X, Y and Z) has been set at the origin of beam A. For consistency, the global axes remain the same for all of the beam arrangements considered.

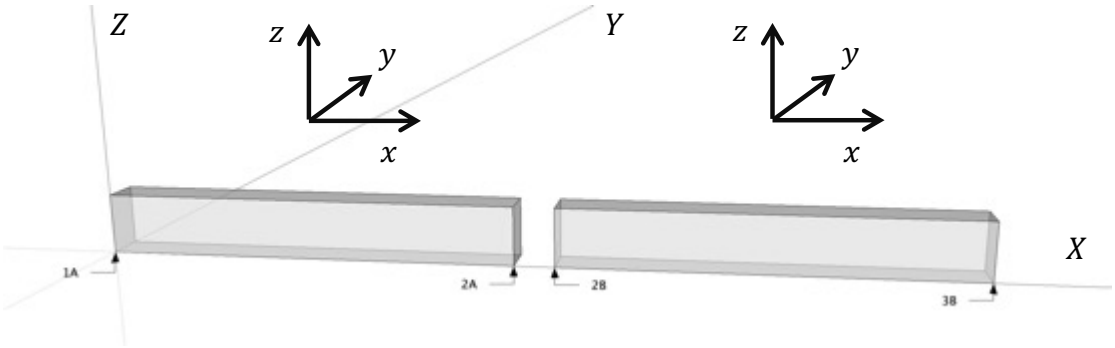

Figure 5. 3 Sketch showing local and global coordinate system considered when modelling two beams in-line (global coordinate system in upper case, local coordinate system in lower case)

With the coordinate systems defined, the next step to derive the coupled impedance matrix for the two beams is to assemble the coupling matrix as set out in Section 5.2. Equation 5. 12 sets out the coupling matrix assembled for two free-free beams coupled in line with six degrees of freedom at each end.

$$\mathbf{coupling}_{2\ beams\ in\ line} =$$

$$\begin{bmatrix}
\mathbf{1} & 0 & 0 & 0 & 0 & 0 & 0 & 0 & 0 & 0 & 0 & 0 & 0 & 0 & 0 & 0 & 0 & 0 \\
0 & \mathbf{1} & 0 & 0 & 0 & 0 & 0 & 0 & 0 & 0 & 0 & 0 & 0 & 0 & 0 & 0 & 0 & 0 \\
0 & 0 & \mathbf{1} & 0 & 0 & 0 & 0 & 0 & 0 & 0 & 0 & 0 & 0 & 0 & 0 & 0 & 0 & 0 \\
0 & 0 & 0 & \mathbf{1} & 0 & 0 & 0 & 0 & 0 & 0 & 0 & 0 & 0 & 0 & 0 & 0 & 0 & 0 \\
0 & 0 & 0 & 0 & \mathbf{1} & 0 & 0 & 0 & 0 & 0 & 0 & 0 & 0 & 0 & 0 & 0 & 0 & 0 \\
0 & 0 & 0 & 0 & 0 & \mathbf{1} & 0 & 0 & 0 & 0 & 0 & 0 & 0 & 0 & 0 & 0 & 0 & 0 \\
0 & 0 & 0 & 0 & 0 & 0 & \mathbf{1} & 0 & 0 & 0 & 0 & 0 & 0 & 0 & 0 & 0 & 0 & 0 \\
0 & 0 & 0 & 0 & 0 & 0 & 0 & \mathbf{1} & 0 & 0 & 0 & 0 & 0 & 0 & 0 & 0 & 0 & 0 \\
0 & 0 & 0 & 0 & 0 & 0 & 0 & 0 & \mathbf{1} & 0 & 0 & 0 & 0 & 0 & 0 & 0 & 0 & 0 \\
0 & 0 & 0 & 0 & 0 & 0 & 0 & 0 & 0 & \mathbf{1} & 0 & 0 & 0 & 0 & 0 & 0 & 0 & 0 \\
0 & 0 & 0 & 0 & 0 & 0 & 0 & 0 & 0 & 0 & \mathbf{1} & 0 & 0 & 0 & 0 & 0 & 0 & 0 \\
0 & 0 & 0 & 0 & 0 & 0 & 0 & 0 & 0 & 0 & 0 & \mathbf{1} & 0 & 0 & 0 & 0 & 0 & 0 \\
0 & 0 & 0 & 0 & 0 & 0 & \mathbf{1} & 0 & 0 & 0 & 0 & 0 & 0 & 0 & 0 & 0 & 0 & 0 \\
0 & 0 & 0 & 0 & 0 & 0 & 0 & \mathbf{1} & 0 & 0 & 0 & 0 & 0 & 0 & 0 & 0 & 0 & 0 \\
0 & 0 & 0 & 0 & 0 & 0 & 0 & 0 & \mathbf{1} & 0 & 0 & 0 & 0 & 0 & 0 & 0 & 0 & 0 \\
0 & 0 & 0 & 0 & 0 & 0 & 0 & 0 & 0 & \mathbf{1} & 0 & 0 & 0 & 0 & 0 & 0 & 0 & 0 \\
0 & 0 & 0 & 0 & 0 & 0 & 0 & 0 & 0 & 0 & \mathbf{1} & 0 & 0 & 0 & 0 & 0 & 0 & 0 \\
0 & 0 & 0 & 0 & 0 & 0 & 0 & 0 & 0 & 0 & 0 & \mathbf{1} & 0 & 0 & 0 & 0 & 0 & 0 \\
0 & 0 & 0 & 0 & 0 & 0 & 0 & 0 & 0 & 0 & 0 & 0 & \mathbf{1} & 0 & 0 & 0 & 0 & 0 \\
0 & 0 & 0 & 0 & 0 & 0 & 0 & 0 & 0 & 0 & 0 & 0 & 0 & \mathbf{1} & 0 & 0 & 0 & 0 \\
0 & 0 & 0 & 0 & 0 & 0 & 0 & 0 & 0 & 0 & 0 & 0 & 0 & 0 & \mathbf{1} & 0 & 0 & 0 \\
0 & 0 & 0 & 0 & 0 & 0 & 0 & 0 & 0 & 0 & 0 & 0 & 0 & 0 & 0 & \mathbf{1} & 0 & 0 \\
0 & 0 & 0 & 0 & 0 & 0 & 0 & 0 & 0 & 0 & 0 & 0 & 0 & 0 & 0 & 0 & \mathbf{1} & 0 \\
0 & 0 & 0 & 0 & 0 & 0 & 0 & 0 & 0 & 0 & 0 & 0 & 0 & 0 & 0 & 0 & 0 & \mathbf{1}
\end{bmatrix}$$

Equation 5. 12

The resultant impedance matrix at the connection point of the two beams is given in Equation 5. 13. The below shows that for two beams coupled in line, the quasi-longitudinal, torsional and bending degrees of freedom in each beam are coupled together at point 2. As the beams have the same orientation, no coupling between translations and rotations of other degrees of freedom, such as between torsion and bending, would occur. However, for beams at different angles to each other, this would not be the case. The full impedance matrix for two beams coupled in line is provided in Appendix B for information.

The response of two beams coupled in a line has been modelled in MATLAB using the matrices given above and the results compared with those from a FEM model. A summary of these is provided in Section 5.4.2.

$$\mathbf{Z}_{2\ beams\ in\ line,\ \ point\ 2} = \begin{bmatrix} Z_{Lx2A2A} + Z_{Lx2B2B} & 0 & 0 & 0 & 0 & 0 \\ 0 & Z_{Tx2A2A} + Z_{Tx2B2B} & 0 & 0 & 0 & 0 \\ 0 & 0 & Z_{vy2AFy2A} + Z_{vy2BFy2B} & Z_{vy2AMz2A} + Z_{vy2BMz2B} & 0 & 0 \\ 0 & 0 & Z_{\alpha z2AFy2A} + Z_{\alpha z2BFy2B} & Z_{\alpha z2AMz2A} + Z_{\alpha z2BMz2B} & 0 & 0 \\ 0 & 0 & 0 & 0 & Z_{vz2AFz2A} + Z_{vz2BFz2B} & Z_{vz2AFz2A} + Z_{vz2BFz2B} \\ 0 & 0 & 0 & 0 & Z_{\alpha y2AFz2A} + Z_{\alpha y2BFz2B} & Z_{\alpha y2AMy2A} + Z_{\alpha y2BMy2B} \end{bmatrix} \quad \text{Equation 5. 13}$$

5.3.3 Two beams in an L-junction

A more common arrangement of beams and columns encountered in buildings is for these to be at 90° angles to each other. The coordinate system, coupling matrices and resultant impedance matrices for two beams in an L-junction have been derived and are presented in the following paragraphs.

In contrast with two beams in line, the local coordinate systems of beams coupled in L-junctions differ. Focussing on the example given in Figure 5. 4 for two beams at 90° to each other, it can be seen that the local *x* axis of beam B is perpendicular to the *x* axis of beam A and to the global *X* axis of the overall system. Similarly, the local *z* axis of beam A is at 90° to the local *z* axis of beam B.

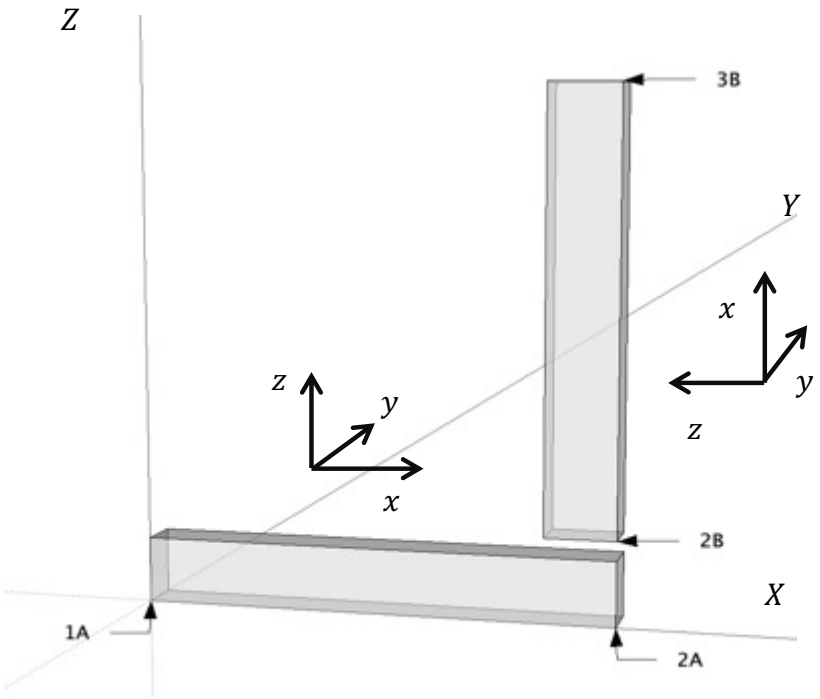

Figure 5. 4 Sketch showing local and global coordinate system considered when modelling two beams in an L-junction (global coordinate system in upper case, local coordinate system in lower case)

As the local coordinate systems for two beams in line and in an L-junction are different, so is the coupling matrix needed to couple the relevant degrees of freedom and points on the beam. The coupling matrix for two beams in an L-junction has been assembled and is provided in Equation 5. 12. One point worth noting in the coupling matrix is the presence of negative numbers. These relate to situations where a given degree of freedom in beam A is coupled to a degree of freedom in beam B which runs in the negative local axis direction. A good example of this is the coupling between quasi-longitudinal waves in beam A in the positive x direction and transverse waves along the negative z axis. When excited, quasi-longitudinal waves in beam A will excite the local z axis in beam B in the negative direction.

$$\mathbf{coupling}_{2\ beams\ in\ L} =$$

$$\begin{bmatrix}
\mathbf{1} & 0 & 0 & 0 & 0 & 0 & 0 & 0 & 0 & 0 & 0 & 0 & 0 & 0 & 0 & 0 & 0 & 0 \\
0 & \mathbf{1} & 0 & 0 & 0 & 0 & 0 & 0 & 0 & 0 & 0 & 0 & 0 & 0 & 0 & 0 & 0 & 0 \\
0 & 0 & \mathbf{1} & 0 & 0 & 0 & 0 & 0 & 0 & 0 & 0 & 0 & 0 & 0 & 0 & 0 & 0 & 0 \\
0 & 0 & 0 & \mathbf{1} & 0 & 0 & 0 & 0 & 0 & 0 & 0 & 0 & 0 & 0 & 0 & 0 & 0 & 0 \\
0 & 0 & 0 & 0 & \mathbf{1} & 0 & 0 & 0 & 0 & 0 & 0 & 0 & 0 & 0 & 0 & 0 & 0 & 0 \\
0 & 0 & 0 & 0 & 0 & \mathbf{1} & 0 & 0 & 0 & 0 & 0 & 0 & 0 & 0 & 0 & 0 & 0 & 0 \\
0 & 0 & 0 & 0 & 0 & 0 & \mathbf{1} & 0 & 0 & 0 & 0 & 0 & 0 & 0 & 0 & 0 & 0 & 0 \\
0 & 0 & 0 & 0 & 0 & 0 & 0 & \mathbf{1} & 0 & 0 & 0 & 0 & 0 & 0 & 0 & 0 & 0 & 0 \\
0 & 0 & 0 & 0 & 0 & 0 & 0 & 0 & \mathbf{1} & 0 & 0 & 0 & 0 & 0 & 0 & 0 & 0 & 0 \\
0 & 0 & 0 & 0 & 0 & 0 & 0 & 0 & 0 & \mathbf{1} & 0 & 0 & 0 & 0 & 0 & 0 & 0 & 0 \\
0 & 0 & 0 & 0 & 0 & 0 & 0 & 0 & 0 & 0 & \mathbf{1} & 0 & 0 & 0 & 0 & 0 & 0 & 0 \\
0 & 0 & 0 & 0 & 0 & 0 & 0 & 0 & 0 & 0 & 0 & \mathbf{1} & 0 & 0 & 0 & 0 & 0 & 0 \\
0 & 0 & 0 & 0 & 0 & 0 & 0 & 0 & 0 & 0 & \mathbf{1} & 0 & 0 & 0 & 0 & 0 & 0 & 0 \\
0 & 0 & 0 & 0 & 0 & 0 & 0 & 0 & 0 & \mathbf{1} & 0 & 0 & 0 & 0 & 0 & 0 & 0 & 0 \\
0 & 0 & 0 & 0 & 0 & 0 & 0 & 0 & \mathbf{1} & 0 & 0 & 0 & 0 & 0 & 0 & 0 & 0 & 0 \\
0 & 0 & 0 & 0 & 0 & 0 & 0 & \mathbf{-1} & 0 & 0 & 0 & 0 & 0 & 0 & 0 & 0 & 0 & 0 \\
0 & 0 & 0 & 0 & 0 & 0 & \mathbf{-1} & 0 & 0 & 0 & 0 & 0 & 0 & 0 & 0 & 0 & 0 & 0 \\
0 & 0 & 0 & 0 & 0 & 0 & 0 & 0 & 0 & 0 & 0 & \mathbf{1} & 0 & 0 & 0 & 0 & 0 & 0 \\
0 & 0 & 0 & 0 & 0 & 0 & 0 & 0 & 0 & 0 & 0 & 0 & 0 & 0 & 0 & 0 & \mathbf{1} & 0 \\
0 & 0 & 0 & 0 & 0 & 0 & 0 & 0 & 0 & 0 & 0 & 0 & 0 & 0 & 0 & \mathbf{1} & 0 & 0 \\
0 & 0 & 0 & 0 & 0 & 0 & 0 & 0 & 0 & 0 & 0 & 0 & 0 & 0 & \mathbf{1} & 0 & 0 & 0 \\
0 & 0 & 0 & 0 & 0 & 0 & 0 & 0 & 0 & 0 & 0 & 0 & 0 & \mathbf{-1} & 0 & 0 & 0 & 0 \\
0 & 0 & 0 & 0 & 0 & 0 & 0 & 0 & 0 & 0 & 0 & 0 & \mathbf{-1} & 0 & 0 & 0 & 0 & 0 \\
0 & 0 & 0 & 0 & 0 & 0 & 0 & 0 & 0 & 0 & 0 & 0 & 0 & 0 & 0 & 0 & 0 & \mathbf{1}
\end{bmatrix}$$

Equation 5. 14

The resultant impedance matrix at the connection point of the two beams in an L-junction is given in Equation 5. 15. The below shows that degrees of freedom of different types, such as quasi-longitudinal and bending can be coupled together to give the response of the beam at the connection point. The full impedance matrix for the two beams coupled in an L-junction is provided in Appendix B for information.

The response of two beams coupled in an L-junction has been modelled in MATLAB using the matrices given above and the results compared with those from a FEM model. A summary of these is provided in Section 5.4.3.

$$\mathbf{Z}_{2\ beams\ in\ L,\ \ point\ 2} = \begin{bmatrix} Z_{Lx2A2A} + Z_{vz2BFz2B} & 0 & 0 & 0 & 0 & -Z_{vz2BMy2B} \\ 0 & Z_{Tx2A2A} + Z_{\alpha z2BMz2B} & -Z_{\alpha z2BFy2B} & 0 & 0 & 0 \\ 0 & -Z_{vy2BMz2B} & Z_{vy2AFy2A} + Z_{vy2BFy2B} & Z_{vy2AMz2A} & 0 & 0 \\ 0 & 0 & Z_{\alpha z2AFy2A} & Z_{\alpha z2AMz2A} + Z_{Tx2B2B} & 0 & 0 \\ 0 & 0 & 0 & 0 & Z_{vz2AFz2A} + Z_{Lx2B2B} & Z_{vz2AMy2A} \\ -Z_{\alpha y2BFz2B} & 0 & 0 & 0 & Z_{\alpha y2AFz2A} & Z_{\alpha y2AMy2A} + Z_{\alpha y2BMy2B} \end{bmatrix} \quad \text{Equation 5. 15}$$

5.3.4 Three and four beams in L-junctions

The principles followed above for two beams in an L-junction can also be applied to three and four beams in L-junctions. The latter scenario, i.e. a beam frame, is the one that is most commonly found in buildings. In between the beam frame, there would typically be a wall, floor or ceiling. A description of the coordinate systems, coupling matrices and coupled impedance matrices for these two scenarios is provided below.

Figure 5. 5 and Figure 5. 6 show the global and local coordinate systems for three and four beams coupled in L-junctions, respectively. As with two beams in an L-junction discussed in the previous section, the local axes of beams B, C and D are rotated in relation to the local axes of beam A, as well as to the global coordinate axes of the system. Therefore, when coupling three or four beams in such arrangements, different degrees of freedom, such as quasi-longitudinal and bending, will be coupled together.

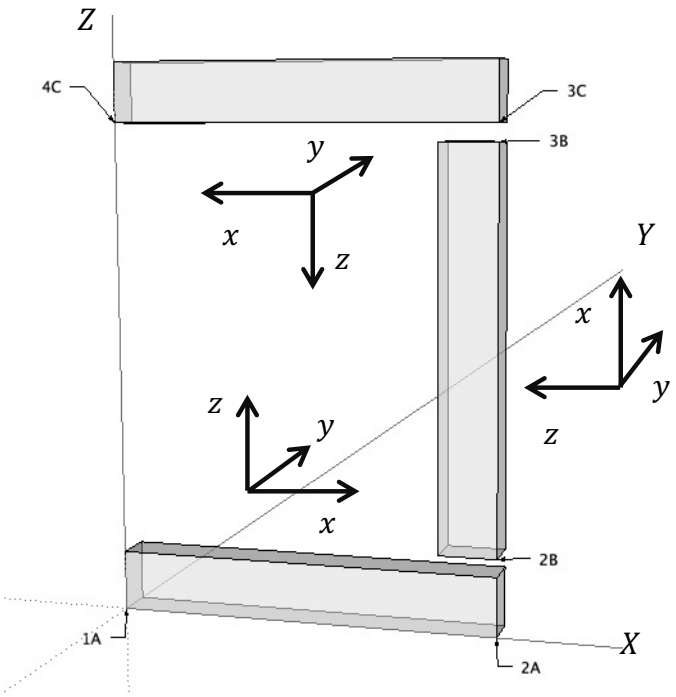

Figure 5. 5 Sketch showing local and global coordinate system considered when modelling three beams in L-junctions (global coordinate system in upper case, local coordinate system in lower case)

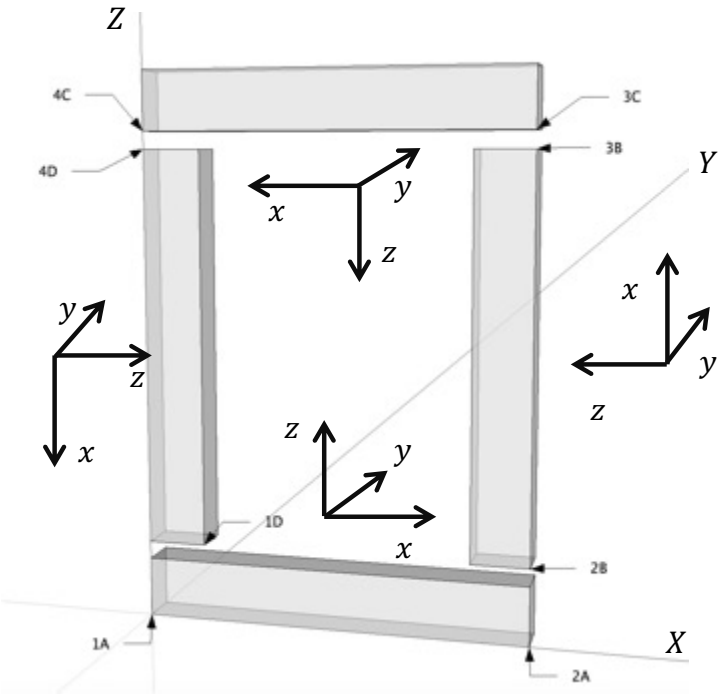

Figure 5. 6 Sketch showing local and global coordinate system considered when modelling a four-beam frame (global coordinate system in upper case, local coordinate system in lower case)

The coupling matrices for three and four beams in L-junctions are given in Equation 5. 16 and Equation 5. 17, respectively. Given the number of degrees of freedom considered, these matrices are rather large. As the local axes of beams B, C and D are rotated in relation to each other, negative numbers are also present in these coupling matrices.

The impedance matrix for three beams coupled in L-junctions at connection point 3 is provided in Equation 5. 18, while Equation 5. 19 and Equation 5. 20 set out the impedance matrices for a beam frame at connections points 4 and 1, respectively. It is worth noting that the impedance matrix for three and four beams coupled in L-junctions at connection point 2 is the same as Equation 5. 15 for two beams in an L-junction and has therefore not been repeated in this section. Similarly, the response at point 3 for four beams in a frame is given by Equation 5. 18 for three beams in L-junctions.

The response of three and four beams coupled in L-junctions has been modelled in MATLAB using the matrices given below and the results compared with those from a FEM model. A summary of these is provided in Sections 5.4.4 and 5.4.5, respectively.

$$\mathbf{coupling}_{3\ beams\ in\ L} =$$

$$\begin{bmatrix}
\mathbf{1} & 0 & 0 & 0 & 0 & 0 & 0 & 0 & 0 & 0 & 0 & 0 & 0 & 0 & 0 & 0 & 0 & 0 & 0 & 0 & 0 & 0 & 0 & 0 \\
0 & \mathbf{1} & 0 & 0 & 0 & 0 & 0 & 0 & 0 & 0 & 0 & 0 & 0 & 0 & 0 & 0 & 0 & 0 & 0 & 0 & 0 & 0 & 0 & 0 \\
0 & 0 & \mathbf{1} & 0 & 0 & 0 & 0 & 0 & 0 & 0 & 0 & 0 & 0 & 0 & 0 & 0 & 0 & 0 & 0 & 0 & 0 & 0 & 0 & 0 \\
0 & 0 & 0 & \mathbf{1} & 0 & 0 & 0 & 0 & 0 & 0 & 0 & 0 & 0 & 0 & 0 & 0 & 0 & 0 & 0 & 0 & 0 & 0 & 0 & 0 \\
0 & 0 & 0 & 0 & \mathbf{1} & 0 & 0 & 0 & 0 & 0 & 0 & 0 & 0 & 0 & 0 & 0 & 0 & 0 & 0 & 0 & 0 & 0 & 0 & 0 \\
0 & 0 & 0 & 0 & 0 & \mathbf{1} & 0 & 0 & 0 & 0 & 0 & 0 & 0 & 0 & 0 & 0 & 0 & 0 & 0 & 0 & 0 & 0 & 0 & 0 \\
0 & 0 & 0 & 0 & 0 & 0 & \mathbf{1} & 0 & 0 & 0 & 0 & 0 & 0 & 0 & 0 & 0 & 0 & 0 & 0 & 0 & 0 & 0 & 0 & 0 \\
0 & 0 & 0 & 0 & 0 & 0 & 0 & \mathbf{1} & 0 & 0 & 0 & 0 & 0 & 0 & 0 & 0 & 0 & 0 & 0 & 0 & 0 & 0 & 0 & 0 \\
0 & 0 & 0 & 0 & 0 & 0 & 0 & 0 & \mathbf{1} & 0 & 0 & 0 & 0 & 0 & 0 & 0 & 0 & 0 & 0 & 0 & 0 & 0 & 0 & 0 \\
0 & 0 & 0 & 0 & 0 & 0 & 0 & 0 & 0 & \mathbf{1} & 0 & 0 & 0 & 0 & 0 & 0 & 0 & 0 & 0 & 0 & 0 & 0 & 0 & 0 \\
0 & 0 & 0 & 0 & 0 & 0 & 0 & 0 & 0 & 0 & \mathbf{1} & 0 & 0 & 0 & 0 & 0 & 0 & 0 & 0 & 0 & 0 & 0 & 0 & 0 \\
0 & 0 & 0 & 0 & 0 & 0 & 0 & 0 & 0 & 0 & 0 & \mathbf{1} & 0 & 0 & 0 & 0 & 0 & 0 & 0 & 0 & 0 & 0 & 0 & 0 \\
0 & 0 & 0 & 0 & 0 & 0 & 0 & 0 & 0 & 0 & \mathbf{1} & 0 & 0 & 0 & 0 & 0 & 0 & 0 & 0 & 0 & 0 & 0 & 0 & 0 \\
0 & 0 & 0 & 0 & 0 & 0 & 0 & 0 & 0 & \mathbf{1} & 0 & 0 & 0 & 0 & 0 & 0 & 0 & 0 & 0 & 0 & 0 & 0 & 0 & 0 \\
0 & 0 & 0 & 0 & 0 & 0 & 0 & 0 & \mathbf{1} & 0 & 0 & 0 & 0 & 0 & 0 & 0 & 0 & 0 & 0 & 0 & 0 & 0 & 0 & 0 \\
0 & 0 & 0 & 0 & 0 & 0 & 0 & \mathbf{-1} & 0 & 0 & 0 & 0 & 0 & 0 & 0 & 0 & 0 & 0 & 0 & 0 & 0 & 0 & 0 & 0 \\
0 & 0 & 0 & 0 & 0 & 0 & \mathbf{-1} & 0 & 0 & 0 & 0 & 0 & 0 & 0 & 0 & 0 & 0 & 0 & 0 & 0 & 0 & 0 & 0 & 0 \\
0 & 0 & 0 & 0 & 0 & 0 & 0 & 0 & 0 & 0 & 0 & \mathbf{1} & 0 & 0 & 0 & 0 & 0 & 0 & 0 & 0 & 0 & 0 & 0 & 0 \\
0 & 0 & 0 & 0 & 0 & 0 & 0 & 0 & 0 & 0 & 0 & 0 & 0 & 0 & 0 & 0 & \mathbf{1} & 0 & 0 & 0 & 0 & 0 & 0 & 0 \\
0 & 0 & 0 & 0 & 0 & 0 & 0 & 0 & 0 & 0 & 0 & 0 & 0 & 0 & 0 & \mathbf{1} & 0 & 0 & 0 & 0 & 0 & 0 & 0 & 0 \\
0 & 0 & 0 & 0 & 0 & 0 & 0 & 0 & 0 & 0 & 0 & 0 & 0 & 0 & \mathbf{1} & 0 & 0 & 0 & 0 & 0 & 0 & 0 & 0 & 0 \\
0 & 0 & 0 & 0 & 0 & 0 & 0 & 0 & 0 & 0 & 0 & 0 & 0 & \mathbf{-1} & 0 & 0 & 0 & 0 & 0 & 0 & 0 & 0 & 0 & 0 \\
0 & 0 & 0 & 0 & 0 & 0 & 0 & 0 & 0 & 0 & 0 & 0 & \mathbf{-1} & 0 & 0 & 0 & 0 & 0 & 0 & 0 & 0 & 0 & 0 & 0 \\
0 & 0 & 0 & 0 & 0 & 0 & 0 & 0 & 0 & 0 & 0 & 0 & 0 & 0 & 0 & 0 & 0 & \mathbf{1} & 0 & 0 & 0 & 0 & 0 & 0 \\
0 & 0 & 0 & 0 & 0 & 0 & 0 & 0 & 0 & 0 & 0 & 0 & \mathbf{-1} & 0 & 0 & 0 & 0 & 0 & 0 & 0 & 0 & 0 & 0 & 0 \\
0 & 0 & 0 & 0 & 0 & 0 & 0 & 0 & 0 & 0 & 0 & 0 & 0 & \mathbf{-1} & 0 & 0 & 0 & 0 & 0 & 0 & 0 & 0 & 0 & 0 \\
0 & 0 & 0 & 0 & 0 & 0 & 0 & 0 & 0 & 0 & 0 & 0 & 0 & 0 & \mathbf{1} & 0 & 0 & 0 & 0 & 0 & 0 & 0 & 0 & 0 \\
0 & 0 & 0 & 0 & 0 & 0 & 0 & 0 & 0 & 0 & 0 & 0 & 0 & 0 & 0 & \mathbf{1} & 0 & 0 & 0 & 0 & 0 & 0 & 0 & 0 \\
0 & 0 & 0 & 0 & 0 & 0 & 0 & 0 & 0 & 0 & 0 & 0 & 0 & 0 & 0 & 0 & \mathbf{-1} & 0 & 0 & 0 & 0 & 0 & 0 & 0 \\
0 & 0 & 0 & 0 & 0 & 0 & 0 & 0 & 0 & 0 & 0 & 0 & 0 & 0 & 0 & 0 & 0 & \mathbf{1} & 0 & 0 & 0 & 0 & 0 & 0 \\
0 & 0 & 0 & 0 & 0 & 0 & 0 & 0 & 0 & 0 & 0 & 0 & 0 & 0 & 0 & 0 & 0 & 0 & \mathbf{-1} & 0 & 0 & 0 & 0 & 0 \\
0 & 0 & 0 & 0 & 0 & 0 & 0 & 0 & 0 & 0 & 0 & 0 & 0 & 0 & 0 & 0 & 0 & 0 & 0 & \mathbf{-1} & 0 & 0 & 0 & 0 \\
0 & 0 & 0 & 0 & 0 & 0 & 0 & 0 & 0 & 0 & 0 & 0 & 0 & 0 & 0 & 0 & 0 & 0 & 0 & 0 & \mathbf{1} & 0 & 0 & 0 \\
0 & 0 & 0 & 0 & 0 & 0 & 0 & 0 & 0 & 0 & 0 & 0 & 0 & 0 & 0 & 0 & 0 & 0 & 0 & 0 & 0 & \mathbf{1} & 0 & 0 \\
0 & 0 & 0 & 0 & 0 & 0 & 0 & 0 & 0 & 0 & 0 & 0 & 0 & 0 & 0 & 0 & 0 & 0 & 0 & 0 & 0 & 0 & \mathbf{-1} & 0 \\
0 & 0 & 0 & 0 & 0 & 0 & 0 & 0 & 0 & 0 & 0 & 0 & 0 & 0 & 0 & 0 & 0 & 0 & 0 & 0 & 0 & 0 & 0 & \mathbf{1}
\end{bmatrix}$$

Equation 5. 16

$$\mathbf{coupling}_{4\ beams\ in\ L} =$$

$$\begin{bmatrix}
\mathbf{1} & 0 & 0 & 0 & 0 & 0 & 0 & 0 & 0 & 0 & 0 & 0 & 0 & 0 & 0 & 0 & 0 & 0 & 0 & 0 & 0 & 0 & 0 & 0 \\
0 & \mathbf{1} & 0 & 0 & 0 & 0 & 0 & 0 & 0 & 0 & 0 & 0 & 0 & 0 & 0 & 0 & 0 & 0 & 0 & 0 & 0 & 0 & 0 & 0 \\
0 & 0 & \mathbf{1} & 0 & 0 & 0 & 0 & 0 & 0 & 0 & 0 & 0 & 0 & 0 & 0 & 0 & 0 & 0 & 0 & 0 & 0 & 0 & 0 & 0 \\
0 & 0 & 0 & \mathbf{1} & 0 & 0 & 0 & 0 & 0 & 0 & 0 & 0 & 0 & 0 & 0 & 0 & 0 & 0 & 0 & 0 & 0 & 0 & 0 & 0 \\
0 & 0 & 0 & 0 & \mathbf{1} & 0 & 0 & 0 & 0 & 0 & 0 & 0 & 0 & 0 & 0 & 0 & 0 & 0 & 0 & 0 & 0 & 0 & 0 & 0 \\
0 & 0 & 0 & 0 & 0 & \mathbf{1} & 0 & 0 & 0 & 0 & 0 & 0 & 0 & 0 & 0 & 0 & 0 & 0 & 0 & 0 & 0 & 0 & 0 & 0 \\
0 & 0 & 0 & 0 & 0 & 0 & \mathbf{1} & 0 & 0 & 0 & 0 & 0 & 0 & 0 & 0 & 0 & 0 & 0 & 0 & 0 & 0 & 0 & 0 & 0 \\
0 & 0 & 0 & 0 & 0 & 0 & 0 & \mathbf{1} & 0 & 0 & 0 & 0 & 0 & 0 & 0 & 0 & 0 & 0 & 0 & 0 & 0 & 0 & 0 & 0 \\
0 & 0 & 0 & 0 & 0 & 0 & 0 & 0 & \mathbf{1} & 0 & 0 & 0 & 0 & 0 & 0 & 0 & 0 & 0 & 0 & 0 & 0 & 0 & 0 & 0 \\
0 & 0 & 0 & 0 & 0 & 0 & 0 & 0 & 0 & \mathbf{1} & 0 & 0 & 0 & 0 & 0 & 0 & 0 & 0 & 0 & 0 & 0 & 0 & 0 & 0 \\
0 & 0 & 0 & 0 & 0 & 0 & 0 & 0 & 0 & 0 & \mathbf{1} & 0 & 0 & 0 & 0 & 0 & 0 & 0 & 0 & 0 & 0 & 0 & 0 & 0 \\
0 & 0 & 0 & 0 & 0 & 0 & 0 & 0 & 0 & \mathbf{1} & 0 & 0 & 0 & 0 & 0 & 0 & 0 & 0 & 0 & 0 & 0 & 0 & 0 & 0 \\
0 & 0 & 0 & 0 & 0 & 0 & 0 & 0 & 0 & 0 & \mathbf{1} & 0 & 0 & 0 & 0 & 0 & 0 & 0 & 0 & 0 & 0 & 0 & 0 & 0 \\
0 & 0 & 0 & 0 & 0 & 0 & 0 & 0 & 0 & \mathbf{1} & 0 & 0 & 0 & 0 & 0 & 0 & 0 & 0 & 0 & 0 & 0 & 0 & 0 & 0 \\
0 & 0 & 0 & 0 & 0 & 0 & 0 & 0 & \mathbf{1} & 0 & 0 & 0 & 0 & 0 & 0 & 0 & 0 & 0 & 0 & 0 & 0 & 0 & 0 & 0 \\
0 & 0 & 0 & 0 & 0 & 0 & 0 & \mathbf{-1} & 0 & 0 & 0 & 0 & 0 & 0 & 0 & 0 & 0 & 0 & 0 & 0 & 0 & 0 & 0 & 0 \\
0 & 0 & 0 & 0 & 0 & 0 & \mathbf{-1} & 0 & 0 & 0 & 0 & 0 & 0 & 0 & 0 & 0 & 0 & 0 & 0 & 0 & 0 & 0 & 0 & 0 \\
0 & 0 & 0 & 0 & 0 & 0 & 0 & 0 & 0 & 0 & \mathbf{1} & 0 & 0 & 0 & 0 & 0 & 0 & 0 & 0 & 0 & 0 & 0 & 0 & 0 \\
0 & 0 & 0 & 0 & 0 & 0 & 0 & 0 & 0 & 0 & 0 & 0 & 0 & 0 & 0 & \mathbf{1} & 0 & 0 & 0 & 0 & 0 & 0 & 0 & 0 \\
0 & 0 & 0 & 0 & 0 & 0 & 0 & 0 & 0 & 0 & 0 & 0 & 0 & 0 & \mathbf{1} & 0 & 0 & 0 & 0 & 0 & 0 & 0 & 0 & 0 \\
0 & 0 & 0 & 0 & 0 & 0 & 0 & 0 & 0 & 0 & 0 & 0 & \mathbf{-1} & 0 & 0 & 0 & 0 & 0 & 0 & 0 & 0 & 0 & 0 & 0 \\
0 & 0 & 0 & 0 & 0 & 0 & 0 & 0 & 0 & 0 & 0 & \mathbf{-1} & 0 & 0 & 0 & 0 & 0 & 0 & 0 & 0 & 0 & 0 & 0 & 0 \\
0 & 0 & 0 & 0 & 0 & 0 & 0 & 0 & 0 & 0 & 0 & 0 & 0 & 0 & 0 & \mathbf{1} & 0 & 0 & 0 & 0 & 0 & 0 & 0 & 0 \\
0 & 0 & 0 & 0 & 0 & 0 & 0 & 0 & 0 & 0 & 0 & 0 & \mathbf{-1} & 0 & 0 & 0 & 0 & 0 & 0 & 0 & 0 & 0 & 0 & 0 \\
0 & 0 & 0 & 0 & 0 & 0 & 0 & 0 & 0 & 0 & 0 & 0 & 0 & \mathbf{-1} & 0 & 0 & 0 & 0 & 0 & 0 & 0 & 0 & 0 & 0 \\
0 & 0 & 0 & 0 & 0 & 0 & 0 & 0 & 0 & 0 & 0 & 0 & 0 & 0 & \mathbf{1} & 0 & 0 & 0 & 0 & 0 & 0 & 0 & 0 & 0 \\
0 & 0 & 0 & 0 & 0 & 0 & 0 & 0 & 0 & 0 & 0 & 0 & 0 & 0 & 0 & \mathbf{1} & 0 & 0 & 0 & 0 & 0 & 0 & 0 & 0 \\
0 & 0 & 0 & 0 & 0 & 0 & 0 & 0 & 0 & 0 & 0 & 0 & 0 & 0 & 0 & 0 & \mathbf{-1} & 0 & 0 & 0 & 0 & 0 & 0 & 0 \\
0 & 0 & 0 & 0 & 0 & 0 & 0 & 0 & 0 & 0 & 0 & 0 & 0 & 0 & 0 & 0 & 0 & \mathbf{1} & 0 & 0 & 0 & 0 & 0 & 0 \\
0 & 0 & 0 & 0 & 0 & 0 & 0 & 0 & 0 & 0 & 0 & 0 & 0 & 0 & 0 & 0 & 0 & 0 & \mathbf{-1} & 0 & 0 & 0 & 0 & 0 \\
0 & 0 & 0 & 0 & 0 & 0 & 0 & 0 & 0 & 0 & 0 & 0 & 0 & 0 & 0 & 0 & 0 & 0 & 0 & \mathbf{-1} & 0 & 0 & 0 & 0 \\
0 & 0 & 0 & 0 & 0 & 0 & 0 & 0 & 0 & 0 & 0 & 0 & 0 & 0 & 0 & 0 & 0 & 0 & 0 & 0 & \mathbf{1} & 0 & 0 & 0 \\
0 & 0 & 0 & 0 & 0 & 0 & 0 & 0 & 0 & 0 & 0 & 0 & 0 & 0 & 0 & 0 & 0 & 0 & 0 & 0 & 0 & \mathbf{1} & 0 & 0 \\
0 & 0 & 0 & 0 & 0 & 0 & 0 & 0 & 0 & 0 & 0 & 0 & 0 & 0 & 0 & 0 & 0 & 0 & 0 & 0 & 0 & 0 & \mathbf{-1} & 0 \\
0 & 0 & 0 & 0 & 0 & 0 & 0 & 0 & 0 & 0 & 0 & 0 & 0 & 0 & 0 & 0 & 0 & 0 & 0 & 0 & 0 & 0 & 0 & \mathbf{1} \\
0 & 0 & 0 & 0 & 0 & 0 & 0 & 0 & 0 & 0 & 0 & 0 & 0 & 0 & 0 & 0 & 0 & 0 & 0 & 0 & 0 & 0 & \mathbf{-1} & 0 \\
0 & 0 & 0 & 0 & 0 & 0 & 0 & 0 & 0 & 0 & 0 & 0 & 0 & 0 & 0 & 0 & 0 & 0 & 0 & 0 & 0 & \mathbf{1} & 0 & 0 \\
0 & 0 & 0 & 0 & 0 & 0 & 0 & 0 & 0 & 0 & 0 & 0 & 0 & 0 & 0 & 0 & 0 & 0 & 0 & 0 & 0 & 0 & \mathbf{1} & 0 \\
0 & 0 & 0 & 0 & 0 & 0 & 0 & 0 & 0 & 0 & 0 & 0 & 0 & 0 & 0 & 0 & 0 & 0 & 0 & 0 & 0 & 0 & 0 & \mathbf{1}
\end{bmatrix}$$

Equation 5. 17

$$\begin{bmatrix}
0 & 0 & 0 & 0 & 0 & 0 & 0 & 0 & 0 & 0 & 0 & 0 & 0 & 0 & 0 & 0 & 0 & 0 & 0 & 0 & 0 & 0 & 0 & \mathbf{1} \\
0 & 0 & 0 & 0 & \mathbf{-1} & 0 & 0 & 0 & 0 & 0 & 0 & 0 & 0 & 0 & 0 & 0 & 0 & 0 & 0 & 0 & 0 & 0 & 0 & 0 \\
0 & 0 & 0 & \mathbf{1} & 0 & 0 & 0 & 0 & 0 & 0 & 0 & 0 & 0 & 0 & 0 & 0 & 0 & 0 & 0 & 0 & 0 & 0 & 0 & 0 \\
0 & 0 & \mathbf{1} & 0 & 0 & 0 & 0 & 0 & 0 & 0 & 0 & 0 & 0 & 0 & 0 & 0 & 0 & 0 & 0 & 0 & 0 & 0 & 0 & 0 \\
0 & \mathbf{1} & 0 & 0 & 0 & 0 & 0 & 0 & 0 & 0 & 0 & 0 & 0 & 0 & 0 & 0 & 0 & 0 & 0 & 0 & 0 & 0 & 0 & 0 \\
\mathbf{1} & 0 & 0 & 0 & 0 & 0 & 0 & 0 & 0 & 0 & 0 & 0 & 0 & 0 & 0 & 0 & 0 & 0 & 0 & 0 & 0 & 0 & 0 & 0 \\
0 & 0 & 0 & 0 & 0 & \mathbf{1} & 0 & 0 & 0 & 0 & 0 & 0 & 0 & 0 & 0 & 0 & 0 & 0 & 0 & 0 & 0 & 0 & 0 & 0
\end{bmatrix}$$

$$\mathbf{Z}_{3\ beams\ in\ L,\ \ point\ 3} = \begin{bmatrix}
Z_{vz3BFz3B} + Z_{Lx3C3C} & 0 & 0 & 0 & 0 & -Z_{vz3BMy3B} \\
0 & Z_{\alpha z3BMz3B} + Z_{Tx3C3C} & -Z_{\alpha z3BFy3B} & 0 & 0 & 0 \\
0 & -Z_{vy3BMz3B} & Z_{vy3BFy3B} + Z_{vy3CFy3C} & Z_{vy3CMz3C} & 0 & 0 \\
0 & 0 & Z_{\alpha z3CFy3C} & Z_{Tx3B3B} + Z_{\alpha z3CMz3C} & 0 & 0 \\
0 & 0 & 0 & 0 & Z_{Lx3B3B} + Z_{vz3CFz3C} & -Z_{vz3CMy3C} \\
-Z_{\alpha y3BFz3B} & 0 & 0 & 0 & -Z_{\alpha y3CFz3C} & Z_{\alpha y3BMy3B} + Z_{\alpha y3CMy3C}
\end{bmatrix}$$

Equation 5. 18

$$\mathbf{Z}_{4\ beams\ in\ L,\ \ point\ 4} = \begin{bmatrix}
Z_{Lx4C4C} + Z_{vz4DFz4D} & 0 & 0 & 0 & 0 & Z_{vz4DMy4D} \\
0 & Z_{Tx4C4C} + Z_{\alpha z4DMz4D} & Z_{\alpha z4DFy4D} & 0 & 0 & 0 \\
0 & Z_{vy4DMz4D} & Z_{vy4CFy4C} + Z_{vy4DFy4D} & Z_{vy4CMz4C} & 0 & 0 \\
0 & 0 & Z_{\alpha z4CFy4C} & Z_{\alpha z4CMz4C} + Z_{Tx4D4D} & 0 & 0 \\
0 & 0 & 0 & 0 & Z_{vz4CFz4C} + Z_{Lx4D4D} & -Z_{vz4CMy4C} \\
Z_{\alpha y4DFz4D} & 0 & 0 & 0 & -Z_{\alpha y4CFz4C} & Z_{\alpha y4CMy4C} + Z_{\alpha y4DMy4D}
\end{bmatrix}$$

Equation 5. 19

$$\mathbf{Z}_{4\ beams\ in\ L,\ \ point\ 1} = \begin{bmatrix}
Z_{Lx1A1A} + Z_{vz1DFz1D} & 0 & 0 & 0 & 0 & Z_{vz1DMy1D} \\
0 & Z_{Tx1A1A} + Z_{\alpha z1DMz1D} & Z_{\alpha z1DFy1D} & 0 & 0 & 0 \\
0 & Z_{vy1DMz1D} & Z_{vy1AFy1A} + Z_{vy1DFy1D} & Z_{vy1AMz1A} & 0 & 0 \\
0 & 0 & Z_{\alpha z1AFy1A} & Z_{\alpha z1AMz1A} + Z_{Tx1D1D} & 0 & 0 \\
0 & 0 & 0 & 0 & Z_{vz1AFz1A} + Z_{Lx1D1D} & Z_{vz1AMy1A} \\
Z_{\alpha y1DFz1D} & 0 & 0 & 0 & Z_{\alpha y1AFz1A} & Z_{\alpha y1AMy1A} + Z_{\alpha y1DMy1D}
\end{bmatrix}$$

Equation 5. 20

5.4 Results and validation of coupling matrices

The coupling matrices have been assembled and the resultant impedance matrices for the coupled beams determined in the previous section. To validate the results, the beam arrangements described in Section 5.4 have been modelled in MATLAB. In addition to this, finite element (FE) models have also been built in COMSOL for each scenario and their results compared with those from the coupling matrices. For each scenario, the beams were excited at the junction points with the response predicted at the same points. The comparisons between the analytical and FE models were therefore carried out in terms of driving point mobilities. This allowed the simplification of the analytical model, offering savings in computation time. The following sections provide a summary of the parameters used in each model, as well as a comparison of their results. A discussion of the results is provided within each sub-section.

The code used to model the beam mobilities in MATLAB is provided in Appendix C.

5.4.1 Model parameters

The material properties used to model the beams in different arrangements are the same as used in Section 4.4.1 to validate the output of the beam mobilities for consistency, with the exception of the length of the beams used. Shorter beams have been modelled in this section, such that the overall length of two beams coupled in line matched the length of the beams modelled in Section 4.4. While it is appreciated that the length of the beams used in the following paragraphs is reasonably small and might not often be encountered in buildings, the results should still highlight the properties of the coupled systems. The properties of the beams used in the validation exercise that follows are summarised in Table 5. 1. Additional information on the damping model considered and other assumptions used in the FE model is also provided.

Table 5. 1 Beam parameters used in MATLAB and COMSOL models to couple beams together

Parameter	Beams A & C	Beams B & D
Beam dimensions (L x W x H)	2.5 m x 0.2 m x 0.3 m	1.5 m x 0.2 m x 0.3 m
Density [1]	2200 kg/m^3	
Young's modulus [1]	27×10^{-9} Pa	
Poisson's ratio [1]	0.2	
Internal loss factor [2]	0.05	
Frequency range	1 – 5000 Hz	

[1] Values for density and Poisson's ratio are as provided in Hopkins (2007). The base value for the Young's modulus is as given in BS EN 1992-1-1:2004 (CEN, 2004).
[2] Hopkins (2007) states that dense concrete has an internal loss factor of 0.005 which is very low. However, beams in buildings will be coupled to other elements and damping of these elements will be much greater. A higher internal loss factor has therefore been used to represent these additional coupling losses.

5.4.1.1 Damping

The effect of hysteretic damping has been included in both the MATLAB and FE models, for consistency with the work described in Section 4.4.1. As such, the complex modulus of elasticity in the analytical and FE models has been taken as $27 \times 10^{-9}(1 + j0.05)$ Pa. The use of such parameter will allow the decay of energy with frequency in the beam to be evaluated.

5.4.1.2 FE model assumptions

The assumptions in the FE model of the coupled beams are as per those set out in Section 4.4.1 for the validation of the beam mobilities.

The work in Section 4.4 only included a single beam, and therefore there was no need to specify junctions between beams. However, to model the coupling between various beams, this is now required. As mentioned in Section 4.4.1, each beam has been modelled as a Bézier polygon. The start and end points of each beam were set in terms of global coordinates and COMSOL automatically coupled the beams together at the relevant points.

With the parameters used in the analytical and FE models defined, the results of the models can now be analysed. The following sections provide graphs showing the driving point mobilities for the coupled beams at the connection points for the various scenarios described in Section 5.3.

5.4.2 Two beams in line

The predicted driving point mobilities at the connection point of two beams coupled in line are given in Figure 5. 7 to Figure 5. 12. The results of the FE model are also provided in these figures for comparison. A discussion of the results obtained is included in the following paragraphs.

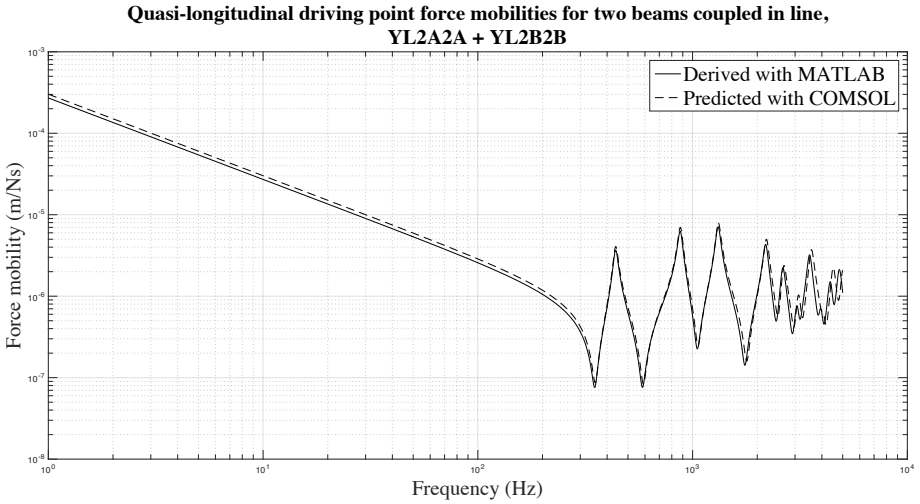

Figure 5. 7 Quasi-longitudinal driving point force mobilities for two beams coupled in line, YL2A2A + YL2B2B

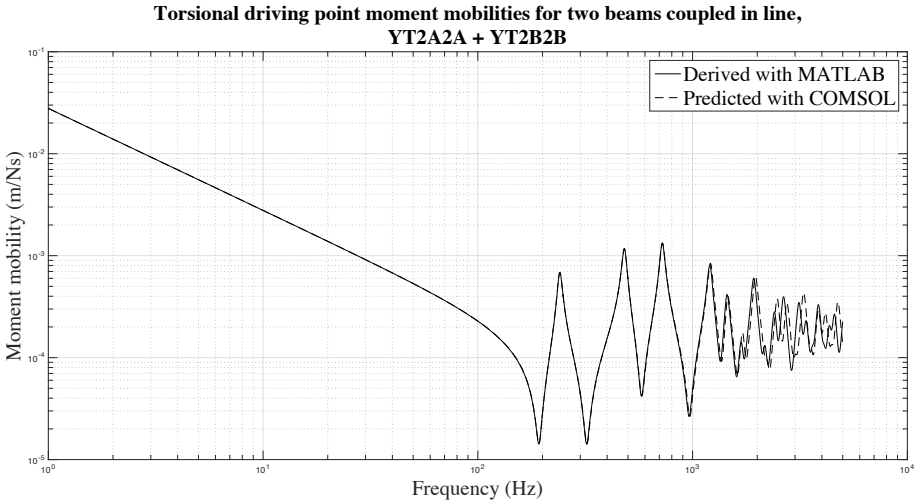

Figure 5. 8 Torsional driving point moment mobilities for two beams coupled in line, YT2A2A + YT2B2B

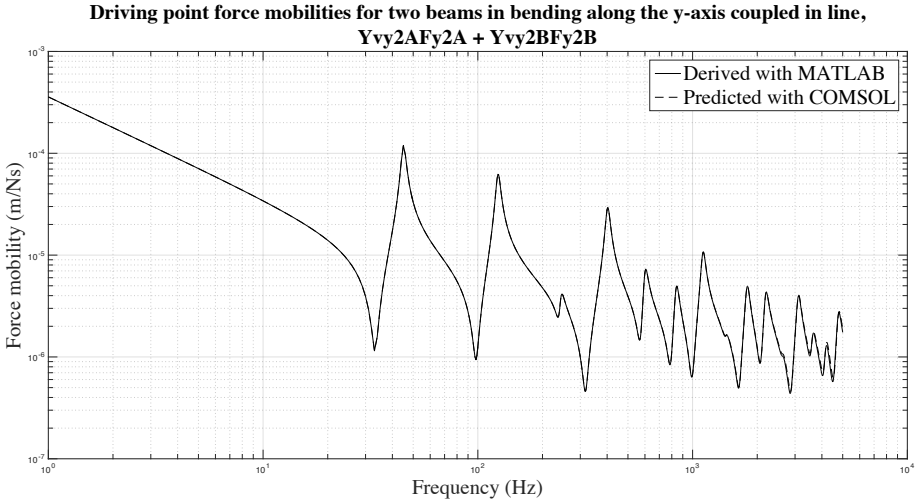

Figure 5. 9 Transverse driving point force mobilities for two beams in bending along the y-axis coupled in line, Yvy2AFy2A + Yvy2BFy2B

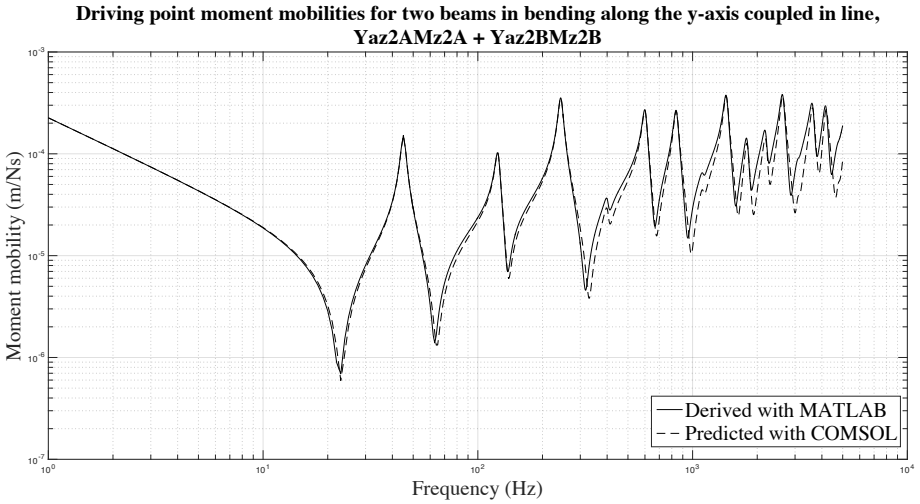

Figure 5. 10 Transverse driving point moment mobilities for two beams in bending along the y-axis coupled in line, Yaz2AMz2A + Yaz2BMz2B

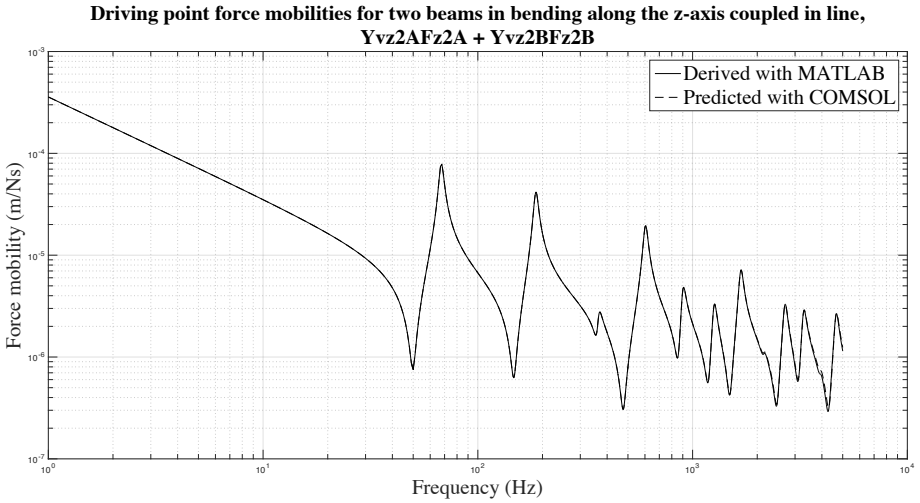

Figure 5. 11 Transverse driving point force mobilities for two beams in bending along the z-axis coupled in line, Yvz2AFz2A + Yvz2BFz2B

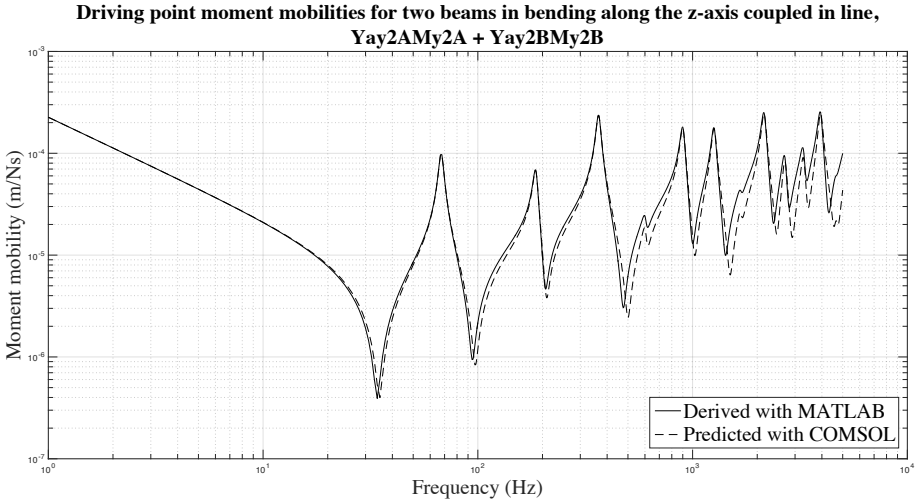

Figure 5. 12 Transverse driving point moment mobilities for two beams in bending along the z-axis coupled in line, Yay2AMy2A + Yay2BMy2B

Figure 5. 7 to Figure 5. 12 present the predicted response of beams A and B coupled in line at the connection point 2. The mass-like behaviour of the beams at low frequencies mentioned in Section 4.4 is still evident when the beams are coupled together and energy decays at a rate of 6 dB per octave. As frequency increases, however, the behaviour of the coupled beams starts to be affected by their damping, causing the amplitude of the resonant and anti-resonant peaks to reduce with frequency as can be seen.

Good agreement was also found between the analytical and FE models. The results of the latter follow the outline of the analytical model quite precisely, and the resonant and anti-resonant peaks of both models are reasonably well matched in both frequency and magnitude. This suggests that the coupling matrices derived for two beams in line are correct. However, as frequency increases, the discrepancies between the analytical and FE models become somewhat more apparent. The use of a finer mesh in the FE model would likely be required to reduce these discrepancies.

5.4.3 Two beams in an L-junction

The predicted driving point mobilities at the connection point of two beams coupled in an L-junction are given in Figure 5. 13 to Figure 5. 18. The results of the FE model are also provided in these figures for comparison. A discussion of the results obtained is included in the following paragraphs.

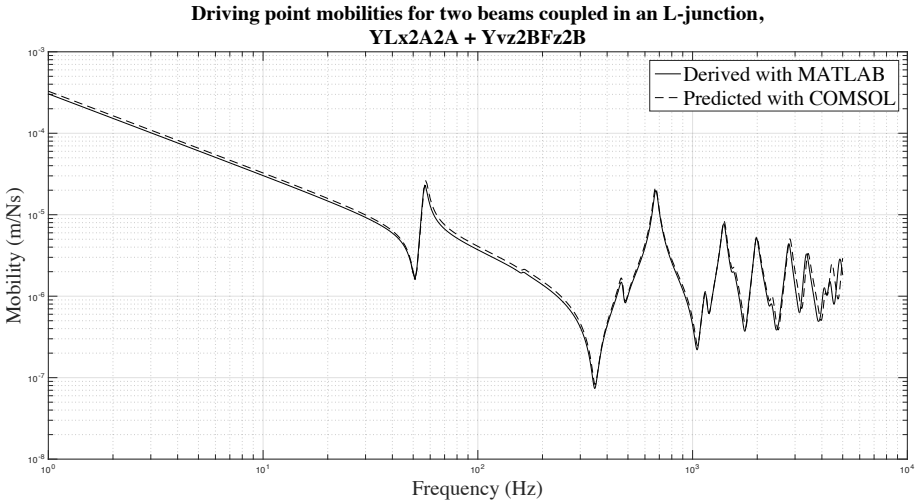

Figure 5. 13 Driving point mobilities for two beams coupled in an L-junction, YLx2A2A + Yvz2BFz2B

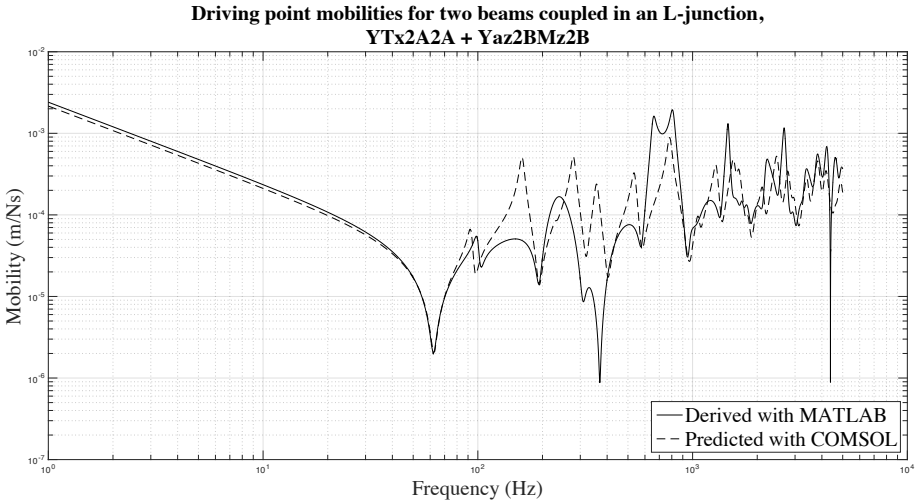

Figure 5. 14 Driving point mobilities for two beams coupled in an L-junction, YTx2A2A + Yaz2BMz2B

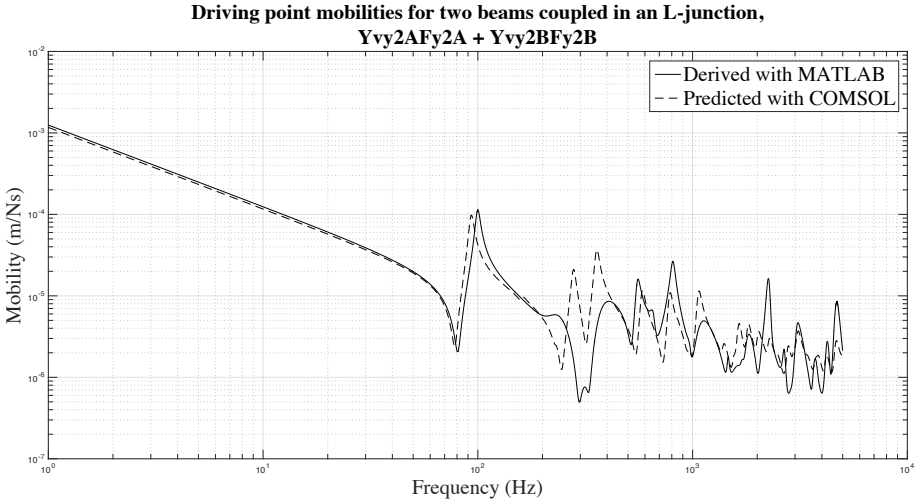

Figure 5. 15 Driving point mobilities for two beams coupled in an L-junction, Yvy2AFy2A + Yvy2BFy2B

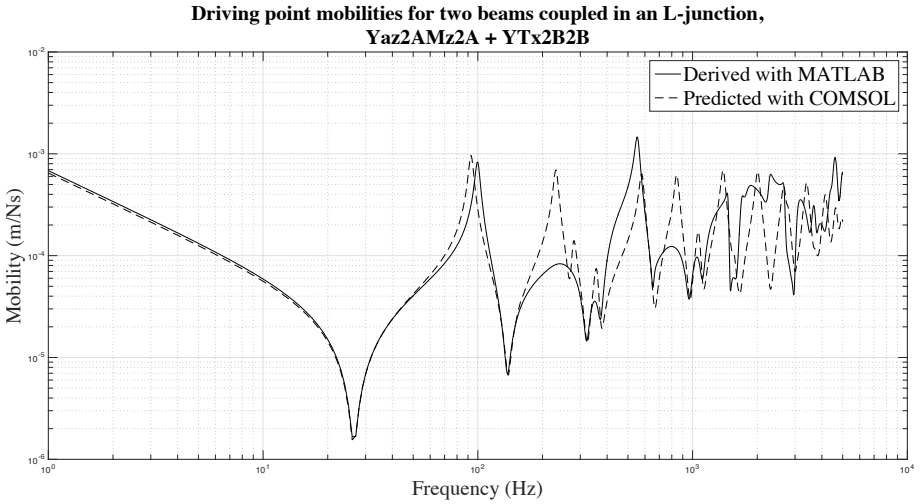

Figure 5. 16 Driving point mobilities for two beams coupled in an L-junction, Yaz2AMz2A + YTx2B2B

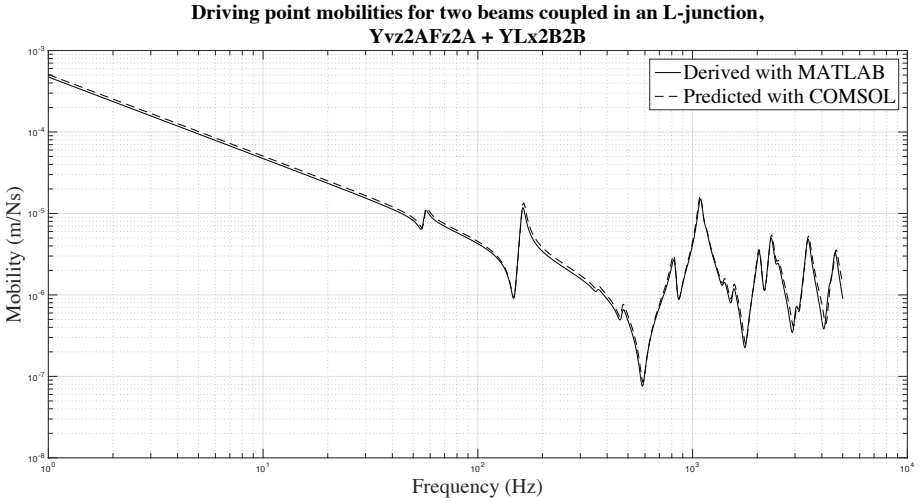

Figure 5. 17 Driving point mobilities for two beams coupled in an L-junction, Yvz2AFz2A + YLx2B2B

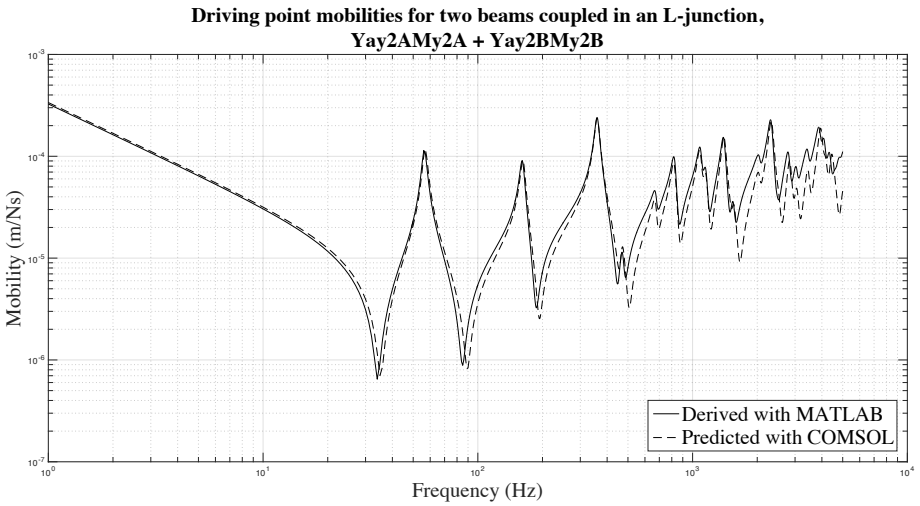

Figure 5. 18 Driving point mobilities for two beams coupled in an L-junction, Yay2AMy2A + Yay2BMy2B

Figure 5. 13 to Figure 5. 18 present the predicted response of beams A and B coupled in an L-junction at the connection point 2. As with two beams in line, the mass-like behaviour of the beams coupled manifests itself as a linear slope that decays at 6 dB per octave at low frequencies. The effect of damping becomes more apparent as frequency increases, where the decay in the amplitude of the resonant and anti-resonant peaks can be seen more prominently.

Figure 5. 13, Figure 5. 17 and Figure 5. 18 show good agreement between the analytical and FE models, with the differences between the two being just noticeable in the figures. The frequency and magnitude of the resonant and anti-resonant peaks are well matched in both models. This suggests that the coupling assigned for these degrees of freedom is correct. As frequency increases, the differences between the analytical and FE models also increase somewhat. A finer mesh in the FE model would likely be required to reduce these discrepancies.

Figure 5. 14, Figure 5. 15 and Figure 5. 16, on the other hand, show more noticeable discrepancies between the analytical and FE predicted responses of the two beams coupled in an L-junction, starting reasonably close to the first modal peak. Although at low frequencies the results of the analytical and FE models are very well matched, as frequency increases, the differences between the models are more apparent. Despite the results of the two models following a similar trend, and the resonant and anti-resonant behaviour of the coupled beams still being evident, the global modes in one of the models seem to be incorrect for all wave types, causing such discrepancies. This could potentially be attributed to assembly errors in the coupling matrices. However, if this was the case, significant discrepancies between the two models

would also be expected at low frequencies and these do not occur. In addition to this, different configurations of the coupling matrices were tested and the errors persisted. The differences between the analytical and FE models could also be attributed to the destructive interference between the torsional and bending degrees of freedom. However, should this be the case, similar results would be expected for the coupling between the other degrees of freedom. Further investigation into the discrepancies between the analytical and FE models in Figure 5. 14 to Figure 5. 16 is required. This will be suggested as part of the further work to be carried out to simplify Shorter & Langley's prediction model. As the same approach for modelling two beams in an L-junction was followed when coupling three and four beams together, it is likely that this unsolved problem in the analytical and / or FE model also affects the comparisons in the sections that follow.

5.4.4 Three beams in L-junctions

The predicted driving point mobilities at the connection point of three beams coupled in an L-junction are given in Figure 5. 19 to Figure 5. 24 for point 3. As previously mentioned, the response of the system at point 2 would be as per the two beams in an L-junction scenario presented in Section 5.4.3. The results of the FE model are also provided in these figures for comparison. A discussion of the results obtained is included in the following paragraphs.

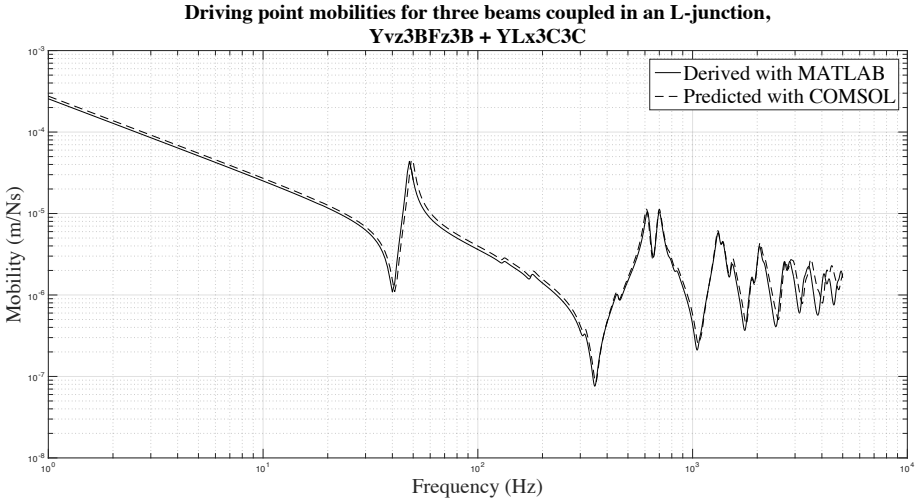

Figure 5. 19 Driving point mobilities for three beams coupled in an L-junction, Yvz3BFz3B + YLx3C3C

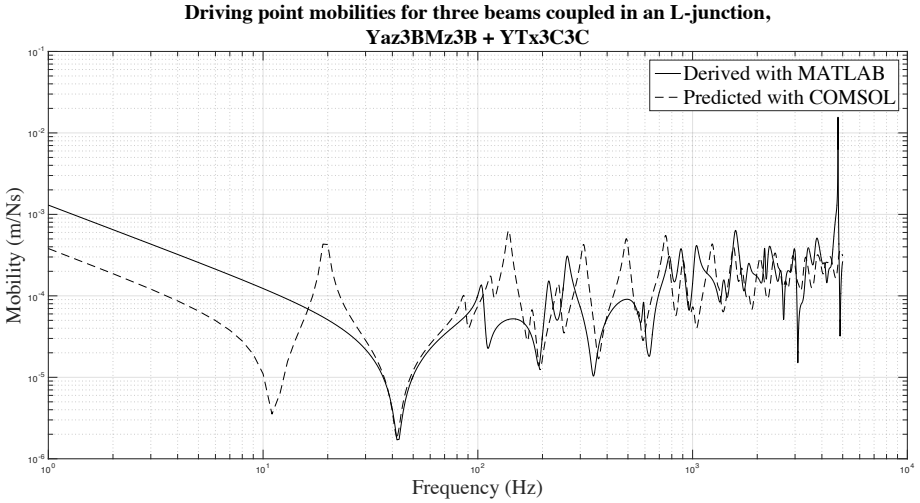

Figure 5. 20 Driving point mobilities for three beams coupled in an L-junction, Yaz3BMz3B + YTx3C3C

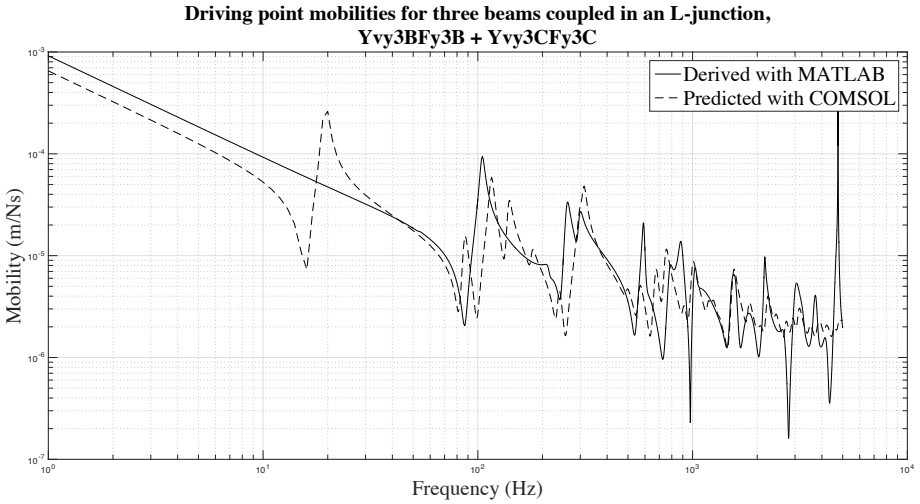

Figure 5. 21 Driving point mobilities for three beams coupled in an L-junction, Yvy3BFy3B + Yvy3CFy3C

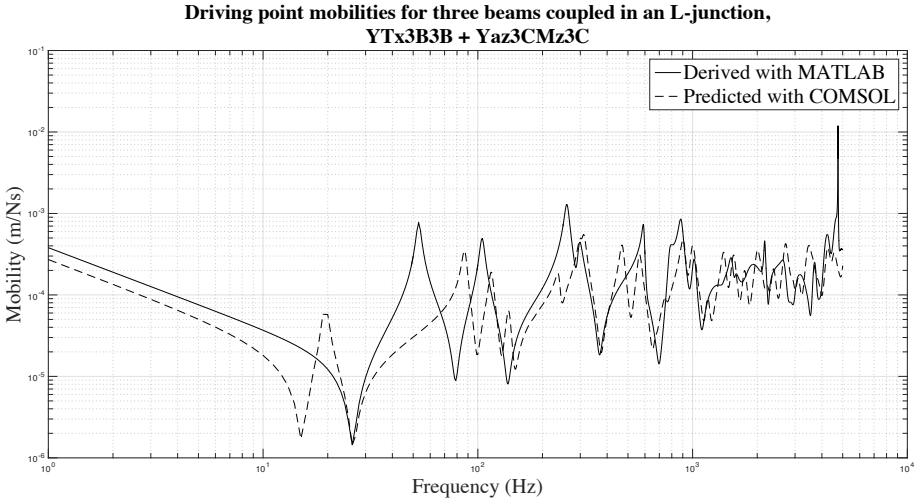

Figure 5. 22 Driving point mobilities for three beams coupled in an L-junction, YTx3B3B + Yaz3CMz3C

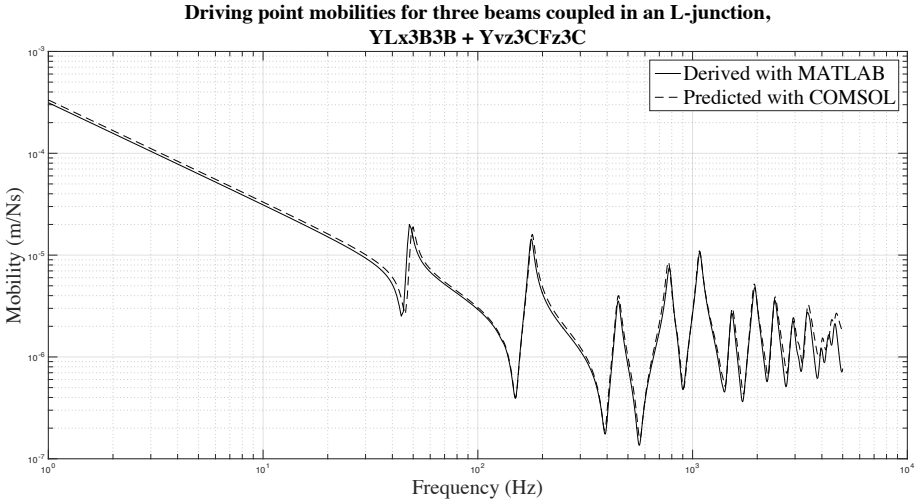

Figure 5. 23 Driving point mobilities for three beams coupled in an L-junction, YLx3B3B + Yvz3CFz3C

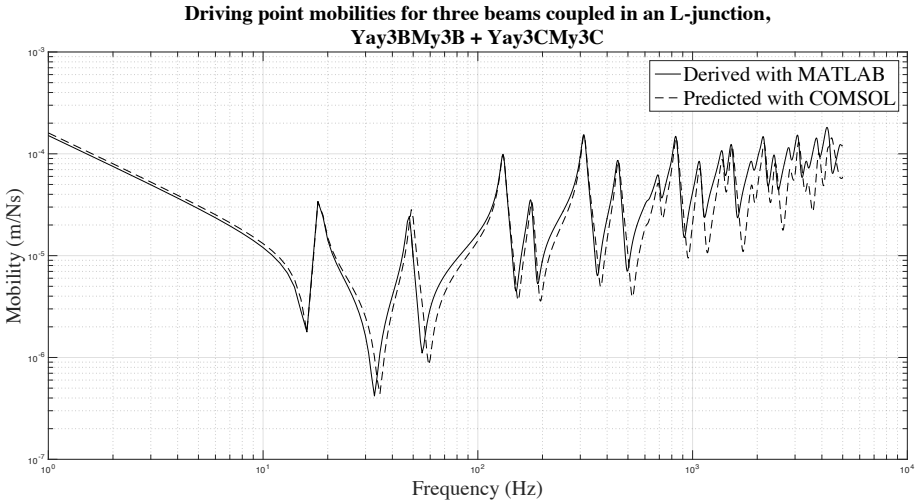

Figure 5. 24 Driving point mobilities for three beams coupled in an L-junction, Yay3BMy3B + Yay3CMy3C

Figure 5. 19 to Figure 5. 24 present the predicted response of beams B and C coupled in an L-junction at connection point 3 (refer to Section 5.3.4 for the relevant notation). As with two beams in line and in an L-junction, the mass-like behaviour of the coupled beams manifests itself as a linear slope that decays at 6 dB per octave at low frequencies. With the increase in frequency, the effect of damping becomes more significant and the amplitude of the resonant and anti-resonant peaks decays.

As with two beams in an L-junction, good agreement is shown in Figure 5. 19, Figure 5. 23 and Figure 5. 24 between the analytical and FE models. The differences between the two models are somewhat more noticeable than in the case of the two beams in an L-junction. The frequency and magnitude of the resonant and anti-resonant peaks are well matched in both models, which suggests that the coupling assigned for these degrees of freedom is correct. As frequency increases, the differences between the analytical and FE models also increase more noticeably than in the previous scenario. These differences could likely be reduced by using a finer mesh in the FE model.

More noticeable discrepancies are shown in Figure 5. 20, Figure 5. 21 and Figure 5. 22 between the analytical and FE models. While for the two beams in an L-junction scenario the response at low frequencies was very well matched, the predicted responses at similar frequencies for three beams in L-junctions are significantly different. This said, the results of the two models follow a similar trend, and the resonant and anti-resonant behaviour of the coupled beams is still evident. The results of the FE model also show additional anti-resonant behaviour at low frequencies, which is not present in the results of the analytical model. This additional anti-resonance could potentially be an effect of the presence of beam A on the response of the coupling between beams B and C at point 3, which is not accounted for in the analytical model.

The errors between the analytical and FE models could also be attributed to assembly errors in the coupling matrices. However, different configurations of the coupling matrices were tested and the errors persisted. The differences between the analytical and FE models could also be attributed to the destructive interference between different degrees of freedom, such as torsional and bending degrees of freedom. However, should this be the case, similar results would be expected for the coupling between the other degrees of freedom. Further investigation into the discrepancies between the analytical and FE models in Figure 5. 20 to Figure 5. 22 is required. This will be suggested as part of the further work to be carried out to simplify Shorter & Langley's prediction model.

5.4.5 Four beams in an L-junction

The predicted driving point mobilities at the connection points of four beams coupled in an L-junction are given in Figure 5. 25 to Figure 5. 30 for point 1 and in Figure 5. 31 to Figure 5. 36 for point 4. The response of the system at points 2 and 3 would be as per the three beams in L-junctions scenario presented in Section 5.4.4. The results of the FE model are also provided in these figures for comparison. A discussion of the results obtained is included in the following paragraphs.

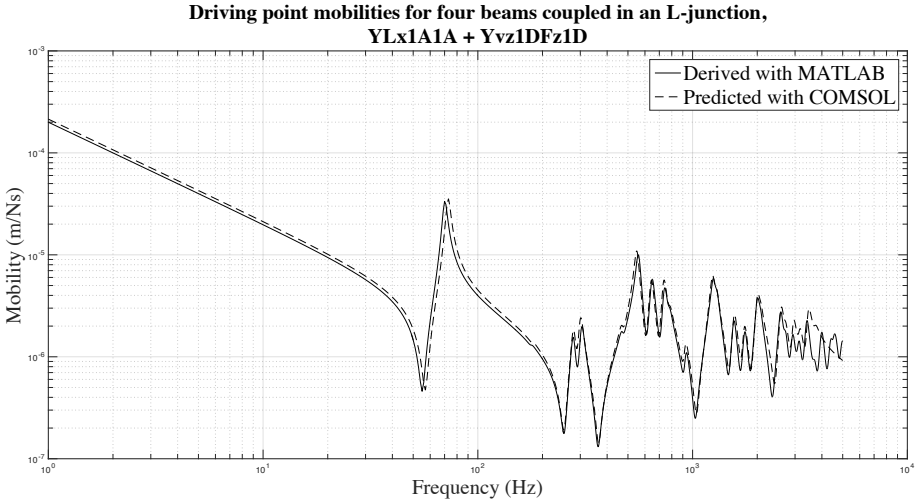

Figure 5. 25 Driving point mobilities for four beams coupled in an L-junction, YLx1A1A + Yvz1DFz1D

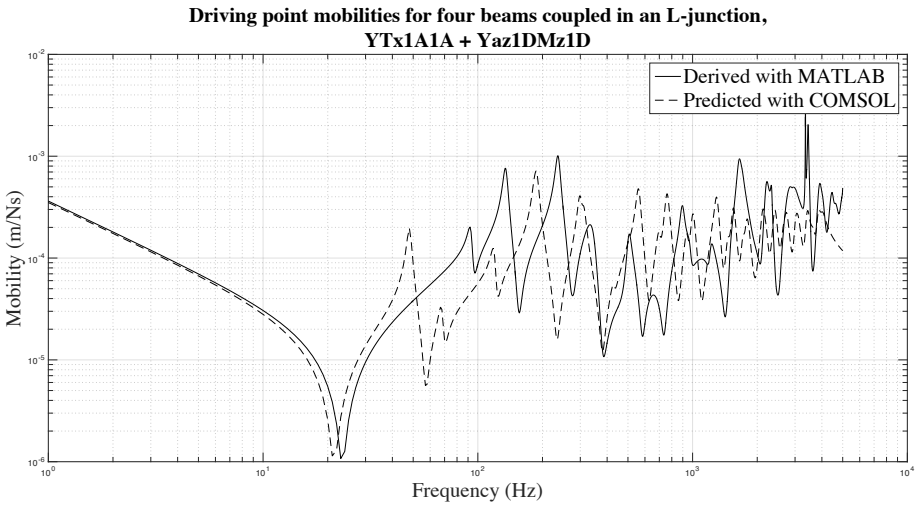

Figure 5. 26 Driving point mobilities for four beams coupled in an L-junction, YTx1A1A + Yaz1DMz1D

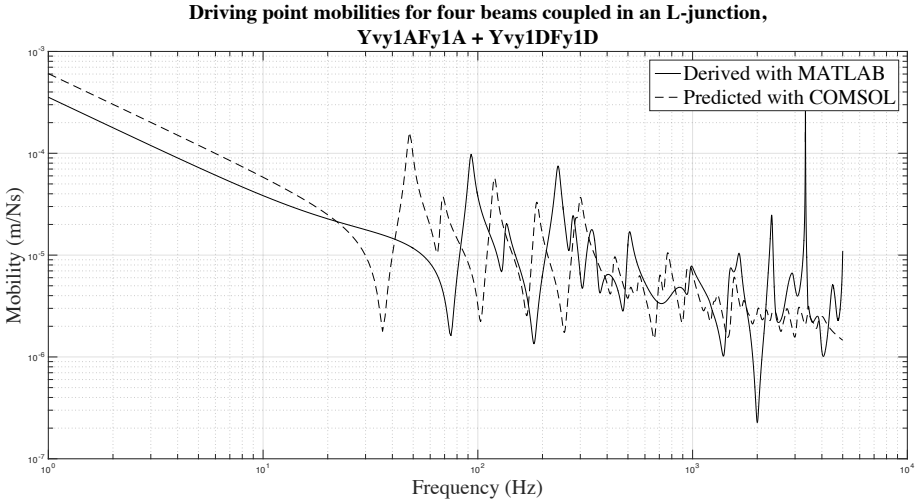

Figure 5. 27 Driving point mobilities for four beams coupled in an L-junction, Yvy1AFy1A + Yvy1DFy1D

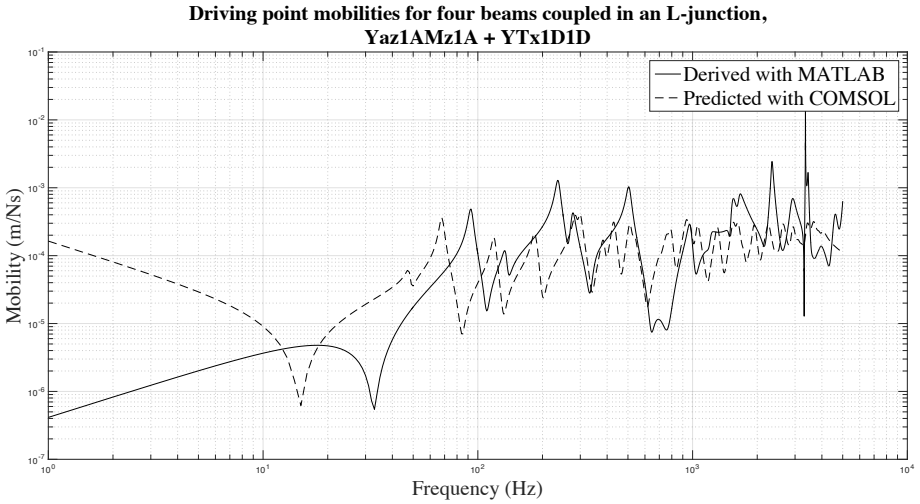

Figure 5. 28 Driving point mobilities for four beams coupled in an L-junction, Yaz1AMz1A + YTx1D1D

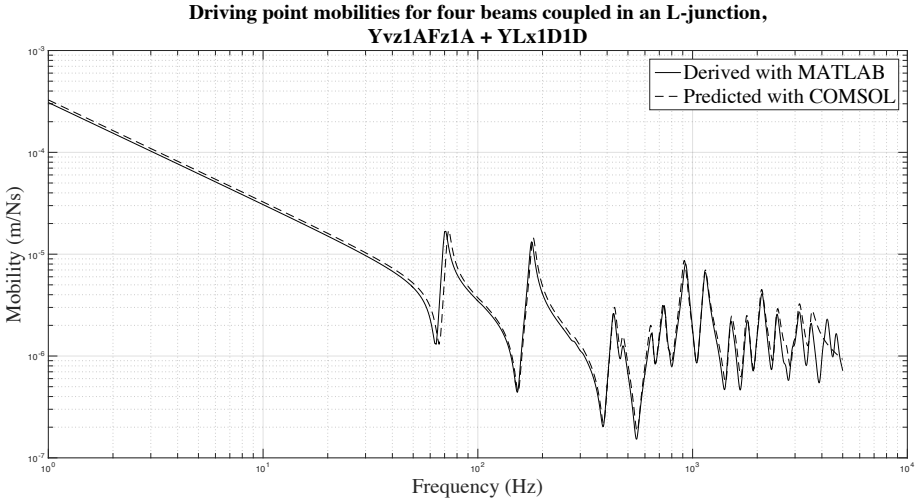

Figure 5. 29 Driving point mobilities for four beams coupled in an L-junction, Yvz1AFz1A + YLx1D1D

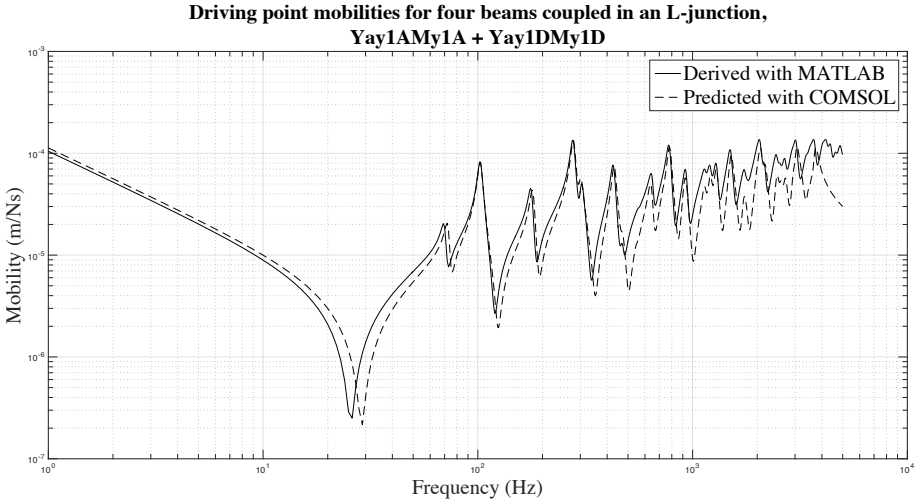

Figure 5. 30 Driving point mobilities for four beams coupled in an L-junction, Yay1AMy1A + Yay1DMy1D

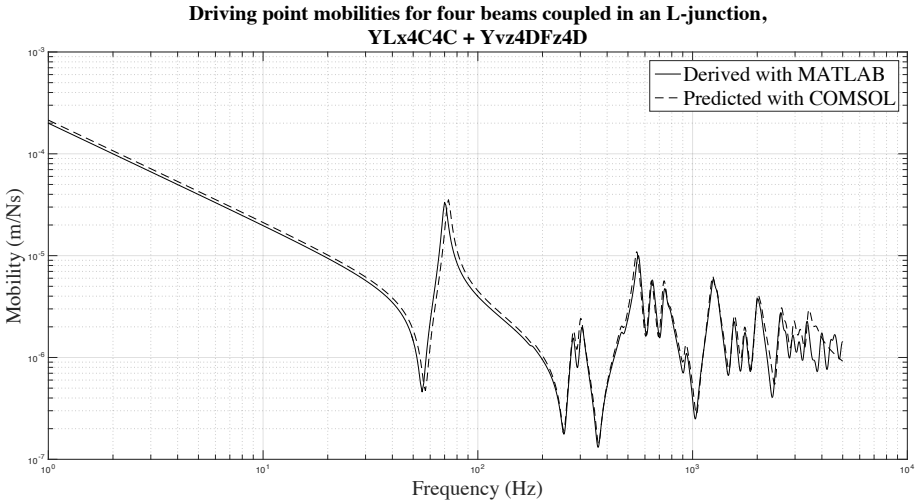

Figure 5. 31 Driving point mobilities for four beams coupled in an L-junction, YLx4C4C + Yvz4DFz4D

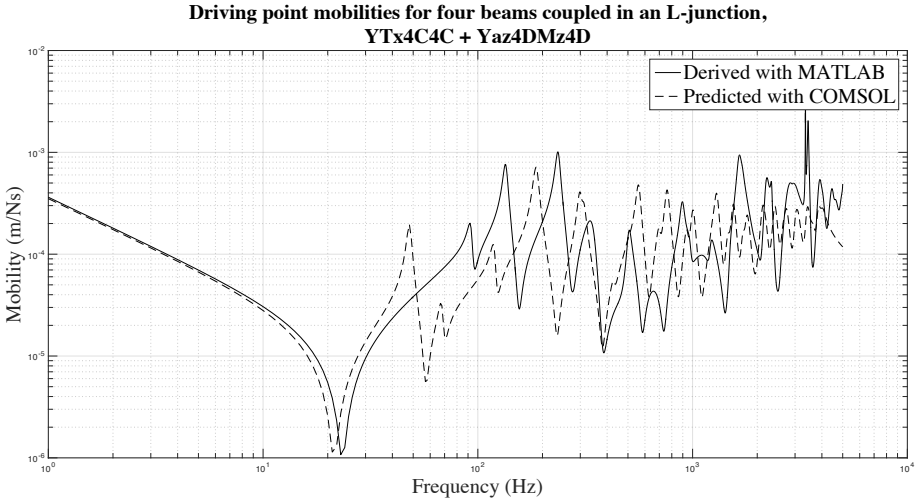

Figure 5. 32 Driving point mobilities for four beams coupled in an L-junction, YTx4C4C + Yaz4DMz4D

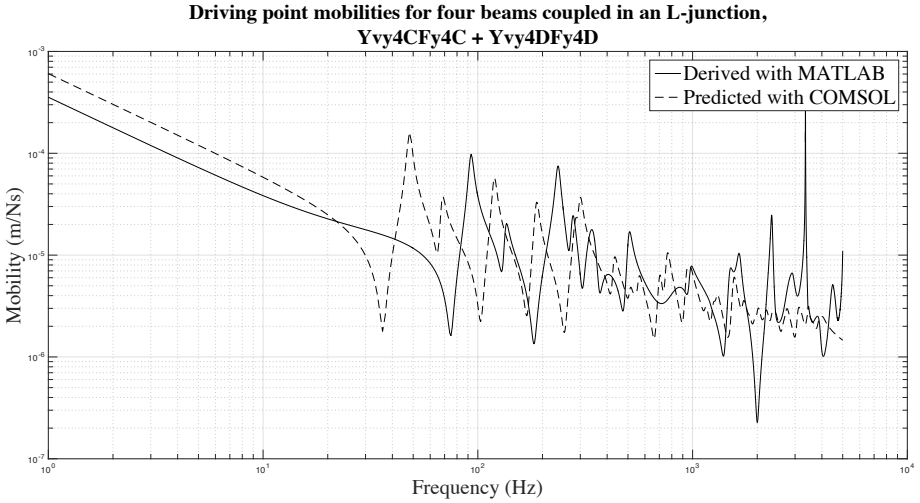

Figure 5. 33 Driving point mobilities for four beams coupled in an L-junction, Yvy4CFy4C + Yvy4DFy4D

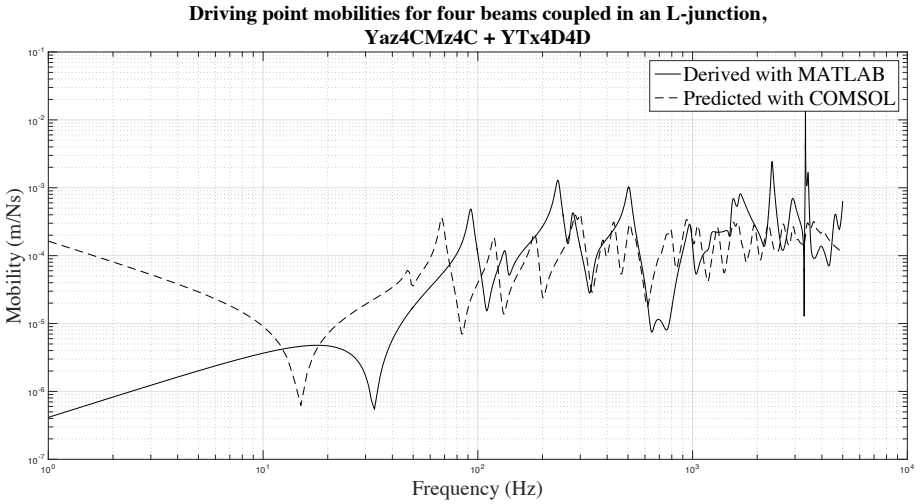

Figure 5. 34 Driving point mobilities for four beams coupled in an L-junction, Yaz4CMz4C + YTx4D4D

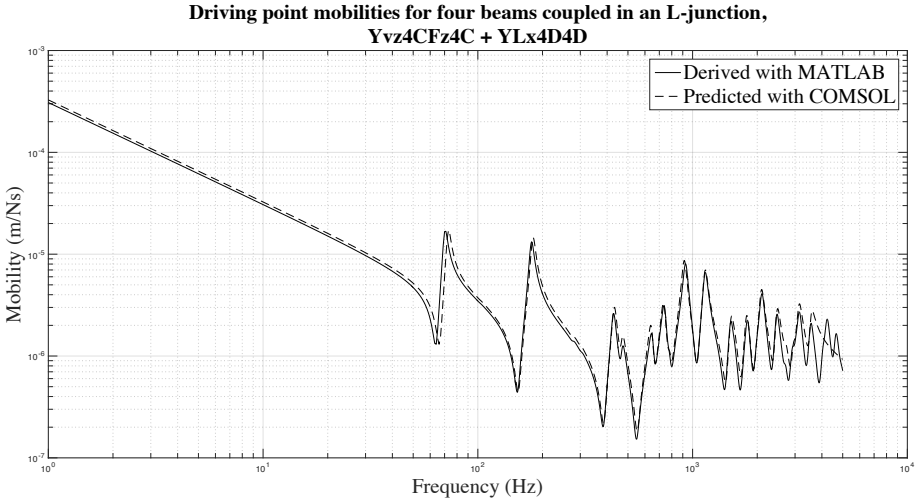

Figure 5. 35 Driving point mobilities for four beams coupled in an L-junction, Yvz4CFz4C + YLx4D4D

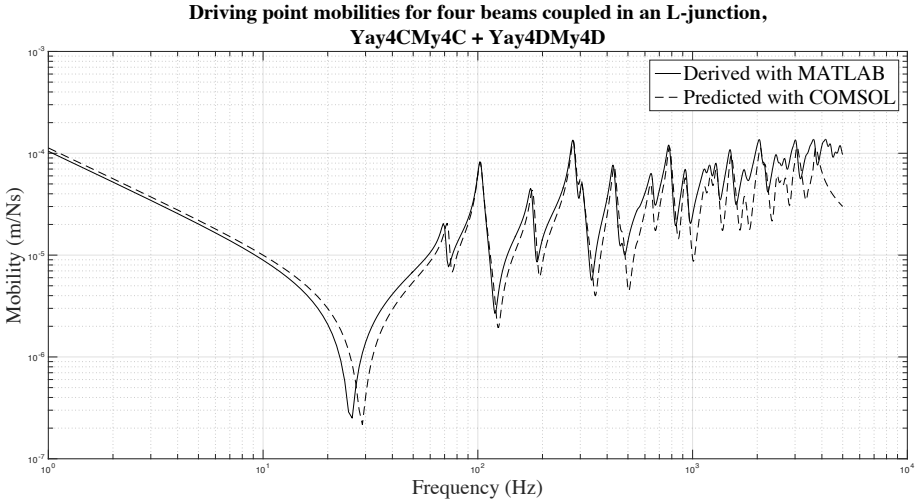

Figure 5. 36 Driving point mobilities for four beams coupled in an L-junction, Yay4CMy4C + Yay4DMy4D

Figure 5. 25 to Figure 5. 36 present the predicted response of beams A, D and C coupled in L-junctions at connection points 1 and 4 (refer to Section 5.3.4 for the relevant notation). The mass-like behaviour of the coupled beams manifests itself in most figures as a linear slope that decays at 6 dB per octave at low frequencies. With the increase in frequency, the effect of damping becomes more significant and the amplitude of the resonant and anti-resonant peaks decays.

Good agreement was found between the results of the analytical and FE models shown in Figure 5. 25, Figure 5. 29, Figure 5. 30, Figure 5. 31, Figure 5. 35 and Figure 5. 36. The differences between the two models are more noticeable than in the case of the two and three beams in L-junctions. The frequency and magnitude of the resonant and anti-resonant peaks are well matched in both models, with the exception of the degrees of freedom shown in Figure 5. 30 and Figure 5. 36, where a small shift in frequency is shown. This could be related to the level of detail included in the FE model. Despite this small shift in frequency, the results suggest that the coupling assigned for these degrees of freedom is correct. As frequency increases, the differences between the analytical and FE models also increase more noticeably than in the previous scenarios. These differences could likely be reduced by using a finer mesh in the FE model.

Figure 5. 26, Figure 5. 27, Figure 5. 28, Figure 5. 32, Figure 5. 33 and Figure 5. 34 reveal more significant discrepancies between the analytical and FE models. While for the two beams in an L-junction scenario the response at low frequencies was very well matched, the predicted responses at similar frequencies for four beams in L-junctions are quite different. This said, the results of the two models follow a

reasonably similar trend. The resonant and anti-resonant behaviour of the coupled beams is still evident. However, the frequencies at which they occur in each model are noticeably different. As per the discussion for three beams coupled in L-junctions, there is a chance that the significant differences between the two models are related to the presence of the coupling between beams A, B and C, which is not accounted for in the analytical model.

The errors between the analytical and FE models could also be attributed to assembly errors in the coupling matrices. As per the previous discussions, different configurations of the coupling matrices were tested and the errors persisted. The differences between the analytical and FE models could also be attributed to the destructive interference between different degrees of freedom, such as torsional and bending degrees of freedom. However, should this be the case, similar results would be expected for the coupling between the other degrees of freedom. Further investigation into the discrepancies between the analytical and FE models in the above figures is required. This will be suggested as part of the further work to be carried out to simplify Shorter & Langley's prediction model.

5.4.6 Computation time

In addition to comparing the results of the analytical and FE models, consideration has also been given to the time each model takes to generate results to demonstrate the different computational requirements of each model. A comparison between the computation time taken for each model to run is provided in Table 5. 2, along with a discussion of the results in the subsequent paragraphs.

Table 5. 2 Comparison of computation times for each model

	Computation time of models	
	Analytical beam functions (MATLAB)	FE model (COMSOL)
Two beams in line	1 minute 14 seconds	3 minutes 59 seconds
Two beams in an L-junction	1 minute 32 seconds	4 minutes 10 seconds
Three beams in L-junctions	1 minute 32 seconds	4 minutes
Four beams in L-junctions	1 minute 56 seconds	8 minutes 26 seconds (total for excitation at points 1 and 4) 4 minutes 13 seconds (for excitation at a single point)

The difference in time taken to run the models is clear from the table. However, it should be noted that the set up of the FE model has a significant impact on the computation time needed. If the number of elements on the beam and the mesh size were optimised, the times shown in Table 5. 2 for the FE model would likely be shorter and more in line with those of the analytical model.

Similarly, if the MATLAB code for the analytical model was to be optimised, there would be potential for the run times given above to also be reduced.

One point worth noting is that the computation time for the FE model only increased marginally with the addition of more beams into to the system. The run times for the analytical model, on the other hand, increased more significantly.

The process for coupling beams together in four different scenarios commonly encountered in buildings has been set out in this chapter, in terms of the coordinate systems to use and the coupling of beams through the use of coupling matrices and impedance addition. This process was modelled in MATLAB and the results of which were compared with those of an FE model for the same scenario. Good agreement was found for most scenarios. However, further work is expected to be required to ascertain the causes of some of the discrepancies found. The computation time for the analytical and FE models has been compared. As expected, the FE model has larger computational requirements. With the beam mobilities derived in Chapter 4 and with the coupling of beams discussed in the present chapter, it is now appropriate to provide additional information on the proposed simplifications to Shorter & Langley's prediction model. This is given in the following chapter.

6 A simplified hybrid model for the prediction of structure-borne noise in buildings

With the results for the coupling of beams validated against FEM, the next step in the proposal for a simplified hybrid model for the prediction of structure-borne noise in buildings is to demonstrate how the work presented in Chapters 4 and 5 can be incorporated into Shorter & Langley's model (2005). The present chapter relates to objective 5 of this thesis and compares the main calculation stages of Shorter & Langley's hybrid model against the proposed simplified model.

6.1 Comparison between Shorter & Langley's and simplified models

As previously mentioned, buildings comprise both low frequency and high frequency elements, such as beams and plates, respectively. Low frequency elements are better modelled using a deterministic approach such as FEM or analytical functions. For high frequency elements, a statistical approach would be more appropriate. Shorter & Langley's hybrid model caters for the properties of these two types of elements in a building / vibro-acoustic system and allows them to be modelled with a flexible approach. For instance, their calculation method can account for the deterministic characteristics of an element without the need to model the whole system deterministically, allowing a solution to the problem encountered at mid-frequencies where neither FE nor SEA are strictly appropriate. (Shorter & Langley, 2005)

The lowest frequency to which SEA can be applied has been studied by many authors, in terms of the lowest number of modes needed to allow accurate statistical averaging. Typical suggested lowest values range from 2 to 30 modes per frequency band. However, as Craik (1988) states, the lower limit of SEA is not only dependent on the number of modes per frequency band, but also on the damping properties of those modes. Therefore, the lower limit of SEA will likely vary depending on the system under consideration, and so will the frequency range in the simplified model.

The various calculation steps of the full hybrid model are set out in Table 6. 1 based on information provided in Shorter & Langley (2005). Also included in this table is a brief description of how the dynamic stiffness beam model presented in the previous sections can be incorporated within the full model. Additional information on the various steps is provided in Sections 6.2 to 6.5.

Table 6. 1 Comparison of full and proposed simplified hybrid models for the prediction of structure-borne sound in buildings

Step	Shorter & Langley's model (2005)	Proposed simplified model	Notes
	System definition		
1	Divide the system into a set of coupled sub-systems, and specify connection regions for each sub-system.	As per Shorter & Langley's model.	Beams are considered to be deterministic systems, and plates (walls, floors and ceilings) statistical.
2	Define the deterministic boundaries for each sub-system.	As per Shorter & Langley's model.	Deterministic boundaries apply to junctions between beams, and between beams and plates, where the sub-system properties are fully known.
3	Specify degrees of freedom for the deterministic sub-systems and the statistical junctions, i.e. junctions between statistical elements only.	As per Shorter & Langley's model.	At least two points need to be considered on each beam when modelling the deterministic elements on their own. These are the excitation point and the reception point. At each end of the beam, the longitudinal, torsional and two bending degrees of freedom need to be accounted for, resulting in a total of 12 degrees of freedom per beam. Additional points, and consequently degrees of freedom, will likely be needed when connecting deterministic and statistical elements. As the simplified model is only intended to model beam framed buildings, i.e. there will always be a beam element in between plates, there are no connections between statistical systems.

Step	Shorter & Langley's model (2005)	Proposed simplified model	Notes
	Assembly of direct field equations		
4	Use finite or boundary element analysis to obtain the dynamic stiffness matrix, D_d, for the deterministic sub-systems at a given frequency. Specify the excitation applied to the system, S_{ff}^{ext}, in terms of a cross-spectral matrix at a given frequency.	Instead of using finite or boundary element analysis techniques to derive the dynamic stiffness matrix, D_d, for the beams, this can be found using the mobilities derived in Chapter 4 and the coupled matrices given in Chapter 5. In a real scenario, the force applied to the system / building can be determined from velocity measurements at the point of entry to the system / building. The input force can then be calculated from the relationship between velocity and mobility discussed in Chapter 4. The cross-spectrum matrix of the force S_{ff}^{ext} is calculated from the cross spectral matrix of the measured velocity and in the simplest case is given by the magnitude squared of a unit force.	The dynamic stiffness matrix is proportional to the inverse of the mobility matrix. Refer to Section 6.3 for the dynamic stiffness matrix. Additional points will be required on the beam to allow coupling to plates.
5	Calculate the direct field dynamic stiffness, $D_{dir}^{(m)}$, for each statistical sub-system. Shorter & Langley (2005) state that boundary element analysis can be used to calculate the direct field dynamic stiffness. However, they also note that using analytical expressions for such calculations would be more computationally effective.	As with the dynamic stiffness matrix for the beams, the direct field dynamic stiffness for each plate can be found from the inverse of the point mobility for the plate.	Refer to Section 6.4 for the direct field dynamic stiffness matrix.

Step	Shorter & Langley's model (2005)	Proposed simplified model	Notes
6	Assemble the total dynamic stiffness matrix for the system.	The total dynamic stiffness matrix for the system can then be assembled with the derived D_d and $D_{dir}^{(m)}$.	
	Assembly of reverberant field equations		
7	Calculate the input power to each statistical sub-system.	As per Shorter & Langley's model.	Use equation in Shorter & Langley to calculate the input power.
8	Calculate the power transfer coefficients, or coupling loss factors, between the statistical sub-systems.	As per Shorter & Langley's model.	As the simplified model is only intended to model beam framed buildings, i.e. there will always be a beam element in between plates, there are no connections between statistical systems.
9	Calculate the total power transfer coefficients for each statistical sub-system.	As per Shorter & Langley's model.	Use equation in Shorter & Langley to calculate the total power transfer coefficients for each sub-system.
10	Calculate the modal overlap factors for each statistical sub-system.	As per Shorter & Langley's model.	Calculate the modal overlap factors for each plate by using the modal density of a plate.
11	Assemble the reverberant power balance equations for the statistical sub-systems, making use of the external input powers calculated in Step 7.	As per Shorter & Langley's model.	Assemble matrix as per Shorter & Langley's model.

Step	Shorter & Langley's model (2005)	Proposed simplified model	Notes
	Solution for reverberant and direct field responses		
12	Find the ensemble average modal energy density in the reverberant field of each statistical sub-system by solving the reverberant power balance equations assembled in Step 11.	As per Shorter & Langley's model.	Solve for the average modal energy density in the reverberant field of each plate using the equations given by Shorter & Langley.
13	Determine the ensemble average cross-spectral response, $\langle S_{qq} \rangle$, using the reverberant energy levels determined.	As per Shorter & Langley's model.	Use equations in Shorter & Langley.
14	Add the energy in the direct and reverberant fields to find the total energy of each statistical sub-system.	As per Shorter & Langley's model.	
15	Repeat Steps 1 to 14 for each frequency of interest.	As per Shorter & Langley's model.	

6.2 Steps 1 to 3 – Define the system

The first steps in Shorter & Langley's (2005) model consist of correctly defining the properties of the system. This should include a description of the coupled sub-systems and their connection regions, as well as the definition of the deterministic boundaries and the specification of degrees of freedom. A description of these items based on the above paper, along with how they are applied in the simplified model, is provided in the following paragraphs.

6.2.1 Boundaries, connection regions and junctions

The definitions of boundaries, connection regions and junctions used by Shorter & Langley (2005) are provided below. Examples of how these can be applied to a beam framed building and to a simpler scenario of a plate in a beam frame are also given.

Coupled sub-systems can have two main types of boundaries. These are deterministic boundaries, which are present where the full properties of the boundary are known, and random boundaries, present when the properties of a boundary are not fully known. A sub-system that is formed by fully deterministic boundaries can be treated as a deterministic sub-system. All other sub-systems containing either only random or a mix of random and deterministic boundaries are considered to be statistical subsystems.

Each deterministic boundary will have connection regions, i.e. areas of the boundary through which energy will transfer between sub-systems, either as a result of the coupling between adjacent sub-systems or due to excitation from external sources. Connection regions can also be divided into coherently and incoherently coupled. The former is possible if the properties of the sub-system are fully known and the connection regions are within a few wavelengths of each other. At low frequencies, sub-systems are more likely to be coherently coupled as the wavelength will be longer and the connection regions will be "closer" together. If the opposite is present, however, i.e. the connection regions are many wavelengths apart and their properties are not fully known, the connection regions would be incoherently coupled. As frequency increases and the wavelength decreases, the connection regions between sub-systems will become incoherently coupled.

In addition to the above, connection regions can be coupled through the following types of junctions:

1. Deterministic junctions: junctions between deterministic sub-systems;
2. Statistical junctions: junctions between statistical sub-systems;
3. Hybrid junctions: junctions between deterministic and statistical sub-systems.

Applying the above to a beam framed building, beams and columns show long wavelength behaviour and therefore would be better modelled deterministically. Plates (walls and floors), on the other hand, have a short wavelength behaviour, meaning a statistical approach would likely produce more accurate results when modelling such elements.

Focussing now on the scenario of a plate in a beam frame, such as a wall within a building, four connection regions could be defined between the plate and the frame, one per beam. In terms of defining the deterministic boundaries for a plate in a beam frame, these would apply to the junctions between the beams, as well as between beams and plates where the sub-system properties are fully known. In this scenario, there would be no connections or boundaries between statistical systems. However, if the plate formed part of the boundaries of a room, a random boundary would exist between the plate and the room volume. Extensive work on the energy flow between plates and volumes is available from sources such as Craik (1988).

As noted in Section 5.2, for the coupling of various elements to be successful, the velocity (or displacement, when working in terms of dynamic stiffness) on both sides of the connection regions will need to be compatible.

6.2.2 Degrees of freedom and connection points

The response of the deterministic sub-systems can be described with degrees of freedom, as used in Chapters 4 and 5. In the case of the beams modelled in the previous chapters, six degrees of freedom have been accounted for at each end of each beam. These included the quasi-longitudinal, torsional and bending along the y- and z-axes degrees of freedom, and resulted in a total of 12 degrees of freedom per beam.

When modelling beams and the coupling between them, a minimum of two points need to be considered on each beam. These are the excitation point and the response point. However, when coupling statistical and deterministic sub-systems together, additional excitation and response points may be needed on the beam. This will increase the number of degrees of freedom that need to be considered.

For simplicity, the discussions in the following sections will refer to a beam coupled to a single plate. The beam has been modelled as having a total of 12 degrees of freedom, six degrees of freedom per end. Deterministic junctions will be present at both ends to couple the beam to the plate.

6.3 Step 4 – Determine the dynamic stiffness matrix and the applied excitation for the deterministic sub-systems

With the overall system defined in steps 1 to 3 above, the dynamic stiffness matrix for the deterministic sub-systems should now be determined, along with the excitation applied to the system. The following paragraphs provide the dynamic stiffness matrix for the beam and details of the excitation applied to it.

Shorter & Langley (2005) mention that finite or boundary element modelling can be used to obtain the dynamic stiffness matrix for the deterministic sub-systems. However, this can also be calculated from the mobility matrices derived in Chapter 4. It is worth noting that if the system under consideration includes more than a single deterministic sub-system, the dynamic stiffness matrix derived ought to be for the coupled deterministic sub-systems. As the scenario under consideration only comprises one deterministic sub-system, the dynamic stiffness matrix will be for the uncoupled beam.

As mentioned in Section 4.1, the dynamic stiffness matrix for a beam is directly proportional to the inverse of the mobility matrix. Equation 6. 1 to Equation 6. 6 set out the dynamic stiffness matrix for a free-free beam with six degrees of freedom at each end. For consistency, the notation used to indicate which degree of freedom the terms refer to and what axis they act on has been kept as per the previous chapters.

$$\mathbf{D}_d = j\omega\mathbf{Y}(\omega)^{-1} \qquad \text{Equation 6. 1}$$

$$\mathbf{D}_d = \begin{bmatrix} \mathbf{D}_{1\mathrm{A}1\mathrm{A}} & \mathbf{D}_{1\mathrm{A}2\mathrm{A}} \\ \mathbf{D}_{2\mathrm{A}1\mathrm{A}} & \mathbf{D}_{2\mathrm{A}2\mathrm{A}} \end{bmatrix} \qquad \text{Equation 6. 2}$$

$$\mathbf{D}_{1\mathrm{A}1\mathrm{A}} = \begin{bmatrix} D_{Lx1A1A} & 0 & 0 & 0 & 0 & 0 \\ 0 & D_{Tx1A1A} & 0 & 0 & 0 & 0 \\ 0 & 0 & D_{v_y1AF_y1A} & D_{v_y1AM_z1A} & 0 & 0 \\ 0 & 0 & D_{w_z1AF_y1A} & D_{w_z1AM_z1A} & 0 & 0 \\ 0 & 0 & 0 & 0 & D_{v_z1AF_z1A} & D_{v_z1AM_y1A} \\ 0 & 0 & 0 & 0 & D_{w_y1AF_z1A} & D_{v_y1AF_y1A} \end{bmatrix} \qquad \text{Equation 6. 3}$$

$$\mathbf{D}_{1\mathrm{A}2\mathrm{A}} = \begin{bmatrix} D_{Lx1A2A} & 0 & 0 & 0 & 0 & 0 \\ 0 & D_{Tx1A2A} & 0 & 0 & 0 & 0 \\ 0 & 0 & D_{v_y1AF_y2A} & D_{v_y1AM_z2A} & 0 & 0 \\ 0 & 0 & D_{w_z1AF_y2A} & D_{w_z1AM_z2A} & 0 & 0 \\ 0 & 0 & 0 & 0 & D_{v_z1AF_z2A} & D_{v_z1AM_y2A} \\ 0 & 0 & 0 & 0 & D_{w_y1F_z2} & D_{v_y1AF_y2A} \end{bmatrix} \qquad \text{Equation 6. 4}$$

$$\mathbf{D}_{2\mathrm{A}1\mathrm{A}} = \begin{bmatrix} D_{Lx2A1A} & 0 & 0 & 0 & 0 & 0 \\ 0 & D_{Tx2A1A} & 0 & 0 & 0 & 0 \\ 0 & 0 & D_{v_y2AF_y1A} & D_{v_y2AM_z1A} & 0 & 0 \\ 0 & 0 & D_{w_z2AF_y1A} & D_{w_z2AM_z1A} & 0 & 0 \\ 0 & 0 & 0 & 0 & D_{v_z2AF_z1A} & D_{v_z2AM_y1A} \\ 0 & 0 & 0 & 0 & D_{w_y2AF_z1A} & D_{v_y2AF_y1A} \end{bmatrix} \qquad \text{Equation 6. 5}$$

$$\mathbf{D}_{2\mathrm{A}2\mathrm{A}} = \begin{bmatrix} D_{Lx2A2A} & 0 & 0 & 0 & 0 & 0 \\ 0 & D_{Tx2A2A} & 0 & 0 & 0 & 0 \\ 0 & 0 & D_{v_y2AF_y2A} & D_{v_y2AM_z2A} & 0 & 0 \\ 0 & 0 & D_{w_z2AF_y2A} & D_{w_z2AM_z2A} & 0 & 0 \\ 0 & 0 & 0 & 0 & D_{v_z2AF_z2A} & D_{v_z2AM_y2A} \\ 0 & 0 & 0 & 0 & D_{w_y2AF_z2A} & D_{v_y2AF_y2A} \end{bmatrix} \qquad \text{Equation 6. 6}$$

In addition to the dynamic stiffness matrix for the deterministic elements, the excitation applied to the system S_{ff}^{ext} needs to be specified in terms of a cross-spectral matrix. As mentioned in Table 6. 1, the cross-spectrum matrix of the force S_{ff}^{ext} can be calculated from the cross-spectral matrix of the measured velocity, which is given by the magnitude squared of a unit force in its simplest scenario.

6.4 Step 5 – Calculate the direct field dynamic stiffness matrix for each statistical sub-system

Using a similar method to that described in Section 6.3 to model the statistical sub-systems would require the properties of these to be known exactly. However, this is not always possible and as Shorter & Langley (2005) state *"there is therefore an unavoidable amount of uncertainty (or missing information) associated with the properties of such subsystems"*.

As such, instead of deriving the global dynamic stiffness matrix for each statistical sub-system, the dynamic behaviour of these sub-systems can be modelled statistically by describing their response as a superposition of direct and reverberant fields. When an excitation is applied to a deterministic boundary of a statistical sub-system, such as the boundary between a plate and a beam, the displacement field generated can describe the direct field within the statistical sub-system. Therefore, the direct field of a statistical sub-system can be coupled with a deterministic sub-system. (Shorter & Langley, 2005)

Shorter & Langley's (2005) model states that the direct field dynamic stiffness matrix for the statistical sub-systems can be calculated using a boundary element model. However, the direct field dynamic stiffness matrix for a plate $\mathbf{D}_{dir}^{(m)}$ can also be derived from its mobility matrix $\mathbf{Y}_{infinite\ plate}$, as shown in Equation 6. 7. The term (m) refers to the *m*th statistical sub-system. In the simple case of a beam coupled to a plate, $m = 1$.

$$\mathbf{D}_{dir}^{(m)} = j\omega \mathbf{Y}_{infinite\ plate}^{-1} \qquad \text{Equation 6. 7}$$

The driving point mobility for an infinite plate in bending along the y-axis can be found from Equation 6. 8, as provided by Su (2003).

$$\mathbf{Y}_{\mathrm{vyiFyj}} = Y_{\infty}\left(H_0^{(2)}(kr_{ij}) - H_0^{(2)}(-jkr_{ij})\right) \quad \text{Equation 6. 8}$$

where

$Y_{\infty} = 8\sqrt{Dm''}$ is the characteristic mobility; Equation 6. 9

$D = \frac{Eh^3}{12(1-\nu^2)}$ is the bending stiffness; Equation 6. 10

$k = \frac{\omega^2 m''}{D}$ is the wavenumber; Equation 6. 11

$H_0^{(2)}$ is a Hankel function of the second order;

And r_{ij} is the distance between points i and j on the plate.

The transfer and moment mobilities for the plate ($\mathbf{Y}_{\mathrm{vyiMzj}}$, $\mathbf{Y}_{\mathrm{aziFyj}}$ and $\mathbf{Y}_{\mathrm{aziMzj}}$, respectively) can be found using the same method as described for the beams in Section 4.3.3. However, these can also be approximated using a simpler finite difference method as set out in Elliott, Moorhouse & Pavíc (2012) for beams.

To allow the plate to be coupled to the two ends of the beam, the number of degrees of freedom on the plate should match those of the beam. This essentially means that the second bending degree of freedom along the z- axis, as well as the longitudinal and transverse shear degrees of freedom will also need to be accounted for. The inclusion of these in the mobility, and subsequently dynamic stiffness matrix, will generate a 12 x 12 matrix as for the beam.

6.5 Step 6 – Assemble the total dynamic stiffness matrix for the system

The next step in Shorter & Langley's (2005) model is the assembly of the total dynamic stiffness matrix for the coupled system $\mathbf{D}_{tot}$. This can be calculated from Equation 6. 14. $\mathbf{D}_{tot}$ for a single beam and plate connected at the two ends of the beam is given by Equation 6. 15.

$$\mathbf{D}_d = j\omega \mathbf{Y}_{beam}^{-1} \quad \text{Equation 6. 12}$$

$$\mathbf{D}_{dir}^{(m)} = j\omega \mathbf{Y}_{plate(\,m)}^{-1} \quad \text{Equation 6. 13}$$

$$\mathbf{D}_{tot} = \mathbf{D}_d + \sum_m \mathbf{D}_{dir}^{(m)} \quad \text{Equation 6. 14}$$

$$\mathbf{D}_{tot} = \begin{bmatrix} \mathbf{D}_{d1A1A} + \mathbf{D}_{dir1A1A} & \mathbf{D}_{d1A2A} + \mathbf{D}_{dir1A2A} \\ \mathbf{D}_{d2A1A} + \mathbf{D}_{dir2A1A} & \mathbf{D}_{d2A2A} + \mathbf{D}_{dir2A2A} \end{bmatrix} \quad \text{Equation 6. 15}$$

At present, the above dynamic stiffness matrix only considers two excitation and response points on the beam and plate. However, in reality, additional points will likely be needed to effectively couple plates to beams along their full length. However, calculating the mobility matrix for each additional point on the beam and plate is expected to have a significant impact on the computation time of the analytical model. Therefore, by introducing more excitation and response points into the system, the advantages of using a dynamic stiffness model as replacement for a FE model will likely diminish. To ascertain the extent of such impact and whether it is feasible to replace FEM with dynamic stiffness models for complex systems, it is suggested that further research work is undertaken.

In summary, the present chapter sets out the main differences between Shorter & Langley's (2005) hybrid deterministic – statistical model and the proposed simplified prediction model. These relate to the calculation of the deterministic and direct field dynamic stiffness matrices for the various sub-systems. The replacement of the FE stage of the model with a dynamic stiffness approach has been proposed, based on the work presented in Chapters 4 and 5. However, given the likely need for additional excitation and response points on the various sub-systems to allow them to be effectively coupled, the use of a simplified model may not be appropriate for complex systems. The simplification of Shorter & Langley's (2005) model ends with the assembly of the total dynamic stiffness matrix for the system under study. The remaining steps of the original model can then be followed to complete the vibro-acoustic analysis of the system.

7 Conclusions

The following conclusions have been drawn from the research set out in the previous chapters:

- An overview of the mechanisms through which ground-borne vibration and structure-borne noise propagate from a source, such as an underground train line, through the soil and into a receiver has been provided. The parameters that affect the generation and propagation of vibration and structure-borne noise are complex and, in some cases, their impact on the propagation of energy is hard to predict.
- Extensive work on the prediction of vibration and structure-borne noise through soil and into buildings has been ongoing since the 1970s, and numerous prediction models have been developed since. These range from empirical calculation tools, which are based on data measured at a number of sites from which relationships are then derived for losses through the soil, foundations and the building itself, through to highly detailed numerical models. Although numerical prediction techniques can be more accurate than an empirical model, the latter are still widely used in the industry. A potential reason for this may be related to the high level of detail often required for such models and the associated large computational costs.
- As most prediction techniques have their limitations, some authors have taken to developing hybrid calculation tools. This type of models combine the best characteristics of two or more calculation techniques and are therefore more likely to provide more accurate results. An example of these is Shorter & Langley's (2005) hybrid FE-SEA model, which allows deterministic elements, such as beams and columns in buildings, to be modelled deterministically, while allowing statistical elements, such as walls and floors, to be modelled statistically. However, there is an inherent computational cost associated with such detailed models.

- Therefore, a simplification to Shorter & Langley's (2005) hybrid FE-SEA model has been proposed for the prediction of structure-borne noise in buildings. The deterministic elements in the model are proposed to be represented through analytical expressions for mobility / dynamic stiffness beam functions with six degrees of freedom each, while the statistical systems would be modelled using SEA as per Shorter & Langley's (2005) model. This approach is expected to provide a better representation of the structural frame of a building and its effect on vibration transmission to other elements within the building, compared with other simplified dynamic stiffness models currently available, and the use of SEA to model walls and floors will allow their resonant behaviour to be accounted for. Such approach is also expected to yield more accurate predictions, while keeping the calculation time to a minimum.
- The first step to allow the simplification of Shorter & Langley's (2005) model was to derive the analytical mobility functions for beams and columns. These have been derived from first principles for free-free beams with six degrees of freedom including quasi-longitudinal, torsional, and bending along the y- and z- axes. The results of the mobility functions were compared against a FE model for the same scenario. Good agreement was achieved between the analytical and FE models.
- With the beam mobilities derived, coupling of beams was the second step in simplifying Shorter & Langley's (2005) model. Beams were coupled in four scenarios including two beams coupled in line and two, three and four beams coupled in L-junctions to each other. The beams were coupled using the impedance addition method for which coupling matrices were developed. These matrices allow the selection of which degrees of freedom are to be coupled. The results of the impedance addition and coupling matrices have been compared against a FE model for the various scenarios.
- For two beams coupled in line, good agreement was achieved between the analytical and FE model. Slight differences in the results of the two models were noticeable at high frequencies.

- For two, three and four beams coupled in L-junctions, positive results were also obtained for some of the coupled degrees of freedom. However, larger discrepancies were encountered particularly when coupling torsional and bending degrees of freedom. Further interrogation of the coupling matrices derived for these scenarios has been suggested.
- Based on the results presented in this thesis, the replacement of FEM in Shorter & Langley's (2005) model with dynamic stiffness functions to model beams and columns in buildings may in fact be feasible. The research herein has shown that, in most instances, good agreement was present between the results of the analytical and FE models and that savings in computational costs may be available. However, to fully confirm this, further work is required. This is further discussed in Section 7.1.
- A comparison between the various stages of the full and simplified hybrid prediction models has been provided, along with suggestions for the next steps to further develop and assemble the proposed simplified model.

7.1 Opportunities for further work

The work presented in this thesis has highlighted a number of areas which would benefit from further study, especially relating to the development of the simplified structure-borne noise prediction model. These are set out below.

- Discrepancies were noted between the results of the analytical and FE models for some degrees of freedom when beams are coupled in L-junctions. One of the potential causes of these differences may be associated with the coupling matrices and how they have been derived. Therefore, it would be worth interrogating the coupling matrices used further to ascertain whether these are the cause of such differences between the analytical and FE models.
- The next step in simplifying Shorter & Langley's (2005) model would be to derive the dynamic stiffness matrix for the statistical elements of the system, using the equations and methodology provided in Chapter 6.4. The dynamic stiffness matrix for the statistical elements would need to account for the same number of degrees of freedom as the beams to allow the elements to be effectively coupled.

- The current analytical model only considers two points on the beam, one at each end. Whilst this is sufficient when coupling beams together at the ends, additional points on the beams would likely be required to allow plates to be effectively coupled to them. Further research could be undertaken on the minimum number of points that would be needed on the beams to allow effective coupling between these elements and reasonably accurate results. If the number of points needed on the beams is large, the benefit of replacing FEM with the dynamic stiffness method to model beams in the simplified model might be somewhat reduced.
- The derivation of the coupling matrices for the scenarios considered herein was done manually and was found to be very time consuming for beams with six degrees of freedom at each end. For more complex scenarios, such as when coupling beams and plates, or when assembling the full structure of a building, such task would become very challenging. Therefore, consideration could be given to the automation of the assembling of coupling matrices. This would help make the process more time efficient and might bring additional benefits in terms of computational costs.
- Additional consideration could also be given to the frequency range in which the dynamic stiffness method would be expected to be used and whether this range matches that of the FEM model being replaced.
- Lastly, if following the above works a simplified deterministic-statistical model is still found to be feasible, the complete simplified model could be assembled. The model could then be verified and validated against Shorter & Langley's (2005) model and on-site measurements.

8 References

Achenbach, J. (1973). *Wave propagation in elastic solids* (1st Edition ed.). Amsterdam: Elsevier Science Publishers B.V.

Alten, K., Friedl, H., & Flesch, R. (2010). Calculating Ground-Borne Noise From Ground-Borne Vibra- tion – A Comparison of Different Approaches. *Proceedings of ISMA 2010 including USD2010* (pp. 3431-3440). ISMA.

ANC. (2012). *ANC Guidelines - Measurement & assessment of groundborne noise & vibration* (2nd ed.). St Albans: The Association of Noise Consultants.

ARUP & ERM. (2017). *High Speed Rail (West Midlands - Crewe) Environmental Statement, Volume 5: Technical appendices, Sound noise and vibration methodology, assumptions and assessment*. Birmingham: High Speed Two (HS2) Limited.

Avillez, J. (2013). *Routine procedure for the assessment of rail-induced vibration*. Loughborough: Loughborough University.

Bahrekazemi, M. (2004). *Train-Induced Ground Vibration and Its Prediction*. Royal Institute of Technology, Division of Soil and Rock Mechanics, Department of Civil and Architectural Engineering. Stockholm: Royal Institute of Technology.

Barkan, D. (1962). *Dynamics of bases and foundations*. New York: McGraw-Hill Book Company, Inc.

Bauchau, O., & Craig, J. (2009). Euler-Bernoulli beam theory. In O. Bauchau, & J. Craig, *Structural Analysis - Solid Mechanics and Its Applications* (Vol. 163). Dordrecht: Springer.

Braile, L. (2010, February 2010). *Seismic Wave Demonstrations and Animations*. Retrieved June 7, 2017, from http://web.ics.purdue.edu/~braile/edumod/waves/WaveDemo.htm

BSI. (1990). *BS 7385-1:1990 Evaluation and measurement for vibration in buildings - Part 1: Guide for measurement of vibrations and evaluation of their effects on buildings*. British Standards Institution. London: British Standards Institution.

BSI. (1992). *BS 6472:1992 Guide to Evaluation of human exposure to vibration in buildings (1 Hz to 80 Hz)*. London: British Standards Institution.

BSI. (2005). *BS ISO 14837-1:2005 Mechanical vibration - ground-borne noise and vibration arising from rail systems - Part 1: General guidance*. London: British Standards Institution.

BSI. (2008). *BS 6472-1:2008 Guide to evaluation of human exposure to vibration in buildings - Part 1: Vibration sources other than blasting*. London: British Standards Insitution.

BSI. (2009). *BS 5228-2:2009 Code of practice for noise and vibration control on construction and open sites - Part 2: Vibration*. British Standads Institution. London: British Standads Institution.

Burroughs, C., Hambric, S., & McDevitt, T. (2000). Power flow in coupled bending and longitudinal waves in beams. *Journal of the Acoustical Society of America, 107*, 3186-3195.

Cardona, J., Romeu, J., Arcos, R., & Balastegui, A. (2010). A ground-borne vibration assessment model for rail systems at-grade. *39th International Congress on Noise Control Engineering 2010 - INTERNOISE*. Lisbon: Sociedade Portuguesa de Acústica.

CEN. (2004). *EN 1992-1-1:2004 Eurocode 2: Design of concrete structures – Part 1-1: general rules and rules for buildings* . Brussels: Comité Européen de Normalisation.

Clouteau, D., Othman, R., Arnst, M., Chebli, H., Degrande, G., Klein, R., . . . Janssens, B. (2004). A numerical model for ground-borne vibrations from underground railway traffic based on a periodic FE-BE formulation. *8th International Workshop on Railway Noise*. Buxton: International Workshop on Railway Noise.

COMSOL Multiphysics. (2018). *Reference Manual - COMSOL Multiphysics 5.3a*. Cambridge: COMSOL Multiphysics.

Cornish, R. (2000). A novel approach to optimizing and stabilizing interior noise quality in vehicles. *Proceedings of the Institute of Mechanical Engineers, Part*

D: Journal of Automobile Engineers. 214, pp. 685-692. Institute of Mechanical Engineers.

Cotoni, V., Shorter, P., & Langley, R. (2007, July). Numerical and experimental validation of a hybrid finite element-statistical energy analysis method. *Journal of the Acoustical Society of America*, 259-270.

Cox, S., Wang, A., Morison, C., Carels, P., Kelly, R., & Bewes, O. (2004). Investigations within the CONVURT Project into effectiveness of different track structures in controlling ground vibration. *Eighth International Workshop on Railway Noise*. Buxton: Eighth International Workshop on Railway Noise.

Craik, R. (1981). Damping of building structures. *Applied Acoustics, 14*, 347-359.

Craik, R. (1982). The prediction of sound transmission through buildings using statistical energy analysis. *Journal of Sound and Vibration, 82*, 505-516.

Craik, R. (1988). *Sound transmission through buildings using statistical energy analysis*. Aldershot, England: Gower Publishing Limited.

Craik, R., & Barry, P. (1992). The internal damping of building materials. *Applied Acoustics, 35*, 139-148.

Craik, R., & Osipov, A. (1995). Structural isolation of walls using elastic interlayers. *Applied Acoustics, 46*, 233-249.

Crandall, S. (1974). Propagation of noise and vibration through soil. In J. Manning, S. Gann, & J. Freidberg, *Prediction and Control of Rail Transit Noise and Vibration*. US Department of Transportation, Report No. PB 233 633.

Cremer, L., Heckl, M., & Ungar, E. (1988). *Structure-Borne Sound: Structural Vibrations and Sound Radiation at Audio Frequencies* (2nd ed.). (E. Ungar, Trans.) Berlin: Springer-Verlag.

Crossrail Ltd. (2016). *Information for developers - December 2016*. London: Crossrail Ltd.

Davis, D. (2010, August 23 - 27). A Review of Prediction Methods for Ground-Borne Noise due to Construction Activities. *Proceedings of 20th International Congress on Acoustics* (pp. 1-6). Sydney: ICA 2010.

Davis, E. (2006, December 3-6). Characterization of structure-borne noise sources using a reverberant or anechoic plate. *Inter-Noise 2006* (pp. 2658-2665). Honolulu: Inter-Noise 2006.

DB, OBERMEYER. (2003). *Erschütterungstechnischen Untersuchungen zur Ermittlung der gebäudespezifischen Übertragungsfaktoren (Vibration analysis for the determination of building-specific transmission factors)*. Munich: Deutsche Bahn.

Eitzenberger, A. (2008). *Train-induced Vibrations in Tunnels – A Review*. Luleå University of Technology, Division of Mining and Geotechnical Engineering. Luleå, Sweden: Luleå University of Technology.

Elliott, A., Moorhouse, A., & Pavíc, G. (2012). Moment excitation and the measurement of moment mobilities. *Journal of Sound and Vibration, 331*, 2499-2519.

Ewing, W., Jardetzky, W., & Press, F. (1957). *Elastic waves in layered media*. New York: McGraw-Hill Book Company, Inc.

Fahy, F., & Gardonio, P. (2007). *Sound and structural vibration. Radiation, transmission and response* (2nd ed.). Oxford: Elsevier.

Fiala, P., Degrande, G., & Augusztinovicz, F. (2007). Numerical modelling of ground-borne noise and vibration in buildings due to surface rail traffic. *Journal of Sound and Vibration, 301*, 718-738.

Forrest, J. (1999). *Modelling of Ground Vibration from Underground Railways*. University of Cambridge. Cambridge: University of Cambridge.

Forrest, J., & Hunt, H. (2006). A three-dimensional tunnel model for calculation of train-induced ground vibration. *Journal of Sound and Vibration, 294*, 687-705.

Gardonio, P., & Brennan, M. (2002). On the Origins and Development of Mobility and Impedance Methods in Structural Dynamics. *Journal of Sound and Vibration, 249*(3), 557-573.

Gordon, C. (nd). *Generic Vibration Criteria for Vibration-Sensitive Equipment*. San Mateo: Colin Gordon & Associates.

Graff, K. (1975 / 1991). *Wave motion in elastic solids* (1975 1st Edition; 1991 Reprint ed.). New York: Dover Publications, Inc.

Gupta, S., Degrande, G., & Lombaert, G. (2009). Experimental validation of a numerical model for subway induced vibrations. *Journal of Sound and Vibration, 321*, 786-812.

Gutowski, T., & Dym, C. (1976). Propagation of ground vibration: A review. *Journal of Sound and Vibration, 49*, 179-193.

Höller, C., & Gibbs, B. (2012). A substitution method for structure-borne source power in heavyweight construction. *19th International Congress on Sound and Vibration 2012. 1*, pp. 1389-1396. Vilnius, Lithuania: International Institute of Acoustics & Vibration.

Höller, C., & Gibbs, B. (2015). Indirect determination of the mobility of structure-borne sound sources. *Journal of Sound and Vibration, 344*, 38-58.

Han, S., Benaroya, H., & Wei, T. (1999). Dynamics of transversely vibration beams using four engineering theories. *Journal of Sound and Vibration, 225*(5), 935-988.

Hanson, C., Ross, J., & Towers, D. (2012). *High-Speed Ground Transportation Noise and Vibration Impact Assessment*. US Department of Transportation, Federal Railroad Administration. Washington: US Department of Transportation.

Hanson, C., Towers, D., & Meister, L. (2006). *Transit Noise and Vibration Impact Assessment*. U.S. Department of Transportation, Federal Transit Administration. Washington: U.S. Department of Transportation.

Hargreaves, J., & Cox, T. (2008). A transient boundary element method model of Schroeder diffuser scattering using well mouth impedance. *Journal of the Acoustical Society of America, 124*(5), 2942-2951.

Heckl, M. (1961). *Compedium of impedance formulas*. Cambridge, Massachusetts: Bolt Beranek and Newman Inc.

Heckl, M., Hauck, G., & Wettschureck, R. (1996). Structure-borne sound and vibration from rail traffic. *Journal of Sound and Vibration, 193*, 175-184.

Heron, K. (1994). Advanced statistical energy analysis. *Philosophical Transactions of the Royal Society of London Series A, 346*, 501-510.

High Speed 2 (HS2) Limited. (2013). *London - West Midlands Environmental Statement, Volume 5, Techincal Appendices, Methodology, assumptions and assessment - Sound, noise and vibration*. London: High Speed 2 (HS2) Limited.

Hong, S., Wang, A., & Vlahopoulos, N. (2006). A hybrid finite element formulation for a beam-plate system. *Journal of Sound and Vibration, 298*(2006), 233-256.

Hood, R., Greer, R., Breslin, M., & Williams, P. (1996). The calculation and assessment of ground-borne noise and perceptible vibration from trains in tunnels. *Journal of Sound and Vibration, 193*(1), 215-225.

Hopkins, C. (2002). Statistical energy analysis of coupled plate systems with low modal density and low modal overlap. *Journal of Sound and Vibration, 251*(2), 193-214.

Hopkins, C. (2007). *Sound Insulation* (1st ed.). Oxford, United Kingdom: Elsevier Ltd.

Hopkins, C. (2009). Experimental statistical energy analysis of coupled plates with wave conversion at the junction. *Journal of Sound and Vibration, 322*, 155-166.

Hopkins, C., & Robinson, M. (2013). On the Evaluation of Decay Curves to Determine Structural Reverberation Times for Building Elements. *Acta Acustica United with Acustica, 99*, 226-244.

Hung, H. (2000). *Vibration of foundations and soils generated by high-speed trains*. National Taiwan University, Department of Civil Engineering. Taipei: National Taiwan University.

Hung, H., & Yang, Y. (2001). A review of researches on ground-borne vibrations with emphasis on those induced by trains. *Proceedings of the National Science Council, Republic of China, Part A. 25*, pp. 1-16. National Science Council, Republic of China.

Hunt, H., & Hussein, M. (2007). Chapter 123: Ground-borne vibration transmission from road and rail systems: prediction and control. In M. Crocker, *Handbook*

of Noise and Vibration Control (pp. 1458-1469). New Jersey: John Wiley & Sons, Inc.

Hussein, M. (2004). *Vibration from underground railways*. University of Cambridge, Girton College. Cambridge: University of Cambridge.

Ibrahim, R. (2008). Recent advances in nonlinear passive vibration isolators. *Journal of Sound and Vibration, 314*, 371-452.

Ishii, K., & Tachibana, H. (1978). Field measurements of structure-borne sound propagation in buildings. *Journal of the Acoustical Society of America, 64*(S27).

ISO. (1997 & 2003). *ISO 2631:1997 Mechanical vibration and shock – Evaluation of human exposure to whole-body vibration, Parts 1 and 2*. Geneva: International Organization for Standardization.

ISO. (1997). *ISO 2631-1:1997 Mechanical vibration and shock - Evaluation of human exposure to whole-body vibration - Part 1: General requirements*. Geneva: International Organization for Standardization.

Jakobsen, J. (1987). Ground vibration from rail traffic. *Journal of Low Frequency Noise and Vibration, 6*, 96-103.

Jakobsen, J. (1989). Transmission of ground-borne vibration in buildings. *Journal of Low Frequency Noise and Vibration, 8*(3), 75-80.

Jean, P., Guigou, C., & Villot, M. (2004). A 2.5D BEM Model for Ground-Structure Interaction. *Building Acoustics, 11*(3), 157-173 .

Jones, C. (1994). Use of numerical models to determine the effectiveness of anti-vibration systems for railways. *Proceedings of the Institution of Civil Engineers - Transport. 105*, pp. 43-51. Institution of Civil Engineers Publishing.

Jones, S. (2010). *Ground vibration from underground railways: how simplifying assumptions limit prediction accuracy*. University of Cambridge, Churchill College. Cambridge: University of Cambridge.

Kling, C., & Scholl, W. (2011). Transient SEA Studies on the Damping of Coupled Building Elements. *Acta Acustica united with Acustica, 97*(2011), 266-277.

Koh, Y., & White, R. (1995). Analysis and control of vibrational power transmision to machinery supporting structures subjected to a multi-excitation system, Part I: Driving point mobility matrix of beams and rectangular plates. *Journal of Sound and Vibration, 196*, 469-493.

Kompella, M., & Bernhard, B. (1993). Measurement of the statistical variation of structural-acoustic characteristics of automotive vehicle. *Proceedings of the SAE Noise and Vibration Conference*. Warrendale PA.

Kuhl, W., & Kaiser, H. (1952). Absorption of structure-borne sound in building materials without and with sand-filled cavities. *Acta Acustica united with Acustica, 2*(4), 179-188.

Kuo, K., Jones, S., Hussein, M., & Hunt, H. (2013). Recent Developments in the Pipe-in-Pipe Model for Underground-Railway Vibration Predictions. In J. Nielsen, D. Anderson, P. Gautier, M. Iida, J. Nelson, D. Thompson, . . . P. de Vos (Ed.), *Noise and Vibration Mitigation for Rail Transportation Systems - Proceedings of the 11th International Workshop on Railway Noise. 126*, pp. 321-328. Uddevalla: Springer.

Kuppelwieser, H., & Ziegler, A. (1996). A tool for predicting vibration and structure-borne noise immissions caused by railways. *Journal of Sound and Vibration, 193*, 261-267.

Kurzweil, L. (1979). Ground-borne noise and vibration from underground rail systems. *Journal of Sound and Vibration, 66*, 363 - 370.

Kwan, A. (1993). Local deformations and rotational degrees of freedom at beam-wall joints. *Computers & Structures, 48*, 615-625.

Lamb, H. (1904, January 1). On the propagation of tremors over the surface of an elastic solid. *Philosophical Transactions of the Royal Society of London, Series A, Containing Papers of a Mathematical or Physical Character, 203*(359-371), pp. 1-42.

Lang, J. (1971). Result of measurements on the control of structure-borne noise from subways. *Seventh International Congress on Acoustics*, (pp. 421-424). Budapest.

Langley, R. S. (1994). Spatially averaged frequency response envelopes for one and two-dimensional structural components. *Journal of Sound and Vibration, 178*(4), 483 - 500.

Langley, R., & Bremner, P. (1999). A hybrid method for the vibration analysis of complex structural-acoustic systems. *Journal of the Acoustical Society of America, 105*, 1657-1671.

Langley, R., Cicirello, A., & Kovalevsky, L. (2012, March 2012). The hybrid FE-SEA method. Cambridge, Cambridgeshire, United Kingdom: University of Cambridge.

Leung, R., & Pinnington, R. (1992). Wave propagation through right-angle joints with compliance: longitudinal incidence wave. *Journal of Sound and Vibration, 153*, 223-237.

Li, H., Wu, W., & Yin, X. (2017). In-plane and bending vibration analysis of a double bottom cabin using dynamic stiffness method. *24th International Congress on Sound and Vibration*. London: ICSV24.

Lotinga, M. (2014). *Investigating the accuracy of a semi-empirical model for rail-induced ground/structure-borne noise and vibration*. University of Salford, Acoustics Research Centre, School of Computing, Science and Engineering. Salford: University of Salford.

Lurcock, D., & Thompson, D. (2014). Predicting groundborne railway noise and vibration in buildings: a comparison of measurements and methods. *40th Anniversary Conference of the Institute of Acoustics 2014. 36*, pp. 139-146. Birmingham: Institute of Acoustics.

Lurcock, D., Thompson, D., & Bewes, O. (2013). Attenuation of railway noise and vibration in two concrete frame multi-storey buildings. *Noise and Vibration MItigation for Rail Transportation - Proceedings of the 11th International Workshop on Railway Noise* (pp. 297-304). Uddevalla: Springer.

Madshus, C., Bessason, B., & Hårvik, L. (1996). Prediction model for low frequency vibration from high speed railways on soft ground. *Journal of Sound and Vibration, 193*(1), 195-203.

Maksimov, D., & Tanner, G. (2011). A hybrid approach for predicting the distribution of vibro-acoustic energy in complex built-up structures. *Journal of the Acoustical Society of America, 130*(3), 1337-1347.

Manning, J., Cann, R., & Fredberg, J. (1974). *Prediction and control of rail transit noise and vibration - a state-of-the-art review*. Department for Transportation, Urban Mass Transportation Administration. Cambridge MA: Department for Transportation.

Meggitt, J., Elliott, A., & Moorhouse, A. (2016). Virtual assemblies and their use in the prediction of vibro-acoustic responses. *Proceedings of the Institute of Acoustics. 38*, pp. 165-172. Kenilworth: Institute of Acoustics.

Melke, J. (1988). Noise and vibration from underground railway lines: proposals for a prediction procedure. *Journal of Sound and Vibration, 120*, 391-406.

Moorhouse, A., & Elliott, A. (2013). The "round trip" theory for reconstruction of Green's functions at passive locations. *Journal of the Acoustical Society of America, 134*, 3605-3612.

Moorhouse, A., Evans, T., & Elliott, A. (2011). Some relationships for coupled structures and their application to measurement of structural dynamic properties in situ. *Mechanical Systems and Signal Processing, 25*, 1574-1584.

Nagy, A., Fiala, P., Márki, F., Augusztinovicz, F., Degrande, G., Jacobs, S., & Brassenx, D. (2004). Prediction of interior noise in buildings, generated by underground rail traffic. *8th International Workshop on Railway Noise*. Buxton: International Workshop on Railway Noise.

Nagy, A., Fiala, P., Márki, F., Augusztinovicz, F., Degrande, G., Jacobs, S., & Brassenx, D. (2006). Prediction of interior noise in buildings generated by underground rail traffic. *Journal of Sound and Vibration, 293*, 680-690.

Nagy, A., Fiala, P., Márki, F., Augusztinovicz, F., Degrande, G., Jacobs, S., & Brassenx, D. (2006). Prediction of interior noise in buildings generated by underground rail traffic. *Journal of Sound and Vibration, 293*(2006), 680-690.

Nelson, J., & Saurenman, H. (1983). *State-of-the-Art Review: Prediction and control of groundborne noise and vibration from rail transit trains*. Washington: US Department of Transportation Urban Mass Transportation Administration.

Nelson, J., & Saurenman, H. (1987). A prediction procedure for rail transportation groundborne noise and vibration. *Transportation Research Record*(1143), 26-35.

Nielsen, J., Anderson, D., Gautier, P., Iida, M., Nelson, J., Thompson, D., . . . de Vos, P. (Eds.). (2015). Noise and Vibration Mitigation for Rail Transportation Systems. *Proceedings of the 11th International Workshop on Railway Noise* (pp. 1-724). Berlin: Springer-Verlag.

O'Hara, G. (1967). Mechanical Impedance and Mobility Concepts. *Journal of the Acoustical Society of America, 41*(5), 1180-1184.

Osipov, A., & Vermeir, G. (1996). Sound transmission in buildings with elastic layers at joints. *Applied Acoustics, 49*(2), 141-162.

Palacios, J., Arcos, R., Prat, M., & Balastegui, A. (2009). Development of frequency-domain source models for railway vibration impact assessment. *Euronoise 2009*. Edingburgh: Euronoise 2009.

Petersson, B., & Plunt, J. (1982). On effective mobilities in the prediction of structure-borne sound transmission between a source structure and a receiving structure, Part I: Theoretical background and basic experimental studies. *Journal of Sound and Vibration, 82*(4), 517-529.

Plewa, K., Eger, T., Oliver, M., & Dickey, J. (2012). Comparison between ISO 2631-1 comfort prediction equations and self-reported comfort values during occupational exposure to whole-body vehicular vibration. *Journal of Low Frequency Noise, Vibration and Active Control, 31*(1), 43-53.

Rücker, W., & Auersch, L. (2007). A User-Friendly Prediction Tool for Railway Induced Ground Vibrations: Emission – Transmission – Immission. In B. Schulte-Werning, D. Thompson, P. Gautier, C. Hanson, B. Hemsworth, J. Nelson, . . . P. de Vos (Ed.), *Noise and Vibration Mitigation for Rail Transportation - Proceedings of the 9th International Workshop on Railway Noise* (pp. 129-135). Munich: Springer.

Rajaram, S., & Saurenman, H. (2013). Challenges in the design and fabrication of elastomeric springs for floating slab tracks. In J. Nielsen, D. Anderson, P. Gautier, M. Iida, J. Nelson, D. Thompson, . . . P. de Vos, *Noise and vibration*

mitigation for rail transportation systems (pp. 619-626). Uddevalla, Sweden: Springer.

Remington, P., Kurzweil, L., & Towers, D. (1987). Chapter 16: Low-frequency noise and vibration from trains. In P. Nelson (Ed.), *Transportation Noise Reference Book*. London: Butterworths.

Robinson, M. (2012). *Prediction of sound and vibration response using Transient Statistical Energy Analysis*. University of Liverpool, School of Architecture. Liverpool: University of Liverpool.

Romeu, J., Balastegui, A., Arcos, R., Sánchez, Á., Palacios, J., & Alarcón, G. (2009). CATdBTren project: New prediction tool of vibration impact for railway infrastructures. *The Sixteenth International Congress on Sound and Vibration* (pp. 1-8). Kraków: ICSV16.

RPS. (2004). *Groundborne Noise and Vibration Predictions - Validation on DLR Greenwich*. London: Crossrail.

RPS. (2005). *Assessment of Noise and Vibration Impacts - Volume 1 of 8: Introduction, Scope and Methodology*. London: Crossrail.

Rubin, S. (1967). Mechanical immittance- and transmission-matrix concepts . *Journal of the Acoustical Society of America, 41*(5), 1171-1179.

Sanayei, M., Anish, K., Moore, J., & Brett, C. (2014). Measurement and prediction of train-induced vibrations in a full-scale building. *Engineering Structures, 77*(2014), 119-128.

Sanayei, M., Kayiparambil P., A., Moore, J., & Brett, C. (2014). Measurement and prediction of train-induced vibrations in a full-scale building. *Engineering Structures, 77*, 119-128.

Sanayei, M., Maurya, P., Zhao, N., & Moore, J. (2012). Impedance modeling: An efficient modeling method for prediction of building floor vibrations. *Structures Congress 2012* (pp. 886-897). Chicago: American Society of Civil Engineers.

Sanayei, M., Zhao, N., Maurya, P., Moore, J., Zapfe, J., & Hines, E. (2011). IMpedance modeling for prediction of train induced floor vibrations.

Structures Congress 2011 (pp. 371-382). Las Vegas: American Society of Civil Engineers.

Saurenman, H., Nelson, J., & Wilson, G. (1982). *Handbook of Urban Rail Noise and Vibration Control*. Cambridge, MA: US Department of Transportation, Urban Mass Transportation Administration.

Sheng, X., Jones, C., & Thompson, D. (2006). Prediction of ground vibration from trains using the wavenumber finite and boundary element methods. *Journal of Sound and Vibration, 293*, 575-586.

Shorter, P., & Langley, R. (2005). On the reciprocity relationship between direct field radiation and diffuse reverberant loading. *Journal of the Acoustical Society of America, 117*, 85-95.

Shorter, P., & Langley, R. (2005). Vibro-acoustic analysis of complex systems. *Journal of Sound and Vibration, 288*, 669-699.

Soize, C. (1993, August). A model and numerical method in the medium frequency range for vibroacoustic predictions using the theory of structural fuzzy. *Journal of the Acoustical Society of America, 94*(2), 849-865.

Späh, M., & Gibbs, B. (2009). Reception plate method for characterisation of structure-borne sound sources in buildings: Assumptions and application. *Applied Acoustics, 70*, 361-368.

Su, X. (2003). *Simplified characterisation of structure-borne sound sources with multi-point connections*. University of Liverpool. Liverpool: University of Liverpool.

Su, X. (2003). *Simplified characterisation of structure-borne sound sources with multi-point connections*. University of Liverpool. Liverpool: University of Liverpool.

Thornely-Taylor, R. (2004a). The prediction of vibration, groundborne and structure-radiated noise from railways using finite difference methods - Part I: Theory. *Proceedings of the Institute of Acoustics. 26*, p. nd. nd: Institute of Acoustics.

Thornely-Taylor, R. (2004b, nd nd). The prediction of vibration, groundborne noise and structure-radiated noise using finite difference methods. *Proceedings of*

the 8th International Workshop on Railway Noise. Buxton. Retrieved April 02, 2017, from Rupert Taylor F.I.O.A: http://ruperttaylor.com/

Thornely-Taylor, R. (2005). Numerical modelling of groundborne noise and vibration from underground railways: geotechnical considerations. *Twelfth International Congress on Sound and Vibration* (pp. 1-8). Lisbon: ICSV12.

Thornely-Taylor, R. (nd, nd nd). *Ground vibration prediction and assessment*. Retrieved April 2, 2017, from Rupert Taylor F.I.O.A: http://ruperttaylor.com/

Timoshenko, S., & Goodier, J. (1970). *Theory of elasticity*. New York: McGraw-Hill.

Toronto Transit Commission. (1976). *Yonge subway northern extension noise and vibration study*. Toronto Transit Commission, Subway Construction Branch. Toronto Transit Commission.

Triepaischajonsak, N., Thompson, D., Jones, C., Ryue, J., & Priest, J. (2010). Ground vibration from trains: experimental parameter characterization and validation of a numerical model. *Proceedings of the Institution of Mechanical Engineers, Part F: Journal of Rail and Rapid Transit. 225*, pp. 140-153. Institution of Mechanical Engineers.

Trochides, A. (1991). Ground-borne vibrations in buildings near subways. *Applied Acoustics, 32*, 289-296.

Ungar, E., & Bender, E. (1975). Vibrations produced in buildings by passage of subway trains; parameter estimation for prelimiary design. *Proceedings of the 4th International Conference on Noise Control Engineering* (pp. 491-498). Sendai: Inter-noise 75.

University of Cambridge. (2014). *REF Impact Case Studies*. Retrieved October 2018, from Research Excellence Framework 2014: https://impact.ref.ac.uk/casestudies/CaseStudy.aspx?Id=8078

Vadillo, E., Herreros, J., & Walker, J. (1996). Subjective reaction to structurally radiated sound from underground railways: field results. *Journal of Sound and Vibration, 193*(1), 65-74.

Verbraken, H., Lombaert, G., & Degrande, G. (2011). Verification of an empirical prediction method for railway induced vibrations by means of numerical simulations. *Journal of Sound and Vibration, 330*, 1692-1703.

Verhas, H. (1979). Prediction of the propagation of train-induced ground vibration. *Journal of Sound and Vibration, 66*(3), 371-376.

Villot, M., Bailhache, S., Guigou, C., & Jean, P. (2015). Prediction of railway induced vibration and ground borne noise exposure in building and associated annoyance. In W. Schröder, *Notes on Numerical Fluid Mechanics and Multidisciplinary Design*. Springer.

Villot, M., Guigou, C., Jean, P., & Picard, N. (2012). *Definition of appropriate procedures to predict exposure in buildings and estimate annoyance - Deliverable D1.6*. RIVAS Railway Induced Vibration Abatement Solutions Collaborative project.

Villot, M., Ropars, P., Jean, P., Bongini, E., & Poisson, F. (2011). Modeling the influence of structural modifications on the response of a building to railway vibration. *Noise Control Engineering Journal, 59*(6), 641-651.

Wang, C., & Lai, J. (2000). Modelling the vibration behaviour of infinite structures by FEM. *Journal of Sound and Vibration, 229*(3), 453-466.

Wang, X., & Hopkins, C. (2016). Bending, longitudinal and torsional wave transmission on Euler-Bernoulli and Timoshenko beams with high propagation losses. *Journal of the Acoustical Society of America, 140*(4), 2312-2332.

With, C. (2008). *Train-induced vibrations on embankments and in buildings - Prediction and validation of some models*. Royal Institue of Technology, Division of Soil and Rock Mechanics, Department of Civil and Architectural Engineering. Stockholm: Royal Institute of Techonology.

Woodhouse, J. (1981). An introduction to statistical energy analysis of structural vibration. *Applied Acoustics, 14*, 455-469.

Yang, Y., & Hsu, L. (2006). A Review of Researches on Ground-Borne Vibrations Due to Moving Trains via Underground Tunnels. *Advances in Structural Engineering, 9*(3), 1-16.

Zapfe, J., Saurenman, H., & Fidell, S. (2009). *TCRP Web-Only Document 48: Ground-Borne Noise and Vibration in Buildings Caused by Rail Transit*.

Contractor's Final Report for TCRP Project D-12. Transportation Research Board of the National Academies. National Academy of Sciences.

Ziegler Consultants. (2009). *Theoretische Grundlagen zum Programm VIBRA-1-2-3 (Theoretical basics of the VIBRA-1-2-3 program)*. Ziegler Consultants.

Appendix A – Mobilities for a free-free beam in bending along the z-axis

Figure A. 1 to Figure A. 4 present the results of the derived mobilities for a finite free-free beam in bending along the Z-axis. A comparison with the results of the FEM model for the same scenario is also provided. These results are similar to those obtained from the derived mobilities for a free-free beam in bending along the Y-axis, presented in Section 4.4.4, and are discussed in the same section.

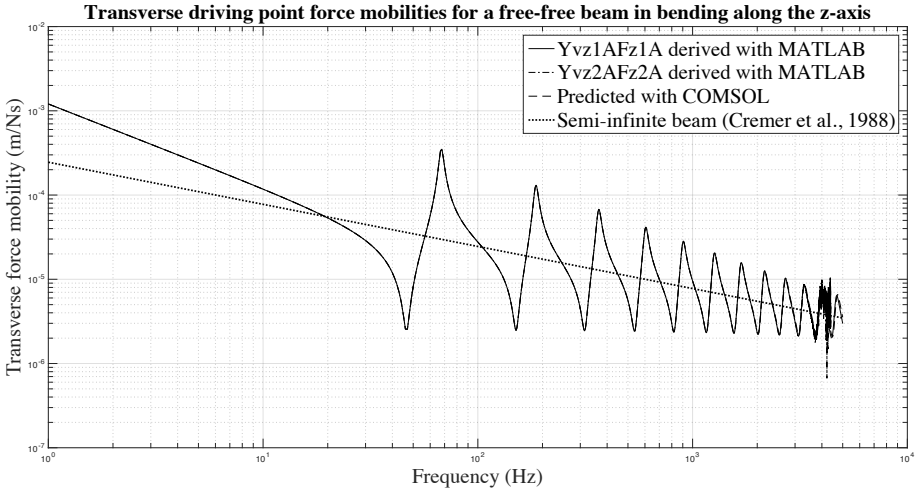

Figure A. 1 Transverse driving point force mobilities for a free-free beam in bending along the z-axis

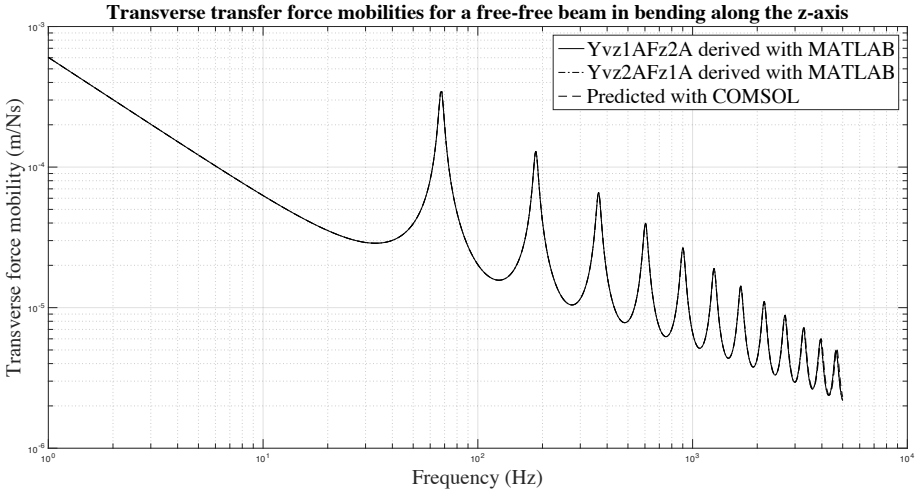

Figure A. 2 Transverse driving point force mobilities for a free-free beam in bending along the z-axis

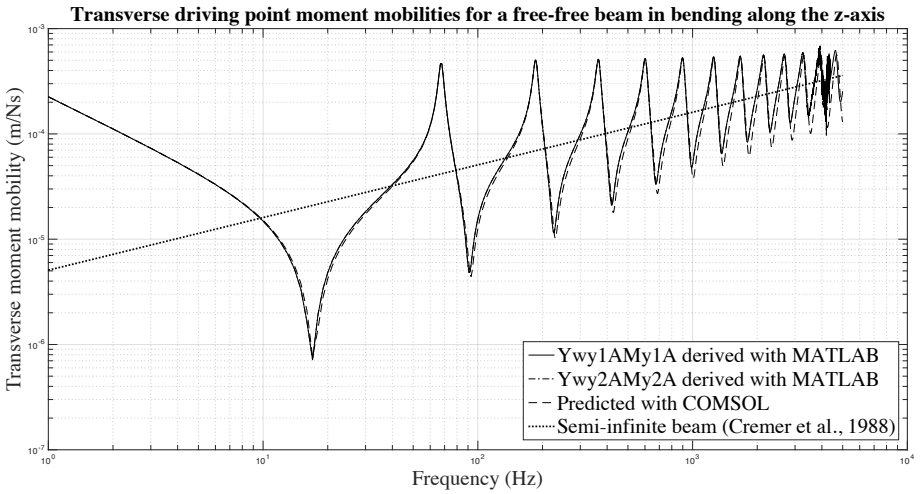

Figure A. 3 Transverse driving point moment mobilities for a free-free beam in bending along the z-axis

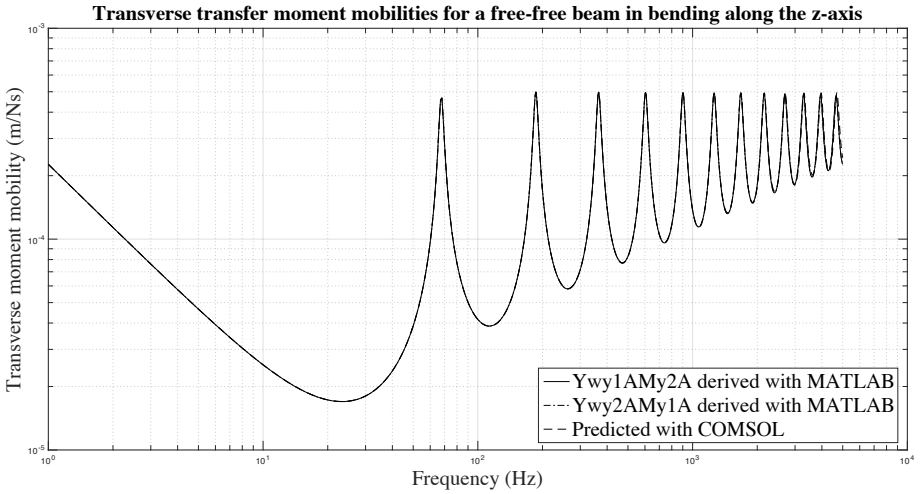

Figure A. 4 Transverse transfer moment mobilities for a free-free beam in bending along the z-axis

Appendix B – Impedance matrices for coupled beams

Coupled impedance matrix for two beams in line

ZLx1a1a	0	0	0	0	0	ZLx1a2a	0	0	0	0	0
0	ZTx1a1a	0	0	0	0	0	ZTx1a2a	0	0	0	0
0	0	Zvy1aFy1a	Zvy1aMz1a	0	0	0	0	Zvy1aFy2a	Zvy1aMz2a	0	0
0	0	Zαz1aFy1a	Zαz1aMz1a	0	0	0	0	Zαz1aFy2a	Zαz1aMz2a	0	0
0	0	0	0	Zvz1aFz1a	Zvz1aMy1a	0	0	0	0	Zvz1aFz2a	Zvz1aMy2a
0	0	0	0	Zαy1aFz1a	Zαy1aMy1a	0	0	0	0	Zαy1aFz2a	Zαy1aMy2a
ZLx2a1a	0	0	0	0	0	ZLx2a2a + ZLx2b2b	0	0	0	0	0
0	ZTx2a1a	0	0	0	0	0	ZTx2a2a + ZTx2b2b	0	0	0	0
0	0	Zvy2aFy1a	Zvy2aMz1a	0	0	0	0	Zvy2aFy2a + Zvy2bFy2b	Zvy2aMz2a+ Zvy2bMz2b	0	0
0	0	Zαz2aFy1a	Zαz2aMz1a	0	0	0	0	Zαz2aFy2a + Zαz2bFy2b	Zαz2aMz2a + Zαz2bMz2b	0	0
0	0	0	0	Zvz2aFz1a	Zvz2aMy1a	0	0	0	0	Zvz2aFz2a + Zvz2bFz2b	Zvz2aMy2a + Zvz2bMy2b
0	0	0	0	Zαy2aFz1a	Zαy2aMy1a	0	0	0	0	Zαy2aFz2a + Zαy2bFz2b	Zαy2aMy2a + Zαy2bMy2b
0	0	0	0	0	0	ZLx3b2b	0	0	0	0	0
0	0	0	0	0	0	0	ZTx3b2b	0	0	0	0
0	0	0	0	0	0	0	0	Zvy3bFy2b	Zvy3bMz2b	0	0
0	0	0	0	0	0	0	0	Zαz3bFy2b	Zαz3bMz2b	0	0
0	0	0	0	0	0	0	0	0	0	Zvz3bFz2b	Zvz3bMy2b
0	0	0	0	0	0	0	0	0	0	Zαy3bFz2b	Zαy3bMy2b

0	0	0	0	0	0
0	0	0	0	0	0
0	0	0	0	0	0
0	0	0	0	0	0
0	0	0	0	0	0
0	0	0	0	0	0
ZLx2b3b	0	0	0	0	0
0	ZTx2b3b	0	0	0	0
0	0	Zvy2bFy3b	Zvy2bMz3b	0	0
0	0	Zαz2bFy3b	Zαz2bMz3b	0	0
0	0	0	0	Zvz2bFz3b	Zvz2bMy3b
0	0	0	0	Zαy2bFz3b	Zαy2bMy3b
ZLx3b3b	0	0	0	0	0
0	ZTx3b3b	0	0	0	0
0	0	Zvy3bFy3b	Zvy3bMz3b	0	0
0	0	Zαz3bFy3b	Zαz3bMz3b	0	0
0	0	0	0	Zvz3bFz3b	Zvz3bMy3b
0	0	0	0	Zαy3bFz3b	Zαy3bMy3b

Beam A
Beam A + B
Beam B

Figure B. 1 Coupled impedance matrix for two beams in an L-junction

Coupled impedance matrix for two beams in an L-junction

ZLx1a1a	0	0	0	0	0	ZLx1a2a	0	0	0	0	0
0	ZTx1a1a	0	0	0	0	0	ZTx1a2a	0	0	0	0
0	0	Zvy1aFy1a	Zvy1aMz1a	0	0	0	0	Zvy1aFy2a	Zvy1aMz2a	0	0
0	0	Zαz1aFy1a	Zαz1aMz1a	0	0	0	0	Zαz1aFy2a	Zαz1aMz2a	0	0
0	0	0	0	Zvz1aFz1a	Zvz1aMy1a	0	0	0	0	Zvz1aFz2a	Zvz1aMy2a
0	0	0	0	Zαy1aFz1a	Zαy1aMy1a	0	0	0	0	Zαy1aFz2a	Zαy1aMy2a
ZLx2a1a	0	0	0	0	0	ZLx2a2a + Zvz2bFz2b	0	0	0	0	-Zvz2bMy2b
0	ZTx2a1a	0	0	0	0	0	ZTx2a2a + Zαz2bMz2b	-Zαz2bFy2b	0	0	0
0	0	Zvy2aFy1a	Zvy2aMz1a	0	0	0	-Zvy2bMz2b	Zvy2aFy2a + Zvy2bFy2b	Zvy2aMz2a	0	0
0	0	Zαz2aFy1a	Zαz2aMz1a	0	0	0	0	Zαz2aFy2a	Zαz2aMz2a + ZTx2b2b	0	0
0	0	0	0	Zvz2aFz1a	Zvz2aMy1a	0	0	0	0	Zvz2aFz2a + ZLx2b2b	Zvz2aMy2a
0	0	0	0	Zαy2aFz1a	Zαy2aMy1a	-Zαy2bFz2b	0	0	0	Zαy2aFz2a	Zαy2aMy2a + Zαy2bMy2b
0	0	0	0	0	0	Zvz3bFz2b	0	0	0	0	-Zvz3bMy2b
0	0	0	0	0	0	0	Zαz3bMz2b	-Zαz3bFy2b	0	0	0
0	0	0	0	0	0	0	-Zvy3bMz2b	Zvy3bFy2b	0	0	0
0	0	0	0	0	0	0	0	0	ZTx3b2b	0	0
0	0	0	0	0	0	0	0	0	0	ZLx3b2b	0
0	0	0	0	0	0	-Zαy3bFz2b	0	0	0	0	Zαy3bMy2b

0	0	0	0	0	0
0	0	0	0	0	0
0	0	0	0	0	0
0	0	0	0	0	0
0	0	0	0	0	0
0	0	0	0	0	0
Zvz2bFz3b	0	0	0	0	-Zvz2bMy3b
0	Zαz2bMz3b	-Zαz2bFy3b	0	0	0
0	-Zvy2bMz3b	Zvy2bFy3b	0	0	0
0	0	0	ZTx2b3b	0	0
0	0	0	0	ZLx2b3b	0
-Zαy2bFz3b	0	0	0	0	Zαy2bMy3b
Zvz3bFz3b	0	0	0	0	-Zvz3bMy3b
0	Zαz3bMz3b	-Zαz3bFy3b	0	0	0
0	-Zvy3bMz3b	Zvy3bFy3b	0	0	0
0	0	0	ZTx3b3b	0	0
0	0	0	0	ZLx3b3b	0
-Zαy3bFz3b	0	0	0	0	Zαy3bMy3b

Beam A
Beam A + B
Beam B

Figure B. 2 Coupled impedance matrix for two beams in an L-junction

Coupled impedance matrix for three beams in an L-junction

ZLx1a1a	0	0	0	0	0	ZLx1a2a	0	0	0	0	0
0	ZTx1a1a	0	0	0	0	0	ZTx1a2a	0	0	0	0
0	0	Zvy1aFy1a	Zvy1aMz1a	0	0	0	0	Zvy1aFy2a	Zvy1aMz2a	0	0
0	0	Zαz1aFy1a	Zαz1aMz1a	0	0	0	0	Zαz1aFy2a	Zαz1aMz2a	0	0
0	0	0	0	Zvz1aFz1a	Zvz1aMy1a	0	0	0	0	Zvz1aFz2a	Zvz1aMy2a
0	0	0	0	Zαy1aFz1a	Zαy1aMy1a	0	0	0	0	Zαy1aFz2a	Zαy1aMy2a
ZLx2a1a	0	0	0	0	0	ZLx2a2a + Zvz2bFz2b	0	0	0	0	-Zvz2bMy2b
0	ZTx2a1a	0	0	0	0	0	ZTx2a2a + Zαz2bMz2b	-Zαz2bFy2b	0	0	0
0	0	Zvy2aFy1a	Zvy2aMz1a	0	0	0	-Zvy2bMz2b	Zvy2aFy2a + Zvy2bFy2b	Zvy2aMz2a	0	0
0	0	Zαz2aFy1a	Zαz2aMz1a	0	0	0	0	Zαz2aFy2a	Zαz2aMz2a + ZTx2b2b	0	0
0	0	0	0	Zvz2aFz1a	Zvz2aMy1a	0	0	0	0	Zvz2aFz2a + ZLx2b2b	Zvz2aMy2a
0	0	0	0	Zαy2aFz1a	Zαy2aMy1a	-Zαy2bFz2b	0	0	0	Zαy2aFz2a	Zαy2aMy2a + Zαy2bMy2b
0	0	0	0	0	0	Zvz3bFz2b	0	0	0	0	-Zvz3bMy2b
0	0	0	0	0	0	0	Zαz3bMz2b	-Zαz3bFy2b	0	0	0
0	0	0	0	0	0	0	-Zvy3bMz2b	Zvy3bFy2b	0	0	0
0	0	0	0	0	0	0	0	0	ZTx3b2b	0	0
0	0	0	0	0	0	0	0	0	0	ZLx3b2b	0
0	0	0	0	0	0	-Zαy3bFz2b	0	0	0	0	Zαy3bMy2b
0	0	0	0	0	0	0	0	0	0	0	0
0	0	0	0	0	0	0	0	0	0	0	0
0	0	0	0	0	0	0	0	0	0	0	0
0	0	0	0	0	0	0	0	0	0	0	0
0	0	0	0	0	0	0	0	0	0	0	0
0	0	0	0	0	0	0	0	0	0	0	0

0	0	0	0	0	0	0	0	0	0	0	0
0	0	0	0	0	0	0	0	0	0	0	0
0	0	0	0	0	0	0	0	0	0	0	0
0	0	0	0	0	0	0	0	0	0	0	0
0	0	0	0	0	0	0	0	0	0	0	0
0	0	0	0	0	0	0	0	0	0	0	0
Zvz2bFz3b	0	0	0	0	-Zvz2bMy3b	0	0	0	0	0	0
0	Zαz2bMz3b	-Zαz2bFy3b	0	0	0	0	0	0	0	0	0
0	-Zvy2bMz3b	Zvy2bFy3b	0	0	0	0	0	0	0	0	0
0	0	0	ZTx2b3b	0	0	0	0	0	0	0	0
0	0	0	0	ZLx2b3b	0	0	0	0	0	0	0
-Zαy2bFz3b	0	0	0	0	Zαy2bMy3b	0	0	0	0	0	0
Zvz3bFz3b + ZLx3c3c	0	0	0	0	-Zvz3bMy3b	ZLx3c4c	0	0	0	0	0
0	Zαz3bMz3b + ZTx3c3c	-Zαz3bFy3b	0	0	0	0	ZTx3c4c	0	0	0	0
0	-Zvy3bMz3b	Zvy3bFy3b + Zvy3cFy3c	Zvy3cMz3c	0	0	0	0	Zvy3cFy4c	Zvy3cMz4c	0	0
0	0	Zαz3cFy3c	ZTx3b3b + Zαz3cMz3c	0	0	0	0	Zαz3cFy4c	Zαz3cMz4c	0	0
0	0	0	0	ZLx3b3b + Zvz3cFz3c	-Zvz3cMy3c	0	0	0	0	Zvz3cFz4c	-Zvz3cMy4c
-Zαy3bFz3b	0	0	0	-Zαy3cFz3c	Zαy3bMy3b + Zαy3cMy3c	0	0	0	0	-Zαy3cFz4c	Zαy3cMy4c
ZLx4c3c	0	0	0	0	0	ZLx4c4c	0	0	0	0	0
0	ZTx4c3c	0	0	0	0	0	ZTx4c4c	0	0	0	0
0	0	Zvy4cFy3c	Zvy4cMz3c	0	0	0	0	Zvy4cFy4c	Zvy4cMz4c	0	0
0	0	Zαz4cFy3c	Zαz4cMz3c	0	0	0	0	Zαz4cFy4c	Zαz4cMz4c	0	0
0	0	0	0	Zvz4cFz3c	-Zvz4cMy3c	0	0	0	0	Zvz4cFz4c	-Zvz4cMy4c
0	0	0	0	-Zαy4cFz3c	Zαy4cMy3c	0	0	0	0	-Zαy4cFz4c	Zαy4cMy4c

Beam A	(green)
Beam A + B	(yellow)
Beam B	(orange)
Beam B + C	(blue)
Beam C	(grey)

Figure B. 3 Coupled impedance matrix for three beams in an L-junction

Coupled impedance matrix for a beam frame (four beams in L-junctions)

ZLx1a1a + Zvz1dFz1d	0	0	0	0	Zvz1dMy1d	ZLx1a2a	0	0	0	0	0
0	ZTx1a1a + Zαz1dMz1d	Zαz1dFy1d	0	0	0	0	ZTx1a2a	0	0	0	0
0	Zvy1dMz1d	Zvy1aFy1a + Zvy1dFy1d	Zvy1aMz1a	0	0	0	0	Zvy1aFy2a	Zvy1aMz2a	0	0
0	0	Zαz1aFy1a	Zαz1aMz1a + ZTx1d1d	0	0	0	0	Zαz1aFy2a	Zαz1aMz2a	0	0
0	0	0	0	Zvz1aFz1a + ZLx1d1d	Zvz1aMy1a	0	0	0	0	Zvz1aFz2a	Zvz1aMy2a
Zαy1dFz1d	0	0	0	Zαy1aFz1a	Zαy1aMy1a + Zαy1dMy1d	0	0	0	0	Zαy1aFz2a	Zαy1aMy2a
ZLx2a1a	0	0	0	0	0	ZLx2a2a + Zvz2bFz2b	0	0	0	0	-Zvz2bMy2b
0	ZTx2a1a	0	0	0	0	0	ZTx2a2a + Zαz2bMz2b	-Zαz2bFy2b	0	0	0
0	0	Zvy2aFy1a	Zvy2aMz1a	0	0	0	-Zvy2bMz2b	Zvy2aFy2a + Zvy2bFy2b	Zvy2aMz2a	0	0
0	0	Zαz2aFy1a	Zαz2aMz1a	0	0	0	0	Zαz2aFy2a	Zαz2aMz2a + ZTx2b2b	0	0
0	0	0	0	Zvz2aFz1a	Zvz2aMy1a	0	0	0	0	Zvz2aFz2a + ZLx2b2b	Zvz2aMy2a
0	0	0	0	Zαy2aFz1a	Zαy2aMy1a	-Zαy2bFz2b	0	0	0	Zαy2aFz2a	Zαy2aMy2a + Zαy2bMy2b
0	0	0	0	0	0	Zvz3bFz2b	0	0	0	0	-Zvz3bMy2b
0	0	0	0	0	0	0	Zαz3bMz2b	-Zαz3bFy2b	0	0	0
0	0	0	0	0	0	0	-Zvy3bMz2b	Zvy3bFy2b	0	0	0
0	0	0	0	0	0	0	0	0	ZTx3b2b	0	0
0	0	0	0	0	0	0	0	0	0	ZLx3b2b	0
0	0	0	0	0	0	-Zαy3bFz2b	0	0	0	0	Zαy3bMy2b
Zvz4dFz1d	0	0	0	0	Zvz3cMy4c	0	0	0	0	0	0
0	Zαz4dMz1d	Zαz4dFy1d	0	0	0	0	0	0	0	0	0
0	Zvy4dMz1d	Zvy4dFy1d	0	0	0	0	0	0	0	0	0
0	0	0	ZTx4d1d	0	0	0	0	0	0	0	0
0	0	0	0	ZLx4d1d	0	0	0	0	0	0	0
Zαy4dFz1d	0	0	0	0	Zαy4dMy1d	0	0	0	0	0	0

0	0	0	0	0	0	Zvz1dFz4d	0	0	0	0	Zvz dMy4d
0	0	0	0	0	0	0	Zαz1dMz4d	Zαz1dFy4d	0	0	0
0	0	0	0	0	0	0	Zvy1dMz4d	Zvy1dFy4d	0	0	0
0	0	0	0	0	0	0	0	0	ZTx1d4d	0	0
0	0	0	0	0	0	0	0	0	0	ZLx1d4d	0
0	0	0	0	0	0	Zαy1dFz4d	0	0	0	0	Zαy1dMy4d
Zvz2bFz3b	0	0	0	0	-Zvz2bMy3b	0	0	0	0	0	0
0	Zαz2bMz3b	-Zαz2bFy3b	0	0	0	0	0	0	0	0	0
0	-Zvy2bMz3b	Zvy2bFy3b	0	0	0	0	0	0	0	0	0
0	0	0	ZTx2b3b	0	0	0	0	0	0	0	0
0	0	0	0	ZLx2b3b	0	0	0	0	0	0	0
-Zαy2bFz3b	0	0	0	0	Zαy2bMy3b	0	0	0	0	0	0
Zvz3bFz3b + ZLx3c3c	0	0	0	0	-Zvz3bMy3b	ZLx3c4c	0	0	0	0	0
0	Zαz3bMz3b + ZTx3c3c	-Zαz3bFy3b	0	0	0	0	ZTx3c4c	0	0	0	0
0	-Zvy3bMz3b	Zvy3bFy3b + Zvy3cFy3c	Zvy3cMz3c	0	0	0	0	Zvy3cFy4c	Zvy3cMz4c	0	0
0	0	Zαz3cFy3c	ZTx3b3b + Zαz3cMz3c	0	0	0	0	Zαz3cFy4c	Zαz3cMz4c	0	0
0	0	0	0	ZLx3b3b + Zvz3cFz3c	-Zvz3cMy3c	0	0	0	0	Zvz3cFz4c	-Zvz3cMy4c
-Zαy3bFz3b	0	0	0	-Zαy3cFz3c	Zαy3bMy3b + Zαy3cMy3c	0	0	0	0	-Zαy3cFz4c	Zαy3cMy4c
ZLx4c3c	0	0	0	0	0	ZLx4c4c + Zvz4dFz4d	0	0	0	0	Zvz4dMy4d
0	ZTx4c3c	0	0	0	0	0	ZTx4c4c + Zαz4dMz4d	Zαz4dFy4d	0	0	0
0	0	Zvy4cFy3c	Zvy4cMz3c	0	0	0	Zvy4dMz4d	Zvy4cFy4c + Zvy4dFy4d	Zvy4cMz4c	0	0
0	0	Zαz4cFy3c	Zαz4cMz3c	0	0	0	0	Zαz4cFy4c	Zαz4cMz4c + ZTx4d4d	0	0
0	0	0	0	Zvz4cFz3c	-Zvz4cMy3c	0	0	0	0	Zvz4cFz4c + ZLx4d4d	-Zvz4cMy4c
0	0	0	0	-Zαy4cFz3c	Zαy4cMy3c	Zαy4dFz4d	0	0	0	-Zαy4cFz4c	Zαy4cMy4c + Zαy4dMy4d

Beam A
Beam A + B
Beam B
Beam B + C
Beam C
Beam C + D
Beam D
Beam D + A

Figure B. 4 Coupled impedance matrix for a beam frame (four beams in L-junctions)

Appendix C – MATLAB code

Base code

```
%% Beam properties
wd = 0.2;                               % Width of beam (m)
l = 4;                                  % Length of beam (m)
h = 0.3;                                % Height of beam (m)
S = wd*h;                               % Cross-sectional area of beam
rho = 2200;                             % Density of beam (kg/m3)
E = (27*10^9)*(1+1i*(0.05));            % Modulus of elasticity of beam (Pa)
nu = 0.20;                              % Poisson's ratio of beam
G = E/(2*(1+nu));                       % Shear modulus of beam
Iy = wd*(h^3)/12;                       % Moment of inertia of beam about y axis (emphasis on
dimension perpendicular to the axis)
Iz = h*(wd^3)/12;                       % Moment of inertia of beam about z axis (emphasis on
dimension perpendicular to the axis)
Ix = (wd*(h^3)+h*(wd^3))/12;            % Polar moment of inertia of beam about x axis
(torsional moment of inertia)
T = G*((h*(wd^3))/3)*(1-((192*wd)/((pi^5)*h))*tanh((pi*h)/(2*wd))); % Torsional stiffnes,
Hopkins (2007)
By = E*Iz;                              % Bending stiffness of beam along y axis
Bz = E*Iy;                              % Bending stiffness of beam along z axis
D = (E*(1-nu))/((1+nu)*(1-2*nu));       % Longitudinal stiffness of beam
m = rho*S;                              % Mass per unit length of beam

% Frequency range
nfreqs = 5000;                          % Number of frequencies
fmax = 5000;                            % Maximum frequency (Hz)
freq = 1:fmax/nfreqs:fmax;              % Frequency array (Hz)
f = freq;

w = 2*pi*freq;                          % Angular frequency (rad/s)
cBy = sqrt(w).*(By/m)^(1/4);            % Phase velocity of bending waves along y axis (m/s)
cBz = sqrt(w).*(Bz/m)^(1/4);            % Phase velocity of bending waves along z axis (m/s)
cL = sqrt(E/rho);                       % Propagation velocity of longitudinal waves (m/s)
cT = sqrt(T/(rho*Ix));                  % Propagation velocity of torsional waves (rad/s)
kBy = w./cBy;                           % Complex wavenumber along y axis (bending)
kBz = w./cBz;                           % Complex wavenumber along z axis (bending)
kL = w/cL;                              % Longitudinal wavenumber
kT = w/cT;                              % Torsional wavenumber

x0 = [0 l];                             % Excitation point on the beam (m)
x = [0; l];                             % Points on the beam we're interested in

% Beam lengths
l_1 = 2.5;                              % Length of beam 1 (m)
l_2 = l-l_1;                            % Length of beam 2 (m)
l_3 = l_1;                              % Length of beam 3 (m)
l_4 = l-l_1;                            % Length of beam 4 (m)

% Excitation and response points on each beam
x0_1 = [0 l_1];                         % Excitation point on beam 1 (m)
x_1 = [0; l_1];                         % Points on beam 1 we're interested in
x0_2 = [0 l_2];                         % Excitation point on beam 2 (m)
x_2 = [0; l_2];                         % Points on beam 2 we're interested in
x0_3 = [0 l_3];                         % Excitation point on beam 3 (m)
x_3 = [0; l_3];                         % Points on beam 3 we're interested in
x0_4 = [0 l_4];                         % Excitation point on beam 4 (m)
x_4 = [0; l_4];                         % Points on beam 4 we're interested in

Zeros = zeros(1,1,length(f));

%% One long beam
%Long beam - Bending mobilities along Y axis
pBy = [x0 l By m];
[Yaa,Yab,Yba,Ybb] = ffbend_beam_mobility(w,pBy,kBy,x);
Ylong_bendy = [Yaa Yab;
    Yba Ybb];
Ylong_forceby_infinite = 1./((1/2)*rho*S.*cBy*(1+1i));
Ylong_momenby_infinite = 1./((1/2)*rho*S.*cBy.*((1-1i)./(kBy.^2)));

%Long beam - Bending mobilities along Z axis
pBz = [x0 l Bz m];
[Yaa,Yab,Yba,Ybb] = ffbend_beam_mobility(w,pBz,kBz,x);
Ylong_bendz = [Yaa Yab;
    Yba Ybb];
Ylong_forcebz_infinite = 1./((1/2)*rho*S.*cBz*(1+1i));
```

```
Ylong_momenbz_infinite = 1./((1/2)*rho*S.*cBz.*((1-1i)./(kBz.^2)));

% Long beam - Longitudinal beam mobilities
pL = [x0 l S rho cL D];
[Ylong_longi] = fflongi_beam_mob(w,pL,kL,x);
Ylong_longi_infinite = 1./(S*sqrt(E*rho));
Ylong_longi_infinite = repmat(Ylong_longi_infinite,nfreqs);

% Long beam - Torsional mobilities
pT = [x0 l cT T];
[Ylong_torsion] = fftorsion_beam_mob(w,pT,kT,x);
rg = sqrt((h^2)/12);          % Radius of gyration of rectangular beam
Ylong_torsion_infinite = 1/(S*(rg^2)*sqrt(G*rho));   % Torsional impedance for a semi-
infinite beam (Heckl, Compedium of impedances)
Ylong_torsion_infinite = repmat(Ylong_torsion_infinite,nfreqs);

% Mobility matrix for long beam with 6 DOFs
Ylong = [Ylong_longi(1,1,:) Zeros(1,1,:) Zeros(1,1,:) Zeros(1,1,:) Zeros(1,1,:) Zeros(1,1,:)
Ylong_longi(1,2,:) Zeros(1,1,:) Zeros(1,1,:) Zeros(1,1,:) Zeros(1,1,:) Zeros(1,1,:);
          Zeros(1,1,:) Ylong_torsion(1,1,:) Zeros(1,1,:) Zeros(1,1,:) Zeros(1,1,:)
Zeros(1,1,:) Zeros(1,1,:) Ylong_torsion(1,2,:)  Zeros(1,1,:) Zeros(1,1,:) Zeros(1,1,:)
Zeros(1,1,:);
          Zeros(1,1,:) Zeros(1,1,:) Ylong_bendy(1,1,:) Ylong_bendy(1,2,:) Zeros(1,1,:)
Zeros(1,1,:) Zeros(1,1,:) Zeros(1,1,:) Ylong_bendy(1,3,:) Ylong_bendy(1,4,:) Zeros(1,1,:)
Zeros(1,1,:);
          Zeros(1,1,:) Zeros(1,1,:) Ylong_bendy(2,1,:) Ylong_bendy(2,2,:) Zeros(1,1,:)
Zeros(1,1,:) Zeros(1,1,:) Zeros(1,1,:) Ylong_bendy(2,3,:) Ylong_bendy(2,4,:) Zeros(1,1,:)
Zeros(1,1,:);
          Zeros(1,1,:) Zeros(1,1,:) Zeros(1,1,:) Zeros(1,1,:) Ylong_bendz(1,1,:)
Ylong_bendz(1,2,:) Zeros(1,1,:) Zeros(1,1,:) Zeros(1,1,:) Zeros(1,1,:) Ylong_bendz(1,3,:)
Ylong_bendz(1,4,:);
          Zeros(1,1,:) Zeros(1,1,:) Zeros(1,1,:) Zeros(1,1,:) Ylong_bendz(2,1,:)
Ylong_bendz(2,2,:) Zeros(1,1,:) Zeros(1,1,:) Zeros(1,1,:) Zeros(1,1,:) Ylong_bendz(2,3,:)
Ylong_bendz(2,4,:);
          Ylong_longi(2,1,:) Zeros(1,1,:) Zeros(1,1,:) Zeros(1,1,:) Zeros(1,1,:)
Zeros(1,1,:) Ylong_longi(2,2,:) Zeros(1,1,:) Zeros(1,1,:) Zeros(1,1,:) Zeros(1,1,:)
Zeros(1,1,:);
          Zeros(1,1,:) Ylong_torsion(2,1,:) Zeros(1,1,:) Zeros(1,1,:) Zeros(1,1,:)
Zeros(1,1,:) Zeros(1,1,:) Ylong_torsion(2,2,:)  Zeros(1,1,:) Zeros(1,1,:) Zeros(1,1,:)
Zeros(1,1,:);
          Zeros(1,1,:) Zeros(1,1,:) Ylong_bendy(3,1,:) Ylong_bendy(3,2,:) Zeros(1,1,:)
Zeros(1,1,:) Zeros(1,1,:) Zeros(1,1,:) Ylong_bendy(3,3,:) Ylong_bendy(3,4,:) Zeros(1,1,:)
Zeros(1,1,:);
          Zeros(1,1,:) Zeros(1,1,:) Ylong_bendy(4,1,:) Ylong_bendy(4,2,:) Zeros(1,1,:)
Zeros(1,1,:) Zeros(1,1,:) Zeros(1,1,:) Ylong_bendy(4,3,:) Ylong_bendy(4,4,:) Zeros(1,1,:)
Zeros(1,1,:);
          Zeros(1,1,:) Zeros(1,1,:) Zeros(1,1,:) Zeros(1,1,:) Ylong_bendz(3,1,:)
Ylong_bendz(3,2,:) Zeros(1,1,:) Zeros(1,1,:) Zeros(1,1,:) Zeros(1,1,:) Ylong_bendz(3,3,:)
Ylong_bendz(3,4,:);
          Zeros(1,1,:) Zeros(1,1,:) Zeros(1,1,:) Zeros(1,1,:) Ylong_bendz(4,1,:)
Ylong_bendz(4,2,:) Zeros(1,1,:) Zeros(1,1,:) Zeros(1,1,:) Zeros(1,1,:) Ylong_bendz(4,3,:)
Ylong_bendz(4,4,:)];

%% Beam 1 mobilities
% Beam 1 - Bending mobilities along Y axis
p_1 = [x0_1 l_1 By m];
[Yaa,Yab,Yba,Ybb] = ffbend_beam_mobility(w,p_1,kBy,x_1);
Ybendy_1 = [Yaa Yab;
    Yba Ybb];
% Beam 1 - Bending mobilities along Z axis
p_1 = [x0_1 l_1 Bz m];
[Yaa,Yab,Yba,Ybb] = ffbend_beam_mobility(w,p_1,kBz,x_1);
Ybendz_1 = [Yaa Yab;
    Yba Ybb];
% Beam 1 - Longitudinal mobilities
pl_1 = [x0_1 l_1 S rho cL D];
[Ylongi_1] = fflongi_beam_mob(w,pl_1,kL,x_1);
% Beam 1 - Torsional mobilities
pt_1 = [x0_1 l_1 cT T];
[Ytorsion_1] = fftorsion_beam_mob(w,pt_1,kT,x_1);

% Mobility matrix for Beam 1 with 6 DOFs
Ybeam_1 = [Ylongi_1(1,1,:) Zeros(1,1,:) Zeros(1,1,:) Zeros(1,1,:) Zeros(1,1,:) Zeros(1,1,:)
Ylongi_1(1,2,:) Zeros(1,1,:) Zeros(1,1,:) Zeros(1,1,:) Zeros(1,1,:) Zeros(1,1,:);
          Zeros(1,1,:) Ytorsion_1(1,1,:) Zeros(1,1,:) Zeros(1,1,:) Zeros(1,1,:) Zeros(1,1,:)
Zeros(1,1,:) Zeros(1,1,:) Ytorsion_1(1,2,:)  Zeros(1,1,:) Zeros(1,1,:) Zeros(1,1,:)
Zeros(1,1,:);
          Zeros(1,1,:) Zeros(1,1,:) Ybendy_1(1,1,:) Ybendy_1(1,2,:) Zeros(1,1,:)
Zeros(1,1,:) Zeros(1,1,:) Zeros(1,1,:) Ybendy_1(1,3,:) Ybendy_1(1,4,:) Zeros(1,1,:)
Zeros(1,1,:);
          Zeros(1,1,:) Zeros(1,1,:) Ybendy_1(2,1,:) Ybendy_1(2,2,:) Zeros(1,1,:)
Zeros(1,1,:) Zeros(1,1,:) Zeros(1,1,:) Ybendy_1(2,3,:) Ybendy_1(2,4,:) Zeros(1,1,:)
Zeros(1,1,:);
```

```
          Zeros(1,1,:) Zeros(1,1,:) Zeros(1,1,:) Zeros(1,1,:) Ybendz_1(1,1,:)
Ybendz_1(1,2,:) Zeros(1,1,:) Zeros(1,1,:) Zeros(1,1,:) Zeros(1,1,:) Ybendz_1(1,3,:)
Ybendz_1(1,4,:);
          Zeros(1,1,:) Zeros(1,1,:) Zeros(1,1,:) Zeros(1,1,:) Ybendz_1(2,1,:)
Ybendz_1(2,2,:) Zeros(1,1,:) Zeros(1,1,:) Zeros(1,1,:) Zeros(1,1,:) Ybendz_1(2,3,:)
Ybendz_1(2,4,:);
          Ylongi_1(2,1,:) Zeros(1,1,:) Zeros(1,1,:) Zeros(1,1,:) Zeros(1,1,:) Zeros(1,1,:)
Ylongi_1(2,2,:) Zeros(1,1,:) Zeros(1,1,:) Zeros(1,1,:) Zeros(1,1,:) Zeros(1,1,:);
          Zeros(1,1,:) Ytorsion_1(2,1,:) Zeros(1,1,:) Zeros(1,1,:) Zeros(1,1,:) Zeros(1,1,:)
Zeros(1,1,:) Ytorsion_1(2,2,:)  Zeros(1,1,:) Zeros(1,1,:) Zeros(1,1,:) Zeros(1,1,:);
          Zeros(1,1,:) Zeros(1,1,:) Ybendy_1(3,1,:) Ybendy_1(3,2,:) Zeros(1,1,:)
Zeros(1,1,:) Zeros(1,1,:) Zeros(1,1,:) Ybendy_1(3,3,:) Ybendy_1(3,4,:) Zeros(1,1,:)
Zeros(1,1,:);
          Zeros(1,1,:) Zeros(1,1,:) Ybendy_1(4,1,:) Ybendy_1(4,2,:) Zeros(1,1,:)
Zeros(1,1,:) Zeros(1,1,:) Zeros(1,1,:) Ybendy_1(4,3,:) Ybendy_1(4,4,:) Zeros(1,1,:)
Zeros(1,1,:);
          Zeros(1,1,:) Zeros(1,1,:) Zeros(1,1,:) Zeros(1,1,:) Ybendz_1(3,1,:)
Ybendz_1(3,2,:) Zeros(1,1,:) Zeros(1,1,:) Zeros(1,1,:) Zeros(1,1,:) Ybendz_1(3,3,:)
Ybendz_1(3,4,:);
          Zeros(1,1,:) Zeros(1,1,:) Zeros(1,1,:) Zeros(1,1,:) Ybendz_1(4,1,:)
Ybendz_1(4,2,:) Zeros(1,1,:) Zeros(1,1,:) Zeros(1,1,:) Zeros(1,1,:) Ybendz_1(4,3,:)
Ybendz_1(4,4,:)];

%% Beam 2 mobilities
% Beam 2 - Bending mobilities along Y axis
p_2 = [x0_2 l_2 By m];
[Yaa,Yab,Yba,Ybb] = ffbend_beam_mobility(w,p_2,kBy,x_2);
Ybendy_2 = [Yaa Yab;
    Yba Ybb];
% Beam 2 - Bending mobilities along Z axis
p_2 = [x0_2 l_2 Bz m];
[Yaa,Yab,Yba,Ybb] = ffbend_beam_mobility(w,p_2,kBz,x_2);
Ybendz_2 = [Yaa Yab;
    Yba Ybb];
% Beam 2 - Longitudinal mobilities
pl_2 = [x0_2 l_2 S rho cL D];
[Ylongi_2] = fflongi_beam_mob(w,pl_2,kL,x_2);
% Beam 2 - Torsional mobilities
pt_2 = [x0_2 l_2 cT T];
[Ytorsion_2] = fftorsion_beam_mob(w,pt_2,kT,x_2);

% Mobility matrix for Beam 2 with 6 DOFs
Ybeam_2 = [Ylongi_2(1,1,:) Zeros(1,1,:) Zeros(1,1,:) Zeros(1,1,:) Zeros(1,1,:) Zeros(1,1,:)
Ylongi_2(1,2,:) Zeros(1,1,:) Zeros(1,1,:) Zeros(1,1,:) Zeros(1,1,:) Zeros(1,1,:);
          Zeros(1,1,:) Ytorsion_2(1,1,:) Zeros(1,1,:) Zeros(1,1,:) Zeros(1,1,:) Zeros(1,1,:)
Zeros(1,1,:) Ytorsion_2(1,2,:)  Zeros(1,1,:) Zeros(1,1,:) Zeros(1,1,:)
Zeros(1,1,:);
          Zeros(1,1,:) Zeros(1,1,:) Ybendy_2(1,1,:) Ybendy_2(1,2,:) Zeros(1,1,:)
Zeros(1,1,:) Zeros(1,1,:) Zeros(1,1,:) Ybendy_2(1,3,:) Ybendy_2(1,4,:) Zeros(1,1,:)
Zeros(1,1,:);
          Zeros(1,1,:) Zeros(1,1,:) Ybendy_2(2,1,:) Ybendy_2(2,2,:) Zeros(1,1,:)
Zeros(1,1,:) Zeros(1,1,:) Zeros(1,1,:) Ybendy_2(2,3,:) Ybendy_2(2,4,:) Zeros(1,1,:)
Zeros(1,1,:);
          Zeros(1,1,:) Zeros(1,1,:) Zeros(1,1,:) Zeros(1,1,:) Ybendz_2(1,1,:)
Ybendz_2(1,2,:) Zeros(1,1,:) Zeros(1,1,:) Zeros(1,1,:) Zeros(1,1,:) Ybendz_2(1,3,:)
Ybendz_2(1,4,:);
          Zeros(1,1,:) Zeros(1,1,:) Zeros(1,1,:) Zeros(1,1,:) Ybendz_2(2,1,:)
Ybendz_2(2,2,:) Zeros(1,1,:) Zeros(1,1,:) Zeros(1,1,:) Zeros(1,1,:) Ybendz_2(2,3,:)
Ybendz_2(2,4,:);
          Ylongi_2(2,1,:) Zeros(1,1,:) Zeros(1,1,:) Zeros(1,1,:) Zeros(1,1,:) Zeros(1,1,:)
Ylongi_2(2,2,:) Zeros(1,1,:) Zeros(1,1,:) Zeros(1,1,:) Zeros(1,1,:) Zeros(1,1,:);
          Zeros(1,1,:) Ytorsion_2(2,1,:) Zeros(1,1,:) Zeros(1,1,:) Zeros(1,1,:) Zeros(1,1,:)
Zeros(1,1,:) Ytorsion_2(2,2,:)  Zeros(1,1,:) Zeros(1,1,:) Zeros(1,1,:) Zeros(1,1,:);
          Zeros(1,1,:) Zeros(1,1,:) Ybendy_2(3,1,:) Ybendy_2(3,2,:) Zeros(1,1,:)
Zeros(1,1,:) Zeros(1,1,:) Zeros(1,1,:) Ybendy_2(3,3,:) Ybendy_2(3,4,:) Zeros(1,1,:)
Zeros(1,1,:);
          Zeros(1,1,:) Zeros(1,1,:) Ybendy_2(4,1,:) Ybendy_2(4,2,:) Zeros(1,1,:)
Zeros(1,1,:) Zeros(1,1,:) Zeros(1,1,:) Ybendy_2(4,3,:) Ybendy_2(4,4,:) Zeros(1,1,:)
Zeros(1,1,:);
          Zeros(1,1,:) Zeros(1,1,:) Zeros(1,1,:) Zeros(1,1,:) Ybendz_2(3,1,:)
Ybendz_2(3,2,:) Zeros(1,1,:) Zeros(1,1,:) Zeros(1,1,:) Zeros(1,1,:) Ybendz_2(3,3,:)
Ybendz_2(3,4,:);
          Zeros(1,1,:) Zeros(1,1,:) Zeros(1,1,:) Zeros(1,1,:) Ybendz_2(4,1,:)
Ybendz_2(4,2,:) Zeros(1,1,:) Zeros(1,1,:) Zeros(1,1,:) Zeros(1,1,:) Ybendz_2(4,3,:)
Ybendz_2(4,4,:)];

%% Beam 3 mobilities
% Beam 3 - Bending mobilities along Y axis
p_3 = [x0_3 l_3 By m];
[Yaa,Yab,Yba,Ybb] = ffbend_beam_mobility(w,p_3,kBy,x_3);
Ybendy_3 = [Yaa Yab;
    Yba Ybb];
% Beam 3 - Bending mobilities along Z axis
p_3 = [x0_3 l_3 Bz m];
```

```
[Yaa,Yab,Yba,Ybb] = ffbend_beam_mobility(w,p_3,kBz,x_3);
Ybendz_3 = [Yaa Yab;
    Yba Ybb];
% Beam 3 - Longitudinal mobilities
pl_3 = [x0_3 l_3 S rho cL D];
[Ylongi_3] = fflongi_beam_mob(w,pl_3,kL,x_3);
% Beam 3 - Torsional mobilities
pt_3 = [x0_3 l_3 cT T];
[Ytorsion_3] = fftorsion_beam_mob(w,pt_3,kT,x_3);

% Mobility matrix for Beam 3 with 6 DOFs
Ybeam_3 = [Ylongi_3(1,1,:) Zeros(1,1,:) Zeros(1,1,:) Zeros(1,1,:) Zeros(1,1,:) Zeros(1,1,:)
Ylongi_3(1,2,:) Zeros(1,1,:) Zeros(1,1,:) Zeros(1,1,:) Zeros(1,1,:) Zeros(1,1,:);
          Zeros(1,1,:) Ytorsion_3(1,1,:) Zeros(1,1,:) Zeros(1,1,:) Zeros(1,1,:) Zeros(1,1,:)
Zeros(1,1,:) Ytorsion_3(1,2,:)  Zeros(1,1,:) Zeros(1,1,:) Zeros(1,1,:)
Zeros(1,1,:);
          Zeros(1,1,:) Zeros(1,1,:) Ybendy_3(1,1,:) Ybendy_3(1,2,:) Zeros(1,1,:)
Zeros(1,1,:) Zeros(1,1,:) Zeros(1,1,:) Ybendy_3(1,3,:) Ybendy_3(1,4,:) Zeros(1,1,:)
Zeros(1,1,:);
          Zeros(1,1,:) Zeros(1,1,:) Ybendy_3(2,1,:) Ybendy_3(2,2,:) Zeros(1,1,:)
Zeros(1,1,:) Zeros(1,1,:) Zeros(1,1,:) Ybendy_3(2,3,:) Ybendy_3(2,4,:) Zeros(1,1,:)
Zeros(1,1,:);
          Zeros(1,1,:) Zeros(1,1,:) Zeros(1,1,:) Zeros(1,1,:) Ybendz_3(1,1,:)
Ybendz_3(1,2,:) Zeros(1,1,:) Zeros(1,1,:) Zeros(1,1,:) Zeros(1,1,:) Ybendz_3(1,3,:)
Ybendz_3(1,4,:);
          Zeros(1,1,:) Zeros(1,1,:) Zeros(1,1,:) Zeros(1,1,:) Ybendz_3(2,1,:)
Ybendz_3(2,2,:) Zeros(1,1,:) Zeros(1,1,:) Zeros(1,1,:) Zeros(1,1,:) Ybendz_3(2,3,:)
Ybendz_3(2,4,:);
          Ylongi_3(2,1,:) Zeros(1,1,:) Zeros(1,1,:) Zeros(1,1,:) Zeros(1,1,:) Zeros(1,1,:)
Ylongi_3(2,2,:) Zeros(1,1,:) Zeros(1,1,:) Zeros(1,1,:) Zeros(1,1,:) Zeros(1,1,:);
          Zeros(1,1,:) Ytorsion_3(2,1,:) Zeros(1,1,:) Zeros(1,1,:) Zeros(1,1,:) Zeros(1,1,:)
Zeros(1,1,:) Ytorsion_3(2,2,:)  Zeros(1,1,:) Zeros(1,1,:) Zeros(1,1,:) Zeros(1,1,:);
          Zeros(1,1,:) Zeros(1,1,:) Ybendy_3(3,1,:) Ybendy_3(3,2,:) Zeros(1,1,:)
Zeros(1,1,:) Zeros(1,1,:) Zeros(1,1,:) Ybendy_3(3,3,:) Ybendy_3(3,4,:) Zeros(1,1,:)
Zeros(1,1,:);
          Zeros(1,1,:) Zeros(1,1,:) Ybendy_3(4,1,:) Ybendy_3(4,2,:) Zeros(1,1,:)
Zeros(1,1,:) Zeros(1,1,:) Zeros(1,1,:) Ybendy_3(4,3,:) Ybendy_3(4,4,:) Zeros(1,1,:)
Zeros(1,1,:);
          Zeros(1,1,:) Zeros(1,1,:) Zeros(1,1,:) Zeros(1,1,:) Ybendz_3(3,1,:)
Ybendz_3(3,2,:) Zeros(1,1,:) Zeros(1,1,:) Zeros(1,1,:) Zeros(1,1,:) Ybendz_3(3,3,:)
Ybendz_3(3,4,:);
          Zeros(1,1,:) Zeros(1,1,:) Zeros(1,1,:) Zeros(1,1,:) Ybendz_3(4,1,:)
Ybendz_3(4,2,:) Zeros(1,1,:) Zeros(1,1,:) Zeros(1,1,:) Zeros(1,1,:) Ybendz_3(4,3,:)
Ybendz_3(4,4,:)];

%% Beam 4 mobilities
% Beam 4 - Bending mobilities along Y axis
p_4 = [x0_4 l_4 By m];
[Yaa,Yab,Yba,Ybb] = ffbend_beam_mobility(w,p_4,kBy,x_4);
Ybendy_4 = [Yaa Yab;
    Yba Ybb];
% Beam 4 - Bending mobilities along Z axis
p_4 = [x0_4 l_4 Bz m];
[Yaa,Yab,Yba,Ybb] = ffbend_beam_mobility(w,p_4,kBz,x_4);
Ybendz_4 = [Yaa Yab;
    Yba Ybb];
% Beam 4 - Longitudinal mobilities
pl_4 = [x0_4 l_4 S rho cL D];
[Ylongi_4] = fflongi_beam_mob(w,pl_4,kL,x_4);
% Beam 4 - Torsional mobilities
pt_4 = [x0_4 l_4 cT T];
[Ytorsion_4] = fftorsion_beam_mob(w,pt_4,kT,x_4);

% Mobility matrix for Beam 4 with 6 DOFs
Ybeam_4 = [Ylongi_4(1,1,:) Zeros(1,1,:) Zeros(1,1,:) Zeros(1,1,:) Zeros(1,1,:) Zeros(1,1,:)
Ylongi_4(1,2,:) Zeros(1,1,:) Zeros(1,1,:) Zeros(1,1,:) Zeros(1,1,:) Zeros(1,1,:);
          Zeros(1,1,:) Ytorsion_4(1,1,:) Zeros(1,1,:) Zeros(1,1,:) Zeros(1,1,:) Zeros(1,1,:)
Zeros(1,1,:) Ytorsion_4(1,2,:)  Zeros(1,1,:) Zeros(1,1,:) Zeros(1,1,:)
Zeros(1,1,:);
          Zeros(1,1,:) Zeros(1,1,:) Ybendy_4(1,1,:) Ybendy_4(1,2,:) Zeros(1,1,:)
Zeros(1,1,:) Zeros(1,1,:) Zeros(1,1,:) Ybendy_4(1,3,:) Ybendy_4(1,4,:) Zeros(1,1,:)
Zeros(1,1,:);
          Zeros(1,1,:) Zeros(1,1,:) Ybendy_4(2,1,:) Ybendy_4(2,2,:) Zeros(1,1,:)
Zeros(1,1,:) Zeros(1,1,:) Zeros(1,1,:) Ybendy_4(2,3,:) Ybendy_4(2,4,:) Zeros(1,1,:)
Zeros(1,1,:);
          Zeros(1,1,:) Zeros(1,1,:) Zeros(1,1,:) Zeros(1,1,:) Ybendz_4(1,1,:)
Ybendz_4(1,2,:) Zeros(1,1,:) Zeros(1,1,:) Zeros(1,1,:) Zeros(1,1,:) Ybendz_4(1,3,:)
Ybendz_4(1,4,:);
          Zeros(1,1,:) Zeros(1,1,:) Zeros(1,1,:) Zeros(1,1,:) Ybendz_4(2,1,:)
Ybendz_4(2,2,:) Zeros(1,1,:) Zeros(1,1,:) Zeros(1,1,:) Zeros(1,1,:) Ybendz_4(2,3,:)
Ybendz_4(2,4,:);
          Ylongi_4(2,1,:) Zeros(1,1,:) Zeros(1,1,:) Zeros(1,1,:) Zeros(1,1,:) Zeros(1,1,:)
Ylongi_4(2,2,:) Zeros(1,1,:) Zeros(1,1,:) Zeros(1,1,:) Zeros(1,1,:) Zeros(1,1,:);
```

```
          Zeros(1,1,:) Ytorsion_4(2,1,:) Zeros(1,1,:) Zeros(1,1,:) Zeros(1,1,:) Zeros(1,1,:)
Zeros(1,1,:) Ytorsion_4(2,2,:)  Zeros(1,1,:) Zeros(1,1,:) Zeros(1,1,:) Zeros(1,1,:);
          Zeros(1,1,:) Zeros(1,1,:) Ybendy_4(3,1,:) Ybendy_4(3,2,:) Zeros(1,1,:)
Zeros(1,1,:) Zeros(1,1,:) Zeros(1,1,:) Ybendy_4(3,3,:) Ybendy_4(3,4,:) Zeros(1,1,:)
Zeros(1,1,:);
          Zeros(1,1,:) Zeros(1,1,:) Ybendy_4(4,1,:) Ybendy_4(4,2,:) Zeros(1,1,:)
Zeros(1,1,:) Zeros(1,1,:) Zeros(1,1,:) Ybendy_4(4,3,:) Ybendy_4(4,4,:) Zeros(1,1,:)
Zeros(1,1,:);
          Zeros(1,1,:) Zeros(1,1,:) Zeros(1,1,:) Zeros(1,1,:) Ybendz_4(3,1,:)
Ybendz_4(3,2,:) Zeros(1,1,:) Zeros(1,1,:) Zeros(1,1,:) Zeros(1,1,:) Ybendz_4(3,3,:)
Ybendz_4(3,4,:);
          Zeros(1,1,:) Zeros(1,1,:) Zeros(1,1,:) Zeros(1,1,:) Ybendz_4(4,1,:)
Ybendz_4(4,2,:) Zeros(1,1,:) Zeros(1,1,:) Zeros(1,1,:) Zeros(1,1,:) Ybendz_4(4,3,:)
Ybendz_4(4,4,:)];

%% Beams coupled in line and in L-junctions

% Coupling beams 1 and 2 in line - 6 DOFs
Ycoupled_IL = ffb_coupled(f,'IL2',Ybeam_1,Ybeam_2);

% Coupling beams 1 and 2 in an L-junction - 6 DOFs
Ycoupled_LJ2 = ffb_coupled(f,'LJ2',Ybeam_1,Ybeam_2);

% Coupling beams 1, 2 and 3 in an L-junction - 6 DOFs
Ycoupled_LJ3 = ffb_coupled(f,'LJ3',Ybeam_1,Ybeam_2,Ybeam_3);

% Coupling beams 1, 2, 3 and 4 in an L-junction - 6 DOFs
Ycoupled_LJ4 = ffb_coupled(f,'LJ4',Ybeam_1,Ybeam_2,Ybeam_3,Ybeam_4);
```

Quasi-longitudinal mobilities

```
% fflongi_beam_mob: function to predict the longitudinal mobility of a free-free
% beam
% Expression for mobility / impedance derived as for an organ pipe
% Daniela Filipe
%
% [Ylaa,Ylab,Ylba,Ylbb] = fflongi_beam_mob(w,p,k,x)
%
% w(1,N) = angular frequency range (Hz)
% p(1,5) = beam parameters: excitation position 1, excitation position 2, length,
%          cross sectional area, density, cL, longitudinal stiffness D
% k(1,N) = wavenumber (1/m)
% x(K,1) = response points along the beam (m)
%
% Ylaa(K,N) = longi mobility at a with excitation at a
% Ylab(K,N) = longi mobility at a with excitation at b
% Ylba(K,N) = longi mobility at b with excitation at a
% Ylbb(K,N) = longi mobility at b with excitation at b


function [Yl] = fflongi_beam_mob(w,p,k,x)

% Check number of input arguments is sufficient
if nargin<4, return, end
if length(p)<7, return, end

Yc = p(1,6)/(1i*p(1,4)*p(1,7));      % Yc = cL/(j*S*D)

kx(1,:) = k*x(1);       % Response points on the beam (response at 0)
kx(2,:) = k*x(2);       % Response points on the beam (response at l)
% kx0(1,:) = k*p(1,1);    % Excitation points on the beam, at 0
% kx0(2,:) = k*p(1,2);    % Excitation points on the beam, at l
kl = k.*p(1,3);

for i = length(kl):-1:1 % Do loop backwards

    Ylaa = Yc.*(cos(kl(1,:))./sin(kl(1,:)));
    Ylab = Yc.*(1./(sin(kl(1,:))));
    Ylba = Yc.*(1./sin(kl(1,:)));
    Ylbb = Yc.*(cos(kl(1,:))./(sin(kl(1,:))));

end

P1o = struct('Ylaa',Ylaa,'Ylab',Ylab,'Ylba',Ylba,'Ylbb',Ylbb);
Yl = [reshape(P1o.Ylaa(1,:),1,1,size(w,2)) reshape(P1o.Ylab(1,:),1,1,size(w,2));
    reshape(P1o.Ylba(1,:),1,1,size(w,2)) reshape(P1o.Ylbb(1,:),1,1,size(w,2))];

end
```

Torsional mobilities

```
% fftorsion_beam_mob: function to predict the torsional mobility of a free-free
% beam
% Expression for mobility / impedance derived from Cremer & Heckl
%
% [Ytaa,Ytab,Ytba,Ytbb] = fftorsion_beam_mob(w,p,k,x)
%
% w(1,N) = angular frequency range (Hz)
% p(1,5) = beam parameters: excitation position 1, excitation position 2, length,
%          cT, torsional stiffness T
% k(1,N) = wavenumber (1/m)
% x(K,1) = response points along the beam (m)
%
% Ytaa(K,N) = torsional mobility at a with excitation at a
% Ytab(K,N) = torsional mobility at a with excitation at b
% Ytba(K,N) = torsional mobility at b with excitation at a
% Ytbb(K,N) = torsional mobility at b with excitation at b


function [Yl] = fftorsion_beam_mob(w,p,k,x)

% Check number of input arguments is sufficient
if nargin<4, return, end
if length(p)<5, return, end

Yc = p(1,4)/(1i*p(1,5));      % Yc = cT/(j*T)

% kx(1,:) = k*x(1);       % Response points on the beam (response at 0)
% kx(2,:) = k*x(2);       % Response points on the beam (response at l)
% kx0(1,:) = k*p(1,1);    % Excitation points on the beam, at 0
% kx0(2,:) = k*p(1,2);    % Excitation points on the beam, at l
kl = k.*p(1,3);

for i = length(kl):-1:1 % Do loop backwards

    Ytaa = Yc.*(cos(kl(1,:))./(-sin(kl(1,:))));
    Ytab = Yc.*(1./(-sin(kl(1,:))));
    Ytba = Yc.*(1./(-sin(kl(1,:))));
    Ytbb = Yc.*(cos(kl(1,:))./(-sin(kl(1,:))));

end

Plo = struct('Ytaa',Ytaa,'Ytab',Ytab,'Ytba',Ytba,'Ytbb',Ytbb);
Yl = [reshape(Plo.Ytaa(1,:),1,1,size(w,2)) reshape(Plo.Ytab(1,:),1,1,size(w,2));
    reshape(Plo.Ytba(1,:),1,1,size(w,2)) reshape(Plo.Ytbb(1,:),1,1,size(w,2))];

end
```

Bending mobilities

```
% ffbeam_mobility: function to predict the flexural mobility of a free-free
% beam, using the closed form equations from "Simplified characterisation of
% structure-borne sound sources with multi-point connections, Appendix A"
%
% [Yaa,Yab,Yba,Ybb] = ffbeam_mobility(w,p,k,x)
%
% w(1,N) = angular frequency range (Hz)
% p(1,5) = beam parameters: excitation position 1, excitation position 2, length,
%          bending stiffness, mass per unit length
% k(1,N) = complex wavenumber (1/m)
% x(K,1) = response points along the beam (m)
%
% Yvf(K,N) = translation force mobility
% Yvm(K,N) = translation moment mobility
% Yaf(K,N) = rotation force mobility
% Yam(K,N) = rotation moment mobility


function [Yaa,Yab,Yba,Ybb] = ffbeam_mobility(w,p,k,x)

% Check number of input arguments is sufficient
if nargin<4, return, end
if length(p)<5, return, end

Yc = w./(p(1,4).*(k.^3));

kx(1,:) = k*x(1);       % Response points on the beam (response at 0)
kx(2,:) = k*x(2);       % Response points on the beam (response at l)
kx0(1,:) = k*p(1,1);    % Excitation points on the beam
kx0(2,:) = k*p(1,2);    % Excitation points on the beam
l = p(1,3);
```

```
kl = k*l;

% Initialising variables
Yvf = zeros(2,length(k));
Yvm = zeros(2,length(k));
Yaf = zeros(2,length(k));
Yam = zeros(2,length(k));

for i = length(x):-1:1 % Do loop backwards

    f1(i,:) = cosh(kx(i,:))-cosh(k.*(l-x(i,:))).*cos(kl)-sinh(k.*(l-x(i,:))).*sin(kl)-
cos(kx(i,:))+cos(k.*(l-x(i,:))).*cosh(kl)-sinh(kl).*sin(k.*(l-x(i,:)));
    f2(i,:) = sinh(kx(i,:))+sinh(k.*(l-x(i,:))).*cos(kl)-sin(kl).*cosh(k.*(l-x(i,:)))-
sin(kx(i,:))+sinh(kl).*cos(k.*(l-x(i,:)))-cosh(kl).*sin(k.*(l-x(i,:)));

    g1_x0 = -(sin(kx0(1,:))+sinh(kx0(1,:))./(2.*(1-cosh(kl).*cos(kl)));
    g2_x0 = (cos(kx0(1,:))+cosh(kx0(1,:)))./(2.*(1-cosh(kl).*cos(kl)));

    df1dx(i,:) = k.*(sinh(kx(i,:))+sinh(k.*(l-x(i,:))).*cos(kl)+cosh(k.*(l-
x(i,:))).*sin(kl)+sin(kx(i,:))+sin(k.*(l-x(i,:))).*cosh(kl)+sinh(kl).*cos(k.*(l-x(i,:))));
    df2dx(i,:) = k.*(cosh(kx(i,:))-cosh(k.*(l-x(i,:))).*cos(kl)+sin(kl).*sinh(k.*(l-
x(i,:)))-cos(kx(i,:))+sinh(kl).*sin(k.*(l-x(i,:)))+cosh(kl).*cos(k.*(l-x(i,:))));

    % Mobilities with excitation at 0
    Yvf(i,:) = (1i/2).*Yc.*(f1(i,:).*g1_x0+f2(i,:).*g2_x0);
    Yvm(i,:) = ((1i.*Yc.*k)./(4.*(1-cosh(kl).*cos(kl)))).*(f2(i,:).*(-
sin(kx0(1,:))+sinh(kx0(1,:)))-f1(i,:).*(cos(kx0(1,:))+cosh(kx0(1,:))));
    Yaf(i,:) = (1i/2).*Yc.*(g1_x0.*df1dx(i,:)+g2_x0.*df2dx(i,:));
    Yam(i,:) = ((1i.*Yc.*k)./(4.*(1-cosh(kl).*cos(kl)))).*(df2dx(i,:).*(-
sin(kx0(1,:))+sinh(kx0(1,:)))-df1dx(i,:).*(cos(kx0(1,:))+cosh(kx0(1,:))));

end
P1o = struct('Yvf',Yvf,'Yvm',Yvm,'Yaf',Yaf,'Yam',Yam);  % Mobilities with excitation at x0


for i = length(x):-1:1 % Do loop backwards
    f1_x0 = 2.*cosh(kx0(2,:))-2.*cos(kx0(2,:));
    f2_x0 = 2.*sinh(kx0(2,:))-2.*sin(kx0(2,:));

    df1_x0dx0 = 2.*k.*sinh(kx0(2,:))+2.*k.*sin(kx0(2,:));
    df2_x0dx0 = 2.*k.*cosh(kx0(2,:))-2.*k.*cos(kx0(2,:));

    g1(i,:) = -(sin(kx(i,:))+sinh(kx(i,:))./(2.*(1-cosh(kl).*cos(kl)));
    g2(i,:) = (cos(kx(i,:))+cosh(kx(i,:)))./(2.*(1-cosh(kl).*cos(kl)));

    dg1dx(i,:) = -k.*(cos(kx(i,:))+cosh(kx(i,:)))./(2.*(1-cosh(kl).*cos(kl)));
    dg2dx(i,:) = k.*(-sin(kx(i,:))+sinh(kx(i,:)))./(2.*(1-cosh(kl).*cos(kl)));

    % Mobilities with excitation at l
    Yvf(i,:) = (1i/2).*Yc.*(f1_x0.*g1(i,:)+f2_x0.*g2(i,:));
    Yvm(i,:) = (1i/2).*Yc.*(g1(i,:).*df1_x0dx0+g2(i,:).*df2_x0dx0);
    Yaf(i,:) = (1i/2).*Yc.*(f1_x0.*dg1dx(i,:)+f2_x0.*dg2dx(i,:));
    Yam(i,:) = ((1i.*Yc)./(4.*(1-cosh(kl).*cos(kl)))).*((-k.*cos(kx(i,:))-
k.*cosh(kx(i,:))).*df1_x0dx0+(-k.*sin(kx(i,:))+k.*sinh(kx(i,:))).*df2_x0dx0);


end
P2o = struct('Yvf',Yvf,'Yvm',Yvm,'Yaf',Yaf,'Yam',Yam);  % Mobilities with excitation at l


% Assembling mobilities for each frequency (3D matrices)
Yaa = [reshape(P1o.Yvf(1,:),1,1,size(w,2)) reshape(P1o.Yvm(1,:),1,1,size(w,2));
    reshape(P1o.Yaf(1,:),1,1,size(w,2)) reshape(P1o.Yam(1,:),1,1,size(w,2))];

Yab = [reshape(P2o.Yvf(1,:),1,1,size(w,2)) reshape(P2o.Yvm(1,:),1,1,size(w,2));
    reshape(P2o.Yaf(1,:),1,1,size(w,2)) reshape(P2o.Yam(1,:),1,1,size(w,2))];

Yba = [reshape(P1o.Yvf(2,:),1,1,size(w,2)) reshape(P1o.Yvm(2,:),1,1,size(w,2));
    reshape(P1o.Yaf(2,:),1,1,size(w,2)) reshape(P1o.Yam(2,:),1,1,size(w,2))];

Ybb = [reshape(P2o.Yvf(2,:),1,1,size(w,2)) reshape(P2o.Yvm(2,:),1,1,size(w,2));
    reshape(P2o.Yaf(2,:),1,1,size(w,2)) reshape(P2o.Yam(2,:),1,1,size(w,2))];

end
```

Coupling function

```
% ffb_coupled: function to couple two free-free beams together in line
% Y_coupled = ffb_coupled(Y1,Y2,f,IL/LJ/TJ/HJ)
%
% Y1 is the matrix containing the mobilities of beam 1
% Y2 is the matrix containing the mobilities of beam 2
% f is the frequency
%
% Nomenclature for types of junctions:
%           IL - In line
%           LJ - L junction
%           TJ - T junction
%           HJ - H junction (intersecting beams)
%
% Number next to the type of junctions is the number of beams being
% coupled, i.e. LJ2 = two beams in an L-junction, LJ4 = four beams in an
% L-junction.


function Ycoupled = ffb_coupled(f,type,Ybeam_1,Ybeam_2,Ybeam_3,Ybeam_4)

% Check number of input arguments is sufficient
if nargin<4, return, end

% One large impedance matrix with the impedances at x0 and l of the 2 beams
% The results of the inversion have been checked and they seem to be
% correct using 1./Y.

if type == 'IL2'
    for i = length(f):-1:1;
        Zbeam_1(:,:,i) = inv(Ybeam_1(:,:,i));
        Zbeam_2(:,:,i) = inv(Ybeam_2(:,:,i));
    end

    % Impedance matrix assembled (1/Y)
    zeros_0 = zeros(size(Zbeam_1));
    Z = [Zbeam_1(:,:,:) zeros_0(:,:,:);
        zeros_0(:,:,:) Zbeam_2(:,:,:)];

     % Coupling matrix that identifies which points of the beams are connected
    coupling = [see Section 5.3.2];

    for i = length(f):-1:1;
        Zalmost_coupled(:,:,i) = Z(:,:,i)*coupling;
        Zcoupled(:,:,i) = coupling.'* Zalmost_coupled(:,:,i);
        Ycoupled(:,:,i) = inv(Zcoupled(:,:,i));
    end

elseif type == 'LJ2'

    for i = length(f):-1:1;
        Zbeam_1(:,:,i) = inv(Ybeam_1(:,:,i));
        Zbeam_2(:,:,i) = inv(Ybeam_2(:,:,i));
    end

    % Impedance matrix assembled (1/Y)
    zeros_0 = zeros(size(Zbeam_1));
    Z = [Zbeam_1(:,:,:) zeros_0(:,:,:);
        zeros_0(:,:,:) Zbeam_2(:,:,:)];

    % Coupling matrix that identifies which points of the beams are connected
    coupling = [see Section 5.3.3];

    for i = length(f):-1:1;
        Zalmost_coupled(:,:,i) = Z(:,:,i)*coupling;
        Zcoupled(:,:,i) = coupling.'* Zalmost_coupled(:,:,i);
        Ycoupled(:,:,i) = inv(Zcoupled(:,:,i));
    end

elseif type == 'LJ3'

    for i = length(f):-1:1;
        Zbeam_1(:,:,i) = inv(Ybeam_1(:,:,i));
        Zbeam_2(:,:,i) = inv(Ybeam_2(:,:,i));
        Zbeam_3(:,:,i) = inv(Ybeam_3(:,:,i));
    end

    zeros_0 = zeros(size(Zbeam_1));
    Z = [Zbeam_1(:,:,:) zeros_0(:,:,:) zeros_0(:,:,:);
        zeros_0(:,:,:) Zbeam_2(:,:,:) zeros_0(:,:,:);
        zeros_0(:,:,:) zeros_0(:,:,:) Zbeam_3(:,:,:)];
```

```
    % Coupling matrix that identifies which points of the beams are connected
    coupling = [see Section 5.3.4];


    for i = length(f):-1:1;
        Zalmost_coupled(:,:,i) = Z(:,:,i)*coupling;
        Zcoupled(:,:,i) = coupling.'* Zalmost_coupled(:,:,i);
        Ycoupled(:,:,i) = inv(Zcoupled(:,:,i));
    end

elseif type == 'LJ4'

    for i = length(f):-1:1;
        Zbeam_1(:,:,i) = inv(Ybeam_1(:,:,i));
        Zbeam_2(:,:,i) = inv(Ybeam_2(:,:,i));
        Zbeam_3(:,:,i) = inv(Ybeam_3(:,:,i));
        Zbeam_4(:,:,i) = inv(Ybeam_4(:,:,i));
    end

    zeros_0 = zeros(size(Zbeam_1));
    Z = [Zbeam_1(:,:,:) zeros_0(:,:,:) zeros_0(:,:,:) zeros_0(:,:,:);
        zeros_0(:,:,:) Zbeam_2(:,:,:) zeros_0(:,:,:) zeros_0(:,:,:);
        zeros_0(:,:,:) zeros_0(:,:,:) Zbeam_3(:,:,:) zeros_0(:,:,:);
        zeros_0(:,:,:) zeros_0(:,:,:) zeros_0(:,:,:) Zbeam_4(:,:,:)];

    % Coupling matrix that identifies which points of the beams are connected
    coupling = [see Section 5.3.4];

    for i = length(f):-1:1;
        Zalmost_coupled(:,:,i) = Z(:,:,i)*coupling;
        Zcoupled(:,:,i) = coupling.'* Zalmost_coupled(:,:,i);
        Ycoupled(:,:,i) = inv(Zcoupled(:,:,i));
    end

else
    return
end

end
```